The Effect of Surface Stress on Interfacial Solitary Waves

Dane Grundy

October 2019

A thesis submitted to the School of Mathematics of the University of East Anglia in partial fulfilment of the requirements for the degree of Doctor of Philosophy (PhD).

The University of East Anglia has been the centre point of my education for the past eight years. I am proud to have been a student, member of staff, and more importantly a contributor to what makes this University the fantastic institute that it is today.

Abstract

A range of physical problems involving solitary wave solutions to the Korteweg-de Vries (KdV) equation are discussed. More specifically, relevance of perturbed forms of the Korteweg-de Vries equation and the effect of surface stress on the propagation of long-wavelength disturbances on the surface of a fluid layer of finite depth is considered. A weakly nonlinear analysis is performed leading to an evolution equation similar to the classic KdV equation, but modified by additional terms due to the viscosity and to the tangential and normal stress at the surface.

A thorough numerical analysis is constructed concerning numerical solutions to the KdV equation including an extensive stability analysis. Solutions which are perturbations of travelling solitary wave solutions are then considered which is mainly focussed on the Korteweg-de Vries-Burgers' (KdV-B) equation. Asymptotic analyses demonstrate the appearance of a decaying oscillatory tail behind a core solitary wave-like solution. The solution in the tail region is determined in the form of a convolution integral involving the Airy function, while the core solution is obtainable explicitly.

Attention is also focussed on the effect of stress at the fluid surface. Constant surface tension leads to a normal stress at the surface, but the presence of an insoluble surfactant or the application of an electric field can also give rise to tangential stresses. In the large Reynolds number limit, the governing equation for the surface elevation contains contributions from two boundary layers in the flow: one is adjacent to the free surface while the other lies at the base of the fluid layer.

All asymptotic results are fully validated by comparison with numerical results obtained using a pseudospectral numerical integrating factor scheme.

Dedication

I dedicate this thesis to Ethan and Ella whose desire and love for learning is a continual inspiration to all my work. I am certain that one day, through all of your hard work, you will both surpass my own achievements and continue to make me proud.

Acknowledgements

First, I acknowledge Dr. Paul Hammerton for four years of invaluable supervision, support and advice throughout my PhD. Thank you for your patience and for taking the time to carefully work through problems with me whenever I was stuck or confused, even with the most simple things. Thank you also for encouraging me to present my work at international conferences and helping to write applications. One of the best parts of my PhD was travelling to share my work through talks and study groups. Finally, thank you for always making time to support my PhD, even when you were exceptionally busy.

I would also like to acknowledge Professor Emilian Părău for excellent supervision, advice and support. Thank you for the conference recommendations and invites, and for giving me the opportunity to present my work at international study groups. Finally, thank you for attending most of my talks, for the helpful feedback, and also for the many pints of beer consumed during these trips.

Next, I would like to thank my mum and dad for always encouraging me to achieve more and push myself to highest of my abilities. I am extremely grateful for your support and encouragement, not just during my PhD, but for everything you have done to help me over the past twenty seven years. In fact, without you I would never have discovered my love for mathematics and would probably have not achieved what I have today.

I would also like to thank Kevin and Tessa for helping to support me during my PhD, and my undergraduate degree. I am extremely appreciative for all your advice, for always helping us out when and where you can, and - most importantly - for the banoffee pie.

A special thank you goes to Mr. Nathan Barbor for reminding me about life outside of the PhD. Thanks for always looking out for me, for listening to me moan and helping me to de-stress, and for constantly making me laugh. Thanks for being my best mate for the past eight years and for keeping me sane during my PhD.

Another special acknowledgement goes to Dr. Tom Coleman. Thank you, sir. Thanks for continually supporting me where you could with the PhD, for being my co-coffee-enthusiast, for all of your invaluable advice and encouragement, for inspiring me to always work hard, for always looking out for me and the children, and for generally being my best mate. You made my whole PhD experience much, much better.

Finally, I would like to acknowledge Emily without whom my PhD would not have been possible. I don't have words to describe how appreciative I am of everything you have done for me. Thank you for supporting me from the beginning to the end; you encouraged me to pursue the PhD when I was unsure if I was even capable of undertaking one. Thank you for listening to me complain about breaking my codes, for listening to me complain when I got stuck, and for helping me when I asked. Thank you for putting up with me when I was feeling down, especially during the final few months, and for helping me to feel positive again. Thanks for being there for me - and the children - when I needed you, and for encouraging me to work hard and to not give up. Thank you for making every day much happier. I am forever grateful of everything that you do for me and for everything you did to support me during the last four years.

I also acknowledge EPSRC for funding the project and for the support of a studentship.

Contents

List of Figures

List of Tables

Table of notation

Unless otherwise stated, the following list of notation is used throughout the thesis:

Symbol	Description	Symbol	Description
g	Acceleration due to gravity (m/s^2)	ρ	Density (kg/m^3)
p	Pressure (N/m^2)	d	Distance (m)
ν	Kinematic viscosity (m^2/s)	μ	Dynamic viscosity (kg/ms)
Re	Reynolds number	Pe	Peclet number
E_b	Electric Weber number	PV	Cauchy Principal Value
i	Imaginary unit $\sqrt{-1}$	e	Euler's number $2.71828\ldots$
Eo	Eötvös/Bond number	α	Marangoni number
ϵ	Permittivity	σ_c	Conductivity
$\mathbf{J}$	Electric current density	ψ	Electric potential
q	Electric charge density	$\mathbf{E}$	Electric field intensity
σ	Surface tension	ϕ	Velocity potential
η	Surface elevation	Γ	Surfactant concentration
κ	Surface curvature	ω	Vorticity
$\mathbf{u}$	Velocity	$\tilde{\omega}$	Surface vorticity
U	Surface velocity	D_s	Surfactant diffusion coefficient
A	Wave amplitude	c	Wave speed
$\widehat{T}_\mathrm{n}$	Normal surface stress	$\widehat{T}_\mathrm{t}$	Tangential surface stress
k	Spectral variable	K	Wave number
$\mathcal{F}$	Fourier transform	$\mathcal{H}$	Hilbert transform

Frequently used abbreviations

In general, abbreviations and acronyms have been kept to a minimum. However, the following may appear in the thesis:

DFT	Discrete Fourier Transform
FFT	Fast Fourier Transform
KdV	Korteweg-de Vries
KdV-B	Korteweg-de Vries-Burgers
LHS	Left-hand side
RHS	Right-hand side
LF	Leapfrog scheme
RK4	Fourth order Runge-Kutta scheme
ODE	Ordinary differential equation
PDE	Partial differential equation

1

Introduction

1.1 Overview of thesis

The main focus of this thesis is examining the effects of surface stress on solitary wave solutions to the Korteweg-de Vries (KdV) equation and other associated equations. Travelling wave solutions are derived directly from the KdV equation in Section 1.3 as a starting point, followed by a detailed and extensive numerical analysis of the travelling solitary wave solution in Chapter 2, where various numerical methods are considered. A suitable stability analysis of each numerical method is then given to determine its suitability for the subsequent work.

After establishing an appropriate numerical scheme, the scheme is expanded on so that various parameters may be added to the governing KdV equation which govern surface stress and other effects of interest. Each parameter is analysed, where possible, using exact solutions and asymptotic and numerical approximations to examine the effects on the generalised soliton solution.

The first of these effects is examined in Chapter 3 which considers adding a diffusive second-order parameter to the KdV equation contributing to diffusive damping. This chapter imposes the solitary wave solution to the unperturbed KdV equation as an initial condition, but assumes that the amplitude is now a slowly varying function of time. The key purpose of Chapter 3 is to provide a solution for the amplitude as a function of time and interpret the results accordingly.

In Chapter 4, a significant part of which continues the work of Hammerton and Bassom (2013), an extensive analysis is given which considers long-wavelength small amplitude

disturbances in an incompressible shallow fluid layer, subject to arbitrary stress conditions on the fluid surface. Then in Chapter 5, a tangential stress condition acting due to a surface boundary layer is considered. A system with an insoluble low concentration surfactant present at the interface between two fluids is examined.

Finally, Chapter 6 looks at other scenarios with a surface stress condition present at the fluid surface. Results are given for a system with a solitary wave disturbance at the free surface, subject to an electric field acting vertically through the fluid. These results are compared with previous chapters and analogies are given. This chapter, and the thesis as a whole, are concluded with suggestions for possible extensions to the existing work and an overall summary of the results presented in the thesis.

1.2 Background

The study of the Korteweg-de Vries (KdV) equation and its associated travelling wave solutions is well developed. Derived and studied in 1895 by Diederik Korteweg and Gustav de Vries (Korteweg and de Vries, 1895), although also known to Boussinesq (Boussinesq, 1877), the KdV equation is a nonlinear partial differential equation with a direct balance between nonlinearity and wave dispersion which has long since been used in the study of nonlinear shallow water waves. The KdV equation is perhaps best known for having travelling **solitary wave** solutions which make up the basis for this thesis.

1.2.1 History of the solitary wave

The solitary wave is sometimes called **Russell's Solitary Wave** after its earliest known observer, John Scott Russell. In 1834 Russell observed what he called **The Great Wave of Translation**:

"I was observing the motion of a boat which was rapidly drawn along a narrow channel by a pair of horses, when the boat suddenly stopped - not so the mass of water in the channel which it had put in motion; it accumulated round the prow of the vessel in a state

of violent agitation, then suddenly leaving it behind, rolled forward with great velocity, assuming the form of a large solitary elevation, a rounded, smooth and well-defined heap of water, which continued its course along the channel apparently without change of form or diminution of speed. I followed it on horseback, and overtook it still rolling on at a rate of some eight or nine miles an hour, preserving its original figure some thirty feet long and a foot to a foot and a half in height. Its height gradually diminished, and after a chase of one or two miles I lost it in the windings of the channel. Such, in the month of August 1834, was my first chance interview with that singular and beautiful phenomenon which I have called the Wave of Translation" - (Russell, 1844).

This early observation of the solitary wave has since been generalised to **soliton** theory, the details of which are discussed in Subsection 1.2.2.

1.2.2 Properties of the solitary wave and soliton theory

A solitary wave is a nonlinear travelling wave which has finite amplitude and propagates with constant speed and constant shape. The solitary wave, as defined in Hereman (2012), is a localised gravity wave that maintains its coherence and, hence, its visibility through properties of nonlinear hydrodynamics.

After his initial observation, John Scott Russell attempted to recreate solitary wave disturbances in laboratory experiments by dropping a weight at one end of a water channel. Through these experiments Russell was able to attribute two main properties to the solitary wave: (i) the wave amplitude A is directly proportional to the wave speed c, and (ii) the width of the wave is inversely proportional to $\sqrt{A}$. In other words, taller waves travel faster and are narrower than shorter waves.

Early experiments (Zabusky and Kruskal, 1965; Russell, 1844) identified another important property of solitary waves. If a solitary wave of larger amplitude is initially propagating behind another solitary wave of smaller amplitude, then the larger of the two waves will eventually catch up the smaller wave. During their interaction, the taller wave will effectively pass through the smaller wave and then emerge essentially unchanged

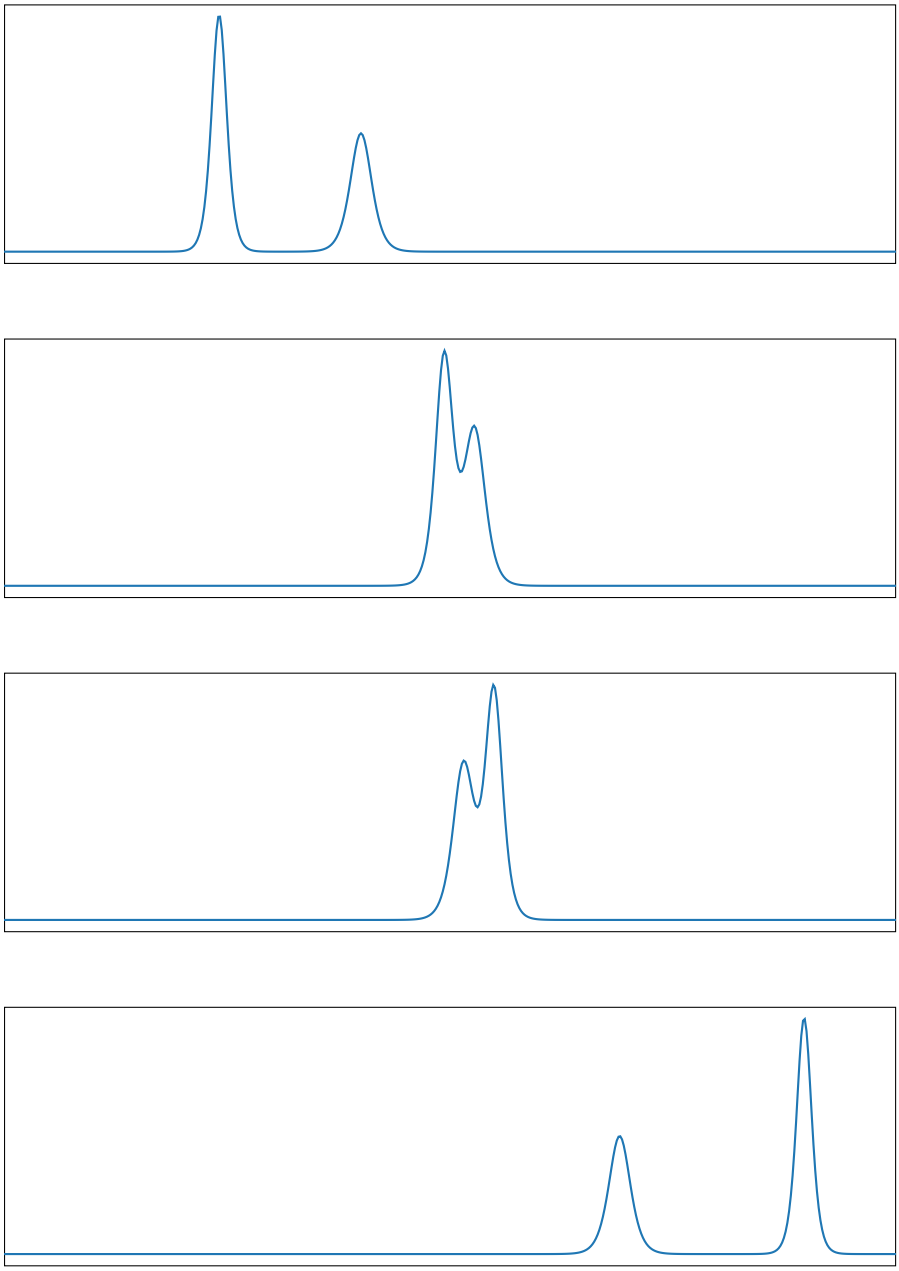

Figure 1.2.1: An interaction between two solitons both travelling to the right. The illustration shows a larger soliton, first catching up, and then passing through a smaller soliton.

(except for a small horizontal phase shift). This property is unique to solitary waves; in the case of other nonlinear travelling waves, the interaction would result in some distortion or merging of the two waves.

This observation led Zabusky and Kruskal (1965) to introduce the term **soliton** to describe solitary waves involved in these interactions. This name is coined as a direct combination of the terms **solitary wave** and **photon** (or **proton**) which emphasises the

particle-like characteristics of retaining their identity following a collision. While there is no universally accepted definition of a soliton, Drazin and Johnson (1989) attribute three properties: a travelling wave solution of a nonlinear equation (i) of permanent form, which is (ii) localised so that it decays or approaches at constant at $\pm\infty$, and (iii) can interact with other solitons and retain its identity.

Figure 1.2.1 is a numerically generated simulation of two solitons interacting with one another. This figure was generated using a numerical scheme defined and discussed in more detail later in Chapter 2. During the course of the thesis, we will often use the terms **solitary wave** and **soliton** interchangeably, as is generally accepted. In the context of the KdV equation it is usual to refer to the single-soliton solution as the solitary wave, but when more than one of them appear as one solution they are usually called solitons, (Drazin and Johnson, 1989).

1.3 Solitary wave solutions to the Korteweg-de Vries equation

The key focus of the thesis will be the study of interfacial solitary water waves. We begin with the KdV equation (Korteweg and de Vries, 1895). The KdV equation is a dispersive nonlinear partial differential equation (PDE) for a surface elevation function η, and can be written as

$$\frac{\partial \eta}{\partial t} + 6\eta\frac{\partial \eta}{\partial x} + a\frac{\partial^3 \eta}{\partial x^3} = 0, \tag{1.3.1}$$

where $\eta(x,t)$ is a function of a characteristic variable which can be denoted by x, and a time variable denoted by t. We restrict our attention to the case when the flow is localised, so we have a boundary condition which states that $\eta \to 0$ as $x \to \pm\infty$.

The coefficient a is a known constant which is directly related to the Eötvös number (also called the Bond number) which characterises the ratio of gravitational forces to interfacial tension forces, and affects the wave dispersion (Davis and Acrivos, 1966). The Bond number is discussed in more detail in Chapter 4 when we start to consider the effects on the surface tension due to surface stress, but for the present we set $a = 1$ which gives the general form of the KdV equation for elevated travelling waves (positive amplitude).

We note that if we were to change the parity of a then we would expect solutions in the form of a travelling waves of depression (negative amplitude), although in a physical system this isn't applicable to water waves.

1.3.1 Derivation of the single soliton solution

The KdV equation has both **solitary** and **cnoidal** surface gravity waves with long wavelength (travelling wave solutions), although the focus of this work concerns solitary waves only. To derive these solutions we switch to the moving frame of reference by introducing a new variable $z = x - ct$, where c is the wave speed, and attempt to solve Equation 1.3.1 for η.

As discussed in Section 1.2, the wave speed is directly proportional to the wave amplitude. In the following derivation of the single soliton solution, the exact relationship between c and A will also be derived. Imposing that $a = 1$, the KdV equation (1.3.1) can be written in the form

$$\frac{\partial \eta}{\partial t} + 6\eta \frac{\partial \eta}{\partial x} + \frac{\partial^3 \eta}{\partial x^3} = 0. \tag{1.3.2}$$

After switching to the moving frame, Equation 1.3.2 becomes

$$-c\frac{\mathrm{d}\eta}{\mathrm{d}z} + 6\eta \frac{\mathrm{d}\eta}{\mathrm{d}z} + \frac{\mathrm{d}^3 \eta}{\mathrm{d}z^3} = 0. \tag{1.3.3}$$

We then integrate with respect to z which gives

$$-c\eta + 3\eta^2 + \frac{\mathrm{d}^2 \eta}{\mathrm{d}z^2} = C_1, \tag{1.3.4}$$

and multiply by $\frac{\mathrm{d}\eta}{\mathrm{d}z}$ to give

$$-c\eta\frac{\mathrm{d}\eta}{\mathrm{d}z} + 3\eta^2\frac{\mathrm{d}\eta}{\mathrm{d}z} + \frac{\mathrm{d}\eta}{\mathrm{d}z}\frac{\mathrm{d}^2 \eta}{\mathrm{d}z^2} = C_1\frac{\mathrm{d}\eta}{\mathrm{d}z},$$

where C_1 is a constant of integration. Integrating once more gives

$$-\frac{c}{2}\eta^2 + \eta^3 + \frac{1}{2}\left(\frac{\mathrm{d}\eta}{\mathrm{d}z}\right)^2 = C_1\eta + C_2,$$

where C_2 is an additional constant of integration. Then rearranging the equation for $(\frac{\mathrm{d}\eta}{\mathrm{d}z})^2$ yields

$$\left(\frac{\mathrm{d}\eta}{\mathrm{d}z}\right)^2 = c\eta^2 - 2\eta^3 + 2C_1\eta + 2C_2. \tag{1.3.5}$$

If we restrict our attention to solitary wave solutions then the flow is localised in z, so we have the boundary conditions

$$\eta, \frac{\mathrm{d}\eta}{\mathrm{d}z}, \frac{\mathrm{d}^2\eta}{\mathrm{d}z^2} \to 0 \qquad \text{as} \qquad |z| \to \infty,$$

since solitary waves decay to zero far from the peak disturbance, by definition. Applying these conditions to Equation 1.3.4 and Equation 1.3.5 gives $C_1 = C_2 = 0$.

We note that without restricting to solitary waves, the right-hand side of Equation 1.3.5 has three real roots for a given domain: η_1, η_2 and η_3, for example. After some work we could derive periodic cnoidal wave solutions which are defined in terms of the Jacobi **cosinus amplitudinus** function $\mathbf{cn}$. This relationship to the $\mathbf{cn}$ function is the reason they are given the name **cn**oidal waves, (Bona and Tropp, 2001).

As discussed earlier the focus of this thesis is solitary waves, so cnoidal waves are not explored any further. In order to obtain real solutions we require that $(\frac{\mathrm{d}\eta}{\mathrm{d}z})^2 \geq 0$, and hence $c\eta^2 - 2\eta^3 \geq 0$. Then with these conditions, Equation 1.3.5 becomes

$$\frac{\mathrm{d}\eta}{\mathrm{d}z} = \pm\sqrt{\eta^2(c-2\eta)} = \pm\eta\sqrt{c-2\eta}.$$

This equation is of separable type so we can find a solution using the method of separation of variables, so that

$$\int \frac{\mathrm{d}\eta}{\eta\sqrt{c-2\eta}} = \pm\int \mathrm{d}z, \tag{1.3.6}$$

and the right-hand side is simply

$$\pm\int \mathrm{d}z = \pm(z+z_0)\,,$$

where z_0 is a constant of integration. Then for the left-hand side of (1.3.6) we try

$$\eta = \frac{c}{2}\operatorname{sech}^2\theta, \tag{1.3.7}$$

for some variable θ to be determined, so that

$$\frac{\mathrm{d}\eta}{\mathrm{d}\theta} = -c\tanh\theta\,\mathrm{sech}^2\,\theta$$

and hence we have

$$\int \mathrm{d}\eta = -c\int \tanh\theta\,\mathrm{sech}^2\,\theta\,\mathrm{d}\theta. \tag{1.3.8}$$

We then substitute Equation 1.3.7 and Equation 1.3.8 into the left-hand side of Equation 1.3.6 which gives

$$\begin{aligned}\int \frac{\mathrm{d}\eta}{\eta\sqrt{c-2\eta}} &= -c\int \frac{\tanh\theta\,\mathrm{sech}^2\,\theta}{\frac{c}{2}\,\mathrm{sech}^2\,\theta\sqrt{c-c\,\mathrm{sech}^2\,\theta}}\,\mathrm{d}\theta \\ &= -\int \frac{2\tanh\theta}{\sqrt{c(1-\mathrm{sech}^2\,\theta)}}\,\mathrm{d}\theta,\end{aligned}$$

Then, using the trigonometric identity

$$1-\mathrm{sech}^2\,\theta = \tanh^2\theta,$$

we have

$$-\int \frac{2\tanh\theta}{\sqrt{c\tanh^2\theta}}\,\mathrm{d}\theta = -\int \frac{2}{\sqrt{c}}\,\mathrm{d}\theta$$

and hence

$$\theta = \mp\frac{\sqrt{c}}{2}(z+z_0).$$

Substituting θ back into equation Equation 1.3.7 yields

$$\eta = \frac{c}{2}\,\mathrm{sech}^2\left(\frac{\sqrt{c}}{2}(z+z_0)\right),$$

where the $\mp$ is no longer necessary since $\mathrm{sech}^2(X)$ is an **even** function, which means that

$$\mathrm{sech}^2(X) = \mathrm{sech}^2(-X).$$

It can then be imposed that $z_0 = 0$ since z_0 simply represents a phase shift denoting the position of the wave peak at $t = 0$. We convert back to x and t and then, finally, the

travelling solitary wave solution is given by

$$\eta(x,t) = A\,\mathrm{sech}^2\left(\frac{\sqrt{c}}{2}(x-ct)\right), \tag{1.3.9}$$

with amplitude A and wave speed $c = 2A$. We note here that changing the coefficients of the derivatives in the KdV equation (1.3.2) will modify this relationship between c and A, although they will remain directly proportional.

The solitary wave solution (1.3.9) will be used in many of the following analyses presented in the thesis, often as an initial condition by setting $t = 0$.

1.3.2 The multiple soliton solution

The single soliton solution is not the only solution to the KdV equation. We have already discussed the possibility of cnoidal wave solutions in Subsection 1.3.1, but there are also various other possible solutions. Some of these include **similarity solutions** and **rational solutions** which are discussed in (Drazin and Johnson, 1989), although these particular examples are not explored here. A further set of solutions which are of interest are the **two-soliton** and **multi-soliton** (or **N-soliton**) solutions.

In Subsection 1.2.2 we discussed the unique property that, following a collision, multiple solitons will emerge essentially unchanged. During a collision between two solitons there is a point when the centres are aligned where the two waves form a single soliton profile, after which the two solitons re-emerge. It is possible to use this single soliton profile as an initial condition to derive the two-soliton solution to the KdV equation. The exact derivation isn't given here, but Brauer (2000) uses Bäcklund transforms to derive a general form of the solution, which is validated using Mathematica, and is given by

$$\eta(x,t) = \frac{(A_1-A_2)\left(c_1\cosh^2\left(\frac{\sqrt{c_2}}{2}z_2\right) + c_2\sinh^2\left(\frac{\sqrt{c_1}}{2}z_1\right)\right)}{\left((\sqrt{c_1}-\sqrt{c_2})\cosh\left(\frac{\sqrt{c_1}}{2}z_1+\frac{\sqrt{c_2}}{2}z_2\right)+(\sqrt{c_1}+\sqrt{c_2})\cosh\left(\frac{\sqrt{c_1}}{2}z_1-\frac{\sqrt{c_2}}{2}z_2\right)\right)^2} \tag{1.3.10}$$

where the wave amplitudes, A_1 and A_2, of each soliton are such that

$$A_1 = \frac{c_1}{2} > A_2 = \frac{c_2}{2} > 0,$$

and $z_1 = x - c_1 t$ and $z_2 = x - c_2 t$ are the respective characteristic variables.

In addition to this, it is also possible to derive the N-soliton solution. This, and the two-soliton solution were originally derived in (Kruskal et al., 1967) using a method of inverse scattering transforms, sometimes called the GGKM analysis, after the authors (Gardner, Green, Kruskal and Miura). A generalisation to the original work is discussed in Drazin and Johnson (1989) where it is shown that taking an initial profile to be

$$\eta(x, 0) = n(n+1)\,\mathrm{sech}^2\, x \tag{1.3.11}$$

results in n unique solitons with different amplitudes as $t \to \infty$. An N-soliton solution with the long-time asymptotics

$$\eta(x, t) = 2\sum_{n=1}^{N} n^2\,\mathrm{sech}^2\left(n(x - 4n^2 t)\right), \quad \text{as} \quad t \to \infty, \tag{1.3.12}$$

can also be constructed, see for example (Kruskal et al., 1967; Drazin and Johnson, 1989).

In this thesis, the main focus will be on the single solitary wave solution applied to different contexts, although numerical examples will be given in Chapter 2 demonstrating multiple solitons emerging from an initial single-soliton profile.

2

A numerical treatment of the Korteweg-de Vries equation

This chapter will compare a variety of techniques which will be used to produce numerical solutions to the Korteweg-de Vries equation. We will use the solitary wave solution (1.3.9) derived in Section 1.3 at time $t = 0$ as an initial condition, and then numerically advance forward in time using three well-defined time step schemes. The aim is to deduce the benefits and the limitations of using each scheme to generate numerical solutions. This chapter will give a detailed comparison of the accuracy of each technique, including stability analyses and efforts to determine time efficiency.

In addition to comparing the time step schemes, this chapter will also consider two techniques for numerically evaluating the spatial derivatives associated with the KdV equation. A comparison highlighting the benefits and limitations will also be made, and as a conclusion we will decide which of the techniques, both for advancing in time and for evaluating spatial derivatives, will be the most efficient to use for future approximations.

Overview of schema

In the following analysis, the spatial derivatives will be handled using two different numerical methods. The first technique we consider will be the **finite difference** method. We will then conduct a similar analysis using the **pseudospectral** method. Each technique will use the solitary wave solution (1.3.9) at $t = 0$ as an initial value. We will then advance in time, first using an **Euler** time step method, then using a **leapfrog** method, and finally using a fourth-order **Runge-Kutta** time step method, to produce a numerical

solution. An attempt will then be made to compare the two spatial methods and the three time step schemes, with the intention of deciding which combination will be the most efficient to use for more complicated systems of equations explored later in the thesis.

2.1 The finite difference method

Finite difference methods approximate spatial and time derivatives using *finite differences* and can produce a numerical solution using difference equations. We begin by subdividing the domain

$$[-x_{\mathrm{m}}, x_{\mathrm{m}}] \times [0, t_{\mathrm{max}}]$$

into

$$(2N+1) \times M$$

equal grid points, where N denotes the number of spatial steps, M denotes the number of time steps, x_{m} is the truncation point of x, and t_{max} denotes the maximum value of time. We define the spatial step size as

$$\Delta x = \frac{\text{length of domain}}{\text{number of elements}} = \frac{2x_{\mathrm{m}}}{2N+1},$$

and define the time step as

$$\Delta t = \frac{t_{\mathrm{max}}}{M}.$$

We then define the nodal points to be

$$x_j = -x_{\mathrm{m}} + j\Delta x, \qquad j = 0, 1, 2, \ldots, 2N+1$$

and

$$t_n = n\Delta t, \qquad n = 0, \ldots, M-1.$$

To set up the scheme η is discretised so we write $\eta(x,t) = \eta(x_j, t_n)$ and so we could write $\eta_{j_1}^{n_1}$ to denote the value of η at grid point (j_1, n_1). Here, subscripts j represent discrete points in space and superscripts n denote discrete levels in time. Applying this

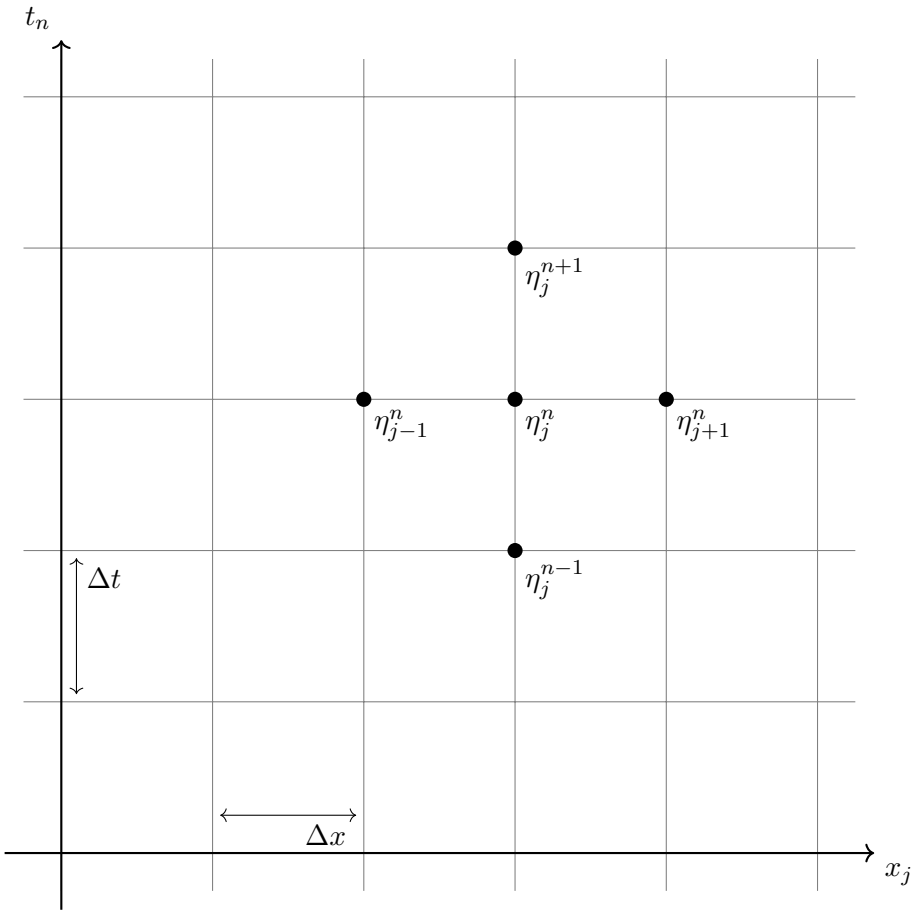

Figure 2.1.1: An illustration of the numerical mesh demonstrating the numerical node structure.

discretisation, η is evaluated over a numerical mesh illustrated by Figure 2.1.1.

The next step is to evaluate the KdV equation in terms of finite difference equations. First, we rearrange Equation 1.3.1 into the following form:

$$\frac{\partial \eta}{\partial t} = -\left(a\frac{\partial^3 \eta}{\partial x^3} + 6\eta\frac{\partial \eta}{\partial x} \right) \tag{2.1.1}$$

and focus our attention on the right-hand side of the equation. The derivatives $\frac{\partial \eta}{\partial x}$ and $\frac{\partial^3 \eta}{\partial x^3}$ need to be written in terms of finite difference approximations. For this analysis we will use **central difference** operators to evaluate the spatial derivatives. These can be defined in several waves depending on the order of the **truncation error**, denoted $\mathcal{E}_{\text{tr}}$, which represents the error conceded in approximating the derivative numerically. For a given step size h, and any given function $f(x)$, the second-order central difference operator for

$\frac{\mathrm{d}f}{\mathrm{d}x}$ is defined in (Mathews et al., 2004) to be

$$\begin{aligned}\frac{\mathrm{d}f}{\mathrm{d}x} &\approx \frac{f(x+h)-f(x-h)}{2h},\\ \frac{\mathrm{d}f}{\mathrm{d}x} &= \frac{f(x+h)-f(x-h)}{2h}+\mathcal{E}_{\mathrm{tr}}.\end{aligned} \tag{2.1.2}$$

This can be derived by taking second-degree Taylor expansions for $f(x+h)$ and $f(x-h)$ around x, so that

$$f(x+h)=f(x)+h\frac{\mathrm{d}f}{\mathrm{d}x}+\frac{h^2}{2!}\frac{\mathrm{d}^2f}{\mathrm{d}x^2}+\frac{h^3}{3!}\frac{\mathrm{d}^3f}{\mathrm{d}x^3}+\mathcal{O}(h^4),$$

and

$$f(x-h)=f(x)-h\frac{\mathrm{d}f}{\mathrm{d}x}+\frac{h^2}{2!}\frac{\mathrm{d}^2f}{\mathrm{d}x^2}-\frac{h^3}{3!}\frac{\mathrm{d}^3f}{\mathrm{d}x^3}+\mathcal{O}(h^4).$$

Combining these we achieve

$$\frac{f(x+h)-f(x-h)}{2h}=\frac{\mathrm{d}f}{\mathrm{d}x}+\mathcal{O}(h^2)$$

and therefore the truncation error $\mathcal{E}_{\mathrm{tr}}=\mathcal{O}(h^2)$. We can reduce the size of the truncation error using higher-degree Taylor expansions around x, and hence derive higher-order central difference approximations. For this example we will use the second-order central difference approximation described above.

Thus, using Equation 2.1.2 with $h=\Delta x$ and $f(x)=\eta(x,t)$, the second-order central difference equation for $\frac{\partial\eta}{\partial x}$ is

$$\frac{\partial\eta}{\partial x}=\frac{\eta(x+\Delta x,t)-\eta(x-\Delta x,t)}{2\Delta x}+\mathcal{O}\left((\Delta x)^2\right), \tag{2.1.3}$$

which in terms of our mesh points i and j can be written as

$$\frac{\partial\eta}{\partial x}=\frac{\eta^n_{j+1}-\eta^n_{j-1}}{2\Delta x}.$$

Increasing the number of mesh points N will decrease the size of Δx and should therefore improve the accuracy of the approximation. It is possible to illustrate the numerical accuracy of these approximations to the derivatives by plotting the exact solution together

with the numerical solution. For this illustration, we choose the solitary wave solution given in Equation 1.3.9,

$$\eta = A\,\mathrm{sech}^2\left(\sqrt{\frac{A}{2}}(x-ct)\right),$$

and the derivative is given by

$$\frac{\partial \eta}{\partial x} = -\sqrt{2}A^{3/2}\,\mathrm{sech}^2\left(\sqrt{\frac{A}{2}}(x-ct)\right)\tanh\left(\sqrt{\frac{A}{2}}(x-ct)\right), \tag{2.1.4}$$

where $A = \frac{c}{2}$ denotes the wave amplitude. Figure 2.1.2 gives a comparison between the numerical central difference equation (2.1.3) approximation to the derivative $\frac{\partial \eta}{\partial x}$, and the exact analytical solution to the derivative Equation 2.1.4, for a varying number of spatial steps N.

In the figure it can be seen that the the approximation appears to map much more closely onto the exact solution for an increased number of steps N. For $N = 32$ the approximation mimics the behaviour of the exact solution, but it is clear from the illustration that there is a reasonably high error in the approximation to the derivative. Increasing the mesh so that $N = 128$, and hence decreasing the step size Δx, results in the approximation mapping a lot more closely onto the exact solution.

We can also use Taylor expansions around x to derive the second-order central difference operator used to give a numerical approximation to the third derivative $\frac{\partial^3 \eta}{\partial x^3}$, although the explicit derivation is not given here. The central difference equation for the third derivative is given by

$$\frac{\partial^3 \eta}{\partial x^3} = \frac{\eta(x+2\Delta x,t) - 2\eta(x+\Delta x,t) + 2\eta(x-\Delta x,t) - \eta(x-2\Delta x,t)}{2(\Delta x)^3} \tag{2.1.5}$$

which in terms of our mesh points i and j can be written as

$$\frac{\partial^3 \eta}{\partial x^3} = \frac{\eta^n_{j+2} - 2\eta^n_{j+1} + 2\eta^n_{j-1} - \eta^n_{j-2}}{2(\Delta x)^3}. \tag{2.1.6}$$

Similar to the first derivative, we illustrate the numerical accuracy of these approximations to the derivatives by plotting the exact solution against the numerical solution. The

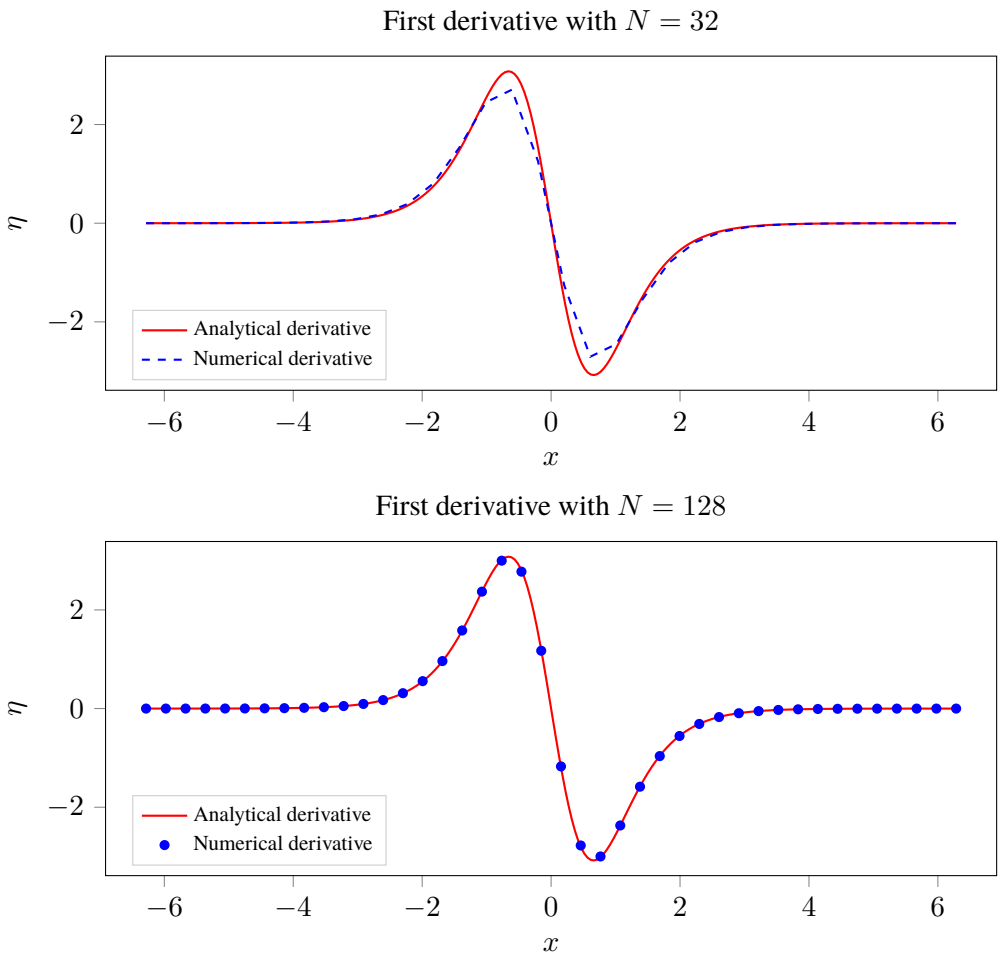

Figure 2.1.2: A comparison between the numerical approximation to the derivative $\frac{\partial \eta}{\partial x}$ using the second-order differential equation (2.1.3), and the exact solution (2.1.4), for $N = 32$ (top) and $N = 128$ (bottom), with parameter values: $A = 4$, $x \in [-2\pi, 2\pi]$.

analytical form of the exact solution to the third derivative is

$$\frac{\partial^3 \eta}{\partial x^3} = 4\sqrt{2}A^{5/2}\,\mathrm{sech}^4\left(\sqrt{\frac{A}{2}}(x - 2At)\right)\tanh\left(\sqrt{\frac{A}{2}}(x - 2At)\right) - 2\sqrt{2}A^{5/2}\,\mathrm{sech}^2\left(\sqrt{\frac{A}{2}}(x - 2At)\right)\tanh^3\left(\sqrt{\frac{A}{2}}(x - 2At)\right). \tag{2.1.7}$$

Figure 2.1.3 gives a comparison between the numerical central difference equation (2.1.5) for the third derivative $\frac{\partial^3 \eta}{\partial x^3}$, and the exact analytical solution, for a varying number of spatial steps N. It is clear from the figure that increasing the value of N results in the numerical approximation mapping much more closely to the exact solution. However, the error in the approximation to the third derivative appears to be greater than that of the

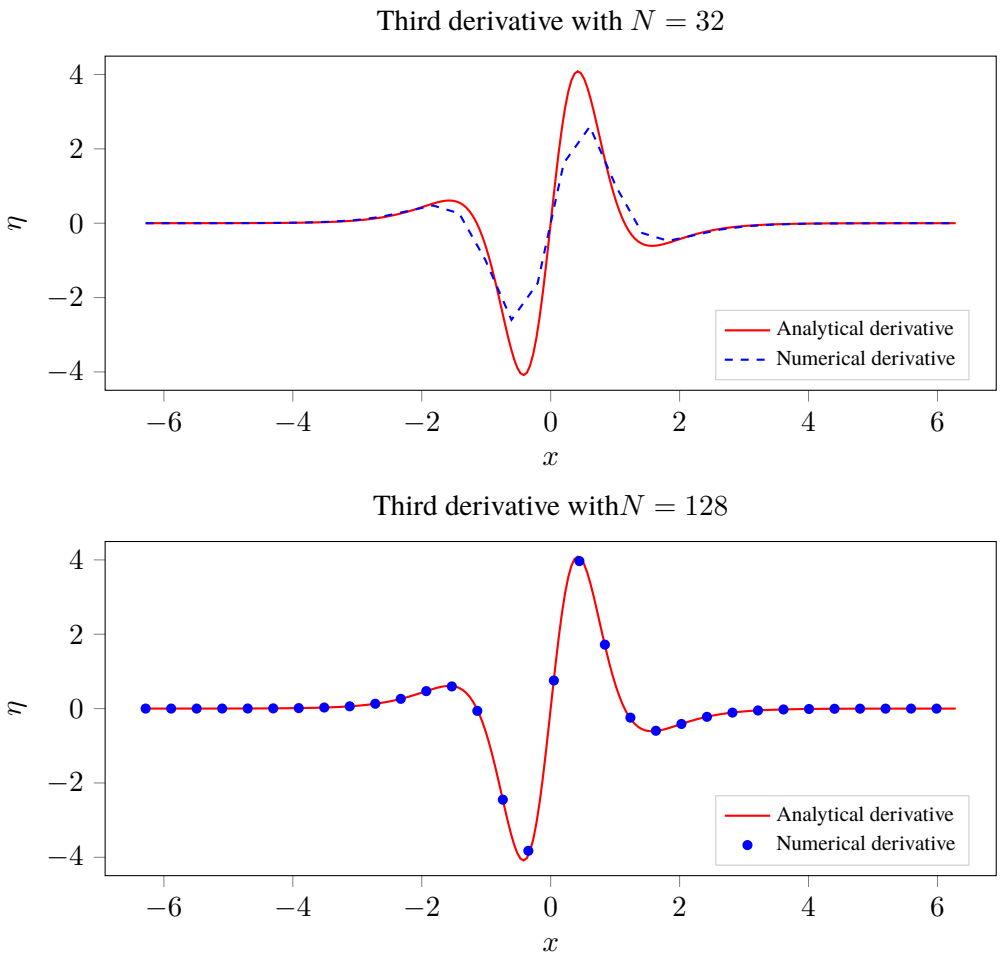

Figure 2.1.3: A comparison between the numerical approximation to the third derivative $\frac{\partial^3 \eta}{\partial x^3}$ using the central difference equation (2.1.5), and the exact solution (2.1.7) , for $N = 32$ (top) and $N = 128$ (bottom), with parameter values: $A = 4$, $x \in [-2\pi, 2\pi]$.

first derivative in x. While increasing the number of steps will improve the accuracy of the approximation, it is not always desirable to set the step size Δx to be too small. Later in the thesis, we will look at solving much more complicated partial differential equations such as a modified KdV equation to include the effects of a surfactant present at the fluid interface, see Equation 5.1.12 for example. This, and similar equations may require Δx to be small enough that this could lead to computationally expensive numerical codes. To avoid having to set the step size too small we can use a higher-order central difference equation to approximate the derivatives so that the truncation error is smaller.

The fourth-order central difference equations for $\frac{\partial \eta}{\partial x}$ and $\frac{\partial^3 \eta}{\partial x^3}$ are given by

$$\frac{\partial \eta}{\partial x} = \frac{-\eta(x + 2\Delta x) + 8\eta(x + \Delta x) - 8\eta(x - \Delta x) + \eta(x - 2\Delta x)}{12\Delta x} \tag{2.1.8}$$

and

$$\frac{\partial^3 \eta}{\partial x^3} = \Big(\eta(x-3\Delta x) - \eta(x+3\Delta x) + 8\eta(x+2\Delta x) - 8\eta(x-2\Delta x) + 13\eta(x-\Delta x) - 13\eta(x+\Delta x)\Big) \Big/ 8(\Delta x)^3 \tag{2.1.9}$$

respectively.

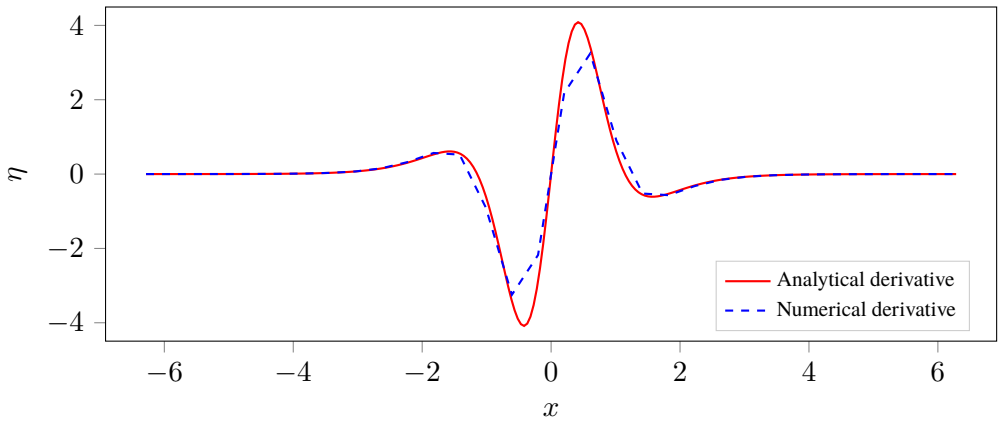

Figure 2.1.4: A comparison between the numerical approximation to the third derivative $\frac{\partial^3 \eta}{\partial x^3}$ using a fourth-order central difference equation (2.1.9), and the exact solution, for $N = 32$ with parameter values: $A = 4$, $x \in [-2\pi, 2\pi]$.

Figure 2.1.4 is an illustration giving a comparison between the exact analytical solution (2.1.7) and the numerical solution using fourth-order central difference equation (2.1.9). Comparing with Figure 2.1.3, we see that although we still retain a noticeable error for a limited number of steps $N = 32$, the approximation maps more closely to the exact solution than it did when using the second-order difference equation.

Going forward, we will use the second-order approximations in the following numerical analysis, with an increased number of steps. While the fourth-order approximation maps closer to the exact solution, the second-order equation is accurate enough for a relatively small number of steps. We also note that when evaluating the end points $j = 0$ and $j = 2N$, using the central difference equations means we attempt to evaluate terms like η_{-1}, and η_{2N+2}, which are undefined and would therefore produce an error.

There are several techniques that can be used to avoid evaluating the derivatives at the end points. One such method, which we have used in the above evaluation, is to introduce

forward difference equations to evaluate the end points at the lower boundary, and **backward difference** equations to evaluate the end points at the upper boundary. These equations are defined and discussed in more detail later.

Another technique would be to set the points to be zero and re-evaluate the difference equations at these points accordingly. For example, at the point $j = 0$ the central difference equation for $\frac{\partial^3 \eta}{\partial x^3}$ would read

$$\frac{\partial^3 \eta}{\partial x^3} = \frac{\eta_{j+2}^n - 2\eta_{j+1}^n + 0 - 0}{2(\Delta x)^3},$$

and similarly, at $j = 2N$ the equation would be

$$\frac{\partial^3 \eta}{\partial x^3} = \frac{0 - 0 + 2\eta_{j-1}^n - \eta_{j-2}^n}{2(\Delta x)^3}.$$

After indicating the potentially high accuracy of the numerical approximations, given a suitably large number of mesh points, we now have a basis for a simple finite difference scheme. How the time derivative $\frac{\partial \eta}{\partial t}$ is evaluated depends on which time step method is chosen.

2.1.1 The Euler time step

Arguably the simplest method for advancing in time is to use the Euler method (sometimes called the forward Euler method). First, we look at the definition of the time derivative of η around $t = 0$

$$\left.\frac{\partial \eta}{\partial t}\right|_{t=0} = \lim_{\delta \to 0} \frac{\eta(x, t + \delta t) - \eta(x, t)}{\delta t}.$$

Then, discretising this equation as before gives

$$\frac{\partial \eta}{\partial t} = \frac{\eta_j^{n+1} - \eta_j^n}{\Delta t},$$

and this equation can be rearranged to

$$\eta_j^{n+1} = \eta_j^n + \Delta t \frac{\partial \eta}{\partial t}.$$

The right-hand side of Equation 2.1.1 can be substituted in place of $\frac{\partial \eta}{\partial t}$ in the above equation, with the central difference equations (Equation 2.1.3 and Equation 2.1.5) in place of the spatial derivatives, and the travelling wave solution Equation 1.3.9 as an initial condition. This approach gives an Euler finite difference scheme for advancing in time. The equation can be written in general as

$$\begin{aligned} \eta_j^{n+1} &= \eta_j^n - \Delta t \left(a \frac{\partial^3 \eta}{\partial x^3} + 6\eta \frac{\partial \eta}{\partial x} \right), \\ &= \Delta t \left(a \frac{\eta_{j+2}^n - 2\eta_{j+1}^n + 2\eta_{j-1}^n - \eta_{j-2}^n}{2(\Delta x)^3} + 6\eta_j^n \frac{\eta_{j+1}^n - \eta_{j-1}^n}{2\Delta x} \right) \end{aligned} \tag{2.1.10}$$

with

$$\eta(x_j, t_0) = A \operatorname{sech}^2 \left(\sqrt{\frac{c}{4a}} x_j \right), \qquad t_0 = 0$$

as the initial condition.

Numerical stability

The Euler finite difference scheme is now set up so we proceed to determine the values for which this scheme is **stable**. First we consider what it means for a scheme to be numerically stable.

"Numerical stability refers to how a malformed input affects the execution of an algorithm. In a numerically stable algorithm, errors in the input lessen in significance as the algorithm executes, having little effect on the final output" - (Macura, 2016).

In other words, errors in an algorithm which is unstable will increase significantly causing the output to diverge from the exact solution. In fact, when instabilities occur, errors can grow exponentially and the algorithm can fail to produce an output at all. A malformed input typically refers to the step sizes chosen before executing the scheme. Fortunately, there are methods to determine the step sizes so that a numerical scheme should produce

a stable output.

In order to determine whether a numerical method will produce reasonable results with a given time step Δt, we need some way to determine stability. There are many forms of stability that have been examined in previous works, but perhaps the one that is the most basic is called **absolute stability**, (LeVeque, 2007). This method is based on using the linear test equation

$$\frac{\mathrm{d}u}{\mathrm{d}t} = \lambda u(t), \tag{2.1.11}$$

where $\lambda \in \mathbb{C}$ is a constant, and applying our time step method to it.

To determine the values for which the KdV equation is stable when evaluating the time derivative using the Euler time step method, we first use the test equation (2.1.11) for η to derive general stability criteria for the Euler method. First, we set

$$\frac{\partial \eta}{\partial t} = \Lambda \eta, \qquad \Lambda = \text{constant}. \tag{2.1.12}$$

Then evaluating the time derivative using the Euler method, the discretised test equation becomes

$$\frac{\eta^{n+1} - \eta^n}{\Delta t} = \Lambda \eta^n.$$

If we set $Z = \Lambda \Delta t$ and rearrange then we have

$$\begin{aligned} \eta^{n+1} &= (1 + \Lambda \Delta t)\eta^n, \\ \eta^{n+1} &= (1 + Z)\eta^n. \end{aligned} \tag{2.1.13}$$

This can the be rearranged again to give

$$\frac{\eta^{n+1}}{\eta^n} = 1 + Z.$$

The term on the left-hand side of this equation is sometimes referred to as the *amplification factor*, which we will denote by G. The system is said to be absolutely stable if $|G| \leq 1$, (LeVeque, 2007). Therefore, we require that

$$|1 + Z| \leq 1, \tag{2.1.14}$$

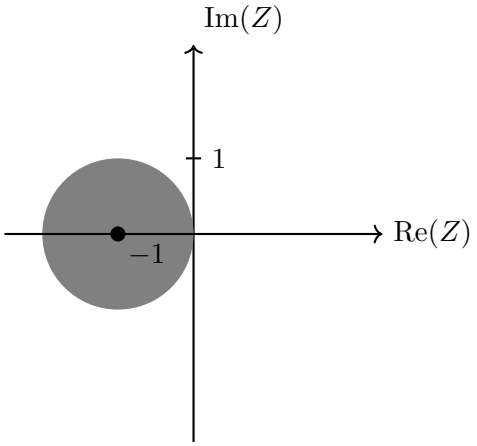

Figure 2.1.5: A plot illustrating the stability region of the Euler time step scheme.

for absolute stability, otherwise the system is unstable. We define the *stability region* as a region in the complex Z plane for which the system is stable, since Λ can be complex. In this case, the stability region is determined by Equation 2.1.14. Or visually, Z must lie inside the unit disk $|Z + 1| = 1$, which is illustrated by Figure 2.1.5.

Now, to determine the values for which the Euler method is stable when applied to the KdV equation, instead of the test equation we use a linearised KdV equation

$$\frac{\partial \eta}{\partial t} = -a\frac{\partial^3 \eta}{\partial x^3}. \tag{2.1.15}$$

The nonlinear term has been dropped since the stability criteria is likely to be most affected by higher-order linear derivatives, which is discussed in more depth in Milewski and Tabak (1999). Determining the stability criteria for nonlinear terms is much more complicated, and is not explored here. In terms of discretised parameters, the linearised KdV equation is written

$$\frac{\eta_j^{n+1} - \eta_j^n}{\Delta t} = -a\frac{\eta_{j+2}^n - 2\eta_{j+1}^n + 2\eta_{j-1}^n - \eta_{j-2}^n}{2(\Delta x)^3}, \tag{2.1.16}$$

which can be rearranged to give

$$\eta_j^{n+1} = \eta_j^n - \frac{a\Delta t}{2(\Delta x)^3}\left(\eta_{j+2}^n - 2\eta_{j+1}^n + 2\eta_{j-1}^n - \eta_{j-2}^n\right).$$

If we compare this to Equation 2.1.13, we see that in this case

$$\Lambda = -\frac{a}{2\eta_j^n(\Delta x)^3}\left(\eta_{j+2}^n - 2\eta_{j+1}^n + 2\eta_{j-1}^n - \eta_{j-2}^n\right),$$

which still has some time dependence contained within η_j^n. Therefore, we cannot use this equation to determine the stability criteria and need to use another approach.

Instead, we use a **Von-Neumann** stability analysis to determine the numerical stability of this scheme. The Von-Neumann method works by splitting the time dependence from the spatial dependence in the solution. First, we assume a solution of the form

$$\eta_j^n = H^n \mathrm{e}^{\mathrm{i}Kx_j} \tag{2.1.17}$$

where K is the wave number, H represents the time dependence of the solution, and the exponential term represents the spatial dependence. In the Von-Neumann method, the amplification factor G is defined as

$$G = \frac{H^{n+1}}{H^n}$$

and states that a scheme is stable if $|G| \leq 1$, in the same way as before. Substituting Equation 2.1.17 into Equation 2.1.16 yields

$$\frac{H^{n+1} - H^n}{\Delta t}\mathrm{e}^{\mathrm{i}Kx_j} = -a\frac{\mathrm{e}^{\mathrm{i}K(x_j+2\Delta x)} - 2\mathrm{e}^{\mathrm{i}K(x_j+\Delta x)} + 2\mathrm{e}^{\mathrm{i}K(x_j-\Delta x)} - \mathrm{e}^{\mathrm{i}K(x_j-2\Delta x)}}{2(\Delta x)^3}H^n.$$

Then, after simplifying we have

$$\begin{aligned} G &= 1 - \frac{\mathcal{W}}{2}\left(\mathrm{e}^{2\mathrm{i}K\Delta x} - \mathrm{e}^{-2\mathrm{i}K\Delta x} - 2\mathrm{e}^{\mathrm{i}K\Delta x} + 2\mathrm{e}^{-\mathrm{i}K\Delta x}\right), \\ &= \left|1 - \mathrm{i}\mathcal{W}\Big(\sin(2K\Delta x) - 2\sin(K\Delta x)\Big)\right| \end{aligned} \tag{2.1.18}$$

where

$$\mathcal{W} = \frac{a\Delta t}{(\Delta x)^3}. \tag{2.1.19}$$

The stability condition is $G \leq 1$, and hence we require a suitable positive real value for

our time step Δt such that

$$\left|1 + \mathrm{i}\mathcal{W}\Big(2\sin(K\Delta x) - \sin(2K\Delta x)\Big)\right| \leq 1 \tag{2.1.20}$$

for the system to be stable. Since $\mathcal{W}$ is real, either $\Delta t = 0$ so $\mathcal{W} = 0$, or the inequality (2.1.20) is an impossible condition. Therefore, the system is **unconditionally unstable** for any chosen positive real value of the time step Δt, and we can assume that this applies to the full nonlinear system as well as the linearised equation.

For further clarification, if we compare Equation 2.1.14 with Equation 2.1.20, we see that for the linearised KdV equation, Z is purely imaginary and therefore will not lie within the unit disk illustrated by Figure 2.1.5.

A brief note on upwinding

The Euler method can be made stable when applied to the linearised KdV equation (2.1.15) by considering another method for dealing with the spatial derivatives. To do this we introduce forward difference or backward difference equations for handling the spatial derivatives, instead of using central difference equations. This method is known as **upwinding**, or sometimes called **downwinding** when using only the backward difference equations.

The $\mathcal{O}\big((\Delta x)^2\big)$ forward difference equation for numerically evaluating the first derivative, in terms of our numerical mesh, is defined by

$$\frac{\partial \eta}{\partial x} = \frac{-3\eta_j^n + 4\eta_{j+1}^n - \eta_{j+2}^n}{2\Delta x},$$

and the $\mathcal{O}\big((\Delta x)^2\big)$ forward difference equation for evaluating the third-order derivative is defined by

$$\frac{\partial^3 \eta}{\partial x^3} = \frac{-5\eta_j^n + 18\eta_{j+1}^n - 24\eta_{j+2}^n + 14\eta_{j+3}^n - 3\eta_{j+4}^n}{2(\Delta x)^3}.$$

The $\mathcal{O}\big((\Delta x)^2\big)$ backward difference equation for numerically evaluating the first deriva-

tive, in terms of our numerical mesh, is defined by

$$\frac{\partial \eta}{\partial x} = \frac{3\eta_j^n - 4\eta_{j-1}^n + \eta_{j-2}^n}{2\Delta x},$$

and the $\mathcal{O}\big((\Delta x)^2\big)$ backward difference equation for evaluating the third-order derivative is defined by

$$\frac{\partial^3 \eta}{\partial x^3} = \frac{5\eta_j^n - 18\eta_{j-1}^n + 24\eta_{j-2}^n - 14\eta_{j-3}^n + 3\eta_{j+4}^n}{2(\Delta x)^3}.$$

As discussed earlier, these equations were used at each of the end points respectively when producing the numerical approximations to each derivative using the central difference equations. This was to avoid errors when attempting to evaluate the undefined end points

$$j \in [-1, -2, -3, 2N+1, 2N+2, 2N+3].$$

Whether the forward or backward difference equation is used for the upwinding method depends on the parity of a as the correct choice depends on the parity of the third derivative. For this analysis we only consider a forward difference equation which corresponds to a positive value of a. We also impose that undefined end points, such as η_{2N+1}, are assumed to be zero, a viable method which was discussed when deciding how to deal with the end points of the central difference equations.

The stability criteria of this scheme can be checked using the Von-Neumann analysis. The resulting amplification factor G looks like

$$G = 1 - \mathcal{W}\left(-5 + 18\mathrm{e}^{\mathrm{i}K\Delta x} - 24\mathrm{e}^{2\mathrm{i}K\Delta x} + 14\mathrm{e}^{3\mathrm{i}K\Delta x} - 3\mathrm{e}^{4\mathrm{i}K\Delta x}\right),$$

and hence the system is stable if

$$\left|1 - \mathcal{W}\left(-5 + 18\mathrm{e}^{\mathrm{i}K\Delta x} - 24\mathrm{e}^{2\mathrm{i}K\Delta x} + 14\mathrm{e}^{3\mathrm{i}K\Delta x} - 3\mathrm{e}^{4\mathrm{i}K\Delta x}\right)\right| \leq 1. \qquad (2.1.21)$$

This condition (2.1.21) is difficult to solve explicitly. Therefore, due to the difficulty in determining stability criteria, and also recognising that the forward difference approx-

imations are perhaps too complicated for evaluating more intricate higher-order terms explored later in the thesis, we instead choose a different method for evaluating any subsequent solutions.

2.1.2 The leapfrog time step

We now consider a different method for advancing in time called the leapfrog method. The key difference between leapfrog method and the Euler method is that leapfrog uses a central difference equation for evaluating the time derivative, instead of a forward difference equation. For this reason the leapfrog time step method is sometimes called the **midpoint method**. When using this method to advance in time, the time derivative is evaluated by

$$\frac{\partial \eta}{\partial t} \approx \frac{\eta(x_j, t_n + \Delta t) - \eta(x_j, t_n - \Delta t)}{2\Delta t} = \frac{\eta_j^{n+1} - \eta_j^{n-1}}{2\Delta t}, \tag{2.1.22}$$

and thus the numerical scheme can be written as

$$\begin{aligned} \frac{\eta_j^{n+1} - \eta_j^{n-1}}{2\Delta t} &= a\frac{\eta_{j+2}^n - 2\eta_{j+1}^n + 2\eta_{j-1}^n - \eta_{j-2}^n}{2(\Delta x)^3} + \eta_j^n \frac{\eta_{j+1}^n - \eta_{j-1}^n}{2\Delta x}, \qquad (2.1.23) \\ \Rightarrow \quad \eta_j^{n+1} &= \eta_j^{n-1} - 2\Delta t \left(a\frac{\eta_{j+2}^n - 2\eta_{j+1}^n + 2\eta_{j-1}^n - \eta_{j-2}^n}{2(\Delta x)^3} + \eta_j^n \frac{\eta_{j+1}^n - \eta_{j-1}^n}{2\Delta x} \right), \end{aligned}$$

where the central difference equations have been used to evaluate the spatial derivatives.

However, when advancing in time we will encounter the undefined term η_j^{-1} in the first time step. For this reason, we use the Euler method for the first iteration, and then use the leapfrog method for each subsequent step. For a large enough mesh size, any instabilities associated with the Euler method will have a negligible effect when only used for the first iteration.

The scheme is now set up, so we proceed to consider the numerical stability associated with this method.

Numerical stability of the leapfrog method

We will determine the stability of leapfrog method using the same approach that we used for the Euler method. In the same way as before, first we will determine the absolute stability of the leapfrog method using the test equation Equation 2.1.12, and substitute Equation 2.1.22 for the derivative in time to give

$$\frac{\eta_j^{n+1} - \eta_j^{n-1}}{2\Delta t} = \Lambda \eta_j^n.$$

Then we substitute $Z = \Lambda \Delta t$ and rearrange to get

$$\frac{\eta_j^{n+1} - \eta_j^{n-1}}{2\eta_j^n} = Z, \tag{2.1.24}$$

and then substitute in the amplification factor $G = \eta^{n+1}/\eta^n$ so that after some simplification we have

$$\frac{G - G^{-1}}{2} = Z.$$

For absolute stability we require that $|G| \leq 1$. Then, to give the boundary of the region of stability, $G = \mathrm{e}^{\mathrm{i}\theta}$ and thus the equation becomes

$$\frac{\mathrm{e}^{\mathrm{i}\theta} - \mathrm{e}^{-\mathrm{i}\theta}}{2} = \mathrm{i}\sin\theta = Z. \tag{2.1.25}$$

Hence the stability region is such that Z is purely imaginary and lies between -1 and 1 on the imaginary axis. In other words $|\mathrm{Im}(Z)| \leq 1$, and $\mathrm{Re}(Z) = 0$. This is illustrated by Figure 2.1.6. Therefore the leapfrog method will only be stable with the linearised KdV equation (2.1.15) if we choose parameters so that $Z \in [-\mathrm{i}, \mathrm{i}]$.

We now consider the exact values for which the leapfrog scheme is stable when applied to the linearised KdV equation. To do this we use the Von-Neumann stability analysis

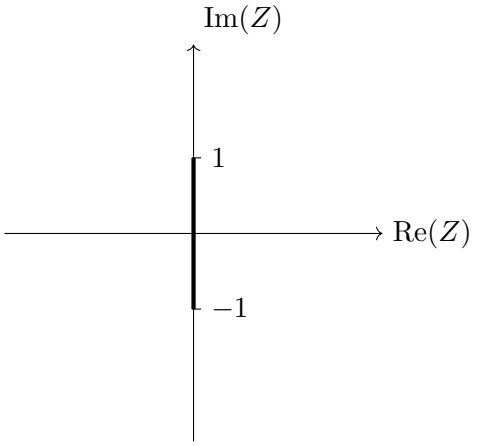

Figure 2.1.6: A plot illustrating the stability region for leapfrog time step schemes.

and substitute a solution of the form Equation 2.1.17 into Equation 2.1.23, which gives

$$\begin{aligned}\frac{H^{n+1}-H^{n-1}}{2\Delta t}\mathrm{e}^{\mathrm{i}Kx_j} &= -aH^n\frac{\mathrm{e}^{\mathrm{i}K(x_j+2\Delta x)}-2\mathrm{e}^{\mathrm{i}K(x_j+\Delta x)}+2\mathrm{e}^{\mathrm{i}K(x_j-\Delta x)}-\mathrm{e}^{\mathrm{i}K(x_j-2\Delta x)}}{2(\Delta x)^3},\\ \Rightarrow\quad \frac{H^{n+1}-H^{n-1}}{2H^n} &= -\frac{a\Delta t}{2(\Delta x)^3}\left(\mathrm{e}^{2\mathrm{i}K\Delta x}-2\mathrm{e}^{\mathrm{i}K\Delta x}+2\mathrm{e}^{-\mathrm{i}K\Delta x}-\mathrm{e}^{-2\mathrm{i}K\Delta x}\right)\end{aligned} \tag{2.1.26}$$

where the nonlinear term has been omitted. Then using Equation 2.1.18 we know that the right-hand side can be rewritten as

$$\frac{\mathrm{i}a\Delta t}{(\Delta x)^3}\big(\sin(2K\Delta x)-2\sin(K\Delta x)\big).$$

Now, we let $\theta = K\Delta x$ and define a function $f(\theta)$ such that

$$f(\theta) = \sin(2\theta) - 2\sin\theta.$$

We look for bounds on $f(\theta)$, and note that $f(\theta)$ is stationary when $\theta = \theta_{\mathrm{m}}$. To determine the stationary points we consider the derivative

$$\frac{\mathrm{d}f}{\mathrm{d}\theta} = 2\cos(2\theta) - 2\cos\theta,$$

then, using standard trigonometric identities we have

$$\begin{aligned}\frac{\mathrm{d}f}{\mathrm{d}\theta} &= 2(2\cos^2\theta - \cos\theta - 1),\\ &= 2(2\cos\theta + 1)(\cos\theta - 1).\end{aligned}$$

Stationary points occur when $\frac{\mathrm{d}f}{\mathrm{d}\theta} = 0$, or in other words

$$\cos\theta = 1,\ -\frac{1}{2}$$

which means that

$$\sin\theta = 0,\ \pm\frac{\sqrt{3}}{2}$$

in $f(\theta)$. Then, using the identity $\sin(2\theta) = 2\sin\theta\cos\theta$, we have

$$f(\theta) = 2\sin\theta(\cos\theta - 1),$$

and therefore, using the bounds on $f(\theta)$ we have

$$\begin{aligned}|f(\theta)| &\leq 2\frac{\sqrt{3}}{2}\left|-\frac{1}{2} - 1\right|,\\ &\leq \frac{3\sqrt{3}}{2}.\end{aligned}$$

Now, if we compare Equation 2.1.26 with the test equation (2.1.24) we see here that

$$\Lambda = \frac{\mathrm{i}a}{(\Delta x)^3}\Big(\sin(2h\Delta x) - 2\sin(h\Delta x)\Big),$$

and hence $Z = \Lambda\Delta t$ must lie on the imaginary axis such that

$$Z \leq \pm\frac{3\sqrt{3}}{2}\mathrm{i}\left(\frac{a\Delta t}{(\Delta x)^3}\right). \tag{2.1.27}$$

From Equation 2.1.25 we know that for absolute stability using the leapfrog method we require that

$$|\mathrm{Im}(Z)| \leq 1,$$

and therefore for the linearised KdV numerical scheme to remain stable with the leapfrog

method, we require

$$\frac{3\sqrt{3}}{2}\left(\frac{a\Delta t}{(\Delta x)^3}\right) \leq 1,$$

or in other words

$$\mathcal{W} = \frac{a\Delta t}{(\Delta x)^3} \leq \frac{2}{3\sqrt{3}}. \tag{2.1.28}$$

which is approximately 0.3849.

Now that we have determined the stability region, it is possible to choose suitable values for the time step Δt, with a given spatial step Δx, to produce numerical solutions to the KdV equation using leapfrog method, without incurring numerical instabilities.

2.1.3 The Runge-Kutta time step

The third and final method that we will examine for advancing in time is called the Runge-Kutta method. The Runge-Kutta method approximates the time derivative using multiple steps. In this analysis we will consider a fourth-order Runge-Kutta method.

First we introduce a function $F(\eta_j^n, t_n)$, where F is simply defined to be the right-hand side of Equation 2.1.1, with the spatial derivatives $\frac{\partial \eta}{\partial x}$ and $\frac{\partial^3 \eta}{\partial x^3}$ evaluated in terms of the central difference equations Equation 2.1.3 and Equation 2.1.5, respectively. Next we introduce four operators, g_1, g_2, g_3, and g_4 which are defined as follows:

$$\begin{aligned}
g_1 &= F(\eta_j^n, t_n), \\
g_2 &= F(\eta_j^n + g_1 \tfrac{\Delta t}{2}, t_n + \tfrac{\Delta t}{2}), \\
g_3 &= F(\eta_j^n + g_2 \tfrac{\Delta t}{2}, t_n + \tfrac{\Delta t}{2}), \\
g_4 &= F(\eta_j^n + g_3 \Delta t, t_n + \Delta t).
\end{aligned}$$

The time step $\eta(x, t_n + \Delta t) = \eta_j^{n+1}$ is then defined to be

$$\eta_j^{n+1} = \eta_j^n + \frac{\Delta t}{6}\Big(g_1 + 2g_2 + 2g_3 + g_4\Big), \tag{2.1.29}$$

and the system is set up.

Numerical stability of Runge-Kutta method

Next we consider the stability of the Runge-Kutta method using the same approach we used for both the Euler method and for the leapfrog method. First, we consider the linear test equation (2.1.12) with the Runge-Kutta method (2.1.29) applied to the time derivative and attempt to find bounds on $Z = \Lambda\Delta t$ in order to determine the absolute stability. We introduce the amplification factor $G = \eta^{n+1}/\eta^n$ and hence we have

$$\begin{aligned} G &= 1 + \frac{1}{6}\left(Z + 2\left(Z + \frac{Z^2}{2}\right) + 2\left(Z + \frac{Z^2 + \frac{Z^3}{2}}{2}\right) + \left(Z + Z^2 + \frac{Z^3 + \frac{Z^4}{2}}{2}\right)\right), \\ &= 1 + \frac{1}{6}\left(Z + 2Z + Z^2 + 2Z + Z^2 + \frac{Z^3}{2} + Z + Z^2 + \frac{Z^3}{2} + \frac{Z^4}{4}\right), \\ &= 1 + \frac{1}{6}\left(6Z + 3Z^2 + Z^3 + \frac{Z^4}{4}\right) \end{aligned}$$

Thus, the amplification factor G is given to be

$$G = 1 + Z + \frac{Z^2}{2} + \frac{Z^3}{6} + \frac{Z^4}{24}, \tag{2.1.30}$$

and for absolute stability we require that $|G| \leq 1$. The stability region for the Runge-

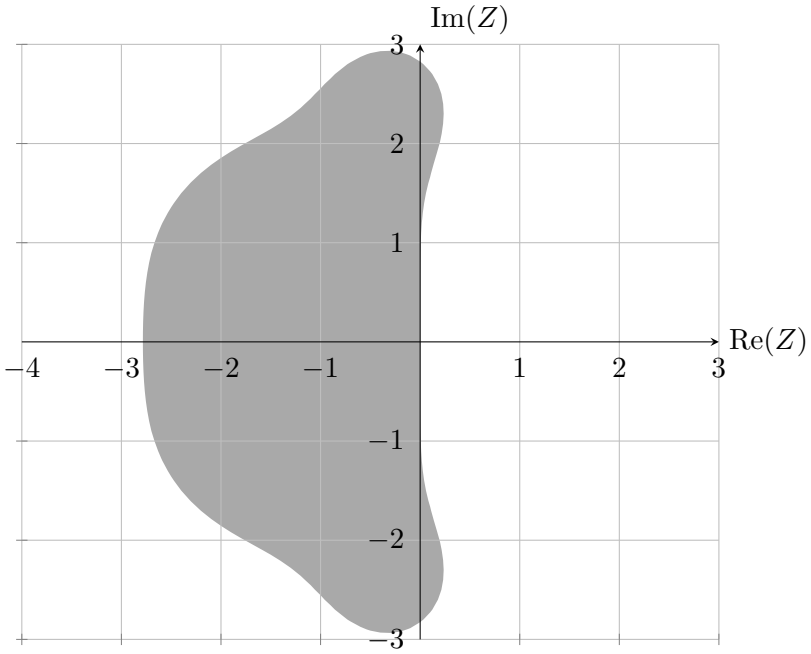

Figure 2.1.7: A plot illustrating the stability region of the fourth-order Runge-Kutta scheme.

Kutta method is illustrated by Figure 2.1.7. We can find the bounds on Z by solving Equation 2.1.30. To do this we consider $\mathrm{Re}(Z)$ and $\mathrm{Im}(Z)$ separately. For the case $\mathrm{Im}(Z) = 0$, we have

$$\frac{2^{2/3}}{3}\left(9\sqrt{29} - 43\right)^{1/3} - \frac{10}{3}\left(\frac{2}{9\sqrt{29} - 43}\right)^{1/3} - \frac{4}{3} \leq \mathrm{Re}(Z) \leq 0$$

and for $\mathrm{Re}(Z) = 0$ we have

$$|\mathrm{Im}(Z)| < 2\sqrt{2}. \tag{2.1.31}$$

Now, similar the leapfrog analysis, we consider the explicit values for which the numerical scheme with the Runge-Kutta method remains stable when applied to the linearised KdV equation (2.1.15). From Equation 2.1.27 we know that Z is purely imaginary and is bounded such that

$$\mathrm{Im}(Z) \leq \frac{3\sqrt{3}}{2}\left(\frac{a\Delta t}{(\Delta x)^3}\right),$$

which is a result of using the central difference equation (2.1.5) to evaluate the third-order derivative. We compare this with the fourth-order Runge-Kutta absolute stability region $|\mathrm{Im}(Z)| < 2\sqrt{2}$, which means that for numerical stability we require

$$\frac{3\sqrt{3}}{2}\left(\frac{a\Delta t}{(\Delta x)^3}\right) < 2\sqrt{2}.$$

In other words, in order to produce a numerically stable solution we should select a suitable value for the size of the time step Δt, for a given Δx, so that

$$\mathcal{W} = \frac{a\Delta t}{(\Delta x)^3} \leq \frac{4\sqrt{2}}{3\sqrt{3}}. \tag{2.1.32}$$

This inequality tells us that the largest value $\mathcal{W}$ can take so that the scheme is stable, sometimes called the critical value which we will denote as $\mathcal{W}_{\mathrm{c}}$, is given by

$$\mathcal{W}_{\mathrm{c}} = \frac{4\sqrt{2}}{3\sqrt{3}} \approx 1.0887.$$

This critical value is approximately three times larger than the critical value obtained for the leapfrog method, which was derived using Equation 2.1.28. It follows that the Runge-Kutta scheme is stable for larger time steps, or equivalently, smaller values of Δx.

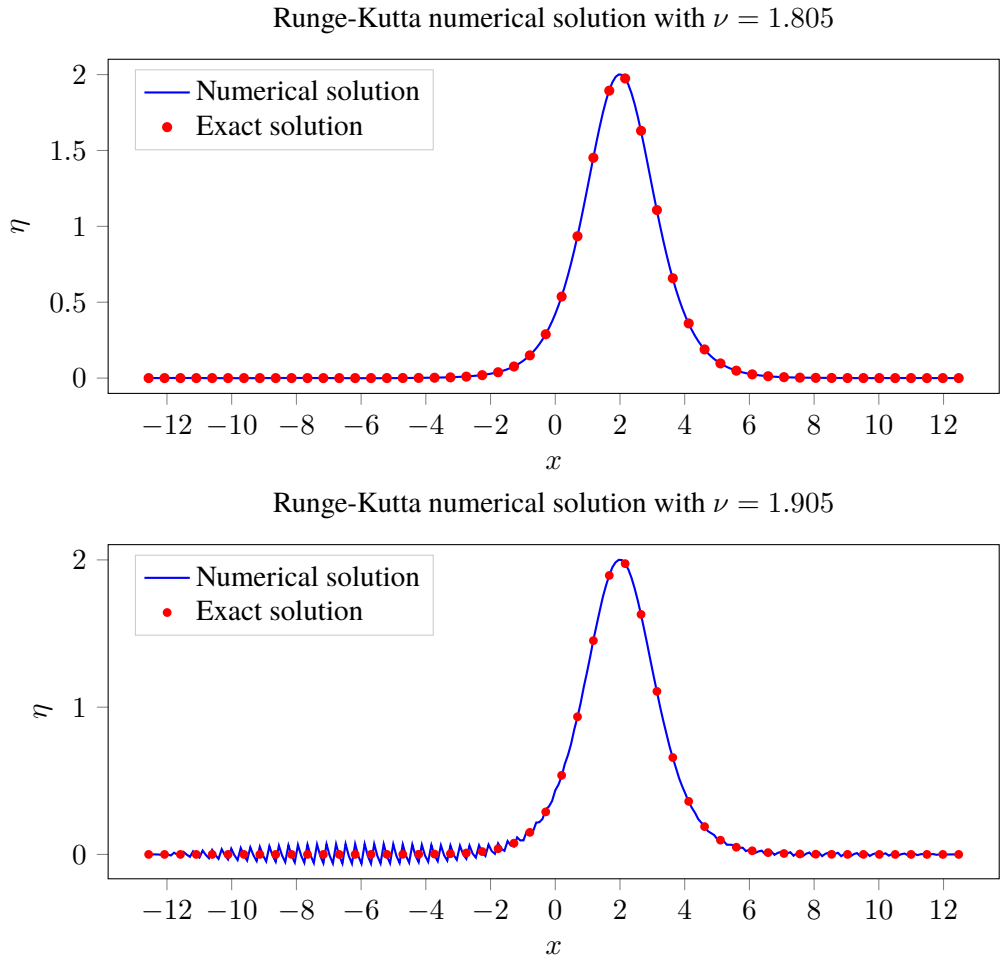

Figure 2.1.8: A plot to demonstrate the critical values of stability parameter $\mathcal{W}$, illustrating a numerical solution with parameter values $A = 2$, $N = 128$, $x \in [-4\pi, 4\pi]$, and $t_{\max} = 2$, comparing $\mathcal{W} = 1.085$ (top) and $\mathcal{W} = 1.095$ (bottom).

We can demonstrate the criticality of $\mathcal{W}$ by choosing two values for the step size Δt, for a given set of parameters so that the respective value of $\mathcal{W}$ is either side of its critical value, say $\mathcal{W} = 1.095$ and $\mathcal{W} = 1.085$ for example. The solutions produced from selecting these values are illustrated by Figure 2.1.8. We can immediately see from the figure that when we exceed the critical value $\mathcal{W}_c$ then the numerical result becomes unstable. This is demonstrated by oscillatory behaviour either side of the main wave crest indicating that the errors in the approximation are growing, causing the result to diverge away from the exact solution.

The stability criteria has been determined for both the leapfrog and Runge-Kutta schemes. We are now able to choose suitable values for our parameters so that the numerical algorithms will produce useful results. Looking forward, we will aim to make meaningful

		Completion time (s)	
Δt	$\mathcal{W}$	Leapfrog	Runge-Kutta
9.1×10^{-6}	0.384	59.14	182.37
2.6×10^{-5}	1.088	Unstable	63.78

Table 2.1.1: A table comparing the completion time when using the leapfrog and fourth-order Runge-Kutta methods to advance the numerical solution to the KdV equation in time, for each respective critical value of $\mathcal{W}$, using the coefficient values: amplitude $A = 2$, maximum time $t_{\text{max}} = 2$, spatial domain $x \in [-4\pi, 4\pi]$, and number of steps $N = 128$.

comparisons between the two methods.

2.1.4 Comparisons between the leapfrog and Runge-Kutta method

We have determined conditions for which both the leapfrog and Runge-Kutta time step method remain numerically stable. We will now use these conditions to produce numerical solutions to the KdV equation and draw comparisons between the two methods. Since the Euler method was shown to be unconditionally unstable, we will not include this in our comparisons.

First we code up each scheme using Python, choosing values for x_{m}, Δx, and t_{max} and then use the respective stability analyses to choose a suitable value for Δt so that the output converges to a numerically stable solution. For the first comparison we will look at the time efficiency of each method. For this comparison to be meaningful, we choose a value of Δt for each method using a given set of parameters so that the respective value of $\mathcal{W}$ is close to the critical value associated with each scheme. This recognises that the Runge-Kutta method is likely to be less time-efficient when using the same value of Δt due to increased complexity of the algorithm for advancing in time, but also accounts for the fact that it remains stable for larger values of Δt.

Table 2.1.1 shows a comparison between the completion times of the leapfrog and Runge-Kutta methods. We have used each method to advance the numerical solution to the KdV equation in time with a different value of Δt corresponding to the critical value of $\mathcal{W}$ for each scheme. It can be seen in the table that the leapfrog method completes much faster

than the Runge-Kutta method, although this is expected since the Runge-Kutta method uses four evaluations to advance each time step, whereas the leapfrog method uses only one, as discussed earlier. However, it is key to note that using Runge-Kutta method allows the use of a much larger time step. The completion times are similar for both methods when using their respective critical stability values.

We note here that the exact values of the times taken for the schemes to complete are entirely hardware dependent and will certainly differ when using different machines. However, the purpose of this examination is merely to demonstrate the difference between the two methods so that a relative comparison can be made. The ability to choose a larger time step is preferable due to the increased complexity of the equations examined later in the thesis. For this reason we favour the use of the Runge-Kutta scheme rather than the leapfrog scheme for which we would have to use a much smaller time step.

Next we consider the **numerical accuracy** of each scheme. It has been shown already that with a sufficiently high number of mesh points, the central difference equations give a very good approximation to the analytical solutions of the spatial derivatives. The **Order of Accuracy**, as defined by LeVeque (2006), "quantifies the rate of convergence of a numerical approximation of a differential equation to the exact solution. A numerical solution to a differential equation is said to be n^{th}-order accurate if the error, $\mathcal{E}$, is proportional to the step-size h to the n^{th} power."

In our numerical schemes, this translates to

$$\mathcal{E} \propto (\Delta t)^n. \tag{2.1.33}$$

To provide a comparison for the order of accuracy for each scheme, we consider the maximum error of each scheme, defined to be

$$\mathcal{E}_{\max} = \max[|\eta - \eta_{\text{ex}}|], \tag{2.1.34}$$

over an interval $x \in [-L, L]$ for time $t = t_{\max}$, where η_{ex} denotes the exact solution.

Table 2.1.2 gives a comparison between the maximum error values calculated when

		Maximum error $\mathcal{E}_{\max}$	
Δt	N	Leapfrog	Runge-Kutta
1×10^{-4}	64	0.0101	0.0100
1×10^{-6}	64	0.01	0.01
1×10^{-4}	256	0.00069	0.00062
1×10^{-6}	256	0.000621	0.000620

Table 2.1.2: A comparison between the maximum error values $\mathcal{E}_{\max}$, for different values of Δt and N, calculated for each time step scheme using the parameter values: amplitude $A = 2$, spatial domain $x \in [-4\pi, 4\pi]$, at time $t = t_{\max} = 5$.

using the leapfrog and Runge-Kutta time step methods to evaluate the numerical problem presented in Equation 2.1.10 (with $a = 1$) compared with the exact solution η_{ex} given in Equation 1.3.9. Each solution was computed using a fixed parameter $A = 2$ over an interval $x \in [-4\pi, 4\pi]$, at time $t = 5$, for various different values of Δt and N.

In each instance we observe that both schemes return a similar value for the maximum error, which decreases as the number of spatial points N is increased. Reducing the size of the time step Δt yields a negligible improvement to the maximum error.

It would appear from the table that the Runge-Kutta method is consistently more accurate than the leapfrog method, although almost negligibly so. Visually, in Figure 2.1.9 it is seen that both approximations map extremely closely to the exact solution.

2.2 The pseudospectral method

In this section, the pseudospectral method is used as an alternative to the finite difference method for evaluating the spatial derivatives. Assuming we have a periodic function $f(x)$ with period L (and L is large when we model solitary waves), we can expand this as a Fourier series

$$f(x) = \sum_{k=-\infty}^{\infty} \widehat{f}(k) \exp\left(\frac{2\mathrm{i}\pi}{L} kx\right) \tag{2.2.1}$$

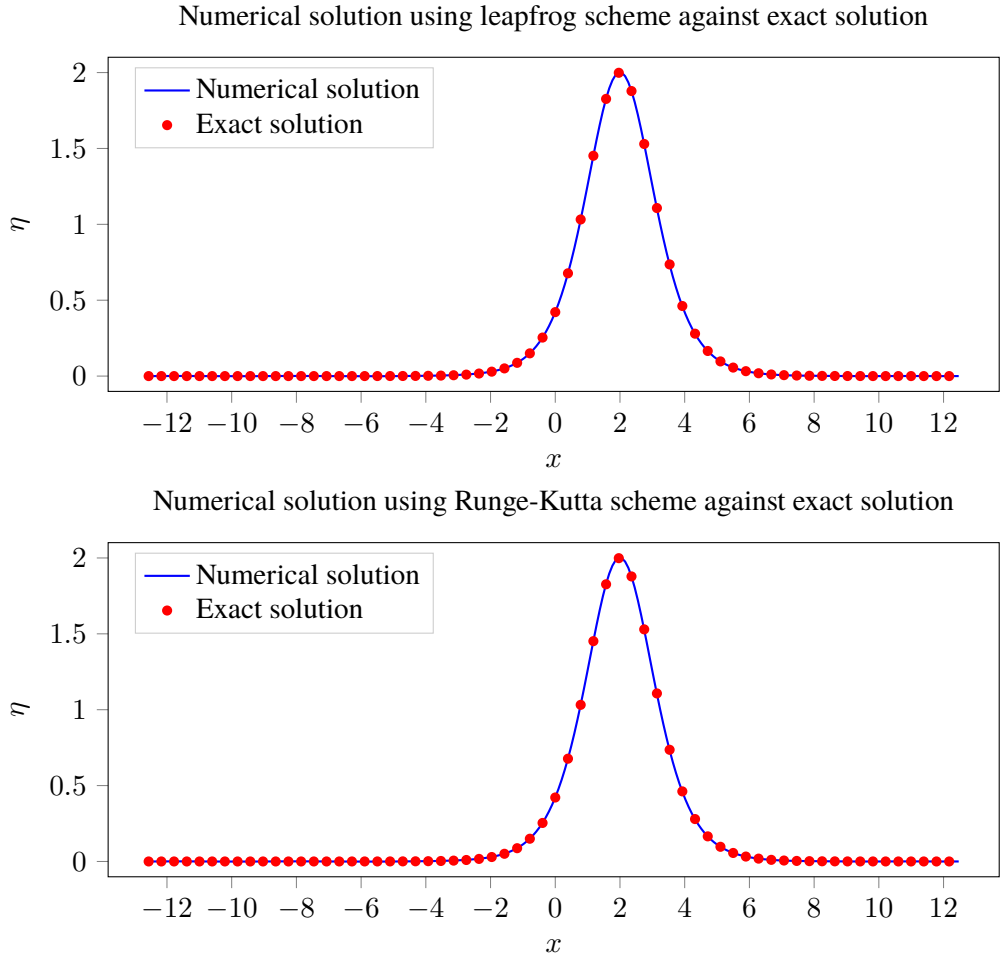

Figure 2.1.9: A comparison between the numerical approximation to the KdV equation using the leapfrog method (top), and fourth-order Runge-Kutta method (bottom), with the exact solution and coefficient values: amplitude $A = 2$, $N = 128$, $x \in [-4\pi, 4\pi]$, and $t_{\max} = 2$.

with Fourier coefficients given by

$$\widehat{f}(k) = \frac{1}{L} \sum_{k=-\infty}^{\infty} f(x) \exp\left(-\frac{2\mathrm{i}\pi}{L} kx\right), \tag{2.2.2}$$

where k is a spectral variable. We also note here that the notation varies for different conventions, and that the sign in the exponential powers can be swapped. One of the main benefits of using this method is that evaluating spatial derivatives is extremely simple. The derivative is given by

$$\frac{\mathrm{d}f}{\mathrm{d}x} = \frac{2\pi}{L} \sum_{k=-\infty}^{\infty} \mathrm{i}k\widehat{f}(k) \exp\left(\frac{2\mathrm{i}\pi}{L} kx\right).$$

In order to use spectral methods for mathematical programming, we use an approximation to the series given in Equation 2.2.2, called the discrete Fourier transform (DFT), which typically has the form

$$\widehat{f}_k = \frac{1}{N}\sum_{k=0}^{N-1} f_j \exp\left(-\frac{2\mathrm{i}\pi}{N} jk\right), \tag{2.2.3}$$

where we have replaced $f(x)$ by N discrete samples, or steps, so that

$$f(x) \approx f\left(\frac{LN}{j}\right) = f_j, \qquad \text{for} \quad j = 0 \ldots N-1.$$

This is known as the DFT of the periodic function $f(x)$. To get back to f, we introduce the inverse discrete Fourier transform (IDFT), which is an approximation to the series given in Equation 2.2.1, which has the form

$$f_j = \sum_{k=0}^{N-1} \widehat{f}_k \exp\left(\frac{2\mathrm{i}\pi}{N} jk\right). \tag{2.2.4}$$

In Python, the discrete Fourier transform can be computed using the fast Fourier transform (FFT) function, and likewise, the inverse transform can be applied using the inverse fast Fourier transform function (IFFT). A much more extensive derivation and discussion of the discrete Fourier transforms used above is presented in Johnson (2011).

For our numerical approximation we transform the surface elevation function $\eta(x,t)$ using a discrete Fourier transform. We impose that $\eta(x,t)$ is periodic on the interval $[-2\pi, 2\pi]$, over N discrete points $x_j = -x_\mathrm{m} + j\Delta x$. The DFT is then given by

$$\widehat{\eta}(k) = \mathcal{F}\left[\eta(x,t)\right] = \frac{1}{N}\sum_{j=0}^{N-1} \eta(x,t)\mathrm{e}^{-\mathrm{i}kx_j}. \tag{2.2.5}$$

The function can $\eta(x,t)$ can be recovered using the inverse transform, defined by

$$\eta(x,t) = \mathcal{F}^{-1}[\widehat{\eta}(k)] = \sum_{j=0}^{N-1} \widehat{\eta}(k)\mathrm{e}^{\mathrm{i}kx_j}. \tag{2.2.6}$$

As discussed, applying the DFT provides a relatively simple way of evaluating the spatial derivatives $\frac{\partial \eta}{\partial x}$ and $\frac{\partial^3 \eta}{\partial x^3}$. Each derivative can be resolved in Fourier space and then

returned to physical space. We have

$$\begin{aligned}\frac{\partial \eta}{\partial x} &= \sum_{j=0}^{N-1} \widehat{\eta} \frac{\mathrm{d}}{\mathrm{d}x}(\mathrm{e}^{\mathrm{i}kx_j}) = \sum_{j=0}^{N-1} (\mathrm{i}k)\widehat{\eta}\mathrm{e}^{\mathrm{i}kx_j}, \\ &= \mathcal{F}^{-1}[(\mathrm{i}k)\widehat{\eta}]\,,\end{aligned}$$

and therefore, using the same logic, the third derivative can be expressed by

$$\frac{\partial^3 \eta}{\partial x^3} = \mathcal{F}^{-1}\left[(\mathrm{i}k)^3\widehat{\eta}\right].$$

The transformed KdV equation can then be represented as

$$\frac{\partial \widehat{\eta}}{\partial t} = -3\mathrm{i}k\widehat{(\eta^2)} - a(\mathrm{i}k)^3\widehat{\eta}$$

noting here that the transformed nonlinear term is represented by the discrete Fourier transform of η^2, using the identity

$$6\eta\frac{\partial \eta}{\partial x} = 3\frac{\partial}{\partial x}\left(\eta^2\right).$$

Similar to the finite difference method, a variety of different time stepping methods can be used to advance forward in time while using the pseudospectral method. We may also advance in either Fourier space or physical space.

The Euler, leapfrog and fourth-order Runge-Kutta methods will be considered again. The key difference between the pseudospectral and finite difference methods is the way in which the spatial derivatives are evaluated. Therefore, we can reuse the time step schemes derived for the finite difference method, and write the KdV equation in the form

$$\frac{\partial \eta}{\partial t} = f(x,t)$$

where the function $f(x,t)$ represents the right-hand side at any given time step n, given by

$$f(x,t) = -3\mathcal{F}^{-1}\left[\mathrm{i}k\widehat{(\eta^2)}\right] - a\mathcal{F}^{-1}\left[(\mathrm{i}k)^3\widehat{\eta}\right]. \tag{2.2.7}$$

Each time step scheme can then be written as follows:

Euler time step

$$\eta^{n+1} = \eta^n + \Delta t f(x,t), \tag{2.2.8}$$

Leapfrog time step

$$\eta^{n+1} = \eta^{n-1} + 2\Delta t f(x,t), \tag{2.2.9}$$

Runge-Kutta time step

$$\eta^{n+1} = \eta^n + \frac{\Delta t}{6}\Big(g_1 + 2g_2 + 2g_3 + g_4\Big), \tag{2.2.10}$$

where

$$\begin{aligned} g_1 &= f(x, t_n), \\ g_2 &= f\big(x + g_1\tfrac{\Delta t}{2}, t_n + \tfrac{\Delta t}{2}\big), \\ g_3 &= f\big(x + g_2\tfrac{\Delta t}{2}, t_n + \tfrac{\Delta t}{2}\big), \\ g_4 &= f\big(x + g_3\Delta t, t_n + \Delta t\big). \end{aligned}$$

We will use Python to numerically solve the KdV equation using each of these step schemes to advance in time. In order to evaluate the DFT of each derivative, we use the Python fast Fourier transform (FFT) algorithm (and IFFT algorithm for the inverse transform), provided by the `NumPy` package. However, in the same manner as the finite difference schemes, we will first conduct a stability analysis to generate stability criteria for each method.

2.2.1 Stability analysis of the pseudospectral method

In the earlier finite difference analysis, presented in Section 2.1, we determined the conditions needed for absolute stability associated with each time step scheme. These are immediately transferable to the pseudospectral method.

In order to determine the stability criteria for each numerical scheme, using the pseudospectral method to approximate the spatial derivatives, we begin with the linearised

KdV equation (2.1.15) and assume a solution of the form

$$\eta = \mathrm{e}^{\mathrm{i}kx} \ .$$

We then use the pseudospectral method discussed in Section 2.2 to evaluate the third-order derivative term to give

$$f(k) = -a(\mathrm{i}k)^3\eta, \tag{2.2.11}$$

so that $f(k)$ denotes the right-hand side of the linearised KdV equation (2.1.15). If the spatial domain is assumed to be periodic on the interval $x \in [-x_\mathrm{m}, x_\mathrm{m}]$, then η can be written as a discrete Fourier series given by

$$\eta = \sum_{n=0}^{N-1} A_n \exp(\mathrm{i}\pi k_n x) \, . \tag{2.2.12}$$

where

$$k_n = \frac{\pi n}{x_\mathrm{m}}, \qquad \text{using equation (2.2.4).}$$

Looking back to the linear test equation (2.1.12), for absolute stability we require that $Z = \Lambda\Delta t$ must lie inside a stable region such that $|k| \leq k_\mathrm{m}$ for each k_n. Using Equation 2.2.11, Λ is given here by

$$\Lambda = \frac{f(k)}{\eta},$$

and thus we have $\Lambda = a(\mathrm{i}k)^3$. Then using the fact that

$$k_m = \frac{\pi(N-1)}{x_\mathrm{m}} = \frac{\pi}{\Delta x}$$

we have

$$\Lambda_\mathrm{m} = a(ik_\mathrm{m})^3 = -\mathrm{i}a\left(\frac{\pi}{\Delta x}\right)^3 .$$

Then the stability condition is such that the section of the imaginary axis $[-\mathrm{i}Z_\mathrm{m}, \mathrm{i}Z_\mathrm{m}]$ lies within the stable region of the chosen step scheme, where

$$Z_\mathrm{m} = \Lambda_\mathrm{m}\Delta t = -\mathrm{i}a\Delta t\left(\frac{\pi}{\Delta x}\right)^3 . \tag{2.2.13}$$

From the finite difference stability analysis we know that this implies that the Euler method is unconditionally unstable as its eigen-solutions will never lie on the imaginary axis, and from the absolute stability examination we know that, for the Euler method, Z must lie in the unit disc $|1 + Z| \leq 1$. We proceed to examine stability conditions for the leapfrog and Runge-Kutta time step methods.

From Equation 2.1.25, we know that for the leapfrog method the absolute stability condition is $|\mathrm{Im}(Z)| \leq 1$, which means that

$$a\Delta t\Big(\frac{\pi}{\Delta x}\Big)^3 \leq 1$$

and therefore the stability region for the leapfrog method when used with the pseudospectral method is given by

$$a\frac{\Delta t}{(\Delta x)^3} \leq \frac{1}{\pi^3},$$

which is approximately 0.0322. Similarly, from Equation 2.1.31 we know that the absolute stability condition of the Runge-Kutta method is $|\mathrm{Im}(Z)| < 2\sqrt{2}$. Hence, when using the pseudospectral method with the Runge-Kutta method to advance in time, the critical stability condition is given by

$$a\frac{\Delta t}{(\Delta x)^3} \leq \frac{2\sqrt{2}}{\pi^3},$$

which is approximately 0.0912. Similar to the finite difference analysis, this value is approximately three times larger than the critical value for the leapfrog method allowing the use of a larger time-step.

2.2.2 Comparisons with the finite difference method

Comparing the two methods directly we see from Table 2.2.1 that the critical stability values $\mathcal{W}_c$ for the pseudospectral method are considerably smaller than those derived earlier for the finite difference method. Thus, while the pseudospectral method is an extremely accurate and simple way of evaluating derivatives, the finite difference method allows for larger time steps and smaller domains for which the system could remain stable.

	Finite difference	Pseudospectral
Leapfrog	0.3849	0.0323
Runge-Kutta	1.0887	0.0912

Table 2.2.1: A table comparing the critical stability values $\mathcal{W}_c$ for the leapfrog and pseudospectral methods when using finite difference or pseudospectral schemes.

The main advantages however to using the pseudospectral method over the finite difference method are accuracy and time efficiency. Whilst the finite difference method is accurate, it becomes less time efficient at higher orders. The pseudospectral method is much more efficient in higher-order systems and is therefore the obvious choice when evaluating more complicated systems of equations. It also offers a higher order of accuracy.

Later in the thesis we consider systems of partial differential equations containing additional higher-order derivatives and transform terms which model the relative effects of surface stresses and gradual damping. Due to the complexity of these equations, we choose to use the pseudospectral method for handling the numerical evaluation of these equations in subsequent chapters.

2.3 The integrating factor method

In the previous sections of this chapter, we have identified that the presence of the linear third-order spatial derivative in the KdV equation results in very limited stability for each of the time step methods that we have considered. For this reason we refer to this term as being *numerically stiff*. This gives us motivation to seek a new method which removes the stiffness associated with the linear term, thus allowing for a more robust and efficient numerical scheme.

One such method is defined by Milewski and Tabak (1999) (and also discussed in Trefethen (2000)), where an **integrating factor** is introduced. The main idea behind this method is to introduce a specially chosen function to be used as an integrating factor, and then introduce a new variable in terms of this integrating factor. These are defined in such

a way so that, when substituted into the transformed KdV equation, the third-order linear derivative term is substituted out, thus removing any associated numerical stiffness. The numerical scheme then advances the substituted variable in time before returning to the original variable.

This method is also applicable to other PDEs where, by modifying the integrating factor, we are able to substitute out other linear derivatives from the given equation. This is discussed in more depth later in Chapter 3 when we begin to consider numerical solutions to the KdV equation with additional terms.

In order to utilise this method, we start by taking the Fourier transform of the KdV equation to give

$$\frac{\partial \widehat{\eta}}{\partial t} + 3\mathrm{i}k\widehat{(\eta^2)} = -a(\mathrm{i}k)^3\widehat{\eta}, \tag{2.3.1}$$

where the Fourier transform of η is given by

$$\widehat{\eta}(k,t) = \mathscr{F}[\eta(x,t)] = \int_{-\infty}^{\infty} \eta(x,t)\mathrm{e}^{-\mathrm{i}kx}\mathrm{d}x,$$

and

$$\widehat{(\eta^2)} = \mathscr{F}[\eta^2].$$

We define the integrating factor denoted by $\widehat{E}$ to be

$$\widehat{E} = \mathrm{e}^{a(\mathrm{i}k)^3 t},$$

where the power of the exponential term is chosen to match the right-hand side of the transformed KdV equation (2.3.1). We then multiply Equation 2.3.1 by $\widehat{E}$ to give

$$\widehat{E}\frac{\partial \widehat{\eta}}{\partial t} + 3\mathrm{i}k\widehat{E}\widehat{(\eta^2)} = -a(\mathrm{i}k)^3\widehat{E}\widehat{\eta} \tag{2.3.2}$$

and introduce a new variable $\widehat{v}$ such that

$$\widehat{v} = \widehat{E}\widehat{\eta}.$$

Then we substitute $\widehat{v}$ into equation Equation 2.3.2 which yields

$$\frac{\partial \widehat{v}}{\partial t} - a(\mathrm{i}k)^3\widehat{v} + 3\mathrm{i}k\widehat{E}\widehat{(\eta^2)} = -a(\mathrm{i}k)^3\widehat{v} \tag{2.3.3}$$

using the fact that

$$\frac{\partial \widehat{v}}{\partial t} = a(\mathrm{i}k)^3\widehat{E}\widehat{\eta} + \widehat{E}\frac{\partial \widehat{\eta}}{\partial t},$$

and hence

$$\widehat{E}\frac{\partial \widehat{\eta}}{\partial t} = \frac{\partial \widehat{v}}{\partial t} - a(\mathrm{i}k)^3\widehat{v}.$$

Then Equation 2.3.3 simplifies and rearranges to

$$\frac{\partial \widehat{v}}{\partial t} = -3\mathrm{i}k\widehat{E}\widehat{(\eta^2)}. \tag{2.3.4}$$

The linear term has been eliminated and the transformed KdV equation is no longer stiff.

We can then set up a numerical scheme using Equation 2.3.4. The spatial element of the system on the right-hand side can be evaluated using the fast Fourier transform (FFT) function in Python, provided by the `NumPy` package, as discussed in the pseudospectral analysis. We choose to evaluate the time derivative, $\frac{\partial \widehat{v}}{\partial t}$, using the Runge-Kutta time step method. It was also mentioned in the pseudospectral analysis that we may advance in either the spectral domain or in physical space. In this example we choose to advance in spectral space.

We begin by rewriting Equation 2.3.4 so that

$$\frac{\partial \widehat{v}}{\partial t} = F(t, \widehat{v}) = \Lambda\mu(\widehat{\eta})\mathrm{e}^{-f(k)t} \tag{2.3.5}$$

where

$$\mu(\widehat{\eta}) = \mathcal{F}[\mathcal{F}^{-1}[\widehat{\eta}]^2], \qquad \Lambda = -3(\mathrm{i}k), \qquad f(k) = -a(\mathrm{i}k)^3.$$

Now, using Equation 2.1.29 we can construct the Runge-Kutta system as follows,

$$\frac{\partial \widehat{v}}{\partial t} = F(t_n, \widehat{v}^n), \qquad n = 0 \ldots \frac{t_{\max}}{\Delta t}, \tag{2.3.6}$$

so that

$$g_1 = F(t_n, \widehat{v}^n)\,, \tag{2.3.7}$$

$$g_2 = F\left(t_n + \frac{\Delta t}{2}, \widehat{v}^n + \frac{\Delta t}{2} g_1\right), \tag{2.3.8}$$

$$g_3 = F\left(t_n + \frac{\Delta t}{2}, \widehat{v}^n + \frac{\Delta t}{2} g_2\right), \tag{2.3.9}$$

$$g_4 = F\big(t_n + \Delta t, \widehat{v}^n + \Delta t g_3\big), \tag{2.3.10}$$

and

$$\widehat{v}^{n+1} = \widehat{v}^n + \frac{\Delta t}{6}\left(g_1 + 2g_2 + 2g_3 + g_4\right), \tag{2.3.11}$$

where the notation $\widehat{v}^n$ denotes $\widehat{v}$ evaluated at a given grid point n, as opposed to an exponent of $\widehat{v}$.

We now adopt a similar approach to that used in (Trefethen, 2000) and evaluate the above system of equations, Equation 2.3.6 through to Equation 2.3.11, with respect to a transformed integrating factor. The motivation behind this is to avoid having the system diverge for real $f(k)$ (for which the integrating factor would grow exponentially). To implement this, we introduce

$$\bar{E} = \mathrm{e}^{f(k)t_n}, \qquad E_1 = \mathrm{e}^{f(k)\frac{\Delta t}{2}}, \qquad E_2 = (E_1)^2 = \mathrm{e}^{f(k)\Delta t}.$$

Transforming the integrating factor in this way gives $\mathcal{O}(1)$ quantities for E_1 and E_2, preventing exponential growth of the integrating factor and also preventing possible divergence. Applying this transformation we have

$$\widehat{\eta}^n = \widehat{\eta}(t_n) = \bar{E}\widehat{v}_n, \qquad \widehat{\eta}^{n+1} = \bar{E}E_2\widehat{v}^{n+1},$$

where, similar to before, the notation $\widehat{\eta}^n$ denotes the function $\widehat{\eta}$ evaluated at the grid point n, as opposed to an exponent term. Then g_1, g_2, g_3, and g_4 are re-evaluated with consideration to the integrating factor. Thus we have

$$g_1 = \Lambda\bar{E}^{-1}\mu(\widehat{\eta}^n), \qquad \text{where} \quad \mu(\widehat{\eta}^n) = \mathcal{F}[\mathcal{F}^{-1}[\widehat{\eta}^n]^2],$$

and we introduce G_1 such that

$$\begin{aligned} G_1 &= \bar{E}\Delta t\, g_1 \\ &= \Lambda\Delta t\, \mu(\widehat{\eta}^n). \end{aligned} \tag{2.3.12}$$

Then for g_2 we have,

$$g_2 = \Lambda\mu(\widehat{v}_a)\bar{E}^{-1}, \qquad \text{where} \qquad \widehat{v}_a = \widehat{v}^n + \frac{\Delta t}{2} g_1.$$

Applying the transformation we can say

$$\begin{aligned} \widehat{\eta}_a &= \bar{E}E_1\widehat{v}_a, \\ &= \bar{E}E_1\left(\widehat{v}^n + \frac{\Delta t}{2} g_1\right), \\ &= E_1\left(\widehat{\eta}^n + \frac{\Delta t}{2}\bar{E} g_1\right), \\ &= E_1\left(\widehat{\eta}^n + \frac{1}{2} g_1\right) \quad \text{(using 2.3.12)}, \end{aligned}$$

and thus we can introduce G_2 such that

$$\begin{aligned} G_2 &= \Lambda\Delta t\, \mu(\widehat{\eta}_a), \\ &= \Delta t\, \bar{E}E_1 g_2. \end{aligned}$$

We continue in this manner for G_3 and G_4, and after some work the system becomes:

$$G_1 = \Delta t\Lambda\mu(\widehat{\eta}^n) = \bar{E}(\Delta t) g_1, \tag{2.3.13}$$

$$G_2 = \Delta t\Lambda\mu\left(E_1\widehat{\eta}^n + \frac{1}{2}E_1 G_1\right) = \bar{E}E_1(\Delta t) g_2, \tag{2.3.14}$$

$$G_3 = \Delta t\Lambda\mu\left(E_1\widehat{\eta}^n + \frac{1}{2}G_2\right) = \bar{E}E_1(\Delta t) g_3, \tag{2.3.15}$$

$$G_4 = \Delta t\Lambda\mu(E_2\widehat{\eta}^n + E_1 G_3) = \bar{E}E_2(\Delta t) g_4, \tag{2.3.16}$$

and thus

$$\widehat{\eta}^{n+1} = E_2\widehat{\eta}^n + \frac{1}{6}\big(E_2 G_1 + 2E_1(G_2 + G_3) + G_4\big). \tag{2.3.17}$$

The function $\eta(x,t)$ can then be recovered by using the inverse transform:

$$\eta(x,t) = \mathcal{F}^{-1}[\widehat{\eta}].$$

The main benefit of using the integrating factor method is the ability to select a time step which is much larger than either of the methods seen previously. While an explicit stability analysis is not explored here, the exclusion of the linear term results in a decrease in numerical stiffness allowing for a much broader stability region, examples of which are given in Trefethen (2000). The ability to select a larger time step means that the algorithms are much more time efficient, which greatly speeds up completion times when generating numerical solutions.

The integrating factor method is readily extendible to additional terms which will be explored later in the thesis, and doing so is also very easy to implement. In fact, the only change necessary to the algorithm is the definition of the integrating factor E. The integrating factor is defined in such a way as to reflect the right-hand side of the governing equation, and incorporate all linear terms which otherwise would result in numerical stiffness. This also extends to integral transform terms which will be examined later in Chapter 5 as part of a surfactant analysis, and Chapter 6 in an electrohydrodynamic system.

Taking account of the reasoning discussed above, for each subsequent chapter in the thesis we use the integrating factor and pseudospectral methods for handling spatial derivatives, and the fourth-order Runge-Kutta method for advancing in time, for all subsequent numerical schemes. We believe that the extensive numerical analysis in this chapter has identified these methods as being the optimal approach applicable to the systems of equations which will be seen later in the thesis.

To conclude this chapter, we will demonstrate this approach by generating various numerical solutions to the Korteweg-de Vries equation (1.3.1) using the integrating factor method described above.

2.4 Numerical solutions to the KdV equation

Now that we have explored a variety of different schemes and have chosen to use the integrating factor method for the remainder of the thesis, we will now use this method to present some simple numerical solutions to the Korteweg-de Vries equation.

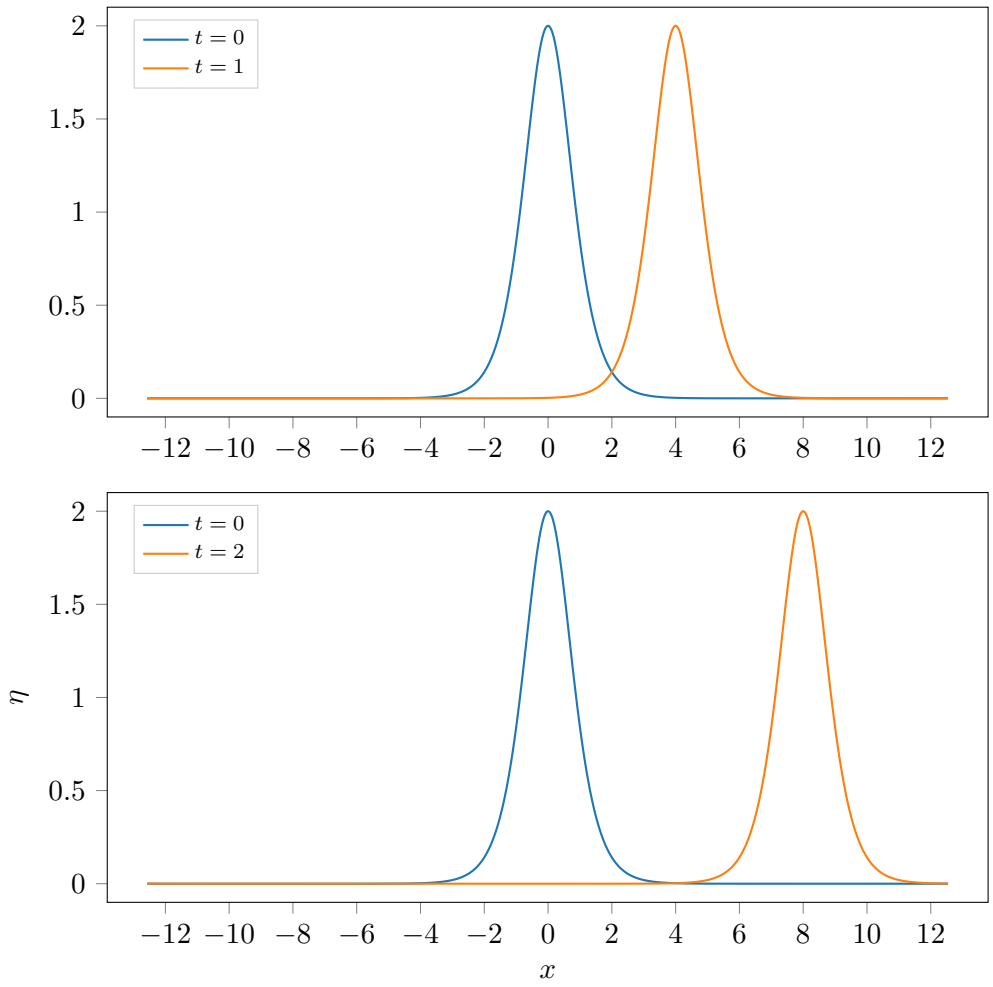

Figure 2.4.1: A plot of the solitary wave solution $\eta(x, 0) = 2\,\mathrm{sech}^2\, x$ for times $t = 0$, 1 and 2, with spatial domain $x \in [-4\pi, 4\pi]$, time step $\Delta t = 0.01$, and number of spatial steps $N = 256$.

If we consider the general form of the KdV equation (1.3.1) and set $a = 1$, then this has a solitary wave solution given by

$$\eta(x,t) = A\,\mathrm{sech}^2\left(\gamma(x - ct)\right), \qquad \gamma = \sqrt{\frac{|A|}{2}}, \tag{2.4.1}$$

using Equation 1.3.9 with $c = 2|A|$. At time $t = 0$ we have

$$\eta(x, 0) = A \operatorname{sech}^2(\gamma x), \tag{2.4.2}$$

then if we set $A = 2$ then the solution is simply

$$\eta(x, 0) = 2 \operatorname{sech}^2 x. \tag{2.4.3}$$

We now use Python to code up the integrating factor system given by Equation 2.3.4, using the Runge-Kutta system presented in equations (2.3.13)-(2.3.17) to advance in time, with Equation 2.4.3 as the initial condition.

Figure 2.4.1 presents a plot of the numerical solution at times $t = 1$ and $t = 2$, each of which is compared with the initial condition. We observe from the illustration that the wave has propagated at a constant speed with no change in its shape or form, which is indicative that the scheme is generating results in accordance with what we'd expect the exact solutions to look like. We also note the use of a relatively large time step size, and small number of spatial steps, which is made possible through use of the integrating factor method since the numerically stiff linear terms have been removed from the system.

If we now fix the shape of the initial wave by imposing that $\gamma = 1$, but change the initial amplitude to $A = 6$ so that

$$\eta(x, 0) = 6 \operatorname{sech}^2 x, \tag{2.4.4}$$

then we have an initial soliton profile which is not an exact solution to the generalised form of the KdV equation (1.3.1). Such a scenario should see the initial profile split into two solitons, as discussed in Section 1.3. This is evidenced by Figure 2.4.2 which is an illustration of such a system for times $t = 0$, 0.15, and 0.5. This illustration has been generated using the same Python script as the one soliton solution, replacing the initial solution (2.4.3) with Equation 2.4.4.

Similarly, if we set $\gamma = 1$ but change the initial amplitude to $A = 12$, so that

$$\eta(x, 0) = 12 \operatorname{sech}^2 x, \tag{2.4.5}$$

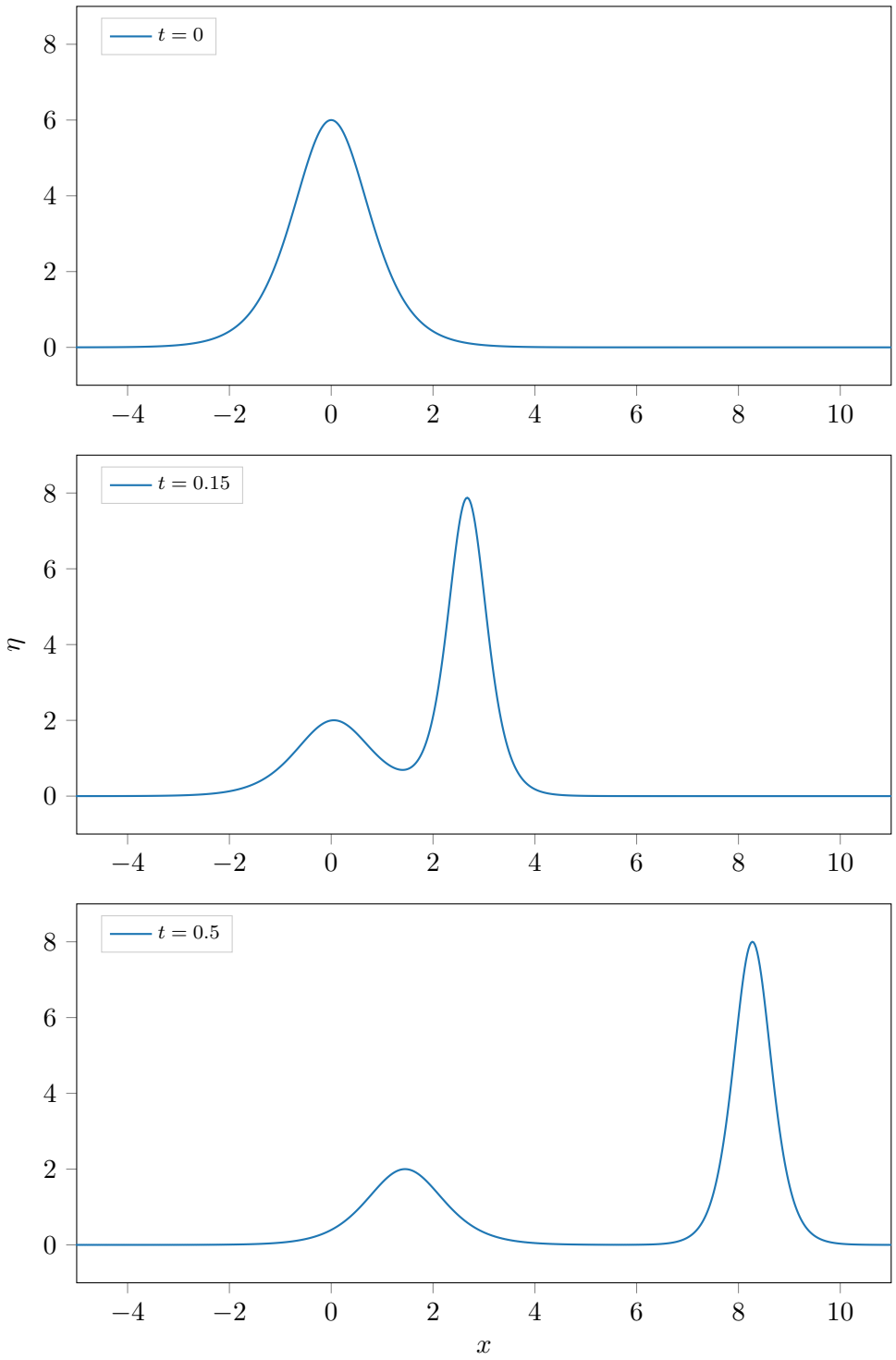

Figure 2.4.2: An illustration of an initial single soliton profile $\eta(x,0) = 6\,\mathrm{sech}^2\,x$ splitting into two solitons, with parameters $x \in [-4\pi, 4\pi]$, $t = 0$, 0.15, and 0.5.

then we have a scenario where we should see the initial single soliton split into three solitons, a scenario which is also discussed in Section 1.3. This can be seen in Figure 2.4.3 which is an illustration of such a scenario at times $t = 0$, 0.05, and 0.25, and has been generated using the same Python script as the one and two soliton solutions, replacing

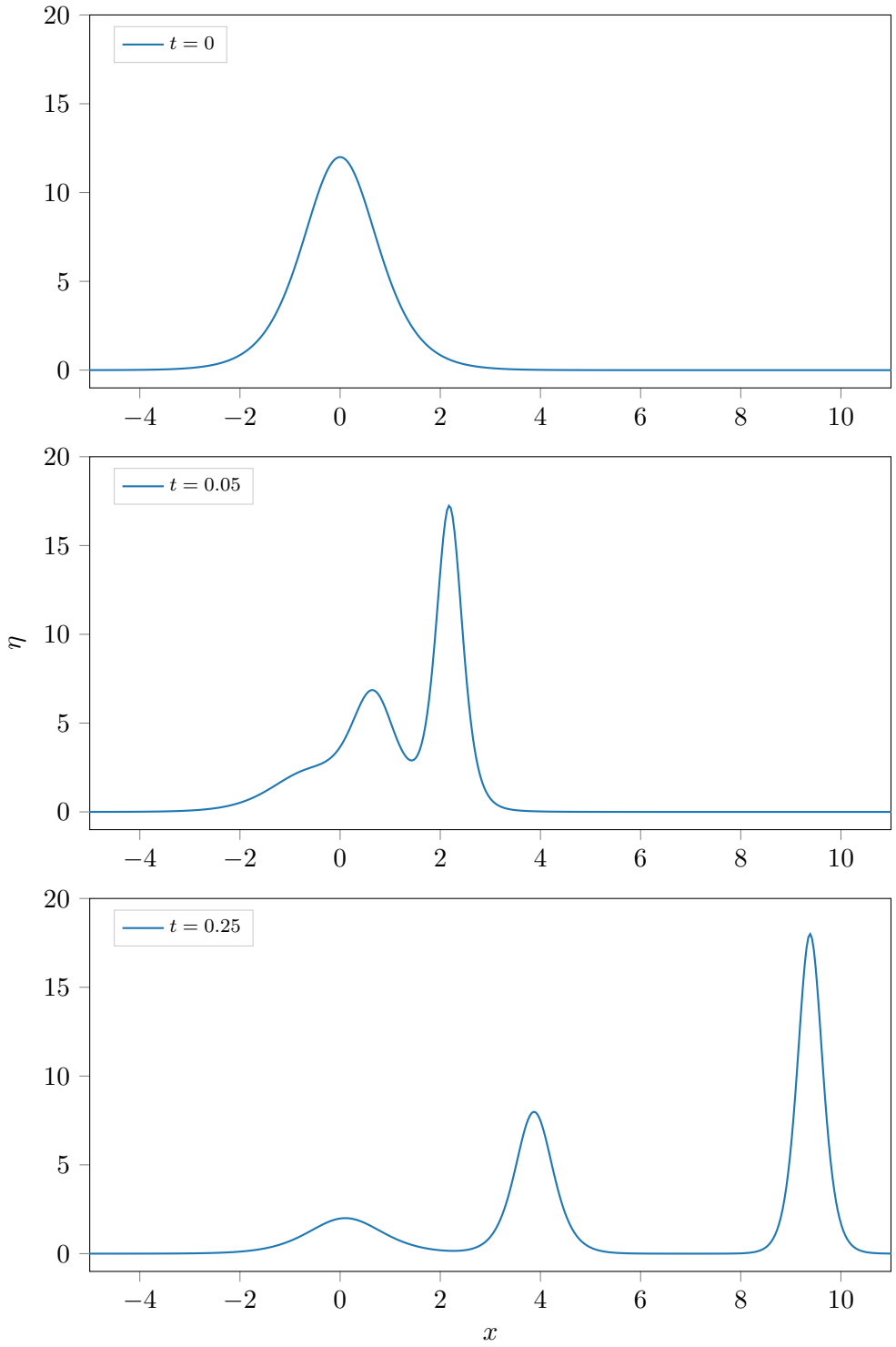

Figure 2.4.3: An illustration of an initial single soliton profile $\eta(x,0) = 12\,\mathrm{sech}^2 x$ splitting into three solitons, with parameters $x \in [-4\pi, 4\pi]$, $t = 0$, 0.05, and 0.25.

the initial solution (2.4.3) with Equation 2.4.5. The reason for such small increments in time is because, in this scenario, the leading soliton has a large amplitude compared with the trailing soliton, which means it travels considerably faster due to the proportionality

between the wave amplitude and the wave speed.

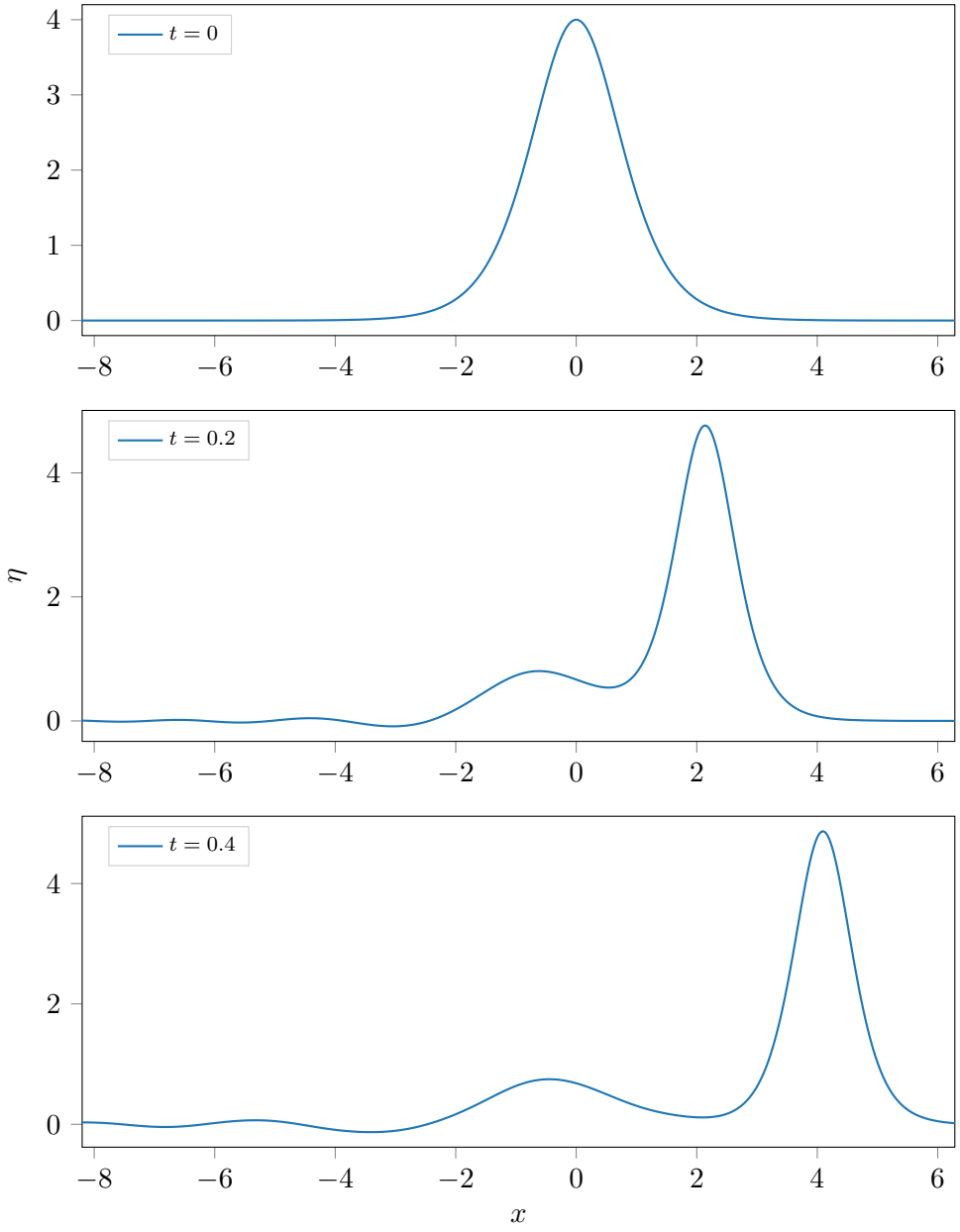

Figure 2.4.4: An illustration of an initial profile $\eta(x,0) = 4\,\mathrm{sech}^2\,x$ which is not an exact solution to the KdV equation, with parameters $x \in [-4\pi, 4\pi]$, $t = 0$, 0.2, and 0.4.

We also consider a scenario where the initial solution is not an exact solution to the KdV equation (1.3.1), and additionally is not an exact multi-soliton case, as above. For this scenario, we again set $\gamma = 1$ and set the initial amplitude to be $A = 4$ so that the initial solution looks like

$$\eta(x,0) = 4\,\mathrm{sech}^2\,x. \tag{2.4.6}$$

Since $A = 4$ cannot be written in the form $N(N-1)$ for $N \in \mathbb{N}$ we should not see an exact split into N solitons, and instead should expect the formation of a dispersive wave component. In fact, Drazin and Johnson (1989) discuss that this particular solution should take the form of two solitons followed by a dispersive wave train. This scenario is illustrated by Figure 2.4.4. We observe from the plots the formation of a decaying oscillatory tail which forms behind the main disturbance. This oscillatory dispersive component is a standard result and will be explored in more depth in Chapter 3 where we consider perturbations to the KdV equation.

Finally, for completeness, we also consider the case of a negative amplitude wave. For clarity, this assumes a negative amplitude solitary wave as a proposed solution to the KdV equation (1.3.1) associated with elevated travelling wave solutions, and not the case where the sign of the third order derivative is also negative which has solutions in the form of waves of depression.

As discussed in Grimshaw and Yuan (2016) and Drazin and Johnson (1989), here we expect that the solution will develop without the emergence of a soliton. The initial pulse will collapse and degenerate into a wave train which disperses into $x < 0$. This is illustrated by Figure 2.4.5. We note that a larger spatial range has been used to allow for the decaying wave train.

We have now demonstrated the integrating factor system which we have selected to use for the remainder of the thesis, to generate several different numerical solutions to the Korteweg-de Vries equation, and will now proceed to look at more complicated systems describing different physical scenarios.

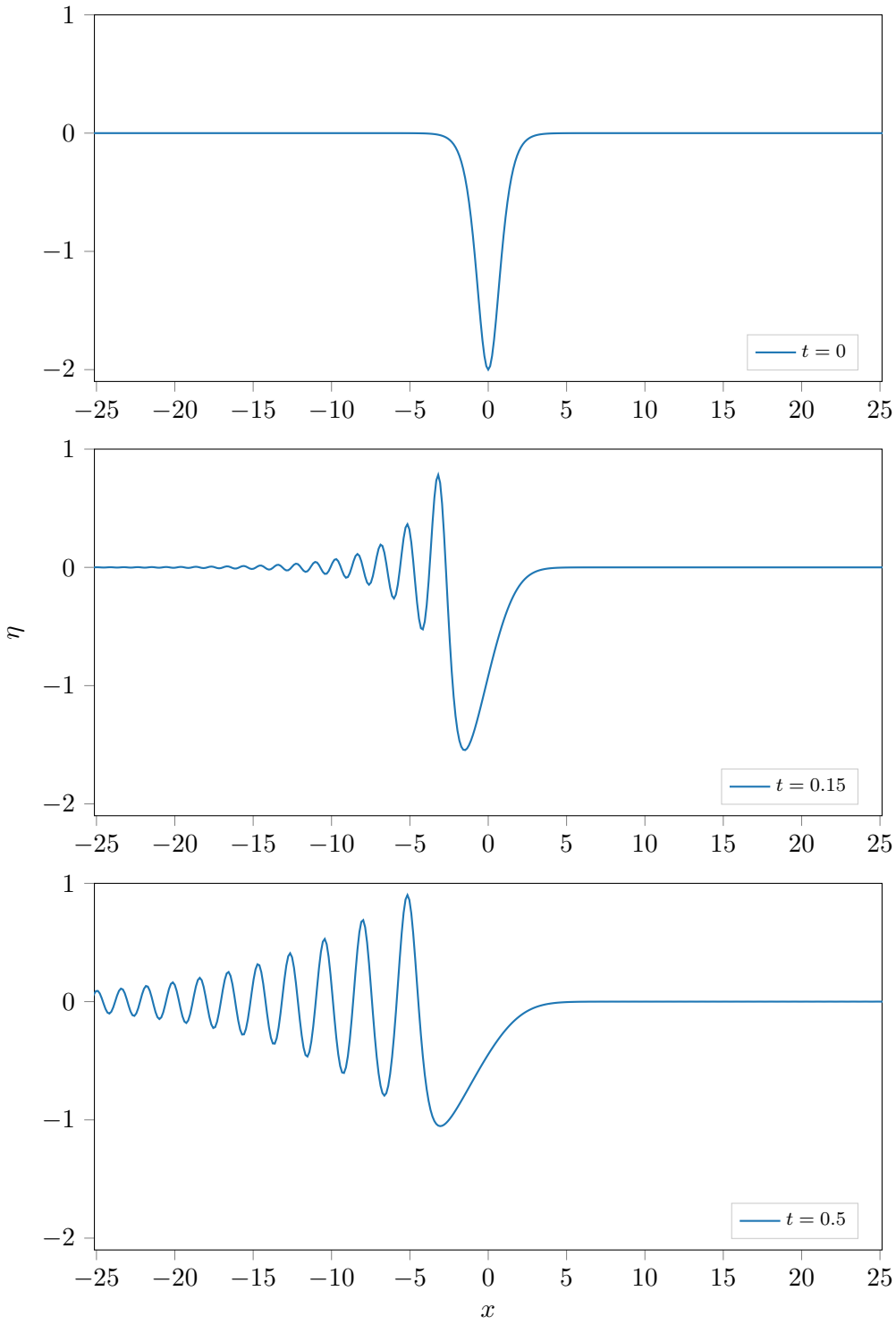

Figure 2.4.5: An illustration of an initial profile $\eta(x,0) = -2\,\mathrm{sech}^2\,x$ which is not an exact solution to the KdV equation (1.3.1), with parameters $x \in [-16\pi, 16\pi]$, $t = 0$, 0.15, and 0.5.

3

Gradual damping of solitary waves and the KdV-Burgers' equation

---

All results in the previous chapter have considered travelling solitary wave solutions to the Korteweg-de Vries equation (1.3.1) without any additional physical effects. In this chapter we will consider a solitary wave (1.3.9) subject to diffusive damping.

Previous work has seen scenarios in which a solitary wave experiences damping due to various different physical scenarios. Ott and Sudan (1970) examined four different forms of damping covering physical situations such as magnetosonic waves damped by electron-ion collisions, ion sound waves damped by ion-neutral collisions and by electron Landau damping, and shallow water waves damped by viscosity. Hammerton and Bassom (2013) examined a system with insoluble surfactant present at the fluid surface, a scenario which is explored in much more depth later, in Chapter 5.

Caputo and Stepanyants (2003) also discuss a variety of different scenarios with generalised soliton damping such as Rayleigh dissipation (Pelinovsky et al., 1993), a Chezy model where damping is due to friction at the solid fluid bottom (Holloway et al., 1999), and Reynolds-type dissipation with effects due to turbulent viscosity (Holloway et al., 1997), to name a few.

In each scenario, the equation governing the fluid can be written as a perturbed KdV equation of the form

$$\frac{\partial \eta}{\partial t} + 6\eta\frac{\partial \eta}{\partial x} + a\frac{\partial^3 \eta}{\partial x^3} = \mathcal{R}(\eta), \tag{3.0.1}$$

where any additional physical processes are governed by the $\mathcal{R}(\eta)$ term on the right-hand

side of Equation 3.0.1.

In each scenario, general solutions are typically not available, and often numerical methods such as those discussed in Chapter 2 are used to produce approximate solutions. We begin by considering a system when $\mathcal{R}(\eta)$ is small and the solution is considered as a perturbation of the soliton solution. In order to develop general methods for examining such a system, in this chapter we choose to focus on the case when the perturbation $\mathcal{R}(\eta)$ represents diffusive damping. This is modelled by adding a diffusive second-order spatial derivative to the right-hand side of the KdV equation, which is kept small so that the effects of the damping over time are gradual. The resulting equation looks like

$$\frac{\partial \eta}{\partial t} + 6\eta\frac{\partial \eta}{\partial x} + a\frac{\partial^3 \eta}{\partial x^3} = \varepsilon\frac{\partial^2 \eta}{\partial x^2} \tag{3.0.2}$$

where $\varepsilon \ll 1$ is a small parameter which controls the magnitude of the diffusion. This equation is widely known as the **Korteweg-de Vries-Burgers' equation** (KdV-B), (sometimes referred to as the Burgers'-KdV equation) and is a direct combination of Burgers' equation

$$\frac{\partial \eta}{\partial t} + 6\eta\frac{\partial \eta}{\partial x} = \varepsilon\frac{\partial^2 \eta}{\partial x^2}, \tag{3.0.3}$$

and the KdV equation (1.3.1). The Burgers' equation has many travelling wave solutions which represent shock waves, although these are not considered here. Although both equations have exact travelling wave solutions, the KdV-B equation has only one known exact, bounded travelling wave solution, given by Feng and Meng (2007) to be

$$\eta(x,t) = \frac{\varepsilon^2}{50a}\operatorname{sech}^2\left(\frac{\varepsilon}{10a}\left(x \mp \frac{6\varepsilon^2}{25a}t\right)\right) - \frac{\varepsilon^2}{25a}\tanh\left(\frac{\varepsilon}{10a}\left(x \mp \frac{6\varepsilon^2}{25a}t\right)\right) \pm \frac{\varepsilon^2}{25a}. \tag{3.0.4}$$

We recall that sech^2 appears in the solitary wave solution (1.3.9) to the KdV equation, and note that the $\tanh$ is seen in the Taylor shock solution to the Burgers' equation. Equation 3.0.4 then appears to be a linear combination of these two solutions, although we do not explore this solution any further here.

The KdV-Burgers' equation (3.0.2) is widely used in the field of wave propagation through cosmic plasmas (Gao, 2015). Particular examples include the propagation of ion-acoustic

waves and magneto-sonic waves, with η denoting perturbations in either ion velocity, ion density or electrostatic wave potential depending on the exact context. Another application of the KdV-B equation is propagation of gas slugs through fluidised beds (Harris and Crighton, 1994), where η describes the voidage fraction, although in this case the perturbation term has the opposite sign and is no longer a dissipative term.

In the present analysis we treat KdV-Burger's equation as a model equation without considering the significance of the solutions to the physical processes discussed above. We will impose a KdV solitary wave solution (1.3.9) as an initial condition and then look at how the inclusion of the diffusive second-order term affects the wave amplitude, assuming that the effects from the diffusive term are applied for time $t > 0$. One of the main purposes for considering this scenario is to formulate a method which can then be used for more complicated scenarios, examined later. Each scenario will consider the same solitary wave solution subject to damping due to a viscous boundary layer at the fluid base, satisfying a no-slip condition at the solid impermeable bottom boundary. The results generated in this chapter will then be used for comparisons with subsequent results.

We will then attempt to construct an asymptotic solution to η expanding around the small parameter ε, and solve up to and including the $\mathcal{O}(\varepsilon)$ correction term. This asymptotic solution will then be used to give a better approximation to the behaviour of the solitary wave subject to the effects due to the diffusion term.

3.1 Leading-order decay due to the diffusive second-order term

Suppose initially that we have a travelling solitary wave solution to the KdV equation (1.3.1), given by

$$\eta(x,t) = A\,\mathrm{sech}^2\left(\sqrt{\frac{c}{4a}}(x-ct)\right), \tag{3.1.1}$$

and then impose that the wave is subject to viscous diffusion for $t > 0$. Such a system is governed by the KdV-Burgers' equation

$$\frac{\partial \eta}{\partial t} + 6\eta \frac{\partial \eta}{\partial x} + a\frac{\partial^3 \eta}{\partial x^3} = \varepsilon \frac{\partial^2 \eta}{\partial x^2} \tag{3.1.2}$$

where the second-order derivative term governs the effects due to slow acting diffusion.

This section will use Equation 3.1.2 such that the diffusion term is relatively small in comparison with the other terms in the equation. The initial solution will be considered in the form of a solitary wave with slowly decaying amplitude A, due to the addition of the diffusion parameter, as the wave propagates in time. We first consider the solitary wave given in Equation 1.3.9. We replace the wave amplitude $\frac{c}{2}$ with a slow-decaying function of time $A(t)$, so that the initial solution to Equation 3.1.2 now takes the form

$$\eta(x,t) = A(t)\,\mathrm{sech}^2\left(\sqrt{\frac{A}{2a}}\Big(x - 2At\Big)\right). \tag{3.1.3}$$

The intention is to find the amplitude function $A(t)$ as an analytic function in terms of t, ε and the initial amplitude $A_0 = \frac{c}{2}$. A similar analysis is given by Ott and Sudan (1970) who were able to find a function describing the amplitude $A(t)$ as a function of time, for each of the physical scenarios discussed therein.

3.1.1 Multiple scale asymptotic analysis

We now attempt to construct a multiple scale analysis with the expectation of finding an analytical solution to the slowly decaying amplitude function $A(\varepsilon t)$. The motivation for this arises from the small parameter ε and the notion of *slow-time*, εt, since the amplitude is expected to decay slowly in time. We start by introducing a new variable $\tau = \varepsilon t$ to denote slow-time, so that the small parameter ε acts as a scale for the time variable t.

Now, the KdV-Burgers' equation (3.1.2) is rewritten in terms of τ and z, where

$$z = x - 2\int^t A(\varepsilon t')\mathrm{d}t',$$

and we assume a solution $\eta = \eta(z, \tau)$. The derivatives in terms of these new variables are given by

$$\frac{\partial}{\partial x} = \frac{\partial}{\partial z}, \quad \text{and} \quad \frac{\partial}{\partial t} = -2A\frac{\partial}{\partial z} + \varepsilon\frac{\partial}{\partial \tau},$$

and therefore the KdV-Burgers' equation (3.1.2) in terms of the new variables becomes

$$\varepsilon\frac{\partial \eta}{\partial \tau} - 2A\frac{\partial \eta}{\partial z} + 6\eta\frac{\partial \eta}{\partial z} + a\frac{\partial^3 \eta}{\partial z^3} = \varepsilon\frac{\partial^2 \eta}{\partial z^2}. \tag{3.1.4}$$

We now attempt to construct a simple asymptotic approximation to $\eta(z, \tau)$ valid for $\varepsilon \ll 1$ which takes the form

$$\eta(z, \tau; \varepsilon) = \eta_0(z, \tau) + \varepsilon\eta_1(z, \tau) + \mathcal{O}(\varepsilon^2), \tag{3.1.5}$$

subject to the condition

$$\eta \to 0, \quad \text{as} \quad |z| \to \infty.$$

Substituting Equation 3.1.5 into Equation 3.1.4, and then equating coefficients of powers of ε, we obtain the leading-order $\mathcal{O}(\varepsilon^0)$ equation

$$-2A\frac{\partial \eta_0}{\partial z} + 6\eta_0\frac{\partial \eta_0}{\partial z} + a\frac{\partial^3 \eta_0}{\partial z^3} = 0. \tag{3.1.6}$$

Then, equating $\mathcal{O}(\varepsilon)$ terms we obtain the differential equation at the next order, given by

$$-2A\frac{\partial \eta_1}{\partial z} + 6\frac{\partial(\eta_0\eta_1)}{\partial z} + a\frac{\partial^3 \eta_1}{\partial z^3} = \frac{\partial^2 \eta_0}{\partial z^2} - \frac{\partial \eta_0}{\partial \tau}. \tag{3.1.7}$$

Equation 3.1.6 is effectively Equation 1.3.3 in terms of η_0, and therefore we can state that the leading-order solution has the form

$$\eta_0 = A(\tau)\,\mathrm{sech}^2\left(\sqrt{\frac{A}{2a}}z\right). \tag{3.1.8}$$

However, the solution to $\eta_1(z, \tau)$ isn't immediately obvious. Instead we use a similar approach to that discussed in Mei (1989) and introduce operators L_0 and L_1 defined to be

$$L_0[U] = \frac{\partial}{\partial z}\left(-2AU + 3U^2 + a\frac{\partial^2 U}{\partial z^2}\right),$$

and

$$L_1[V] = \frac{\partial}{\partial z}\left(-2AV + 6UV + a\frac{\partial^2 U}{\partial z^2}\right),$$

where U and V represent the leading-order and the $\mathcal{O}(\varepsilon)$ solutions respectively. Then, applying these operators to Equation 3.1.6 and Equation 3.1.7 we have

$$L_0[\eta_0] = 0, \qquad \text{and} \qquad L_1[\eta_1] = \frac{\partial^2 \eta_0}{\partial z^2} - \frac{\partial \eta_0}{\partial \tau}. \tag{3.1.9}$$

It can now be shown by straightforward partial integration that L_0 and L_1 are adjoint operators of each other. Applying the condition $\eta_0, \eta_1 \to 0$ as $|z| \to \infty$,

$$\begin{aligned}
\int_{-\infty}^{\infty} \eta_0 L_1[\eta_1]\mathrm{d}z &= \int_{-\infty}^{\infty} \eta_0 \frac{\partial}{\partial z}\left(-2A\eta_1 + 6\eta_0\eta_1 + a\frac{\partial^2 \eta_1}{\partial z^2}\right)\mathrm{d}z, \\
&= -\int_{-\infty}^{\infty} \frac{\partial \eta_0}{\partial z}\left(-2A\eta_1 + 6\eta_0\eta_1 + a\frac{\partial^2 \eta_1}{\partial z^2}\right)\mathrm{d}z, \\
&= -\int_{-\infty}^{\infty} \eta_1 \frac{\partial}{\partial z}\left(-2A\eta_0 + 3\eta_0^2\right)\mathrm{d}z - a\int_{-\infty}^{\infty} \frac{\partial \eta_0}{\partial z}\frac{\partial^2 \eta_1}{\partial z^2}\mathrm{d}z, \\
&= -\int_{-\infty}^{\infty} \eta_1 \frac{\partial}{\partial z}\left(-2A\eta_0 + 3\eta_0^2 + a\frac{\partial^2 \eta_0}{\partial z^2}\right)\mathrm{d}z \\
&= -\int_{-\infty}^{\infty} \eta_1 L_0[\eta_0]\,\mathrm{d}z.
\end{aligned}$$

Thus we have

$$\int_{-\infty}^{\infty} \eta_0 L_1[\eta_1]\,\mathrm{d}z + \int_{-\infty}^{\infty} \eta_1 L_0[\eta_0]\,\mathrm{d}z = 0, \tag{3.1.10}$$

which is exactly the required condition for L_0 and L_1 to be considered adjoint operators, (Mei, 1989). Then, using Equation 3.1.9 we know that $L_0[\eta_0] = 0$, and Equation 3.1.10 becomes

$$\int_{-\infty}^{\infty} \eta_0 L_1[\eta_1]\mathrm{d}z = \int_{-\infty}^{\infty} \eta_0\left(\frac{\partial^2 \eta_0}{\partial z^2} - \frac{\partial \eta_0}{\partial \tau}\right)\mathrm{d}z = 0, \tag{3.1.11}$$

which is a definite integral in terms of the leading-order solution η_0 only. Since η_0 has already been defined in Equation 3.1.8, we can evaluate the integral in Equation 3.1.11 which will remove z, and thus we should be able to rearrange the result into an ordinary differential equation for A in terms of t only. For simplicity we set

$$\gamma = \sqrt{\frac{A}{2a}}, \qquad \text{and} \quad \theta = \gamma z, \tag{3.1.12}$$

and hence Equation 3.1.11) becomes

$$\frac{1}{\gamma}\int_{-\infty}^{\infty}\eta_0\left(\gamma^2\frac{\partial^2\eta_0}{\partial\theta^2}-\frac{\partial\eta_0}{\partial\tau}\right)\mathrm{d}\theta=0 \tag{3.1.13}$$

into which we directly substitute $\eta_0 = A\,\mathrm{sech}^2\,\theta$, from Equation 3.1.8. Evaluating each of the derivatives in (3.1.13) individually, we have

$$\frac{\partial^2\eta_0}{\partial\theta^2}=2A\,\mathrm{sech}^2\,\theta\left(2\tanh^2\theta-\mathrm{sech}^2\,\theta\right) \tag{3.1.14}$$

and

$$\frac{\partial\eta_0}{\partial\tau}=\mathrm{sech}^2\,\theta\frac{\mathrm{d}A}{\mathrm{d}\tau}(1-\theta\tanh\theta)-4\gamma A\,\mathrm{sech}^2\,\theta\tanh\theta. \tag{3.1.15}$$

Before substituting these back into Equation 3.1.13, we first note that $\tanh\theta$ is an **odd** function, which means that

$$\int_{-\infty}^{\infty}\tanh\theta\,\mathrm{d}\theta=0.$$

Then, since $\mathrm{sech}^2(\theta)$ is an **even** function, the final term in Equation 3.1.15 is equal to zero, since

$$\int_{-\infty}^{\infty}\mathrm{sech}^2\,\theta\tanh\theta\,\mathrm{d}\theta=0.$$

We omit this term, and thus after substituting Equation 3.1.14 and Equation 3.1.15 into Equation 3.1.13 we have

$$2\gamma^2A^2\int_{-\infty}^{\infty}2\tanh^2\theta\,\mathrm{sech}^4\,\theta-\mathrm{sech}^6\,\theta\,\mathrm{d}\theta \\ -A\frac{\mathrm{d}A}{\mathrm{d}\tau}\int_{-\infty}^{\infty}\mathrm{sech}^4\,\theta\Big(1-\theta\tanh\theta\Big)\,\mathrm{d}\theta=0.$$

We evaluate each integral using Maple, which gives

$$\int_{-\infty}^{\infty}2\tanh^2\theta\,\mathrm{sech}^4\,\theta-\mathrm{sech}^6\,\theta\,\mathrm{d}\theta=-\frac{8}{15},$$

and

$$\int_{-\infty}^{\infty}\mathrm{sech}^4\,\theta(1-\theta\tanh\theta)\,\mathrm{d}\theta=1.$$

Then, writing $\gamma^2 = \frac{A}{2a}$, Equation 3.1.13 simplifies to

$$\frac{\mathrm{d}A}{\mathrm{d}\tau} + \frac{8}{15a}A(\tau)^2 = 0. \tag{3.1.16}$$

Equation 3.1.16 is a first-order ordinary differential equation for $A(\tau)$ of separable type and can therefore be solved using the method of separable variables. First, we write

$$\int \frac{\mathrm{d}A}{A^2} = -\frac{8}{15a}\int \mathrm{d}\tau.$$

Then, using the initial condition $A(t=0) = A_0$, after simplification we have

$$A(t) = \frac{A_0}{1 + \frac{8}{15a}A_0\varepsilon t} \tag{3.1.17}$$

which is a function describing the leading-order amplitude as a function of time. This agrees with the solution derived in (Ott and Sudan, 1970). We observe that as t increases, the value of the amplitude $A(t)$ decreases gradually from its initial value $A(0) = A_0$, as predicted.

We will now construct a numerical solution to the amplitude so that we can directly compare with the asymptotic solution (3.1.17).

3.1.2 Comparisons between the asymptotic and numerical solutions

Now that we have determined an analytical function which describes the slowly decreasing amplitude, we will compare this with a numerical solution. To construct the numerical solution we will use the integrating factor method from Chapter 2, applied to Equation 3.1.2, using

$$\eta(x,0) = A_0\,\mathrm{sech}^2\left(\sqrt{\frac{A_0}{2a}}x\right) \tag{3.1.18}$$

as an initial condition. Here we are imposing a solitary wave solution for time $t = 0$ and then applying the diffusive damping for $t > 0$. The expectation is that we will see a gradual decay in amplitude and wave speed. First we take the Fourier transform of the KdV-Burgers' equation (3.1.2), and group together the linear derivatives in space on the

right-hand side of the equation. This gives us

$$\begin{aligned}\frac{\partial\widehat{\eta}}{\partial t}+3\mathrm{i}k\widehat{(\eta^2)} &= -a(\mathrm{i}k)^3\widehat{\eta}+(\mathrm{i}k)^2\varepsilon\widehat{\eta},\\ &= \left(\mathrm{i}ak^3-\varepsilon k^2\right)\widehat{\eta}\end{aligned} \tag{3.1.19}$$

An integrating factor is then introduced in order to eliminate both linear terms on the right-hand side, which takes the form

$$\widehat{E}=\exp\Big(-(\mathrm{i}ak^3-\varepsilon k^2)t\Big). \tag{3.1.20}$$

where the exponent is chosen so that it reflects the negative right-hand side of Equation 3.1.19. We start by multiplying Equation 3.1.19 by $\widehat{E}$, and then we introduce the new function $\widehat{v}$ where

$$\widehat{v}=\widehat{E}\widehat{\eta}$$

and substitute it into the governing equation, which gives

$$\begin{aligned}\frac{\partial\widehat{v}}{\partial t}+\left(a\mathrm{i}k^3-\varepsilon^2k^2\right)\widehat{v}+3\mathrm{i}k\widehat{E}\widehat{(\eta^2)} &= \left(a\mathrm{i}k^3-\varepsilon^2k^2\right)\widehat{v},\\ \frac{\partial\widehat{v}}{\partial t}+3\mathrm{i}k\widehat{E}\widehat{(\eta^2)} &= 0.\end{aligned}$$

The linear spatial terms have gone, so we now advance the spectral function $\widehat{v}$ in time using the fourth-order Runge-Kutta equations (2.3.13) - (2.3.17). We can then recover η with an inverse Fourier transform. We will generate numerical solutions with this scheme using Python, similar to Chapter 2.

Figure 3.1.1 is a plot of the numerical solution to Equation 3.0.2 for two different values of ε, together with an undamped soliton solution (3.1.1) for comparisons. We have used Equation 3.1.18 as an initial condition and then applied the diffusive second-order term for $t>0$. Each solution in the figure is essentially a snapshot of the travelling wave at time $t_{\max}=5$.

We observe from the plots that the solitary wave solutions subject to the diffusive damping due to the second-order term have indeed decayed in both wave amplitude and wave speed. We see that increasing the size of ε, which increases the magnitude of the damping

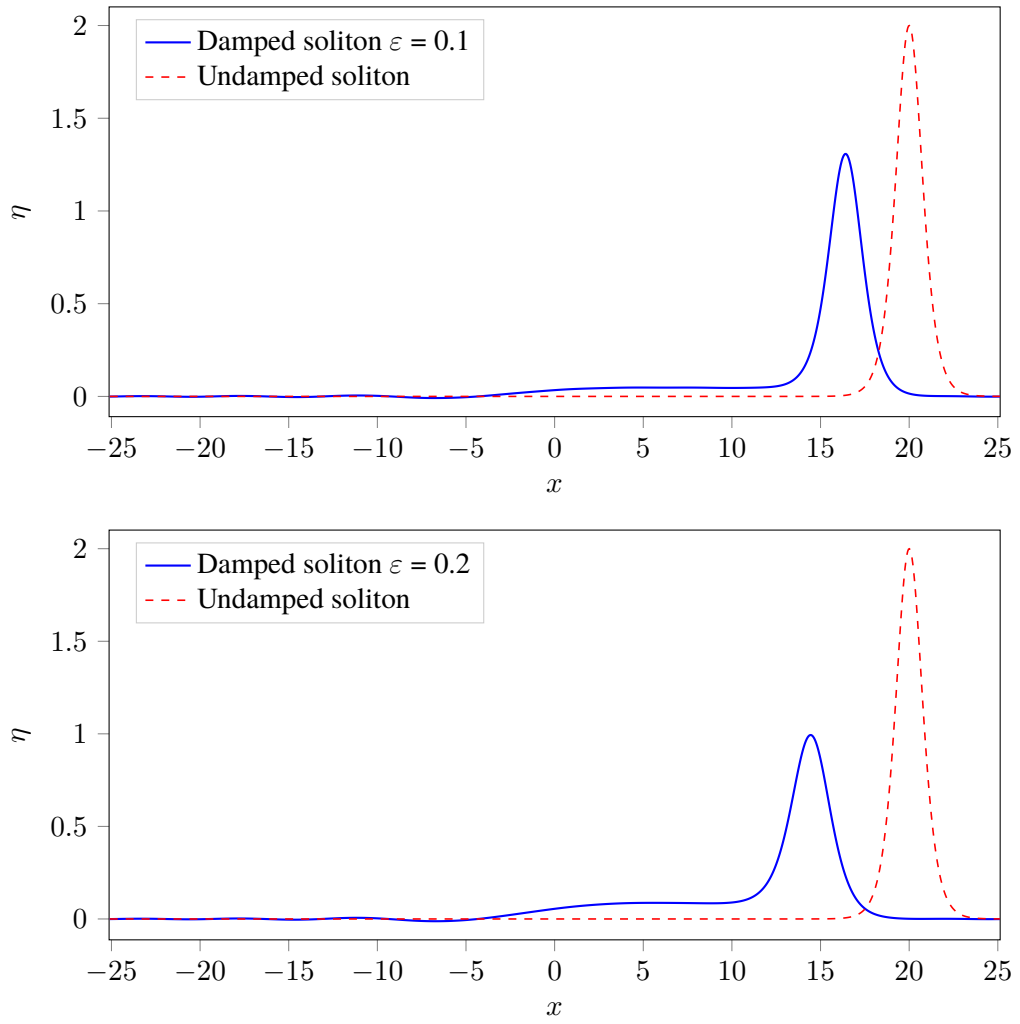

Figure 3.1.1: A plot comparing a solitary wave affected by diffusive damping compared with an unaffected solitary wave, using parameter values: $t_{\max} = 5$, $x \in [-8\pi, 8\pi]$, $A_0 = 2$, $\varepsilon = 0.1$ (top) and $\varepsilon = 0.2$ (bottom).

effects due to diffusivity, results in a larger decay in amplitude and a further decrease in the wave speed. This is evidenced by direct comparisons with the unaffected solitary wave solution, which has maintained a constant amplitude and constant wave speed.

We also observe a change in the wave form for the damped solitary waves. Notably we draw particular attention to the elevated *shelf* which forms behind the main wave crest, followed by a slowly decaying tail. This shelf-tail structure is not specific to diffusive soliton damping associated with the KdV-Burgers' equation, and various examples of this change in wave form have been given in Grimshaw et al. (2003), Karpman and Maslov (1978) and Pelinovsky and Grimshaw (1997), for different physical processes. The magnitude of the elevated shelf increases with increasing ε. The decaying oscillatory

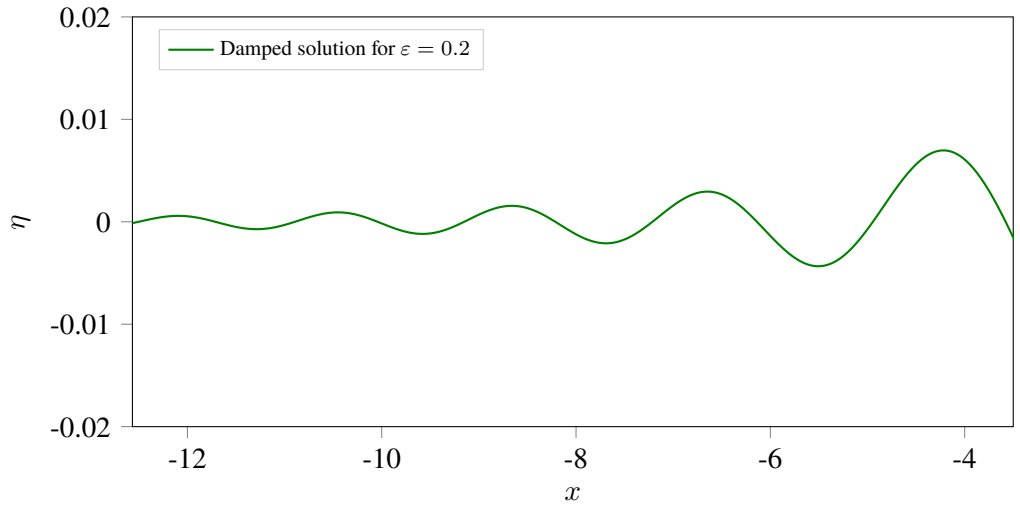

Figure 3.1.2: A close-up of the slowly decaying tail region of the solitary wave solution affected by diffusive damping, using parameter values: $t_{\max} = 2$, $x \in [-4\pi, 4\pi]$, and $\varepsilon = 0.2$.

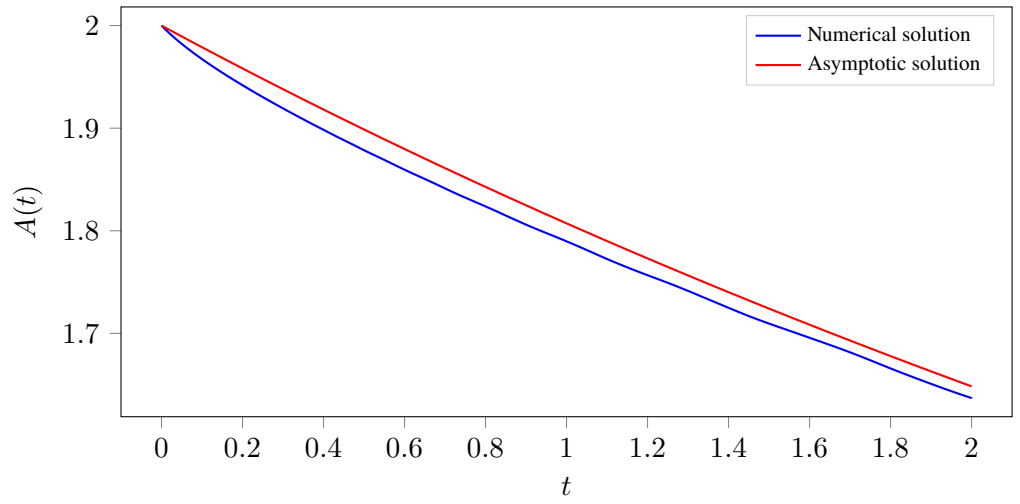

Figure 3.1.3: A comparison between the asymptotic and numerical solutions to the decay in amplitude for diffusive damping, using parameter values: $t_{\max} = 2$, $x \in [-4\pi, 4\pi]$, $A_0 = 2$, $\varepsilon = 0.1$.

tail is perhaps better observed by Figure 3.1.2 which illustrates a close-up of the tail region.

Next we look specifically at the amplitude of the wave. In order to obtain the numerical solution for the amplitude, we use the `max` function which is built into Python to generate such a solution, which is updated with each iteration used to advance the numerical solution to the solitary wave in time. This is then compared to the asymptotically derived solution to the amplitude given in Equation 3.1.17.

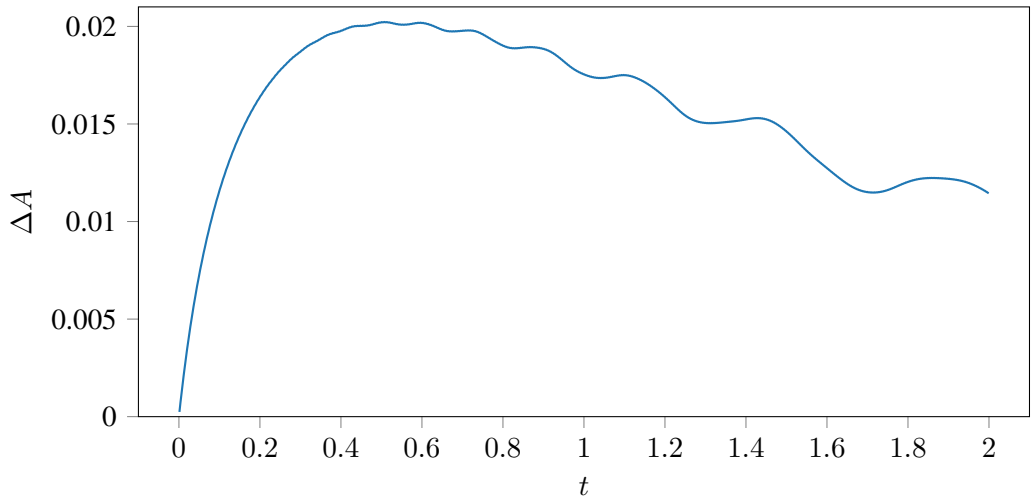

Figure 3.1.4: Difference in amplitude value of numerically and asymptotically derived amplitudes, for parameters: $\varepsilon = 0.1$, $A_0 = 2$, and $t_{\max} = 2$.

Figure 3.1.3 gives a comparison between the numerically derived and asymptotically derived wave amplitude. We observe an excellent agreement, less than 5% difference in value, between the numerical and asymptotic solutions, although we note that both solutions are subject to error since the asymptotic solution only considers leading-order behaviour, and the numerical solution is subject to the usual numerical error as discussed in Chapter 2.

We also observe that the agreement between the two solutions is worse at the beginning but gets better as time increases. This is best illustrated by Figure 3.1.4 which shows the average difference between the two results over the given time period. We initially see a large increase in the difference between to two solutions followed by a seemingly linear decrease. This could potentially be explained by evaluating higher-order terms in the asymptotic solution.

Now that we have derived a reasonable approximation to the wave amplitude we will proceed to examine the solution at the next order. This ideally will improve our asymptotically derived approximation to the wave amplitude.

3.2 Evaluation of the first-order correction term

In this section we evaluate the $\mathcal{O}(\varepsilon)$ correction term η_1 in the asymptotic solution (3.1.5) to the KdV-Burgers' equation (3.1.2). It is our expectation that, by considering the solution for higher-order terms, we will be able to determine a more accurate approximation to the decay in amplitude due to the diffusivity associated with the second-order derivative. The $\mathcal{O}(\varepsilon)$ differential equation (3.1.7) in general is not solvable explicitly, so instead we will find approximate solutions to η_1.

3.2.1 Reformulation

We start by considering the Korteweg-de Vries-Burgers' equation (3.1.2) in its dimensional form given by

$$\frac{\partial \eta^\star}{\partial t^\star} + 6\eta^\star \frac{\partial \eta^\star}{\partial x^\star} + a\frac{\partial^3 \eta^\star}{\partial x^{\star 3}} = \varepsilon^\star \frac{\partial^2 \eta^\star}{\partial x^{\star 2}} \tag{3.2.1}$$

with boundary conditions $\eta^\star \to 0$ as $x^\star \to \pm\infty$, and where the * super-script indicates that a variable has dimension. If $\varepsilon^\star = 0$ then travelling wave solutions exist in the form

$$\eta^\star = 2a\gamma^2 \operatorname{sech}^2\left(\gamma(x^\star - 4a\gamma^2 t^\star)\right), \tag{3.2.2}$$

where γ is an arbitrary constant, defined earlier in Equation 3.1.12. This can be rewritten as

$$\eta^\star = 2a\gamma^2 \operatorname{sech}^2\theta,$$

where

$$\theta = \gamma(x^\star - \xi^\star), \qquad \frac{\partial \xi^\star}{\partial t^\star} = 4a\gamma^2,$$

and the reason for this choice of notation becomes clear in the subsequent analysis for the $\varepsilon \neq 0$ case.

We now consider the case when $\varepsilon \neq 0$ and use

$$\eta^\star(x^\star, 0) = 2a\gamma^2 \operatorname{sech}^2(\gamma x^\star),$$

as the initial condition. We solve for $t > 0$, corresponding to the model problem from Section 3.1 of taking a travelling wave solution and switching on the damping term at $t = 0$. The analysis is simplified by non-dimensionalising, so we set

$$\eta^\star = a\gamma^2\eta, \quad t^\star = \frac{t}{a\gamma^3}, \quad x^\star = \frac{x}{\gamma}, \quad \varepsilon^\star = a\gamma\varepsilon$$

which after substitution into Equation 3.2.1 yields

$$\frac{\partial \eta}{\partial t} + 6\eta\frac{\partial \eta}{\partial x} + \frac{\partial^3 \eta}{\partial x^3} = \varepsilon\frac{\partial^2 \eta}{\partial x^2}, \tag{3.2.3}$$

with the initial condition

$$\eta(x, 0) = 2\operatorname{sech}^2 x.$$

Comparing with the $\varepsilon = 0$ solution (3.2.2) previously determined, we seek solutions of the form

$$\eta = 2\gamma^2 \upsilon(\theta, t), \tag{3.2.4}$$

where γ is now a function of t and

$$\theta = \gamma(x - \xi - \chi), \qquad \text{where} \quad \frac{\partial \xi}{\partial t} = 4\gamma^2, \quad \text{and} \quad \chi = \chi(t). \tag{3.2.5}$$

The reason for including $\chi(t)$ in the definition of θ is seen later. When $\varepsilon = 0$ the solution of Equation 3.2.3 is given by

$$\eta = 2\gamma^2 \operatorname{sech}^2\theta, \qquad \text{with} \quad \gamma(t) = 1, \quad \xi(t) = 4t, \quad \chi(t) = 0 \tag{3.2.6}$$

and hence we take

$$\upsilon = \operatorname{sech}^2\theta, \quad \gamma(0) = 1, \quad \xi(0) = \chi(0) = 0$$

as our initial solution.

Then, substituting (3.2.4) and (3.2.5) into Equation 3.2.3, it can be shown that υ satisfies

$$\frac{\partial \upsilon}{\partial t} + \gamma^3\left(\frac{\partial^3 \upsilon}{\partial \theta^3} + 12\upsilon\frac{\partial \upsilon}{\partial \theta} - 4\frac{\partial \upsilon}{\partial \theta}\right) = \varepsilon\gamma^2\frac{\partial^2 \upsilon}{\partial \theta^2} - \frac{\theta}{\gamma}\frac{\partial \gamma}{\partial t}\frac{\partial \upsilon}{\partial \theta} + \gamma\frac{\partial \chi}{\partial t}\frac{\partial \upsilon}{\partial \theta} - \frac{2\upsilon}{\gamma}. \quad (3.2.7)$$

Recalling that when $\varepsilon = 0$, the amplitude, wave number and propagation speed are all constant, we then seek a solution for $\varepsilon \ll 1$ where γ and χ are functions of a slow time, $\tau = \varepsilon t$. In this case Equation 3.2.7 becomes

$$\frac{\partial \upsilon}{\partial t} + \gamma^3\left(\frac{\partial^3 \upsilon}{\partial \theta^3} + 12\upsilon\frac{\partial \upsilon}{\partial \theta} - 4\frac{\partial \upsilon}{\partial \theta}\right) = \varepsilon\gamma^2\left(\frac{\partial^2 \upsilon}{\partial \theta^2} + \mu_0\left(\upsilon + \frac{\partial(\theta\upsilon)}{\partial \theta}\right) + \mu_1\frac{\partial \upsilon}{\partial \theta}\right), \quad (3.2.8)$$

where

$$\mu_0 = -\frac{1}{\gamma^3}\frac{\partial \gamma}{\partial \tau}, \quad \text{and} \quad \mu_1 = \frac{1}{\gamma}\frac{\partial \chi}{\partial \tau}, \quad (3.2.9)$$

and, at this stage, μ_0 and μ_1 are functions of τ to be determined.

As discussed, we are interested in the perturbation away from the $\varepsilon = 0$ solution for the case $\varepsilon \ll 1$. In order to reduce complexity, we introduce two new parameters:

$$\delta = \frac{\varepsilon}{\gamma}, \quad \text{and} \quad \tilde{t} = \int^t \gamma^3 \mathrm{d}t \quad (3.2.10)$$

so that the full perturbation can be written in terms of one small parameter, δ. Then, substituting (3.2.10) into Equation 3.2.8 and rearranging yields

$$\frac{\partial \upsilon}{\partial \tilde{t}} = 4\frac{\partial \upsilon}{\partial \theta} - 12\upsilon_0\frac{\partial \upsilon}{\partial \theta} - \frac{\partial^3 \upsilon}{\partial \theta^3} + \delta\left(\frac{\partial^2 \upsilon}{\partial \theta^2} + \mu_0\left(\upsilon + \frac{\partial(\theta\upsilon)}{\partial \theta}\right) + \mu_1\frac{\partial \upsilon}{\partial \theta}\right), \quad (3.2.11)$$

noting that

$$\frac{\partial \delta}{\partial \tilde{t}} = \delta^2\mu_0.$$

We now consider an asymptotic expansion valid for small δ, in the form

$$\upsilon(\theta, \tilde{t}; \delta) = \upsilon_0(\theta) + \delta F(\theta, \tilde{t}) + \delta^2 G(\theta, \tilde{t}) + \mathcal{O}(\delta^3) \quad (3.2.12)$$

and substitute into Equation 3.2.11. At leading order we have

$$\frac{\partial^3 \upsilon_0}{\partial \theta^3} + 12\upsilon\frac{\partial \upsilon_0}{\partial \theta} - 4\frac{\partial \upsilon_0}{\partial \theta} = 0,$$

and hence from Equation 3.2.6 we know that

$$v_0(\theta) = \operatorname{sech}^2 \theta.$$

The next two perturbation terms satisfy

$$\frac{\partial F}{\partial \tilde{t}} = -L[F] + R[v_0], \tag{3.2.13}$$

and

$$\frac{\partial G}{\partial \tilde{t}} = -L[G] + R[F] - \mu_0 F - 6\frac{\partial (F^2)}{\partial \theta} \tag{3.2.14}$$

with $F(\theta, 0) = G(\theta, 0) = 0$, where the operators $L[\cdot]$ and $R[\cdot]$ differ from those given in Section 3.1, and are here defined to be

$$L[V] = \frac{\partial^3 V}{\partial \theta^3} + 12\frac{\partial (v_0 V)}{\partial \theta} - 4\frac{\partial V}{\partial \theta}, \tag{3.2.15}$$

and

$$R[V] = \frac{\partial^2 V}{\partial \theta^2} + \mu_0 \left(V + \frac{\partial (\theta V)}{\partial \theta} \right) + \mu_1 \frac{\partial V}{\partial \theta}, \tag{3.2.16}$$

respectively.

When comparing the predictions of the asymptotic analysis with numerical results generated later, one key comparison is the maximum amplitude of the solution, η_{M}, and its position, x_{M}, as functions of time. The maximum is located at

$$\theta_{\text{M}} = \frac{\delta}{2}\frac{\partial F_0}{\partial \theta} + \mathcal{O}(\delta^2)$$

where $F_0 = F(0, \tilde{t})$, and hence

$$\eta_{\text{M}}(t) = 2\gamma^2 \left(1 + \varepsilon \frac{F_0}{\gamma} \right), \tag{3.2.17}$$

and

$$x_{\text{M}} = \frac{\varepsilon}{2}\frac{F_0}{\gamma^2} + \frac{1}{\varepsilon}\int_0^\tau 4\gamma^2 + \varepsilon\gamma\mu_1 \, \mathrm{d}\tau, \tag{3.2.18}$$

correct to the $\mathcal{O}(\varepsilon)$ term.

In the next part of the analysis we look at the evolution of F with time, focussing in particular on the validity of the perturbation expansions over different time scales.

3.2.2 Analytic solutions of the linear perturbation equation

We now consider solutions of the perturbation equation

$$\frac{\partial F}{\partial \tilde{t}} = -L[F] + R[\upsilon_0], \qquad F(\theta, 0) = 0, \tag{3.2.19}$$

for different ranges of time. Here the operators R and L are defined in Equation 3.2.16 and Equation 3.2.15, and υ_0 and the scaled time variable $\tilde{t}$ is defined in Equation 3.2.10.

Small t expansion

Looking at the case when $t \ll 1$, then we have

$$\gamma \sim 1 - \mu_0 \varepsilon t, \qquad \text{and} \qquad \tilde{t} \sim t.$$

We can then expand F as a power series in $\tilde{t}$ so that

$$F = \sum_{r=1} F_r(\theta) \tilde{t}^r, \qquad F_1 = R[\upsilon_0],$$

and

$$F_r = -\frac{1}{r} L\left[F_{r-1}\right], \qquad r \geq 2.$$

Then, solving for $F_r(\theta)$ and setting $\theta = 0$ gives

$$F(0, \tilde{t}) = 2(\mu_0 - 1)\tilde{t} + 384\tilde{t}^3 + \mathcal{O}(\tilde{t}^4) \tag{3.2.20}$$

and

$$\left.\frac{\partial F}{\partial \theta}\right|_{\theta=0} = -2\mu_1 \tilde{t} + (48 + 8\mu_0)\tilde{t}^2 + \mathcal{O}(\tilde{t}^3). \tag{3.2.21}$$

Looking at the equation for $G(\theta,\tilde{t})$ for $\tilde{t} \ll 1$ shows that $G = O(\tilde{t}^2)$. Hence from Equation 3.2.17 and the definitions of μ_0, μ_1 and $\tilde{t}$, the maximum wave amplitude and its position are given by

$$\eta_{\text{M}} = 2 - 4\varepsilon t + \mathcal{O}\big(\varepsilon t^3, \varepsilon^2 t^2\big)$$

and

$$x_{\text{M}} = 4t + 24t^2\varepsilon + \mathcal{O}\big(\varepsilon t^3, \varepsilon^2 t^2\big)$$

respectively.

Carefully taking account of the higher-order correction terms in the definition of η, θ and $\tilde{t}$ shows that these results are independent of μ_0 and μ_1 for all orders. It is only at later times that the values of μ_0 and μ_1 become important. While the leading-order term in these expansions is valid when $\varepsilon t = o(1)$, the first correction term is only valid when $t = o(1)$, so we now consider the form of solution when $t = \mathcal{O}(1)$.

Solution for t=$\mathcal{O}(1)$

Before considering the solution for F when $t = \mathcal{O}(1)$ we note that when F satisfies Equation 3.2.19, and decay conditions, then there are three integral constraints on F, given by

$$\int_{-\infty}^{\infty} v_0 F \,\mathrm{d}\theta = 2\left(\mu_0 - \frac{8}{15}\right)\tilde{t}, \tag{3.2.22}$$

$$\int_{-\infty}^{\infty} F \,\mathrm{d}\theta = 2\mu_0\tilde{t}, \tag{3.2.23}$$

and

$$\int_{-\infty}^{\infty} \theta F \,\mathrm{d}\theta = 8\left(\mu_0 - \frac{4}{5}\right)\tilde{t}^2 - 2\mu_1\tilde{t}. \tag{3.2.24}$$

These constraints are derived in Appendix A.

Examining the right-hand side of each constraint, we note that there is no choice of μ_0 and μ_1 which results in all three equations being independent of $\tilde{t}$. Therefore, since the right-hand side of each constraint is a function of $\tilde{t}$, we conclude that there is no solution which decays as θ tends to both $+\infty$ and $-\infty$.

However, it is still worthwhile to consider which stationary solutions are possible that are bounded in space, and how they must be modified to simultaneously satisfy the three integral constraints.

Stationary solution

We begin by considering the solution $F = \widehat{F}(\theta)$ in which case $\frac{\partial \widehat{F}}{\partial \bar{t}} = 0$ and Equation 3.2.13 becomes

$$\frac{\partial^3 \widehat{F}}{\partial \theta^3} + 12\frac{\partial(\upsilon_0 \widehat{F})}{\partial \theta} - 4\frac{\partial \widehat{F}}{\partial \theta} = \frac{\partial^2 \upsilon_0}{\partial \theta^2} + \mu_0\left(\upsilon_0 + \frac{\partial(\theta \upsilon_0)}{\partial \theta}\right) + \mu_1 \frac{\partial \upsilon_0}{\partial \theta}. \tag{3.2.25}$$

Then, integrating once with respect to θ, it can be noted that

$$\widehat{F} = \frac{\partial \upsilon_0}{\partial \theta} = -2\tanh\theta\,\mathrm{sech}^2\,\theta$$

is a homogeneous solution of the second-order linear equation obtained. By writing

$$\widehat{F} = H(\theta)\frac{\partial \upsilon_0}{\partial \theta},$$

and solving the second-order equation for $\frac{\partial H}{\partial \theta}$, the particular integral corresponding to each term on the right-hand side of Equation 3.2.25 can be constructed, and the general solution for $\widehat{F}(\theta)$ is given by

$$\begin{aligned}\widehat{F} = {} & \bar{a}\cosh^2\theta + \left(\frac{\mu_0}{8} - \frac{1}{15}\right)\sinh\theta\cosh\theta + \bar{b}\tanh\theta + \left(\bar{b} - \frac{\mu_0}{8} + \frac{1}{5}\right)(1 - \tanh\theta) \\ & + \left(\frac{\mu_0}{8}\theta(2 - \theta\tanh\theta) + \bar{c}\tanh\theta - \bar{d}(1 - \theta\tanh\theta)\right)\mathrm{sech}^2\,\theta,\end{aligned}$$

which has been verified using Maple. Here, $\bar{a}$, $\bar{b}$, and $\bar{c}$ are arbitrary constants and

$$\bar{d} = 3\bar{b} - \frac{3}{8}\mu_0 - \frac{1}{4}\mu_1 + \frac{3}{5}.$$

To ensure that $\widehat{F}$ does not grow exponentially as $\theta \to \pm\infty$, the coefficients of the first two terms must be set to zero and hence, $\bar{a} = 0$ and $\mu_0 = \frac{8}{15}$.

Looking at the next two terms it is clear that the boundary condition $\widehat{F} \to 0$ can not be satisfied at both $\theta = \pm\infty$. It is to be expected that the disturbance tends to zero rapidly in front of the propagating disturbance and hence we set $\bar{b} = 0$. This assumption is validated by the numerical results presented in Subsection 3.2.3. With these conditions imposed, the stationary solution takes the form

$$\begin{aligned}\widehat{F} = \frac{1}{15}\operatorname{sech}^2\theta\left(2\theta + \left(6 - \frac{15}{4}\mu_1\right)(\theta\tanh\theta - 1) - \theta^2\tanh\theta\right) \\ + \frac{2}{15}(1 - \tanh\theta) + \bar{c}\tanh\theta\operatorname{sech}^2\theta.\end{aligned} \tag{3.2.26}$$

Then, since $\mu_0 = \frac{8}{15}$, from Equation 3.2.22 we have

$$\int_{\infty}^{\infty} F\operatorname{sech}^2\theta \mathrm{d}\theta = 0.$$

Imposing this condition on $\widehat{F}$, since $\operatorname{sech}^2\theta$ is exponentially small away from the core region, and using the standard integral identities in Appendix A fixes $\mu_1 = \frac{8}{15}$. Thus $\widehat{F}$ is determined apart from the coefficient $\bar{c}$, so we have

$$\begin{aligned}\widehat{F} &= \widehat{F}_0 + \bar{c}\tanh\theta\operatorname{sech}^2\theta, \\ \widehat{F}_0 &= \frac{1}{15}\operatorname{sech}^2\theta\left(2\theta + \left(6 - \frac{15}{4}\mu_1\right)(\theta\tanh\theta - 1) - \theta^2\tanh\theta\right) \\ &\quad + \frac{2}{15}(1 - \tanh\theta).\end{aligned} \tag{3.2.27}$$

Moreover, since $\mu_0 = \mu_1 = \frac{8}{15}$, then $\gamma(\tau)$, which describes the evolution of the wave amplitude and wave number, is given by solving Equation 3.2.9,

$$\frac{\mathrm{d}\gamma}{\mathrm{d}\tau} = -\frac{8\gamma^3}{15} \quad \Rightarrow \quad \gamma = \left(1 + \frac{16}{15}\tau\right)^{-1/2} \tag{3.2.28}$$

and using (3.2.9), the speed of propagation is given by

$$\frac{\partial\xi}{\partial t} + \varepsilon\frac{\partial\chi}{\partial\tau} = 4\gamma^2 + \frac{8}{15}\gamma\varepsilon.$$

The maximum disturbance amplitude is therefore given by

$$\begin{aligned}\eta_{\text{M}} &= \frac{2}{1+\frac{16}{15}\tau}\left(1+\varepsilon\widehat{F}(0,\tilde{t})+\mathcal{O}(\varepsilon^2)\right)\\ &\sim 2\left(1+\varepsilon\left(\widehat{F}(0,\tilde{t})-\frac{16}{15}t\right)\right), \qquad \text{as} \quad \varepsilon t\to 0.\end{aligned}$$

However, as previously noted, this solution does not satisfy the required boundary as $\theta \to -\infty$. In fact, as

$$\theta \to -\infty, \qquad \widehat{F} \to \frac{4}{15},$$

and hence we write

$$F = \begin{cases} \widetilde{F}(\theta,\tilde{t}), & \theta < -\theta_{\text{M}},\\ \widehat{F}(\theta), & \theta > -\theta_{\text{M}}. \end{cases}$$

Here $\widetilde{F}(\theta,\tilde{t})$ describes the transition from 0 as $\theta \to -\infty$, to $\frac{4}{15}$ at $\theta = -\theta_{\text{M}}$, which we describe as the **tail region**. The value of θ_{M} will be discussed later.

Matching of the stationary solution to the tail solution involves using the integral constraints Equation 3.2.23 and Equation 3.2.24. The contribution to these integrals from the stationary solution is evaluated using the identities in Appendix A, so we have

$$\int_{-\theta_{\text{M}}}^{\infty} \widehat{F}\,\mathrm{d}\theta \sim \frac{4}{15}(\theta_{\text{M}}-1) \tag{3.2.29}$$

and

$$\int_{-\theta_{\text{M}}}^{\infty} \theta\widehat{F}\,\mathrm{d}\theta \sim \frac{1}{15}\left(\frac{\pi^2}{4}-2\theta_{\text{M}}^2\right)+\bar{c} \tag{3.2.30}$$

as $\theta_{\text{M}} \to \infty$.

Oscillatory tail solution

In the tail region ($\theta > -\theta_{\text{M}}$), the leading order solution $v_0(\theta)$ is exponentially small and hence $R[v_0] \to 0$. Thus, for the tail region we consider the solution of

$$\frac{\partial\widetilde{F}}{\partial\tilde{t}}+\frac{\partial^3\widetilde{F}}{\partial\theta^3}-4\frac{\partial\widetilde{F}}{\partial\theta}=0, \tag{3.2.31}$$

which is derived using Equation 3.2.15 and Equation 3.2.13 with $\upsilon_0 \to 0$ and $F = \widetilde{F}$. We also require that

$$\widetilde{F} \to \frac{4}{15}, \quad \frac{\partial \widetilde{F}}{\partial \theta} \to 0, \quad \text{as} \quad \theta \to -\theta_{\text{M}}, \quad \text{and} \quad \widetilde{F} \to 0 \quad \text{as} \quad \theta \to -\infty,$$

in order to match to the stationary solution. Then in terms of a similarity variable z, given by

$$z = \frac{\theta + 4\tilde{t} + C}{T}, \qquad \text{where} \qquad T = (3\tilde{t})^{1/3},$$

Equation 3.2.31 becomes

$$T\frac{\partial \widetilde{F}}{\partial T} + \frac{\partial^3 \widetilde{F}}{\partial z^3} - z\frac{\partial \widetilde{F}}{\partial z} = 0, \tag{3.2.32}$$

and the matching condition for $\widetilde{F}$ becomes

$$\widetilde{F} \to \frac{4}{15}, \quad \frac{\partial \widetilde{F}}{\partial z} \to 0, \quad \text{as} \quad z \to \infty.$$

The solution of Equation 3.2.32 can be obtained by taking the Fourier transform with respect to z. However, a more concise derivation is possible by observing that $\frac{\partial \widetilde{F}}{\partial z} = \text{Ai}(z)$ is one solution and writing $\widetilde{F}$ as a spatial convolution with the Airy function

$$\widetilde{F} = \int_{-\infty}^{\infty} g(z - y, T)\text{Ai}(y)\text{d}y$$

which we rewrite

$$\widetilde{F} = g * \text{Ai} \tag{3.2.33}$$

where $*$ denotes the spatial convolution. The function $g(z, T)$ is obtained by substituting Equation 3.2.33 into Equation 3.2.32 to give

$$T\frac{\partial g}{\partial T} = z\frac{\partial g}{\partial z}.$$

This is satisfied if $g(z,T) = \Psi(Tz)$ for any Ψ such that the convolution integral exists. Thus the leading-order solution for the tail is given by

$$\widetilde{F}(z,\tilde{t}) = \int_{-\infty}^{\infty} \Psi(T(z-y))\,\mathrm{Ai}(y)\,\mathrm{d}y.$$

We note that when comparing the analytic solution in the tail region with a numerical solution, it is more convenient to consider the first derivative of F since the matching condition is $\frac{\partial \widetilde{F}}{\partial z} \to 0$ as $z \to \pm\infty$.

Using the solution above we can then write

$$\frac{\partial \widetilde{F}}{\partial z} = T\int_{-\infty}^{\infty} \Phi(T(z-y))\,\mathrm{Ai}(y)\,\mathrm{d}y, \tag{3.2.34}$$

where $\frac{\mathrm{d}\Psi}{\mathrm{d}z} = \Phi(z)$.

As $z \to \infty$, the tail solution $\widetilde{F}$ must match to the stationary solution (3.2.27), and it is found that

$$\int^{z} \widetilde{F}\mathrm{d}z, \quad \text{and} \quad \int^{z} z\widetilde{F}\mathrm{d}z$$

are required in the matching. In Section A.3 it is shown that if Φ decays exponentially as $|z| \to \infty$, then

$$\widetilde{F} \to K_0, \qquad \int_{-\infty}^{z} \widetilde{F}\mathrm{d}z \to K_0 z - \frac{K_1}{T},$$

and

$$\int_{-\infty}^{z} z\widetilde{F}\mathrm{d}z \to \frac{1}{2}\left(K_0 z^2 - \frac{K_2}{T^2}\right),$$

where

$$K_0 = \int_{-\infty}^{\infty} \Phi(x)\,\mathrm{d}x, \qquad K_1 = \int_{-\infty}^{\infty} x\Phi(x)\,\mathrm{d}x, \qquad K_2 = \int_{-\infty}^{\infty} x^2\Phi(x)\,\mathrm{d}x.$$

Matching of the stationary and tail solutions

To summarise the structure of the solution that we have constructed so far, we have

$$F(\theta,T)=\begin{cases}\widetilde{F}=\int_{-\infty}^{\infty}\Psi(Ty)\mathrm{Ai}(z-y)\,\mathrm{d}y, & \theta<-\theta_{\mathrm{M}},\\ \\ \widehat{F}=\widehat{F}_0+\bar{c}\tanh\theta\,\mathrm{sech}^2\theta, & \theta>-\theta_{\mathrm{M}},\end{cases}\tag{3.2.35}$$

where

$$\Psi(x)=\int_{-\infty}^{x}\Phi(x')\,\mathrm{d}x',\quad\text{and}\quad z=\frac{\theta+4\tilde{t}+C}{T}$$

and $\widehat{F}_0$ is given by Equation 3.2.27. In the region about $\theta=-\theta_{\mathrm{M}}$ both $\widehat{F}$ and $\widetilde{F}$ are constant, and it is in this region that the matching occurs. This fixes $K_0=\frac{4}{15}$. The constants $\bar{c}$ and C are now determined in terms of $\Phi(x)$ using the integral constraints.

Using Equation 3.2.29 and Equation 3.2.30, we have

$$\begin{aligned}\int_{-\infty}^{\infty}F\,\mathrm{d}\theta&=\int_{-\theta_{\mathrm{M}}}^{\infty}\widehat{F}\,\mathrm{d}\theta+T\int_{-\infty}^{z_{\mathrm{M}}}\widetilde{F}\,\mathrm{d}z\\&=\frac{4}{15}(\theta_{\mathrm{M}}-1)+\frac{4}{15}\big(4\tilde{t}-\theta_{\mathrm{M}}+C\big)-K_1\\&=\frac{16}{15}\tilde{t}+\frac{4}{15}(C-1)-K_1,\end{aligned}$$

which is consistent with Equation 3.2.23 if

$$C=1+\frac{15}{4}K_1.$$

It can be shown that the tail solution $\widetilde{F}$ is unaltered by the choice of value for K_1, so we set $K_1=0$, and hence

$$z=(3\tilde{t})^{-1/3}(\theta+4\tilde{t}+1).\tag{3.2.36}$$

Similarly, using Equation 3.2.29 and Equation 3.2.30, we have

$$\begin{aligned}\int_{-\infty}^{\infty}\theta F\,\mathrm{d}\theta &= \int_{-\theta_{\mathrm{M}}}^{\infty}\theta\widehat{F}\,\mathrm{d}\theta + T\int_{-\infty}^{z_{\mathrm{M}}}\left(Tz-(4\tilde{t}+1)\right)\widetilde{F}\,\mathrm{d}z\\ &= \frac{1}{15}\left(\frac{\pi^2}{4}-2\theta_{\mathrm{M}}^2\right)+\bar{c}+\frac{2}{15}(\theta_{\mathrm{M}}^2-(1+4\tilde{t})^2)-\frac{1}{2}K_2\\ &= -\frac{32}{15}\tilde{t}^2-\frac{16}{15}\tilde{t}+\bar{c}-\frac{1}{15}\left(2-\frac{1}{4}\pi^2\right)-\frac{1}{2}K_2.\end{aligned}$$

This is consistent with the third integral constraint given in Equation 3.2.24 if

$$\bar{c}=\frac{1}{15}\left(2-\frac{1}{4}\pi^2\right)+\frac{1}{2}K_2.$$

Thus, assuming that the function which determines the tail solution, $\Phi(x)$, is known then the perturbation solution governed by Equation 3.2.13 is known for all $\tilde{t}$ once the stationary form of the solution is reached. However, without knowledge of the small $\tilde{t}$ solution, $\Phi(x)$ is undetermined, except that

$$\int_{-\infty}^{\infty}\Phi(x)\,\mathrm{d}x=\frac{4}{15}\qquad\text{and}\qquad\int_{-\infty}^{\infty}x\Phi(x)\,\mathrm{d}x=0,$$

and the stationary solution is related to $\Phi(x)$ via

$$\bar{c}=\frac{1}{15}\left(2-\frac{1}{4}\pi^2\right)+\frac{1}{2}\int_{-\infty}^{\infty}x^2\Phi(x)\mathrm{d}x. \tag{3.2.37}$$

In Subsection 3.2.3, we will compare these asymptotic predictions with numerical results, focussing in particular on the development of the tail behind the main disturbance, and the maximum amplitude η_{M}. However, first the validity of this composite description must be considered as t increases.

In the stationary region, it has been demonstrated that the perturbation $\delta F(\theta,t)$ is small compared with the leading-order term, as long as $\delta=\frac{\varepsilon}{\gamma}$ is small. Now, since

$$\gamma\sim(\varepsilon t)^{-1/2}\quad\text{as}\quad t\to\infty,$$

then the first perturbation term remains small compared with the leading-order term until $t=\mathcal{O}(\varepsilon^{-3})$. However, it is not guaranteed that the next perturbation term $\delta^2G(\theta,t)$

is smaller than $\delta F(\theta,t)$. In other words, the first non-uniformity in the expansion may occur when the second and third terms in the perturbation expansion become comparable in size.

By considering the equation for G, there will be no free parameter in the particular integral of the stationary solution. This points to the presence of a term proportional to t in the stationary solution for G, leading to a non-uniformity in the expansion when $\varepsilon t = \mathcal{O}(1)$. This is seen more precisely by observing that

$$\frac{\mathrm{d}}{\mathrm{d}t}\left(\int_{-\infty}^{\infty} v_0 G\,\mathrm{d}\theta\right) = \int_{-\infty}^{\infty} v_0\left(R[F] - \mu_0 F - 6\frac{\partial(F^2)}{\partial\theta}\right)\mathrm{d}\theta,$$

where the right-hand side is a non-zero constant. This expression indicates how the breakdown in the asymptotic description can be eliminated and this is described in the next part of the analysis.

Solution for τ=$\mathcal{O}(1)$

In the previous section $F(\theta,t)$ was determined by assuming that a stationary solution develops which is independent of t. It was seen that this represents a small perturbation until $t = \mathcal{O}(\varepsilon^{-3})$, but that non-uniformity in the perturbation series may arise earlier due to the next term $\delta^2 G(\theta,t)$ becoming comparable in size to $\delta F(\theta,t)$. This can be analysed by recognising that the stationary solution is not truly independent of time, but instead evolves on the slow time scale $\tau = \varepsilon t$.

Thus, in the stationary core we have $F = F(\theta,\tau)$, and hence Equation 3.2.13 becomes

$$L[F] = R[v_0], \tag{3.2.38}$$

and Equation 3.2.14 becomes

$$L[G] = R[F] - \mu_0 F - 6\frac{\partial(F^2)}{\partial\theta} - \frac{1}{\gamma^2}\frac{\partial F}{\partial\tau}. \tag{3.2.39}$$

The solvability conditions are now subtly different from those used in the asymptotic

analysis for the case $t = \mathcal{O}(1)$. Then, noting from Appendix A that

$$\int_{-\infty}^{\infty} v_0 L[V]\,\mathrm{d}\theta = 0$$

for any function $V(\theta)$ that decays sufficiently rapidly to zero as $\theta \to \pm\infty$, since $v_0 = \operatorname{sech}^2\theta$ the solvability conditions become:

$$\int_{-\infty}^{\infty} v_0\left(\frac{\partial^2 v_0}{\partial\theta^2} + \mu_0\left(v_0 + \frac{\partial(\theta v_0)}{\partial\theta}\right) + \mu_1\frac{\partial v_0}{\partial\theta}\right)\mathrm{d}\theta = 0,$$
$$\int_{-\infty}^{\infty} v_0\left(\frac{\partial^2 F}{\partial\theta^2} + \mu_0\frac{\partial(\theta v)}{\partial\theta} + \mu_1\frac{\partial F}{\partial\theta} - 6\frac{\partial(F^2)}{\partial\theta} - \frac{1}{\gamma^2}\frac{\partial F}{\partial\tau}\right)\mathrm{d}\theta = 0.$$

The first of these integrals can be evaluated using the integral identities involving hyperbolic functions given in Appendix A, which fixes $\mu_0 = \frac{8}{15}$ as before. However, μ_1 is left undetermined at this order. The stationary solution for F is given by Equation 3.2.26 which we write in the form

$$F = \overline{F} + \mu_1(\tau)g + \widetilde{c}(\tau)\tanh\theta\operatorname{sech}^2\theta, \tag{3.2.40}$$

where

$$\overline{F} = \frac{1}{15}\big(2(1-\tanh\theta) + \operatorname{sech}^2\theta\big(2\theta - \theta^2\tanh\theta - 6(1-\theta\tanh\theta)\big)\big),$$
$$g = \frac{1}{4}(1-\theta\tanh\theta)\operatorname{sech}^2\theta.$$

Substituting into the second solvability condition, all the terms involving $\widetilde{c}$ cancel out, and so the evolution of $\widetilde{c}$ with τ can not be determined at this order. The remaining terms simplify to

$$I_1 + \mu_1 I_2 = \frac{1}{\gamma^2}\frac{\mathrm{d}\mu_1}{\mathrm{d}\tau}I_3,$$

where

$$I_1 = \int_{-\infty}^{\infty} v_0\frac{\partial}{\partial\theta}\left(\frac{\partial\overline{F}}{\partial\theta} + \mu_0\theta\overline{F} - 6\overline{F}^2\right)\mathrm{d}\theta = \frac{176}{225},$$
$$I_2 = \int_{-\infty}^{\infty} v_0\frac{\partial}{\partial\theta}\left(\frac{\partial g}{\partial\theta} + \mu_0\theta g - 12g\overline{F} + \overline{F}\right)\mathrm{d}\theta = -\frac{2}{5},$$
$$I_3 = \int_{-\infty}^{\infty} v_0 g\,\mathrm{d}\theta = \frac{1}{4}.$$

Here the integrals are evaluated using standard results for hyperbolic functions and checked using MAPLE. Using these numerical values, the ordinary differential equation for $\mu_1(\tau)$ can be written as

$$G\frac{\mathrm{d}\mu_1}{\mathrm{d}\tau} - 3\frac{\partial\gamma}{\partial\tau}\mu_1 = -\frac{88}{15\gamma^4}\frac{\partial\gamma}{\partial\tau}. \tag{3.2.41}$$

Then, using the result

$$\frac{\partial\gamma}{\partial\tau} = -\frac{8}{15}\gamma^3$$

from Equation 3.2.28, we can solve Equation 3.2.41 to give

$$\mu_1(\tau) = \frac{88}{45} + C\gamma^3.$$

The stationary solution Equation 3.2.40 breaks down as $\tau \to 0$, but can be matched to the $t = \mathcal{O}(1)$ solution given by Equation 3.2.27. This then fixes $\mu_1(0) = \frac{8}{15}$ and hence

$$\mu_1(\tau) = \frac{8}{45}\left(11 - 8\gamma^3\right).$$

However, μ_0 does not vary with τ, and hence the expression for $\gamma(\tau)$ previously derived for $t = \mathcal{O}(1)$ remains valid when $\tau = \mathcal{O}(1)$. Thus the stationary solution, which is valid for $\varepsilon t = \mathcal{O}(1)$, is given by

$$\eta(x,t) = 2\gamma\left(\gamma\upsilon_0(\theta) + \varepsilon\left(\overline{F}(\theta) + \frac{8}{15}(11 - 8\gamma^3)g(\theta)\right)\right), \tag{3.2.42}$$

where

$$\gamma = \left(1 + \frac{16}{15}\tau\right)^{-\frac{1}{2}}$$

and where

$$\theta = \gamma\left(x + \frac{1}{\varepsilon}\left(\frac{15}{2}\log\gamma\right) - \left(\frac{11}{3\gamma} + \frac{4}{3}\gamma^2 - 5\right)\right). \tag{3.2.43}$$

The fact that $\widetilde{c}(\tau)$ is not determined at this order is hardly surprising since the term $\varepsilon c\tanh\theta\,\mathrm{sech}^2\,\theta$ in the perturbation series for υ can be interpreted as an $O(\varepsilon)$ correction to the propagation speed and therefore would be determined at the next order.

Summary of asymptotic results

The asymptotic analysis presented has demonstrated the solution to be a slowly varying core with propagation speed varying on the slow time scale τ, followed by a tail evolving on the faster time scale and consisting of a near horizontal shelf followed by a decaying oscillation. The structure of the tail is described by a convolution integral involving a single function undetermined by the asymptotic analysis. In the next section this function is determined numerically, but the main means of validating the asymptotic theory is by considering the maximum amplitude of the wave and its position.

From Equation 3.2.17, the asymptotic prediction of the maximum amplitude for the different time scales is given by

$$\eta_{\text{M}} = \begin{cases} 2(1-2\varepsilon t)\,, & \text{for } t = \text{o}(1) \qquad (3.2.44a) \\ 2\gamma^2\left(1+\varepsilon\tilde{F}(0,\tilde{t})\right), & \text{for } t = \mathcal{O}(1), \qquad (3.2.44b) \\ 2\gamma^2\left(1+\varepsilon\left(\dfrac{2}{9\gamma}-\dfrac{16}{45}\gamma^2\right)\right), & \text{for } t = \mathcal{O}(\varepsilon^{-1}), \qquad (3.2.44c) \end{cases}$$

where $\gamma = (1+\frac{16}{15}\varepsilon t)^{-1/2}$, as before. The corresponding results for the position of the maximum amplitude are given by

$$x_{\text{M}} = \begin{cases} 4t + 24\varepsilon t^2, & t = \text{o}(1) \qquad (3.2.45a) \\ 4t + \varepsilon\left(\dfrac{1}{2}\dfrac{\partial\tilde{F}}{\partial\theta}\bigg|_{\theta=0} + \dfrac{8}{15}t - \dfrac{32}{15}t^2\right), & t = \mathcal{O}(1) \qquad (3.2.45b) \\ \dfrac{15}{4\varepsilon}\log\left(\dfrac{1}{\gamma}\right) + \dfrac{11}{3\gamma} + \dfrac{4}{3}\gamma^2 - 5 + \dfrac{\varepsilon}{2\gamma^2}\widetilde{c}(\tau), & t = \mathcal{O}(\varepsilon^{-1}). \qquad (3.2.45c) \end{cases}$$

The functions $\widetilde{F}(0,\tilde{t})$ and $\frac{\partial}{\partial\theta}\widetilde{F}(0,\tilde{t})$ are obtained from the numerical solution of Equation 3.2.19, with the asymptotic analysis for the case $t = \mathcal{O}(1)$ demonstrating that

$$\widetilde{F}(0,\tilde{t}) \to -\frac{2}{15}, \quad \text{and} \quad \frac{\partial\widetilde{F}}{\partial\theta}\bigg|_{\theta=0} \to \bar{c} \quad \text{as} \quad \tilde{t}\to\infty.$$

As noted earlier, the function $\widetilde{c}(\tau)$ can only be determined by considering higher-order terms, which is not pursued here. However, as $\tau \to 0$ then $\widetilde{c} \to \bar{c}$, and hence as $\varepsilon t \to 0$ the final results for both maximum amplitude and position match the $t = \mathcal{O}(1)$ result.

Similarly letting $t \to 0$ and using the asymptotic form of $\widetilde{F}(0,\tilde{t})$ and $\frac{\partial}{\partial\theta}\widetilde{F}(0,\tilde{t})$ given in the analysis for the case $t = \mathcal{O}(1)$, Equation 3.2.44b and Equation 3.2.45b agree with Equation 3.2.44a and Equation 3.2.45a.

3.2.3 Numerical results

Numerical solutions of the KdV-Burgers' equation (3.2.3) and the linear perturbation equation (3.2.13) are obtained using a pseudospectral scheme, but with linear terms absorbed into an integrating factor following the method of Milewski and Tabak (1999), as discussed in Chapter 2. The Fourier transform of Equation 3.2.3 takes the form

$$\frac{\partial\widehat{\eta}}{\partial t} + 3\mathrm{i}k\mathcal{F}\left[(\mathcal{F}^{-1}[\widehat{\eta}])^2\right] - \mathrm{i}k^3\widehat{\eta} = -\varepsilon k^2\widehat{\eta}. \tag{3.2.46}$$

Then, writing

$$V = \mathrm{e}^{h(k)t}\widehat{\eta},$$

where $h(k) = -\mathrm{i}k^3 + \varepsilon k^2$, Equation 3.2.46 becomes

$$\frac{\partial V}{\partial t} = -3\mathrm{i}k\mathrm{e}^{h(k)t}\mathcal{F}\left[\left(\mathcal{F}^{-1}[\mathrm{e}^{-h(k)t}V]\right)^2\right].$$

This scheme was first used to solve the dimensionless KdV-B equation (3.2.3) with $\varepsilon = 0.1$, and initial condition

$$\eta = 2\,\mathrm{sech}^2\,x.$$

Guided by the asymptotic analysis that predicts a slowly decaying tail behind a stationary core, propagating to the right, a large spatial range $[-40\pi, 40\pi]$ was taken, with $N = 2^{15}$ spatial points, giving a spatial step size $\Delta x \approx 0.04$. We have chosen to use a large spatial range and time step in order to capture a more detailed view of the decaying tail. This also ensures that we can generate results for larger times without any interference to the main peak from the oscillating tail due to using a periodic numerical domain.

Results are given in Figure 3.2.1 for $t = 10, 20$, illustrating the main disturbance propagating to the right at speed $C \approx 4$ with the maximum amplitude decreasing with

time. Behind the core is a constant elevated shelf, extending back to $x \approx 0$, followed by a decaying oscillatory tail, which agrees with the asymptotic analysis described in Subsection 3.2.2. Direct comparison of the numerical results with the analytical results are discussed in the next part of the analysis. The asymptotic analysis presented in

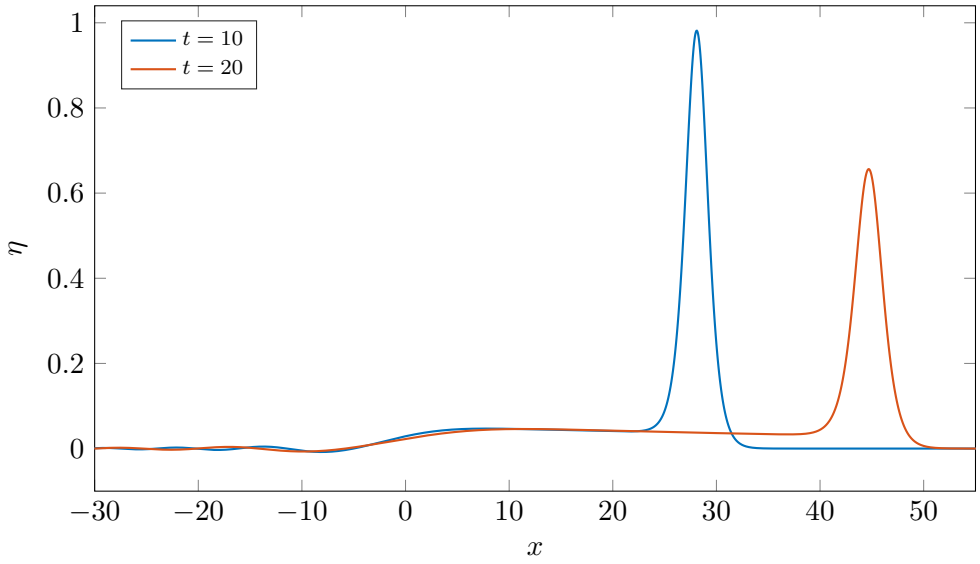

Figure 3.2.1: Plot of $\eta(x,t)$ for $\varepsilon = 0.1$ at times $t = 10$, 20, showing the decay in amplitude with increasing t and the development of a decaying tail.

Subsection 3.2.2 relates to the solution of the perturbation equation Equation 3.2.13. While this is a linear equation for $F(\theta,\tilde{t})$, a similar scheme to that described above is used. The presence of the $\frac{\partial(\upsilon_0 F)}{\partial\theta}$ term requires two discrete Fourier transforms, which is akin to the treatment of the nonlinear term in the first scheme, with the other terms that are linear in F removed using the integrating factor $\mathrm{e}^{h_1(k)\tilde{t}}$, where $h_1(k) = -\mathrm{i}k^3 - 4\mathrm{i}k$. The system to be solved is then

$$\frac{\partial V}{\partial\tilde{t}} = -12\mathrm{i}k\mathrm{e}^{h_1(k)\tilde{t}}\mathcal{F}\left[\upsilon_0\mathcal{F}^{-1}\left[\mathrm{e}^{-h_1(k)\tilde{t}}V\right]\right] + \mathcal{F}\left[\frac{\partial^2\upsilon_0}{\partial\theta^2} + \frac{8}{15}\left(\upsilon_0 + \frac{\partial(\theta\upsilon_0)}{\partial\theta} + \frac{\partial\upsilon_0}{\partial\theta}\right)\right],$$

where $\upsilon_0 = \operatorname{sech}^2\theta$ as before. Note that the final transform term is independent of $\tilde{t}$ and hence is only evaluated once.

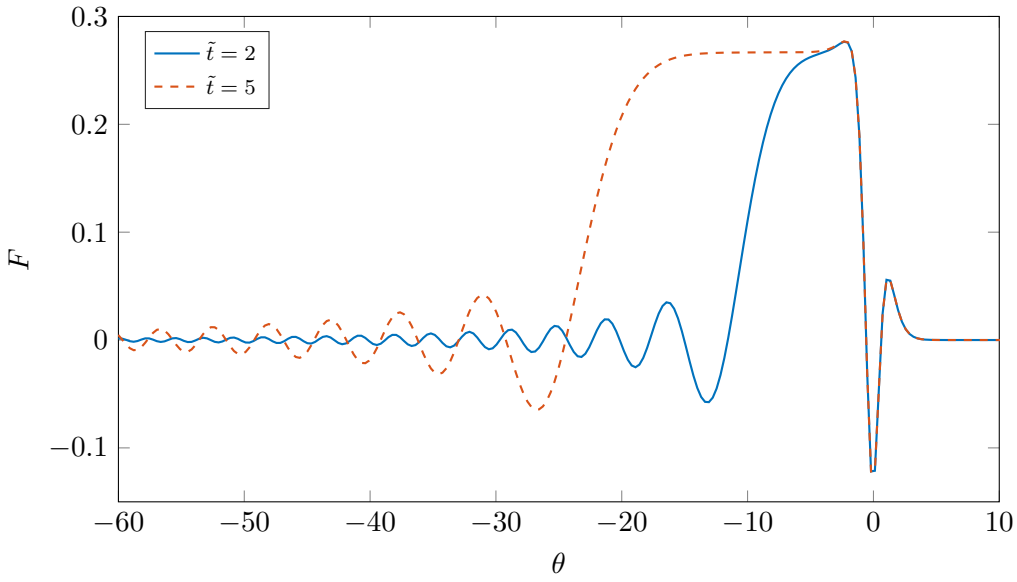

Figure 3.2.2: Plot of numerical solution $F(\theta, \tilde{t})$ for $\tilde{t} = 2$ and $\tilde{t} = 5$ illustrating the development of a stationary core about $\theta = 0$, a constant shelf behind the core, followed by a slowly decaying oscillating tail.

Numerical results for perturbation equation

We now consider numerical solutions of the perturbation equation (3.2.14). In figure 3.2.2, numerical results for $F(\theta, \tilde{t})$ are plotted for $\tilde{t} = 2, 5$. The first thing to note is that the core stationary solution (the solution around $\theta = 0$) has already approached a stationary form at $\tilde{t} = 2$. Ahead of the core, the solution decreases rapidly to zero confirming the stationary solution analysis presented in Subsection 3.2.2.

Behind the stationary core, a shelf of constant amplitude has appeared by $\tilde{t} = 5$ and the matching range between core and the tail discussed in the matching analysis corresponds to the region $-15 < \theta < -5$. Results for larger $\tilde{t}$ show that the extent of the shelf increases as $\tilde{t}$ increases. The stationary form of the solution around $\theta = 0$ is now compared with the predicted analytic form of the stationary core (Equation 3.2.27). Focussing first on the value of $F(0, \tilde{t})$, the numerical results confirm the $\tilde{t}$ limit $F(0, \tilde{t}) \to -\frac{2}{15}$ from Equation 3.2.27, with $F(0, \tilde{t})$ attaining 95% of its limiting value when $\tilde{t} = 0.7$ and 99% by $\tilde{t} = 1.1$. The undetermined coefficient $\bar{c}$ appearing in the stationary solution can be directly extracted from the numerical results in a number of different ways. Directly from

the numerical solution,

$$\left.\frac{\partial F}{\partial \theta}\right|_{\theta=0} \to \bar{c} \quad \text{as} \quad t \to \infty.$$

Alternatively, using the integral constraint Equation 3.2.30

$$\bar{c} \sim \int_{-\theta_M}^{\infty} \theta \widehat{F}\, \mathrm{d}\theta - \frac{1}{15}\left(\frac{\pi^2}{4} - 2{\theta_M}^2\right),$$

where θ_M is taken to be in the overlap region. A third method for calculating $\bar{c}$ comes by comparing the numerically computed value of $F - \widehat{F}_0$ with

$$\bar{c} \tanh\theta \operatorname{sech}^2\theta \quad \text{at} \quad \theta = \operatorname{arctanh}\left(\frac{1}{\sqrt{3}}\right),$$

the position of the maximum of $\tanh\theta \operatorname{sech}^2\theta$. At $\tilde{t} = 5$ all three methods give

$$\bar{c} = 0.0451$$

correct to 3 significant figures.

In Figure 3.2.3 numerical results for $\tilde{t} = 0.5, 1, 2$ are compared with the analytic results using the numerically obtained value of $\bar{c}$. It is seen that there is good agreement between numerical and analytic solutions over the main part of the stationary core, even for $\tilde{t} = 0.5$. When $\tilde{t} = 2$, results are indistinguishable over the range $-5 < \theta < 5$. Looking now at the tail region, it was shown in the tail region analysis of Subsection 3.2.2 that the solution $\widetilde{F}$ can be written in terms of a single universal function $\Phi(x)$, The method used to extract this function from the numerical solution is to compare the derivative of the numerical solution and that of the analytic solution. From Equation 3.2.34, we have the convolution

$$\frac{\partial \widetilde{F}}{\partial z} = h * \mathrm{Ai}(z),$$

where

$$h(z, \tilde{t}) = T\Phi(Tz), \qquad T = (3\tilde{t})^{1/3},$$

and where

$$z = (3\tilde{t})^{-1/3}(\theta + 4\tilde{t} + 1)$$

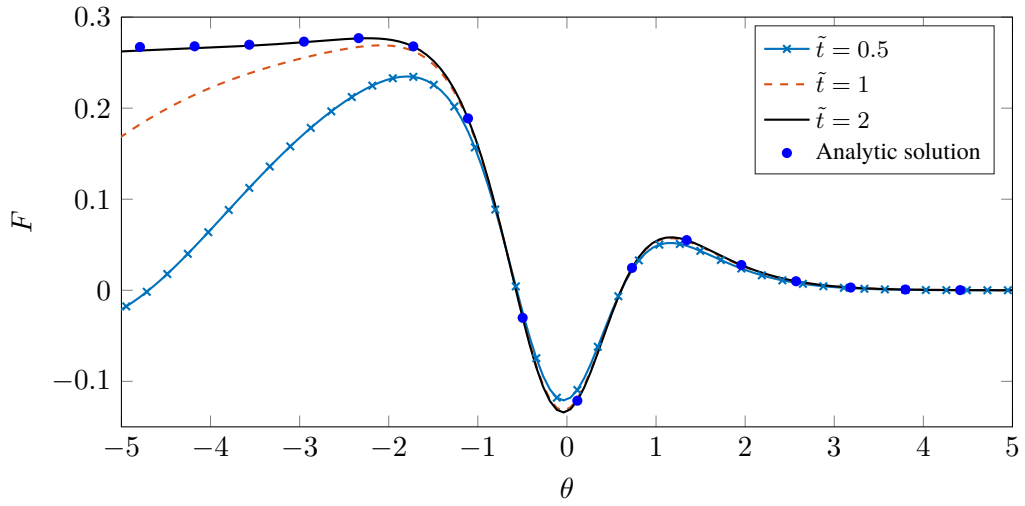

Figure 3.2.3: Plot of numerical results for $F(\theta, \tilde{t})$ for $\tilde{t} = 0.5$, 1.0 and 2.0 along with the analytic solution Equation 3.2.27 with $\bar{c} = 0.0451$ (symbols).

from Equation 3.2.36. Taking Fourier transforms with respect to z and using the convolution theorem gives

$$h(z, \tilde{t}) = \mathcal{F}^{-1}\left[\frac{\mathcal{F}\left[\frac{\partial \tilde{F}}{\partial z}\right]}{\exp\left(\frac{\mathrm{i}k^3}{3}\right)}\right], \tag{3.2.47}$$

since

$$\mathcal{F}[\mathrm{Ai}] = \exp\left(\frac{\mathrm{i}k^3}{3}\right).$$

Then to obtain a numerical approximation of h, and hence Φ, we define $Q(z, t)$ to be the computed value of $\frac{\partial F}{\partial z}$ for $\theta < \theta_{\mathrm{M}}$, and 0 elsewhere. Thus, $h(z, \tilde{t})$ is then given by

$$h(z, \tilde{t}) = \mathcal{F}^{-1}\left[\frac{\mathcal{F}[Q]}{\exp\left(\frac{\mathrm{i}k^3}{3}\right)}\right].$$

The exact value of the Fourier transform of the Airy function is used rather than the discrete transform over the finite range of the numerical calculation. This proves a better approach since the slow decay of $\mathrm{Ai}(z)$, accompanied by a shortening wavelength as $z \to -\infty$, leads to inaccuracy in the large wave number components of the discrete transform of the Airy function over a finite spatial range.

The function $\Phi(x)$, extracted from the numerical solution at $\tilde{t} = 5$, is shown in Figure 3.2.4. The extraction of $\Phi(x)$ at $\tilde{t} = 10$ produced indistinguishable results. Thus

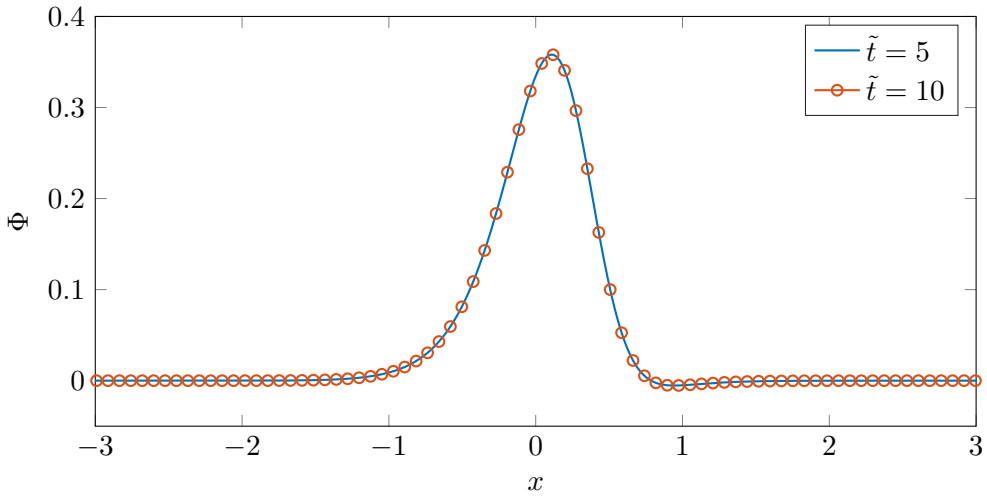

Figure 3.2.4: Plot of $\Phi(x)$ for $\tilde{t} = 5$ and $\tilde{t} = 10$ with h extracted from the numerical solution of F using Equation 3.2.47.

the extracted value of Φ can be used to give the solution in the tail region for all $\tilde{t} > 5$. Finally, the computed value of

$$\int_{-\infty}^{\infty} x^2 \Phi(x) \mathrm{d}x = 0.153$$

which, using Equation 3.2.37, gives a value of $\bar{c} = 0.0453$ which agrees to within 0.5% of the value extracted from the stationary solution.

Comparison between numerical results and perturbation analysis

We now consider how the numerical solution of the full nonlinear equation (3.2.3) compares with the perturbation expansion. If we consider the perturbation form given by Equation 3.2.12, we define

$$F_{\mathrm{N}}(\theta, t) = \frac{\gamma}{\varepsilon}\left(\frac{\eta_{\mathrm{N}}}{2\gamma^2} - \operatorname{sech}^2\theta\right), \qquad \gamma = \left(1 + \frac{16}{15}\varepsilon t\right)^{-\frac{1}{2}}, \tag{3.2.48}$$

where the N subscript denotes the numerical solution, and θ is given by (3.2.43). If we consider $\varepsilon \ll 1$, and $1 \ll t \ll \varepsilon^{-1}$, then F_{N} should agree with the asymptotic result Equation 3.2.35. For the stationary region, where $\theta = \mathcal{O}(1)$, in Subsection 3.2.2 it was seen that as t increases the asymptotic solution F approaches the stationary form $\widehat{F}$, with excellent agreement for $\tilde{t} > 2$.

The most direct check of the validity of the asymptotic predictions presented in Subsection 3.2.2 is by considering the maximum in the waveform and its location, and comparing numerical results with the asymptotic results. In figure Figure 3.2.5, the asymptotic prediction of the maximum amplitude of the disturbance is compared with the numerical results for $\varepsilon = 0.1$. The numerical results are compared with the two asymptotic predictions from (3.2.44b) and (3.2.44c), given by

$$\eta_{\text{M1}} = \frac{2}{1+\frac{16}{15}\varepsilon t}\left(1-\frac{2}{15}\varepsilon\right), \tag{3.2.49}$$

$$\eta_{\text{M2}} = \frac{2}{1+\frac{16}{15}\varepsilon t}\left(1+\varepsilon\left(\frac{2}{9}\left(1+\frac{16}{15}\varepsilon t\right)^{1/2}-\frac{16}{45}\left(1+\frac{16}{15}\varepsilon t\right)^{-1}\right)\right). \tag{3.2.50}$$

As noted earlier, the term $2/(1+\frac{16}{15}\varepsilon t)$ remains valid as a leading-order approximation

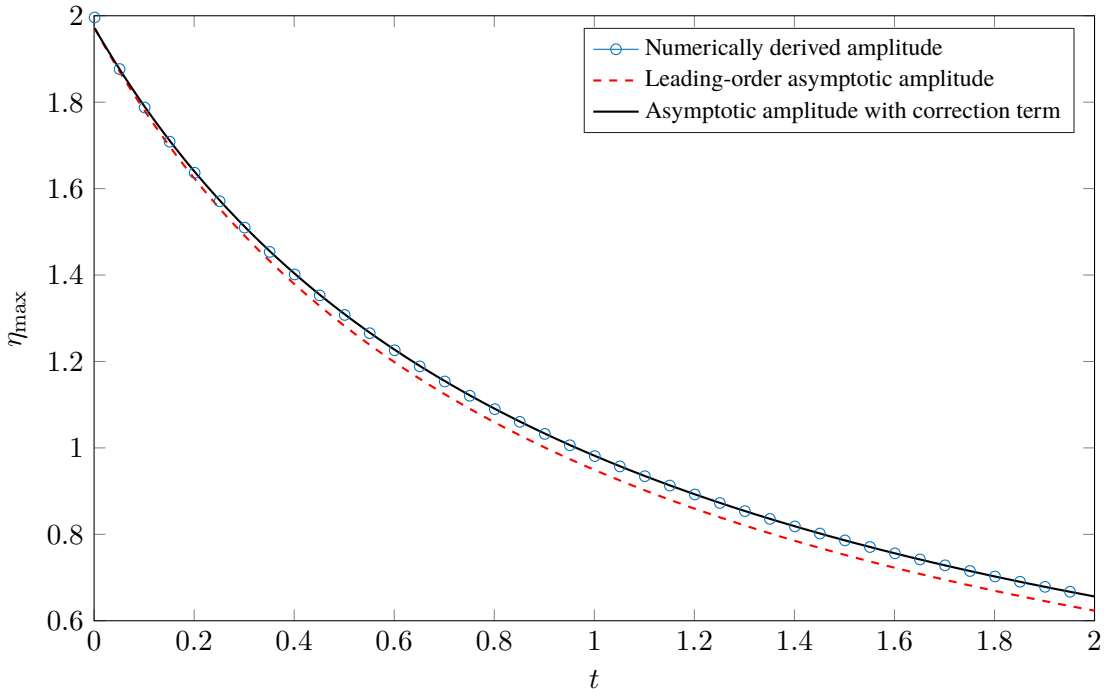

Figure 3.2.5: Comparison of the maximum value of η as a function of $\tau = \varepsilon t$ obtained numerically (circles) for $\varepsilon = 0.1$ and the asymptotic predictions η_{M1} (solid line) given by Equation 3.2.49 and η_{M2} (dashed line) given by Equation 3.2.50.

of the amplitude across the whole range of time studied, though the first correction term becomes comparable with the leading-order term when $t = \mathcal{O}(\varepsilon^{-3})$, at which point the wave amplitude is $\mathcal{O}(\varepsilon^2)$. Excellent agreement is seen over a large time range as illustrated in Figure 3.2.5, and also when comparing x_{M} with its numerical solution, although this is not shown here.

3.3 Summary of chapter

In this chapter we have produced a description of the evolution of a weakly damped solitary wave due to the inclusion of a diffusive second-order parameter governed by the Korteweg-de Vries-Burgers' equation. We began by deriving an asymptotic function describing the leading-order decay in wave amplitude for small values of time t. In order to extract the amplitude as a function of time we used a solvability condition similar to the work presented in Mei (1989).

Comparisons with the numerically derived approximation to the amplitude led to further analysis of the asymptotic correction term at the next order covering three different time regimes: $t = o(1)$, $t = \mathcal{O}(1)$ and $t = \mathcal{O}(\varepsilon^{-1})$. We drew comparisons with other analyses applicable to the different time regimes and all asymptotic results were validated by careful comparisons with the numerical results generated using the integrating factor method discussed in Chapter 2.

Of particular note is the tail region analysis leading to a description of the tail as a convolution of the Airy function and a characteristic function specific to the KdV-Burgers' equation (3.1.2). The form of this function was extracted from the numerical solution, and while other perturbations $\varepsilon\mathcal{R}(\eta)$ to the KdV equation (1.3.1), as given by Equation 3.0.1 will have different characteristic functions describing the tail region, exactly the same methods may be used to determine such a function.

The transformation of the wave structure in the evolution of the damped solitary wave is significant and appears in subsequent results presented in the thesis. We note in particular the elevated constant shelf followed by the decaying tail region to be a general transformation of the wave form for a dissipated sech^2 solitary wave. This is further discussed in Chapter 4 where we present results, with comparisons, for a solitary wave with decaying amplitude due to a no-slip condition at the solid bottom boundary. In addition to this, further comparisons are made in Chapter 5 where we present solitary waves experiencing decay due to an insoluble surfactant at the fluid surface.

4

Flows with tangential surface stress

Directly continuing the work of presented in Hammerton and Bassom (2013), we now consider flows with a variable surface tension parameter. The previous work considered two scenarios resulting in variable surface tension and leading to a tangential surface stress condition at the fluid surface. The first case, which is presented in Chapter 5, is the presence of an insoluble surfactant with low concentration at the fluid interface. The second scenario, which is briefly discussed in Chapter 6, examines a flow positioned between two electric plates which generate an electric field acting vertically through the fluid body. Both cases include the effects of a no-slip condition at the solid impermeable bottom boundary, resulting in a viscous boundary layer.

The motivation for this chapter, and indeed much of the thesis, arises from unexplained behaviour of the existing solutions to the system with an insoluble surfactant at the free surface, presented in Hammerton and Bassom (2013). These results saw rapid growth in amplitude for certain parameter values, using a solitary wave as an initial condition. No explanation could be found for this sudden energy gain of the system and was therefore left as an open problem to be revisited. There was also no development of an elevated shelf behind the peak disturbance, as observed in the KdV-Burgers' system presented in Subsection 3.2.3 and discussed in Kaup and Newell (1978). This transformation we would expect when using a solitary wave as an initial solution to a perturbed KdV equation, as discussed in Grimshaw et al. (2003); Pelinovsky and Grimshaw (1997). It also appears from the results presented in Hammerton and Bassom (2013) that the formation of a slowly decaying oscillatory tail region may be present, but this is not discussed at any depth.

In this chapter, we first construct a thorough analysis which will rework the existing formulation given in Hammerton and Bassom (2013), with the intention of filling in any gaps in the analysis to help identify any errors or inconsistencies. We then examine the effects of the no-slip condition at the solid bottom boundary using a similar multi-scale asymptotic analysis to that given in Section 3.1.

4.1 Formulation

We will first construct a formulation for the system in which we will derive the governing equations for flows with tangential surface stress, defining any necessary scaling parameters.

Consider a viscous fluid layer with average depth d above an impermeable, horizontal plate (illustrated by Figure 4.1.1). Cartesian coordinates are orientated so that $\hat{\mathbf{x}}$ points horizontally and $\hat{\mathbf{y}}$ points vertically upward. For now we will focus attention on the lower

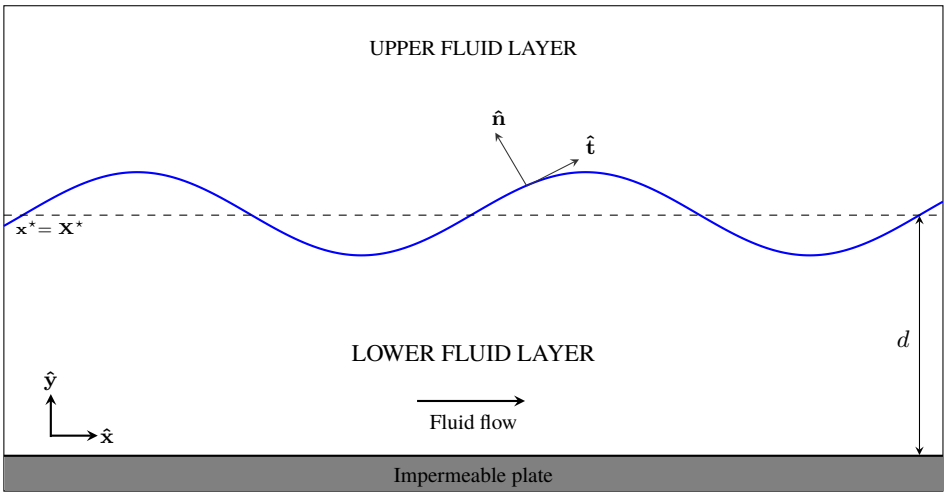

Figure 4.1.1: An illustration of a fluid layer comprising of a viscous lower fluid with average depth d, and a passive upper fluid, positioned above a solid impermeable bottom boundary.

fluid, and assume a passive upper fluid layer. The lower fluid is subject to interface stress given by

$$\mathbf{T}^\star = T_{\mathrm{n}}^\star \hat{\mathbf{n}} + T_{\mathrm{t}}^\star \hat{\mathbf{t}}$$

where the star notation $(^\star)$ denotes a dimensional quantity, and $\hat{\mathbf{n}}$, $\hat{\mathbf{t}}$ represent the outward normal and tangent unit vectors, respectively, at the fluid surface $\mathbf{x}^\star = \mathbf{X}^\star$. The kinematic condition takes the form

$$\hat{\mathbf{n}} \cdot \frac{\partial \mathbf{X}^\star}{\partial t} = \mathbf{u}^\star \cdot \hat{\mathbf{n}} \tag{4.1.1}$$

where $\mathbf{u}^\star$ is the fluid velocity. The surface stress balances (Batchelor, 2000) take the form

$$T_{\mathrm{n}}^\star = 2\mu \hat{\mathbf{n}} \cdot \mathbf{e}^\star \cdot \hat{\mathbf{n}} - p^\star \qquad \text{(normal stress balance)} \tag{4.1.2}$$

$$T_{\mathrm{t}}^\star = 2\mu \hat{\mathbf{t}} \cdot \mathbf{e}^\star \cdot \hat{\mathbf{n}} \qquad \text{(tangential stress balance)} \tag{4.1.3}$$

where $\mathbf{e}^\star$ is the rate of strain tensor, $p^\star$ is the pressure at surface, and μ is the dynamic viscosity. These can be combined to give the vector stress balance

$$\mathbf{T}^\star = -p^\star \hat{\mathbf{n}} + 2\mu \hat{\mathbf{n}} \cdot \mathbf{e}^\star.$$

Here, $\mathbf{e}^\star$ is taken from the Batchelor (1989) definition:

$$\mathbf{e}^\star = \mathrm{e}_{ij}^\star = \frac{1}{2}\left(\frac{\partial u_i^\star}{\partial x_j^\star} + \frac{\partial u_j^\star}{\partial x_i^\star}\right).$$

The incompressible Navier-Stokes equations are

$$\frac{\partial \mathbf{u}^\star}{\partial t^\star} + \mathbf{u}^\star \cdot \nabla \mathbf{u}^\star = -\frac{1}{\rho}\nabla p^\star + \nu \nabla^2 \mathbf{u}^\star - g\hat{\mathbf{y}}$$

where g is acceleration due to gravity and ν is the kinematic viscosity. These equations can be non-dimensionalised using a small amplitude, shallow water wave velocity scale $\sqrt{gd}$, and the resulting dimensionless parameters are

$$\mathbf{x}^\star = d\mathbf{x}, \quad \mathbf{t}^\star = \sqrt{\frac{d}{g}}\mathbf{t}, \quad \mathbf{u}^\star = \sqrt{dg}\,\mathbf{u}, \quad p^\star = \rho d g p, \quad \mathbf{T}^\star = \rho d g \mathbf{T}.$$

The dimensionless system is therefore

$$\frac{\partial \mathbf{u}}{\partial t} + \mathbf{u} \cdot \nabla \mathbf{u} + \hat{\mathbf{y}} = -\nabla p + \frac{1}{\mathrm{Re}}\nabla^2 \mathbf{u}, \qquad \nabla \cdot \mathbf{u} = 0 \tag{4.1.4}$$

where Re is the Reynolds Number such that

$$\mathrm{Re} = \frac{\rho d\sqrt{dg}}{\mu} = \frac{d\sqrt{dg}}{\nu}.$$

The dimensionless interface conditions then become

$$\hat{\mathbf{n}} \cdot \frac{\partial \mathbf{X}}{\partial t} = \mathbf{u} \cdot \hat{\mathbf{n}} \qquad \text{(kinematic condition)} \tag{4.1.5}$$

$$p = 2\mathrm{Re}^{-1}\, \hat{\mathbf{n}} \cdot \mathbf{e} \cdot \hat{\mathbf{n}} - T_{\mathrm{n}} \qquad \text{(normal stress balance)} \tag{4.1.6}$$

$$2\mathrm{Re}^{-1}\, \hat{\mathbf{t}} \cdot \mathbf{e} \cdot \hat{\mathbf{n}} = T_{\mathrm{t}} \qquad \text{(tangential stress balance)} \tag{4.1.7}$$

We will look specifically at large Reynolds number flows, as consistent with water waves, which means that the terms with Re^{-1} in the stress balance equations will become relatively small. If we consider flows of finite depth with wavelength much larger than water depth, in the absence of any surface stress condition, we return to an analysis of nonlinear water waves consistent with the derivation of standard KdV equation seen in Vanden-Broeck (2010). Hence we consider weakly nonlinear waves of the form

$$f(\mathbf{x} - ct\hat{\mathbf{x}}, \tau), \qquad c = \mathcal{O}(1), \quad \tau = \widehat{\varepsilon} t$$

where τ is a suitable slow-time with $\widehat{\varepsilon}$ a small parameter to be determined. We switch to a moving frame of reference

$$\mathbf{x}' = \mathbf{x} - ct\hat{\mathbf{x}}, \qquad \mathbf{u}' = \mathbf{u} - c\hat{\mathbf{x}}$$

so we expect the main peak disturbance to evolve over a large time scale. We are specifically choosing c to ensure that in the moving frame only the slow time variable will appear in the analysis, so waves will evolve on one slow time scale and we have a slow modulation of the wave form. Omitting superscripts, the momentum equation in the moving frame becomes

$$\widehat{\varepsilon} \frac{\partial \mathbf{u}}{\partial \tau} + \mathbf{u} \cdot \nabla \mathbf{u} + \hat{\mathbf{y}} = -\nabla p + \mathrm{Re}^{-1}\, \nabla^2 \mathbf{u} \tag{4.1.8}$$

where the fluid velocity is now $\mathbf{u} = -c\hat{\mathbf{x}}$ on $y = -1$.

Next, we consider the flow close to the fluid surface. Let s be the arc-length along the surface from some fixed point such that

$$s = \int_a^b \mathrm{d}s = \int_a^b \sqrt{1 + \left(\frac{\mathrm{d}y}{\mathrm{d}x}\right)^2}\,\mathrm{d}x.$$

We can then write the position vector of surface as

$$\mathbf{X} = x(s,\tau)\hat{\mathbf{x}} + y(s,\tau)\hat{\mathbf{y}},$$

with a dependence on τ, recognising that the surface position will evolve on the slow time scale. Then we have

$$\left(\frac{\partial x}{\partial s}\right)^2 + \left(\frac{\partial y}{\partial s}\right)^2 = 1. \tag{4.1.9}$$

The normal and tangential unit vectors are given by

$$\hat{\mathbf{n}} = -\frac{\partial y}{\partial s}\hat{\mathbf{x}} + \frac{\partial x}{\partial s}\hat{\mathbf{y}}, \quad \text{and} \quad \hat{\mathbf{t}} = \frac{\partial x}{\partial s}\hat{\mathbf{x}} + \frac{\partial y}{\partial s}\hat{\mathbf{y}},$$

and the surface curvature is defined in Batchelor (2000) as

$$\kappa = \frac{\partial^2 x}{\partial s^2}\frac{\partial y}{\partial s} - \frac{\partial^2 y}{\partial s^2}\frac{\partial x}{\partial s}. \tag{4.1.10}$$

The fluid velocity written in normal and tangential components is

$$\mathbf{u} = u\hat{\mathbf{t}} + v\hat{\mathbf{n}}$$

and the kinematic condition

$$\hat{\mathbf{n}} \cdot \frac{\partial \mathbf{X}}{\partial t} = \mathbf{u} \cdot \hat{\mathbf{n}}$$

becomes

$$\begin{aligned}\left(-\frac{\partial y}{\partial s}\hat{\mathbf{x}} + \frac{\partial x}{\partial s}\hat{\mathbf{y}}\right) \cdot \left(\widehat{\varepsilon}\frac{\partial x}{\partial \tau}\hat{\mathbf{x}} + \widehat{\varepsilon}\frac{\partial y}{\partial \tau}\hat{\mathbf{y}}\right) &= \left(u\hat{\mathbf{t}} + v\hat{\mathbf{n}}\right) \cdot \hat{\mathbf{n}}, \\ \Rightarrow \qquad \widehat{\varepsilon}\left(\frac{\partial x}{\partial s}\frac{\partial y}{\partial \tau} - \frac{\partial y}{\partial s}\frac{\partial x}{\partial \tau}\right) &= v \end{aligned} \tag{4.1.11}$$

on $n = 0$, where n is the distance normal to the surface. In order to write the hydro-

dynamic quantities in terms of orthogonal curvilinear coordinates s and n, we use the identities derived in the appendices of Acheson (1990) and Batchelor (2000) in which vector quantities such as $\nabla \cdot \mathbf{u}$ are expressed in terms of scale factors

$$h_i = \frac{\partial \mathbf{x}}{\partial \zeta_i} \cdot \mathbf{a}_i \tag{4.1.12}$$

where ζ_i is the i^{th} orthogonal coordinate and $\mathbf{a}_i$ is the corresponding coordinate unit vector. Here, we have

$$\zeta_1 = s, \quad \zeta_2 = n \quad \text{and} \quad \mathbf{a}_1 = \hat{\mathbf{t}}, \quad \mathbf{a}_2 = \hat{\mathbf{n}}.$$

In addition to this, the change in position vector $\mathbf{x}$ is given by

$$\delta\mathbf{x} = h_{\mathrm{s}}\, \delta s\, \hat{\mathbf{t}} + h_{\mathrm{n}}\, \delta n\, \hat{\mathbf{n}} \tag{4.1.13}$$

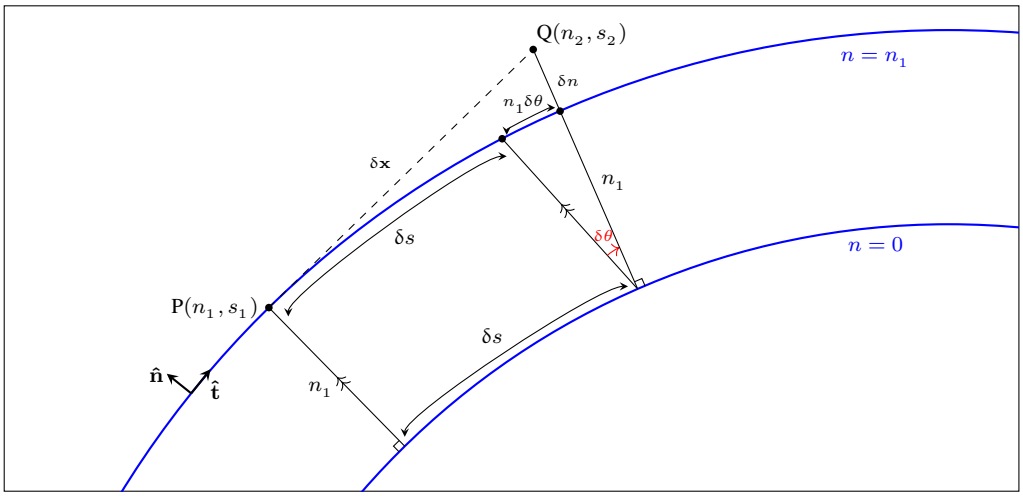

Figure 4.1.2: Orthogonal curvilinear coordinate system illustrating derivation of requisite scaling factors h_i.

Then for any given point P on the surface $n = n_1$ with position $s = s_1$, and any given point Q with position (s_2, n_2) such that

$$s_2 = s_1 + \delta s, \quad \text{and} \quad n_2 = n_1 + \delta n$$

then the path $\overrightarrow{\mathrm{PQ}} = \delta\mathbf{x}$ is given by

$$\delta\mathbf{x} = (\delta s + n_1\delta\theta)\hat{\mathbf{t}} + \delta n\,\hat{\mathbf{n}}$$

as illustrated by Figure 4.1.2. Then the surface curvature κ by definition (Batchelor, 2000) is

$$\kappa = \frac{\mathrm{d}\theta}{\mathrm{d}s}, \quad \text{so} \quad \delta\theta = \kappa\,\delta s.$$

Hence we have

$$\delta\mathbf{x} = (1 + n_1\kappa)\delta s\,\hat{\mathbf{t}} + \delta n\,\hat{\mathbf{n}}.$$

Then using Equation 4.1.12 we have

$$h_\mathrm{s} = \frac{\partial\mathbf{x}}{\partial s}\cdot\hat{\mathbf{t}} = 1 + \kappa n_1.$$

and

$$h_\mathrm{n} = \frac{\partial\mathbf{x}}{\partial n}\cdot\hat{\mathbf{n}} = 1$$

To summarise, for any n, the requisite scaling factors are

$$h_\mathrm{s} = 1 + \kappa n, \quad \text{and} \quad h_\mathrm{n} = 1, \tag{4.1.14}$$

where κ is the surface curvature defined in Equation 4.1.10, which agree with those examined in Longuet-Higgins (1953). Since the normal scaling factor h_n is simply 1, we will write $h_\mathrm{s} = h$ for the remainder of the analysis.

We now obtain expressions for key hydrodynamic quantities in terms of the coordinates s and n. The continuity equation is

$$\nabla\cdot\mathbf{u} = \frac{1}{h}\frac{\partial u}{\partial s} + \frac{\partial v}{\partial n} + \frac{\kappa v}{h} = 0, \tag{4.1.15}$$

and the vorticity is given by

$$\boldsymbol{\omega} = \nabla\times\mathbf{u} = \frac{\widehat{\mathbf{b}}}{h}\left(\frac{\partial v}{\partial s} - \frac{\partial(hu)}{\partial n}\right),$$

where $\widehat{\mathbf{b}} = \hat{\mathbf{n}} \times \hat{\mathbf{t}}$ is the **binormal** vector. Since $\boldsymbol{\omega} = \omega\widehat{\mathbf{b}}$, we can then write

$$\omega = \frac{1}{h}\frac{\partial v}{\partial s} - \frac{\partial u}{\partial n} - \frac{\kappa u}{h}. \tag{4.1.16}$$

Then, using the identity $\nabla^2\mathbf{u} = -\nabla \times \boldsymbol{\omega}$ we have

$$\nabla^2\mathbf{u} = -\frac{\partial \omega}{\partial n}\hat{\mathbf{t}} + \frac{1}{h}\frac{\partial \omega}{\partial s}\hat{\mathbf{n}}.$$

From the Batchelor (1989) definition of the strain tensor in terms of general orthonormal coordinates , we have

$$\hat{\mathbf{n}} \cdot \mathbf{e} \cdot \hat{\mathbf{n}} = e_{22} = \frac{\partial v}{\partial n}$$

and also

$$\begin{aligned}
\hat{\mathbf{t}} \cdot \mathbf{e} \cdot \hat{\mathbf{n}} &= e_{12}, \\
&= \frac{1}{2h}\frac{\partial v}{\partial s} + \frac{h}{2}\frac{\partial}{\partial n}\left(\frac{u}{h}\right), \\
&= \frac{1}{2h}\left(\frac{\partial v}{\partial s} + h\frac{\partial u}{\partial n} - u\kappa\right).
\end{aligned}$$

On $n = 0$, $h = 1$ and so using the kinematic condition Equation 4.1.11 we have

$$v = \widehat{\varepsilon}\left(\frac{\partial x}{\partial s}\frac{\partial y}{\partial \tau} - \frac{\partial x}{\partial \tau}\frac{\partial y}{\partial s}\right) = \mathcal{O}(\widehat{\varepsilon}).$$

Hence from Equation 4.1.16, the vorticity on the surface is given by

$$\omega(s, n = 0) = \omega_0 = -\frac{\partial u}{\partial n} - \kappa U + \mathcal{O}(\widehat{\varepsilon}) \tag{4.1.17}$$

where $U = U(s)$ is the tangential velocity at the surface. Using the continuity equa-

tion (4.1.15) at the surface, the strain coordinates are given by

$$\begin{aligned}\hat{\mathbf{n}}\cdot\mathbf{e}\cdot\hat{\mathbf{n}} &= \frac{\partial v}{\partial n},\\ &= -\frac{1}{h}\left(\frac{\partial u}{\partial s}+\kappa v\right), \quad \text{(from the continuity equation)}\\ &= -\frac{\partial u}{\partial s}-\kappa v,\\ &= -\frac{\partial U}{\partial s}+\mathcal{O}(\widehat{\varepsilon}),\end{aligned}$$

and

$$\begin{aligned}\hat{\mathbf{t}}\cdot\mathbf{e}\cdot\hat{\mathbf{n}} &= \frac{1}{2h}\left(\frac{\partial v}{\partial s}+h\frac{\partial u}{\partial n}-u\kappa\right),\\ &= -\frac{1}{2}\left(\omega_0+2\kappa U\right)+\mathcal{O}(\widehat{\varepsilon})\end{aligned}$$

using the vorticity equation (4.1.16), and the surface vorticity equation (4.1.17). Next, the tangential stress balance is re-evaluated to give

$$\begin{aligned}T_{\mathrm{t}} &= 2\mathrm{Re}^{-1}\,\hat{\mathbf{t}}\cdot\mathbf{e}\cdot\hat{\mathbf{n}},\\ &= -\mathrm{Re}^{-1}\,\left(\omega_0+2\kappa U\right)+\mathcal{O}(\widehat{\varepsilon}),\end{aligned}$$

so at leading order we have

$$\Delta^{-2}\,T_{\mathrm{t}}+\omega_0+2\kappa U=0, \qquad \Delta^{-2}\,=\mathrm{Re}. \tag{4.1.18}$$

The reason for choosing this definition for Δ is due to the appearance of $(\mathrm{Re})^{-1/2}$ terms later in the large Reynolds number analysis. The normal stress balance is also re-evaluated to give

$$\begin{aligned}p+T_{\mathrm{n}}-2\mathrm{Re}^{-1}\,\hat{\mathbf{n}}\cdot\mathbf{e}\cdot\hat{\mathbf{n}} &= 0,\\ p+2\mathrm{Re}^{-1}\,\frac{\partial U}{\partial s}+T_{\mathrm{n}} &= \mathcal{O}(\widehat{\varepsilon})\end{aligned}$$

which at leading order is given by

$$p+2\Delta^2\frac{\partial U}{\partial s}+T_{\mathrm{n}}=0. \tag{4.1.19}$$

The tangential component of the momentum equation (4.1.8) at the surface is therefore

$$\widehat{\varepsilon}\frac{\partial U}{\partial \tau}+U\frac{\partial U}{\partial s}+\frac{\partial}{\partial s}\left(y-T_{\mathrm{n}}-2\Delta^{2}\frac{\partial U}{\partial s}\right)=-\Delta^{2}\frac{\partial \omega}{\partial n}. \tag{4.1.20}$$

The non-dimensional vorticity equation becomes

$$\begin{aligned}\frac{\partial \boldsymbol{\omega}}{\partial t}&=\nabla\times(\mathbf{u}\times\boldsymbol{\omega})+\frac{1}{\mathrm{Re}}\nabla^{2}\boldsymbol{\omega},\\&=\mathbf{u}\cdot\nabla\boldsymbol{\omega}+\frac{1}{\mathrm{Re}}\nabla^{2}\boldsymbol{\omega},\end{aligned}$$

which is derived from taking the curl of equation (4.1.8) and therefore we have

$$\widehat{\varepsilon}\frac{\partial \boldsymbol{\omega}}{\partial \tau}-\mathbf{u}\cdot\nabla\boldsymbol{\omega}=\Delta^{2}\nabla^{2}\boldsymbol{\omega}.$$

Then using standard vector identities, and the vorticity definition (4.1.16), this can be written as

$$\widehat{\varepsilon}h\frac{\partial \omega}{\partial \tau}+u\frac{\partial \omega}{\partial s}+vh\frac{\partial \omega}{\partial n}=\Delta^{2}\left(\frac{\partial}{\partial s}\left(\frac{1}{h}\frac{\partial \omega}{\partial s}\right)+\kappa\frac{\partial \omega}{\partial n}+h\frac{\partial^{2}\omega}{\partial n^{2}}\right), \tag{4.1.21}$$

and from Equation 4.1.18, the surface vorticity given by

$$\omega_{0}=-2\kappa U-\Delta^{-2}T_{\mathrm{t}}. \tag{4.1.22}$$

This summarises the initial formulation. We have defined a system of equations: notably the normal stress balance (4.1.19), the tangential momentum equation (4.1.20), and the vorticity equation (4.1.21), which will now be used as we proceed to focus on a long wave approximation, large Reynolds number flow.

4.1.1 Long wave approximation

Consider now a large Reynolds number limit (here we have $\Delta \ll 1$), and restrict attention to disturbances with wavelength $\mathcal{O}(\varepsilon^{-1})$ and amplitude $\mathcal{O}(\delta)$, where $\delta, \varepsilon \ll 1$.

The fluid surface is parameterised by

$$x = s + h(S), \quad y = \delta\eta(S), \qquad S = \varepsilon s$$

for surface elevation η and some function $h(S)$ to be determined. The large wavelength, small amplitude approximation motivates this choice of scaling for y and s. The wave amplitude of the main disturbance is $\mathcal{O}(\delta)$. Then assuming the position x varies with arc-length s, we have

$$\left(\frac{\partial x}{\partial s}\right)^2 + \left(\frac{\partial y}{\partial s}\right)^2 = 1 + \varepsilon\frac{\partial h}{\partial S} + \left(\delta\varepsilon\frac{\partial \eta}{\partial S}\right)^2 + \mathcal{O}(\varepsilon^2).$$

However, from Equation 4.1.9 we know that

$$\left(\frac{\partial x}{\partial s}\right)^2 + \left(\frac{\partial y}{\partial s}\right)^2 = 1,$$

so a leading-order balance fixes the scale of f such that

$$\varepsilon\frac{\partial h}{\partial S} = -\delta^2\varepsilon^2\left(\frac{\partial \eta}{\partial S}\right)^2,$$

and hence

$$h = \delta^2\varepsilon\xi = \mathcal{O}(\delta^2\varepsilon),$$

where

$$\frac{\partial \xi}{\partial S} = -\left(\frac{\partial \eta}{\partial S}\right)^2.$$

The function $\xi(S)$ doesn't enter subsequent analysis, but it is important to determine the correct scaling,

$$x = s + \delta^2\varepsilon\xi(S).$$

We then express the normal and tangential unit vectors at the surface in terms of the Cartesian unit vectors. The normal unit vector $\hat{\mathbf{n}}$ is given by

$$\hat{\mathbf{n}} = -\frac{\partial y}{\partial s}\hat{\mathbf{x}} + \frac{\partial x}{\partial s}\hat{\mathbf{y}},$$

where

$$\frac{\partial x}{\partial s} = 1 + \delta^2\varepsilon^2\frac{\partial \xi}{\partial S}, \qquad \text{and} \quad \frac{\partial y}{\partial s} = \delta\varepsilon\frac{\partial \eta}{\partial S},$$
$$= 1 + \mathcal{O}(\delta^2\varepsilon^2).$$

We can then write

$$\hat{\mathbf{n}} = -\delta\varepsilon\frac{\partial \eta}{\partial S}\hat{\mathbf{x}} + \hat{\mathbf{y}} + \mathcal{O}(\delta^2\varepsilon^2) \tag{4.1.23}$$

for the normal unit vector, and the tangential unit vector can be written as

$$\begin{aligned}\hat{\mathbf{t}} &= \frac{\partial x}{\partial s}\hat{\mathbf{x}} + \frac{\partial y}{\partial s}\hat{\mathbf{y}},\\ &= \hat{\mathbf{x}} + \delta\varepsilon\frac{\partial \eta}{\partial S}\hat{\mathbf{y}} + \mathcal{O}(\delta^2\varepsilon^2).\end{aligned} \tag{4.1.24}$$

Note that $\hat{\mathbf{n}} \cdot \hat{\mathbf{t}} = 0$, as required. Recalling the definition of the surface curvature from Equation 4.1.10,

$$\kappa = \frac{\partial^2 x}{\partial s^2}\frac{\partial y}{\partial s} - \frac{\partial^2 y}{\partial s^2}\frac{\partial x}{\partial s},$$

we now note that

$$\frac{\partial^2 x}{\partial s^2} = \mathcal{O}(\delta^2\varepsilon^3), \quad \text{and} \quad \frac{\partial^2 y}{\partial s^2} = \delta\varepsilon^2\frac{\partial^2 \eta}{\partial S^2},$$

and hence

$$\kappa = -\delta\varepsilon^2\frac{\partial^2 \eta}{\partial S^2} + \mathcal{O}(\delta^3\varepsilon^4).$$

Then the kinematic condition is

$$\begin{aligned}\hat{\mathbf{n}} \cdot \tfrac{\partial \mathbf{X}}{\partial t} &= \mathbf{u} \cdot \hat{\mathbf{n}}\\ \left(-\delta\varepsilon\tfrac{\partial \eta}{\partial S}\hat{\mathbf{x}} + \hat{\mathbf{y}}\right) \cdot \widehat{\varepsilon}\tfrac{\partial}{\partial \tau}(x\hat{\mathbf{x}} + y\hat{\mathbf{y}}) &= \left(u\left(\hat{\mathbf{x}} + \delta\varepsilon\tfrac{\partial \eta}{\partial S}\hat{\mathbf{y}}\right) + v\left(-\delta\varepsilon\tfrac{\partial \eta}{\partial S}\hat{\mathbf{x}} + \hat{\mathbf{y}}\right)\right) \cdot \left(-\delta\varepsilon\tfrac{\partial \eta}{\partial S}\hat{\mathbf{x}} + \hat{\mathbf{y}}\right)\\ -\delta\varepsilon\widehat{\varepsilon}\tfrac{\partial \eta}{\partial S}\tfrac{\partial \eta}{\partial \tau} + \widehat{\varepsilon}\tfrac{\partial y}{\partial \tau} &= \left(\left(u - \delta\varepsilon v\tfrac{\partial \eta}{\partial s}\right)\hat{\mathbf{x}} + \left(\delta\varepsilon u\tfrac{\partial \eta}{\partial S} + v\right)\hat{\mathbf{y}}\right) \cdot \left(-\delta\varepsilon\tfrac{\partial \eta}{\partial S}\hat{\mathbf{x}} + \hat{\mathbf{y}}\right)\\ \widehat{\varepsilon}\left(\tfrac{\partial y}{\partial \tau} - \delta\varepsilon\tfrac{\partial \eta}{\partial \tau}\tfrac{\partial \eta}{\partial S}\right) &= v + \delta\varepsilon u\tfrac{\partial \eta}{\partial S} - \delta\varepsilon\tfrac{\partial \eta}{\partial S}\left(u - \delta\varepsilon v\tfrac{\partial \eta}{\partial S}\right)\\ \delta\widehat{\varepsilon}\left(\tfrac{\partial \eta}{\partial \tau} - \varepsilon\tfrac{\partial \eta}{\partial \tau}\tfrac{\partial \eta}{\partial S}\right) &= v\left(1 + \delta^2\varepsilon^2\left(\tfrac{\partial \eta}{\partial S}\right)^2\right)\end{aligned}$$

and finally, after rearranging we have the vertical velocity at the surface,

$$v = \delta\widehat{\varepsilon}\frac{\partial \eta}{\partial \tau} + \mathcal{O}(\delta^2\varepsilon^2, \delta\varepsilon\widehat{\varepsilon}), \qquad \text{at} \quad n = 0. \tag{4.1.25}$$

We now start to consider how the flow will behave for each of the example scenarios with a surface stress condition at the fluid interface: flows with a surfactant present at the fluid interface, and flows with an electric field generated vertically through the fluid body. In each case, the flow in the upper fluid layer doesn't affect the lower fluid analysis.

For the surfactant scenario we don't include the upper fluid in the analysis, only the fluid flow in the lower fluid affecting the surfactant density at the surface. In the case with the electric field, the upper fluid with different electrical properties modifies the surface charge density. We will solve this for the electric field, but again, don't need to solve for the upper fluid flow. Hence, the upper fluid is considered passive.

We now examine the lower fluid layer as a body of water and solve for the resulting flow. We find that for large Reynolds number the lower fluid consists of an inviscid, irrotational main fluid body, plus two boundary layers.

In the main part of the lower fluid layer we consider inviscid, irrotational flow. However, it was shown earlier in Equation 4.1.22 that the vorticity at the fluid surface is non-zero. For large Reynolds number flows we expect a thin boundary layer, of thickness δ_{B} say, below the free surface in which the vorticity decays from ω_0 at the surface to zero in order to match to the main irrotational layer.

In addition to this, in order to satisfy the no-slip condition at the bottom of the fluid, a viscous boundary layer of thickness δ_{N} is present in which the tangential velocity decays from its free-stream value in the inviscid main body to zero on the rigid lower surface. Such a system is illustrated by Figure 4.1.3.

We now proceed to solve the system for each boundary layer and then match the solutions to the main fluid body.

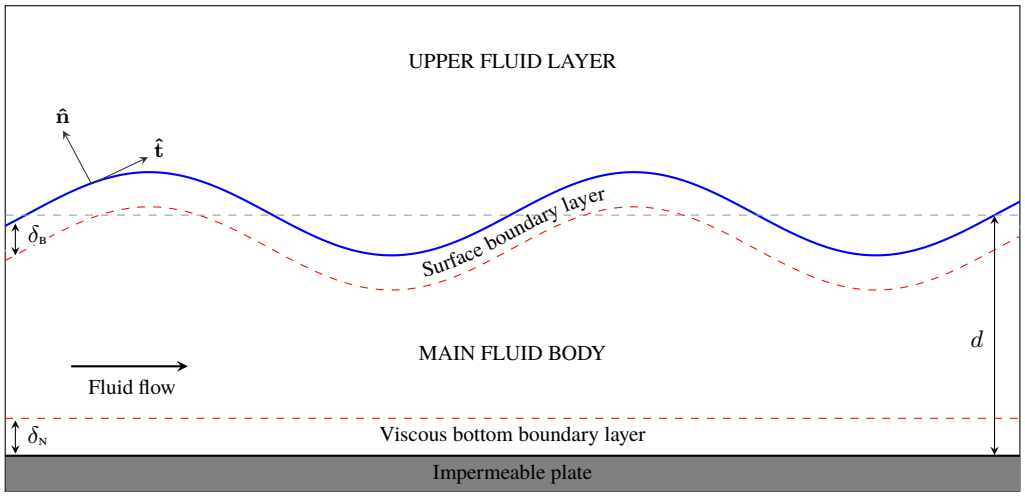

Figure 4.1.3: Illustration of the viscous fluid layer and passive upper layer with boundary layers of thickness δ_N and δ_B at the solid bottom and fluid interface, respectively.

Surface boundary layer

We assume that the surface boundary layer has thickness given by δ_B. We then write $n = -\delta_B N$ so that $N = \mathcal{O}(1)$ in the boundary layer, and is positive.

In the original fixed frame of reference, amplitude disturbances were $\mathcal{O}(\delta)$, so moving horizontally at speed c in the moving frame we set

$$u = -c + \delta\tilde{u} + \mathcal{O}(\delta^2\varepsilon^2), \quad \text{and} \quad v = \delta\widetilde{\varepsilon v}, \tag{4.1.26}$$

where the scaling for v follows from Equation 4.1.25. We now write the general stress applied at the interface in generic form

$$\mathbf{T} = [T_n]\widehat{T}_n\hat{\mathbf{n}} + [T_t]\widehat{T}_t\hat{\mathbf{t}},$$

where $\widehat{T}_n = \widehat{T}_n(S)$ and $\widehat{T}_t = \widehat{T}_t(S)$ are $\mathcal{O}(1)$ quantities, and $[T_n]$ and $[T_t]$ are scaling parameters for the normal and tangential stress, respectively. Now, from Equation 4.1.22 the surface vorticity in terms of the new scaling parameters becomes

$$\omega(S,0) = 2\delta\varepsilon^2\frac{\partial^2\eta}{\partial S^2}(-c + \delta\tilde{u}) - \Delta^{-2}[T_t]\widehat{T}_t$$

which is a combination of vorticity due to a contribution from hydrodynamic flow and from tangential shear stress. Hence we can write

$$\omega = 2c\delta\varepsilon^2\widetilde{\omega}_1 + [T_{\mathrm{t}}]\Delta^{-2}\,\widetilde{\omega}_2 + \mathcal{O}(\delta^2\varepsilon^2), \tag{4.1.27}$$

and at the surface

$$\widetilde{\omega}_1(S,0) = -\frac{\partial^2\eta}{\partial S^2}, \qquad \widetilde{\omega}_2(S,0) = -\widehat{T}_{\mathrm{t}}. \tag{4.1.28}$$

The vorticity equation from Equation 4.1.21 is

$$\widehat{\varepsilon}h\frac{\partial\omega}{\partial\tau} + u\frac{\partial\omega}{\partial s} + hv\frac{\partial\omega}{\partial n} = \Delta^2\left(\frac{\partial}{\partial s}\left(\frac{1}{h}\frac{\partial\omega}{\partial s}\right) + \kappa\frac{\partial\omega}{\partial n} + h\frac{\partial^2\omega}{\partial n^2}\right)$$

and from Equation 4.1.14,

$$\begin{aligned} h &= 1 + \kappa n \\ &= 1 - \delta\delta_{\mathrm{B}}\varepsilon^2\frac{\partial^2\eta}{\partial s^2}N \approx 1. \end{aligned}$$

In terms of the new scaling parameters, the vorticity equation at the surface becomes

$$\frac{\widehat{\varepsilon}}{\varepsilon}\frac{\partial\widetilde{\omega}_i}{\partial\tau} - c\frac{\partial\widetilde{\omega}_i}{\partial S} + \delta\left(\tilde{u}\frac{\partial\widetilde{\omega}_i}{\partial S} - \tilde{v}\frac{\partial\widetilde{\omega}_i}{\partial N}\right) = \frac{\Delta^2}{\delta_{\mathrm{B}}^2\varepsilon}\left(\frac{\partial^2\widetilde{\omega}_i}{\partial N^2} + \delta\delta_{\mathrm{B}}\varepsilon^2\left(\frac{\partial^2\eta}{\partial S^2}\frac{\partial\widetilde{\omega}_i}{\partial N} + \frac{\delta_{\mathrm{B}}}{\delta}\frac{\partial^2\widetilde{\omega}_i}{\partial S^2}\right)\right) \tag{4.1.29}$$

for $\widetilde{\omega}_i$, $(i = 1, 2)$, and where c is an $\mathcal{O}(1)$ quantity. In order to describe the vorticity decay across the layer, we require a derivative with respect to N to enter at leading-order. Since $c = \mathcal{O}(1)$, this requires that

$$\delta_{\mathrm{B}} = \frac{\Delta}{\varepsilon^{1/2}}, \tag{4.1.30}$$

and hence, for the boundary layer to be thin we require that $\Delta \ll \varepsilon^{1/2}$. Here we are assuming that $\widehat{\varepsilon} \ll \varepsilon$, and the motivation for this assumption will be discussed later. This fixes the leading-order vorticity equation for each component $\widetilde{\omega}_i$ to be

$$\frac{\partial^2\widetilde{\omega}_i}{\partial N^2} = -c\frac{\partial\widetilde{\omega}_i}{\partial S}. \tag{4.1.31}$$

In terms of the newly scaled variables, the tangential momentum equation (4.1.20) at the

surface $N = 0$ becomes

$$\frac{\widehat{\varepsilon}}{\varepsilon}\frac{\partial \widetilde{U}}{\partial \tau} - c\frac{\partial \widetilde{U}}{\partial S} + \delta U\frac{\partial \widetilde{U}}{\partial S} + \frac{\partial \eta}{\partial S} - \frac{1}{\delta}\frac{\partial T_{\mathrm{n}}}{\partial S} - 2\delta_{\mathrm{B}}^2\varepsilon^2\frac{\partial^2 \widetilde{U}}{\partial S^2} = \frac{1}{\delta}\frac{\partial \widetilde{\omega}_i}{\partial N}\bigg|_{N=0} \tag{4.1.32}$$

where $\widetilde{U}(S) = \tilde{u}(S, 0)$. To evaluate the right-hand side of Equation 4.1.32, we need to solve Equation 4.1.31 subject to the matching condition at the surface

$$\widetilde{\omega}_i(S, 0) \to f_i(S), \quad \text{as} \quad N \to 0,$$

where $f_i(S) = \widetilde{\omega}_i(S, 0)$ is the surface vorticity function. We also need to solve Equation 4.1.31 subject to the matching condition

$$\widetilde{\omega}_i \to 0 \quad \text{as} \quad N \to \infty.$$

In order to calculate $\frac{\partial \widetilde{\omega}_i}{\partial N}\big|_{N=0}$ we refer to Appendix B, where it is shown that

$$\frac{\partial \widetilde{\omega}_i}{\partial N}\bigg|_{N=0} = \sqrt{c}\,\mathscr{T}\left[\frac{\mathrm{d}f_i}{\mathrm{d}S}\right].$$

The integral transform $\mathscr{T}[\varrho]$ is also defined in Appendix B by Equation B.0.5, such that

$$\mathscr{T}[\varrho(X)] \equiv \frac{1}{\sqrt{\pi}}\int_0^\infty \frac{\varrho(X+Y)}{\sqrt{Y}}\,\mathrm{d}Y,$$

where $\varrho(X)$ is some given function of some given X. In addition to these results, it is also shown that

$$\int_0^\infty \widetilde{\omega}_i \mathrm{d}N = \frac{1}{\sqrt{c}}\,\mathscr{T}[f_i]$$

which is needed later, and the appropriate f_i follows from Equation 4.1.28.

We can now use this result to write the tangential momentum equation (4.1.32) at the surface $N = 0$ in the form

$$\begin{aligned}\frac{\widehat{\varepsilon}}{\varepsilon}\frac{\partial \widetilde{U}}{\partial \tau} - c\frac{\partial \widetilde{U}}{\partial S} + \delta U\frac{\partial \widetilde{U}}{\partial S} + \frac{\partial \eta}{\partial S} - \frac{1}{\delta}\frac{\partial T_{\mathrm{n}}}{\partial S} &= 2c\delta_{\mathrm{B}}\varepsilon^2\frac{\partial \widetilde{\omega}_1}{\partial N}\bigg|_{N=0} + \frac{[T_{\mathrm{t}}]}{\delta\delta_{\mathrm{B}}\varepsilon}\frac{\partial \widetilde{\omega}_2}{\partial N}\bigg|_{N=0} \\ &= 2c^{3/2}\delta_{\mathrm{B}}\varepsilon^2\,\mathscr{T}\left[\frac{\partial f_1}{\partial S}\right] + \frac{\sqrt{c}[T_{\mathrm{t}}]}{\delta\delta_{\mathrm{B}}\varepsilon}\,\mathscr{T}\left[\frac{\partial f_2}{\partial S}\right],\end{aligned}$$

where terms of $\mathcal{O}(\delta_{\text{B}}^2\varepsilon^2)$ have been omitted. This simplifies to

$$\frac{\widehat{\varepsilon}}{\varepsilon}\frac{\partial \widetilde{U}}{\partial \tau} - c\frac{\partial \widetilde{U}}{\partial S} + \delta U\frac{\partial \widetilde{U}}{\partial S} + \frac{\partial \eta}{\partial S} - \beta\frac{\partial \widehat{T}_{\text{n}}}{\partial S} = -2c^{3/2}\delta_{\text{B}}\varepsilon^2\,\mathscr{T}\left[\frac{\partial^3\eta}{\partial S^3}\right] - \alpha\sqrt{c}\,\mathscr{T}\left[\frac{\partial \widehat{T}_{\text{t}}}{\partial S}\right], \tag{4.1.33}$$

where

$$\alpha = \frac{[T_{\text{t}}]}{\delta\delta_{\text{B}}\varepsilon} \qquad \text{and} \qquad \beta = \frac{[T_{\text{n}}]}{\delta}. \tag{4.1.34}$$

Next we specify the magnitudes of some of the small quantities. When we begin to consider the systems involving surfactants, or an electric field, we will be looking for modifications to soliton-like solutions. We therefore require that the time derivative and quadratic nonlinear term have the same magnitude. This is consistent with the standard KdV equation derivation (Vanden-Broeck, 2010). In order to achieve this balance, the relation

$$\widehat{\varepsilon} = \delta\varepsilon \tag{4.1.35}$$

is therefore imposed, which gives the slow time scale for slow modulation of the wave form and is consistent with our earlier assumption that $\widehat{\varepsilon} \ll \varepsilon$. With this scaling the tangential momentum equation at the surface becomes

$$\frac{\partial \eta}{\partial S} - c\frac{\partial \widetilde{U}}{\partial S} = -\delta\left(\frac{\partial \widetilde{U}}{\partial \tau} + \widetilde{U}\frac{\partial \widetilde{U}}{\partial S}\right) + \beta\frac{\partial \widehat{T}_{\text{n}}}{\partial S} - \alpha\sqrt{c}\,\mathscr{T}\left[\frac{\partial \widehat{T}_{\text{t}}}{\partial S}\right] - 2\delta_{\text{B}}\varepsilon^2 c^{3/2}\,\mathscr{T}\left[\frac{\partial^3\eta}{\partial S^3}\right]. \tag{4.1.36}$$

With these new scaling parameters, the continuity equation (4.1.15) becomes

$$\begin{aligned}\nabla\cdot\mathbf{u} &= \frac{1}{h}\frac{\partial u}{\partial s} + \frac{\partial v}{\partial n} + \frac{\kappa v}{h} = 0,\\ &= \delta\varepsilon\frac{\partial \tilde{u}}{\partial S} - \frac{\delta\delta_{\text{B}}\varepsilon}{\delta_{\text{B}}}\frac{\partial \tilde{v}}{\partial N} - \delta^2\delta_{\text{B}}\varepsilon^3\frac{\partial^2\eta}{\partial S^2}\tilde{v} = 0,\\ &\Rightarrow \frac{\partial \tilde{u}}{\partial S} - \frac{\partial \tilde{v}}{\partial N} = \mathcal{O}(\delta\delta_{\text{B}}\varepsilon^2),\end{aligned} \tag{4.1.37}$$

and the vorticity definition (Equation 4.1.16) is

$$\begin{aligned}\omega &= \frac{1}{h}\frac{\partial v}{\partial s} - \frac{\partial u}{\partial n} - \frac{\kappa u}{h},\\ &= \delta\delta_{\text{B}}\varepsilon^2\frac{\partial \tilde{v}}{\partial S} + \frac{\delta}{\delta_{\text{B}}}\frac{\partial \tilde{u}}{\partial N} + (-c+\delta\tilde{u})\delta\varepsilon^2\frac{\partial^2\eta}{\partial S^2},\\ &= \frac{\delta}{\delta_{\text{B}}}\frac{\partial \tilde{u}}{\partial N} + \mathcal{O}(\delta\varepsilon^2).\end{aligned}$$

We compare this with Equation 4.1.27,

$$\begin{aligned}\omega &= \frac{[T_{\mathrm{t}}]}{\Delta^2}\widetilde{\omega}_2 + 2\delta\varepsilon^2 c^2 \widetilde{\omega}_1, \\ &= \frac{\alpha\delta}{\delta_{\mathrm{B}}}\widetilde{\omega}_2 + 2\delta\varepsilon^2 c^2 \widetilde{\omega}_1\end{aligned}$$

using the definitions of α (4.1.34) and δ_{B} (4.1.30). Hence we can write

$$\frac{\partial \tilde{u}}{\partial N} - \alpha\widetilde{\omega}_2 = \mathcal{O}(\delta_{\mathrm{B}}\varepsilon^2). \tag{4.1.38}$$

Here we see that α characterises the change in tangential velocity through the boundary layer and hence the case of general interest is when $\alpha = \mathcal{O}(1)$. If we can develop a theory for this general case, then later we can consider limiting behaviour for when α is small or large.

At leading-order we solve Equation 4.1.38 to give

$$\frac{\partial \tilde{u}}{\partial N} = \alpha\widetilde{\omega}_2,$$

so

$$\tilde{u}(S,N) = \alpha\int_0^N \widetilde{\omega}_2(S,N')\mathrm{d}N' + c_1(S),$$

for some arbitrary function c_1. On $N = 0$, we have $\tilde{u}(S,0) = \widetilde{U}(S)$, so

$$\tilde{u}(S,N) = \widetilde{U}(S) + \alpha\int_0^N \widetilde{\omega}_2(S,N')\mathrm{d}N', \tag{4.1.39}$$

and then, using Equation 4.1.37, we can write

$$\begin{aligned}\frac{\partial \tilde{v}}{\partial N} = \frac{\partial \tilde{u}}{\partial S} &= \frac{\partial \widetilde{U}}{\partial S} + \alpha\int_0^N \frac{\partial}{\partial S}\Big(\widetilde{\omega}_2(S,N')\Big)\mathrm{d}N', \\ &= \frac{\partial \widetilde{U}}{\partial S} - \frac{\alpha}{c}\int_0^N \frac{\partial^2}{\partial N'^2}\Big(\widetilde{\omega}_2(S,N')\Big)\mathrm{d}N',\end{aligned}$$

since

$$\frac{\partial \widetilde{\omega}_2}{\partial S} = -\frac{1}{c}\frac{\partial^2 \widetilde{\omega}_2}{\partial N^2},$$

from Equation 4.1.31. Then evaluating the integral yields

$$\begin{aligned}\frac{\partial \tilde{v}}{\partial N} &= \frac{\partial \widetilde{U}}{\partial S} - \frac{\alpha}{c}\frac{\partial \widetilde{\omega}_2}{\partial N} + \frac{\alpha}{c}\frac{\partial \widetilde{\omega}_2}{\partial N}\bigg|_{N=0} \\ &= \frac{\partial \widetilde{U}}{\partial S} - \frac{\alpha}{c}\frac{\partial \widetilde{\omega}_2}{\partial N} - \frac{\alpha}{\sqrt{c}}\mathscr{T}\left[\frac{\mathrm{d}\widehat{T}_{\mathrm{t}}}{\mathrm{d}S}\right]\end{aligned}$$

using Equation B.0.7 and Equation 4.1.35. Finally, integrating with respect to N, we have

$$\tilde{v} = N\frac{\partial \widetilde{U}}{\partial S} - \frac{\alpha}{c}\widetilde{\omega}_2 - \frac{\alpha N}{\sqrt{c}}\mathscr{T}\left[\frac{\mathrm{d}\widehat{T}_{\mathrm{t}}}{\mathrm{d}S}\right] + c_2(S)$$

for some arbitrary function c_2. Now, on the surface

$$\tilde{v}(S,0) = \frac{\delta}{\delta_{\mathrm{B}}}\frac{\partial \eta}{\partial \tau}, \quad \text{and} \quad \widetilde{\omega}_2 = -\widehat{T}_{\mathrm{t}},$$

where the value of $v(S,0)$ is fixed by the kinematic condition Equation 4.1.25. So at the surface we have

$$\frac{\delta}{\delta_{\mathrm{B}}}\frac{\partial \eta}{\partial \tau} = \frac{\alpha}{c}\widehat{T}_{\mathrm{t}} + c_2(S),$$

and therefore

$$c_2(S) = \frac{\delta}{\delta_{\mathrm{B}}}\frac{\partial \eta}{\partial \tau} - \frac{\alpha}{c}\widehat{T}_{\mathrm{t}}.$$

Finally, we have

$$\tilde{v} = N\left(\frac{\partial \widetilde{U}}{\partial S} - \frac{\alpha}{\sqrt{c}}\mathscr{T}\left[\frac{\mathrm{d}\widehat{T}_{\mathrm{t}}}{\mathrm{d}S}\right]\right) - \frac{\alpha}{c}\left(\widetilde{\omega}_2 + \widehat{T}_{\mathrm{t}}\right) + \frac{\delta}{\delta_{\mathrm{B}}}\frac{\partial \eta}{\partial \tau}. \tag{4.1.40}$$

This solution for the vertical velocity in the surface boundary layer needs to be matched to the irrotational flow. In the main fluid layer, in the fixed frame of reference $u, v = \mathcal{O}(\delta)$ and hence in the moving frame the fluid velocity at the surface is given by

$$u = -c + \delta\tilde{u}, \qquad v = \delta\delta_{\mathrm{B}}\varepsilon\tilde{v}$$

using Equation 4.1.26, where the scaling $\widehat{\varepsilon} = \delta\varepsilon$ on v is taken from Equation 4.1.35.

In order to match to the main fluid layer, we need to calculate the $N \to \infty$ limit of $\tilde{u}$ and $\tilde{v}$ from Equation 4.1.39 and Equation 4.1.40, respectively. Using (4.1.39) as $N \to \infty$,

we have

$$\begin{aligned}\tilde{u} \to \widetilde{U}_{\text{B}} &= \widetilde{U} + \alpha \int_0^\infty \widetilde{\omega}_2 \mathrm{d}N, \\ &= \widetilde{U} + \frac{\alpha}{\sqrt{c}} \mathscr{T}[f_2]\end{aligned}$$

which means that

$$\widetilde{U}_{\text{B}} = \widetilde{U} - \frac{\alpha}{\sqrt{c}} \mathscr{T}\left[\widehat{T}_{\text{t}}\right], \tag{4.1.41}$$

using $f_2(S) = -\widehat{T}_{\text{t}}$ from Equation 4.1.28, and where $\widetilde{U}_{\text{B}}$ denotes the $N \to \infty$ limit of $\tilde{u}$.

Similarly, using (4.1.40) as $N \to \infty$, we have

$$\begin{aligned}\tilde{v} \to \widetilde{V}_{\text{b}} &= \frac{\delta}{\delta_{\text{B}}}\frac{\partial \eta}{\partial \tau} - \frac{\alpha}{c}\widehat{T}_{\text{t}} + \left(N\frac{\partial \widetilde{U}}{\partial S} - \frac{\alpha N}{\sqrt{c}}\mathscr{T}\left[\frac{\mathrm{d}\widehat{T}_{\text{t}}}{\mathrm{d}S}\right]\right)_{N\to\infty} \\ &= \frac{\delta}{\delta_{\text{B}}}\frac{\partial \eta}{\partial \tau} - \frac{\alpha}{c}\widehat{T}_{\text{t}} + \left(N\frac{\partial \widetilde{U}_{\text{B}}}{\partial S}\right)_{N\to\infty}\end{aligned}$$

using Equation 4.1.41, which means that

$$\widetilde{V}_{\text{b}} = \frac{\delta}{\delta_{\text{B}}}\frac{\partial \eta}{\partial \tau} - \frac{\alpha}{c}\widehat{T}_{\text{t}} + \left(N\frac{\partial \widetilde{U}_{\text{B}}}{\partial S}\right)_{N\to\infty} \tag{4.1.42}$$

where $\widetilde{V}_{\text{b}}$ denotes the $N \to \infty$ limit of $\tilde{v}$.

Hence, the conditions which match the surface boundary layer velocity to the irrotational velocity field are given by

$$u \to -c + \delta\widetilde{U}_{\text{B}} \qquad \text{and} \qquad v \to \delta\widetilde{V}_{\text{B}}, \tag{4.1.43}$$

where $\widetilde{U}_{\text{B}}$ is defined in Equation 4.1.41 and $\widetilde{V}_{\text{B}}$ is defined to be

$$\begin{aligned}\widetilde{V}_{\text{B}} &= \delta_{\text{B}}\varepsilon\widetilde{V}_{\text{b}}, \\ &= \delta\varepsilon\frac{\partial \eta}{\partial \tau} - \delta_{\text{B}}\varepsilon\frac{\alpha}{c}\widehat{T}_{\text{t}} + \delta_{\text{B}}\varepsilon\left(N\frac{\partial \widetilde{U}_{\text{B}}}{\partial S}\right)_{N\to\infty}\end{aligned}$$

Before we solve for the main fluid layer we need to consider the viscous boundary layer at the solid bottom boundary.

Base boundary layer

Within the boundary layer at the flat bottom we define the position coordinates to be

$$X = \varepsilon x, \qquad y = -1 + \delta_{\text{N}} Y,$$

and we set

$$\mathbf{u} = (-c + \delta U)\hat{\mathbf{x}} + \delta\delta_{\text{N}}\varepsilon V\hat{\mathbf{y}}, \qquad p = -y + \delta P,$$

where δ_{N} represents the thickness of the lower boundary layer.

The Navier-Stokes equations together with the continuity equation describe a standard set of boundary layer equations, as discussed in Dewey Jr and Gross (1967). With the above parametrisations, the dimensionless continuity equation from Equation 4.1.4 becomes

$$\begin{aligned}
\nabla\cdot\mathbf{u} = \frac{\partial u}{\partial x} + \frac{\partial v}{\partial y} &= 0,\\
\varepsilon\frac{\partial u}{\partial X} + \frac{1}{\delta_{\text{N}}}\frac{\partial v}{\partial Y} &= 0,\\
\delta\varepsilon\frac{\partial U}{\partial X} + \frac{\delta\delta_{\text{N}}\varepsilon}{\delta_{\text{N}}}\frac{\partial V}{\partial Y} &= 0,\\
\Rightarrow \quad \frac{\partial U}{\partial X} + \frac{\partial V}{\partial Y} &= 0.
\end{aligned} \tag{4.1.44}$$

Next, taking the x-component of the dimensionless Navier-Stokes equations from Equation 4.1.4 where $\frac{1}{\text{Re}} = \Delta^2$, together with the above parametrisations and Equation 4.1.35, we have

$$\begin{aligned}
\frac{\partial u}{\partial t} + u\frac{\partial u}{\partial x} + v\frac{\partial u}{\partial y} &= -\frac{\partial p}{\partial x} + \Delta^2\frac{\partial^2 u}{\partial y^2},\\
\widehat{\varepsilon}\frac{\partial u}{\partial \tau} + \varepsilon u\frac{\partial u}{\partial X} + \frac{v}{\delta_{\text{N}}}\frac{\partial u}{\partial Y} &= -\varepsilon\frac{\partial p}{\partial X} + \frac{\Delta^2}{\delta_{\text{N}}^2}\frac{\partial^2 u}{\partial Y^2},\\
\delta^2\varepsilon\frac{\partial U}{\partial \tau} - c\delta\varepsilon\frac{\partial U}{\partial X} + \delta^2\varepsilon U\frac{\partial U}{\partial X} + \delta^2\varepsilon V\frac{\partial U}{\partial Y} &= -\delta\varepsilon\frac{\partial P}{\partial X} + \frac{\delta\Delta^2}{\delta_{\text{N}}^2}\frac{\partial^2 U}{\partial Y^2},\\
\Rightarrow \quad c\frac{\partial U}{\partial X} - \frac{\partial P}{\partial X} + \frac{\Delta^2}{\delta_{\text{N}}^2\varepsilon}\frac{\partial^2 U}{\partial Y^2} &= \delta\left(\frac{\partial U}{\partial \tau} + U\frac{\partial U}{\partial X} + V\frac{\partial U}{\partial Y}\right).
\end{aligned} \tag{4.1.45}$$

Similar to the surface boundary layer, in order to describe velocity decay in the base boundary layer we require a derivative with respect to Y to appear at leading-order. This

implies that

$$\frac{\Delta^2}{\delta_{\text{N}}^2\varepsilon} = \left(\frac{\delta_{\text{B}}}{\delta_{\text{N}}}\right)^2 = \mathcal{O}(1)$$

and hence $\delta_{\text{N}} = \delta_{\text{B}}$, which means that the bottom boundary layer thickness is the same as the surface boundary layer thickness.

Then, taking the y-component of the dimensionless Navier-Stokes equations from Equation 4.1.4, together with the above parametrisations we have

$$\begin{aligned}
\frac{\partial v}{\partial t} + u\frac{\partial v}{\partial x} + v\frac{\partial v}{\partial y} + 1 &= -\frac{\partial p}{\partial y} + \Delta^2\frac{\partial^2 v}{\partial y^2},\\
\widehat{\varepsilon}\frac{\partial v}{\partial \tau} + \varepsilon u\frac{\partial v}{\partial X} + \frac{v}{\delta_{\text{N}}}\frac{\partial v}{\partial Y} + 1 &= 1 - \frac{\delta}{\delta_{\text{N}}}\frac{\partial P}{\partial Y} + \frac{\delta_{\text{B}}^2\varepsilon}{\delta_{\text{N}^2}}\frac{\partial^2 v}{\partial Y^2},\\
\delta^2\delta_{\text{N}}\varepsilon^2\frac{\partial V}{\partial \tau} + \delta\delta_{\text{N}}\varepsilon^2(-c+\delta U)\frac{\partial V}{\partial X} + \delta^2\delta_{\text{N}}\varepsilon^2 V\frac{\partial V}{\partial Y} &= -\frac{\delta}{\delta_{\text{N}}}\frac{\partial P}{\partial Y} + \frac{\delta\delta_{\text{B}}^2\varepsilon^2}{\delta_{\text{N}}}\frac{\partial^2 V}{\partial Y^2},\\
\delta\delta_{\text{B}}^2\varepsilon^2\frac{\partial V}{\partial \tau} + \delta\delta_{\text{B}}^2\varepsilon^2 U\frac{\partial V}{\partial X} - c\delta_{\text{B}}^2\varepsilon^2\frac{\partial V}{\partial X} + \delta\delta_{\text{B}}^2\varepsilon^2 V\frac{\partial V}{\partial Y} &= -\frac{\partial P}{\partial Y} + \delta_{\text{B}}^2\varepsilon^2\frac{\partial^2 V}{\partial Y^2}, \qquad (4.1.46)
\end{aligned}$$

and so at leading-order we have

$$\frac{\partial P}{\partial Y} = \mathcal{O}\big(\delta_{\text{B}}^2\varepsilon^2\big) = \text{o}(\Delta^2), \qquad \text{since} \quad \Delta = \delta_{\text{B}}^2\varepsilon.$$

Hence, the boundary layer equations governing the bottom boundary layer take the form

$$\begin{aligned}
&\frac{\partial U}{\partial X} + \frac{\partial V}{\partial Y} = 0, \qquad \frac{\partial P}{\partial Y} = \text{o}(\Delta^2),\\
&c\frac{\partial U}{\partial X} - \frac{\partial P}{\partial X} + \frac{\partial^2 U}{\partial Y^2} = \delta\left(\frac{\partial U}{\partial \tau} + U\frac{\partial U}{\partial X} + V\frac{\partial U}{\partial Y}\right). \qquad (4.1.47)
\end{aligned}$$

In order to match to the main inviscid flow, we consider the $Y \to \infty$ limit and set

$$\lim_{Y\to\infty} U(X,Y) = \overline{U}(X). \qquad (4.1.48)$$

Then setting

$$f = U - \overline{U},$$

so that

$$f(X,0) = -\overline{U}(X), \qquad \text{and} \qquad f \to 0 \quad \text{as} \quad Y \to \infty,$$

the continuity equation (4.1.44) becomes

$$\begin{aligned} \frac{\partial U}{\partial X} + \frac{\partial V}{\partial Y} &= 0, \\ \Rightarrow \quad \frac{\mathrm{d}\overline{U}}{\mathrm{d}X} + \frac{\partial f}{\partial X} + \frac{\partial V}{\partial Y} &= 0. \end{aligned}$$

In addition to this, Equation 4.1.44 becomes

$$\begin{aligned} c\frac{\partial U}{\partial X} - \frac{\partial P}{\partial X} + \frac{\partial^2 U}{\partial Y^2} &= \mathcal{O}(\delta), \\ \Rightarrow c\frac{\mathrm{d}\overline{U}}{\mathrm{d}X} + c\frac{\partial f}{\partial X} - \frac{\partial P}{\partial X} + \frac{\partial^2 f}{\partial Y^2} &= \mathcal{O}(\delta). \end{aligned}$$

As $Y \to \infty$, $f \to 0$, so

$$\frac{\partial P}{\partial X} = c\frac{\mathrm{d}\overline{U}}{\mathrm{d}X}, \tag{4.1.49}$$

but $\frac{\partial P}{\partial Y} = 0$ so Equation 4.1.49 holds throughout. Therefore, we have

$$c\frac{\partial f}{\partial X} + \frac{\partial^2 f}{\partial Y^2} = \mathcal{O}(\delta).$$

This in essence is identical in structure to the surface boundary layer. Then integrating the continuity equation from (4.1.47), we obtain

$$V \to \overline{V} = -Y\frac{\mathrm{d}\overline{U}}{\mathrm{d}X} + \frac{1}{\sqrt{c}}\mathscr{T}\left[\frac{\mathrm{d}\overline{U}}{\mathrm{d}X}\right], \tag{4.1.50}$$

as $Y \to \infty$.

We have shown using scaling arguments that the thickness of the lower boundary layer is the same order as the thickness of the boundary layer at the surface. However, although the thickness is the same as the upper layer, the boundary layer at the fluid bottom is a different kind of boundary layer. The base boundary layer describes a decay in tangential velocity from its free-stream value in the main inviscid fluid body to zero on the solid bottom boundary, while the surface boundary layer represents decay of vorticity across the layer.

At this point we note that although we have derived matching conditions for matching the base boundary layer to the main flow, we have not fully solved the boundary layer prob-

lem. The pressure gradient in the boundary layer is given by Equation 4.1.49, although this is given in terms of $\overline{U}$ which has not been solved explicitly. Given the geometry of the surface wave, it is reasonable to expect $\bar{U}$ to have a turning point for some X. If so, then there will be a region in the fluid where the pressure gradient becomes negative.

An adverse pressure gradient can cause flow reversal in the boundary layer which can lead to boundary layer separation (Smith, 1986). The flow reversal is usually caused by adverse pressure gradient imposed on the boundary layer by the potential flow. Boundary layer separation is prominent in laminar flows; examples include high-speed flow past an airfoil (Atik et al., 2005), and uniform shear flow around a circular cylinder (Wu and Chen, 2000).

However, boundary layer separation can also occur in horizontal flows over a flat plate with adverse pressure gradients (Canepa et al., 2006). While we make no attempt to solve the boundary layer problem either explicitly or numerically in this thesis, further investigation may be needed to decide if the proposed flow structure is correct. Going forward, we use the assumption that separation does not occur in this system, where the base boundary layer has a similar structure to that discussed in Sugimoto (1996), and leave the problem open to future discussion.

We now proceed to solve for the main fluid layer, and use the matching conditions to match each boundary layer to the main fluid flow.

4.1.2 The potential flow

We solve for the potential flow away from each of the boundary layers, and match to the boundary layers using the matching conditions defined earlier. In the main fluid layer we write

$$\begin{aligned}\mathbf{u} &= -c\hat{\mathbf{x}} + \frac{\delta}{\varepsilon}\nabla\phi, \\ &= \left(-c + \delta\frac{\partial\phi}{\partial X}\right)\hat{\mathbf{x}} + \frac{\delta}{\varepsilon}\frac{\partial\phi}{\partial y}\hat{\mathbf{y}},\end{aligned} \tag{4.1.51}$$

where the scaling on $\phi(X, y)$ is chosen so that the horizontal disturbance velocity is $\mathcal{O}(\delta)$.

First, we will match to the lower boundary layer. The horizontal component of velocity in the main fluid is given by

$$-c + \delta \frac{\partial \phi}{\partial X}$$

and the horizontal component of velocity in the lower boundary layer is given by

$$-c + \delta \overline{U},$$

where $\overline{U}$ is defined by

$$\overline{U}(X) = \lim_{Y \to \infty} U(X, Y)$$

from Equation 4.1.48. Thus, matching to the lower boundary layer we have

$$\lim_{y \to -1} \left[-c + \delta \frac{\partial \phi}{\partial X} \right] = -c + \delta \overline{U}.$$

Similarly, matching the vertical component of velocity we have

$$\lim_{y \to -1} \left[\frac{\delta}{\varepsilon} \frac{\partial \phi}{\partial y} \right] = \delta \delta_{\text{B}} \varepsilon \overline{V} \hat{\mathbf{y}},$$

where $\overline{V}$ is defined to be

$$\overline{V} = -Y \frac{\partial \overline{U}}{\partial X} + \frac{1}{\sqrt{c}} \mathscr{T} \left[\frac{\partial \overline{U}}{\partial X} \right], \quad \text{where } Y = \frac{y+1}{\delta_{\text{B}}},$$

from Equation 4.1.50. Therefore looking at the horizontal components we can say

$$\begin{aligned} \lim_{y \to -1} \left[\frac{\partial \phi}{\partial X} \right] &= \lim_{y \to -1} [U] \\ &= \overline{U} \end{aligned}$$

and hence

$$\frac{\partial^2 \phi}{\partial X^2} = \frac{\partial \overline{U}}{\partial X}$$

as $y \to -1$. Then, looking at the vertical components we can say

$$\begin{aligned}\lim_{y\to-1}\left[\frac{\partial\phi}{\partial y}\right] &= \delta_{\text{B}}\varepsilon^2\overline{V} \\ &= \varepsilon^2\left(-\delta_{\text{B}}Y\frac{\partial\overline{U}}{\partial X}+\frac{\delta_{\text{B}}}{\sqrt{c}}\mathscr{T}\left[\frac{\partial\overline{U}}{\partial X}\right]\right),\end{aligned}$$

and hence

$$\begin{aligned}\lim_{y\to-1}\left[\frac{\partial\phi}{\partial y}\right] &= \varepsilon^2\left(-(1+y)\frac{\partial\overline{U}}{\partial X}+\frac{\delta_{\text{B}}}{\sqrt{c}}\mathscr{T}\left[\frac{\partial\overline{U}}{\partial X}\right]\right), \\ &= \varepsilon^2\left(-(1+y)\frac{\partial^2\phi}{\partial X^2}+\frac{\delta_{\text{B}}}{\sqrt{c}}\mathscr{T}\left[\frac{\partial^2\phi}{\partial X^2}\right]\right).\end{aligned} \tag{4.1.52}$$

We now solve for the flow in the main layer. The potential flow satisfies the relation

$$\varepsilon^2\frac{\partial^2\phi}{\partial X^2}+\frac{\partial^2\phi}{\partial y^2}=0, \tag{4.1.53}$$

which is the continuity equation (4.1.44) in terms of ϕ. In order to solve for ϕ, we can expand for small ε and write

$$\phi(X,y;\varepsilon)=\phi_0(X,y)+\varepsilon^2\phi_1(X,y)+\mathcal{O}(\varepsilon^4). \tag{4.1.54}$$

Then substituting Equation 4.1.54 into Equation 4.1.53, at leading-order we have

$$\frac{\partial^2\phi_0}{\partial y^2}=0$$

and hence, after integrating we have

$$\phi_0=(y+1)A(X)+B(X)$$

for some arbitrary functions A, B to be determined. We choose $(y+1)$ as our variable when integrating as we know that the boundary layer will be a function of $Y=\frac{y+1}{\delta_{\text{B}}}$. Then using the matching condition Equation 4.1.52 at leading-order, as $y\to-1$ we have

$$\frac{\partial\phi_0}{\partial y}=0,$$

so $A(X) = 0$. Then we will write $B(X) = G(X,t)$ so that

$$\phi = G(X,t) + \varepsilon^2 \phi_1(X,y) + \mathcal{O}(\varepsilon^4)$$

where $G(X,t)$ is a function that will be determined later. Now, at $\mathcal{O}(\varepsilon^2)$ we have

$$\frac{\partial^2 \phi_0}{\partial X^2} + \frac{\partial^2 \phi_1}{\partial y^2} = \frac{\partial^2 G}{\partial X^2} + \frac{\partial^2 \phi_1}{\partial y^2} = 0$$

and hence, after integrating, we have

$$\frac{\partial \phi_1}{\partial y} = -(y+1)\frac{\partial^2 G}{\partial X^2} + C(X),$$

for some arbitrary function C to be determined. To derive C we use the matching condition Equation 4.1.52 again at $\mathcal{O}(\varepsilon^2)$, so as $y \to -1$ we have

$$\begin{aligned}\frac{\partial \phi_1}{\partial y} &= -(1+y)\frac{\partial^2 \phi_0}{\partial X^2} + \frac{\delta_{\text{B}}}{\sqrt{c}}\mathscr{T}\left[\frac{\partial^2 \phi_0}{\partial X^2}\right] \\ &= -(1+y)\frac{\partial^2 G}{\partial X^2} + \frac{\delta_{\text{B}}}{\sqrt{c}}\mathscr{T}\left[\frac{\partial^2 G}{\partial X^2}\right]\end{aligned}$$

which means that matching to the main layer gives

$$-(y+1)\frac{\partial^2 G}{\partial X^2} + C(X) = -(1+y)\frac{\partial^2 G}{\partial X^2} + \frac{\delta_{\text{B}}}{\sqrt{c}}\mathscr{T}\left[\frac{\partial^2 G}{\partial X^2}\right]$$

as $y \to -1$, and hence

$$C(X) = \frac{\delta_{\text{B}}}{\sqrt{c}}\mathscr{T}\left[\frac{\partial^2 G}{\partial X^2}\right].$$

Therefore we have

$$\frac{\partial \phi_1}{\partial y} = -(1+y)\frac{\partial^2 G}{\partial X^2} + \frac{\delta_{\text{B}}}{\sqrt{c}}\mathscr{T}\left[\frac{\partial^2 G}{\partial X^2}\right]$$

throughout the main flow. Now to get $\phi_1(X,y)$, we integrate again to get

$$\phi_1(X,y) = -\frac{(1+y)^2}{2}\frac{\partial^2 G}{\partial X^2} + (1+y)\frac{\delta_{\text{B}}}{\sqrt{c}}\mathscr{T}\left[\frac{\partial^2 G}{\partial X^2}\right] + D(X)$$

where D is an arbitrary function which represents some $\mathcal{O}(\varepsilon^2)$ correction to ϕ, and can

therefore be incorporated into $G(X,t)$. Hence, we set $D(X) = 0$ and obtain

$$\phi_1(X,y) = -\frac{(y+1)^2}{2}\frac{\partial^2 G}{\partial X^2} + (y+1)\frac{\delta_{\text{B}}}{\sqrt{c}}\mathscr{T}\left[\frac{\partial^2 G}{\partial X^2}\right]$$

to give

$$\phi = G(X,t) + \varepsilon^2\left(-\frac{1}{2}(1+y)^2\frac{\partial^2 G}{\partial X^2} + \frac{\delta_{\text{B}}}{\sqrt{c}}(1+y)\mathscr{T}\left[\frac{\partial^2 G}{\partial X^2}\right]\right) + \mathcal{O}(\varepsilon^4, \delta_{\text{B}}\varepsilon^4). \tag{4.1.55}$$

We can also solve for $\mathcal{O}(\varepsilon^4)$ and $\mathcal{O}(\varepsilon^6)$, which would equate to the functions $\phi_2(X,y)$ and $\phi_3(X,y)$ respectively in the small ε expansion of ϕ given by Equation 4.1.54, through repeated evaluation of

$$\frac{\partial^2 \phi_{r+1}}{\partial y^2} = -\frac{\partial^2 \phi_r}{\partial X^2}.$$

This eventually yields

$$\begin{aligned}\phi = G(X,t) - \frac{1}{2!}\varepsilon^2(1+y)^2\frac{\partial^2 G}{\partial X^2} + \varepsilon^2\frac{\delta_{\text{B}}}{\sqrt{c}}(1+y)\mathscr{T}\left[\frac{\partial^2 G}{\partial X^2}\right] \\ + \frac{1}{4!}\varepsilon^4(1+y)^4\frac{\partial^4 G}{\partial X^4} - \frac{1}{6!}\varepsilon^6(1+y)^6\frac{\partial^6 G}{\partial X^6} + \mathcal{O}(\varepsilon^8, \delta_{\text{B}}\varepsilon^4).\end{aligned} \tag{4.1.56}$$

In the subsequent analysis, it will be seen why $\mathcal{O}(\varepsilon^4)$ and $\mathcal{O}(\varepsilon^6)$ terms are retained, but $\mathcal{O}(\delta_{\text{B}}\varepsilon^4)$ and smaller terms are dropped. We now obtain an equation governing $G(X,t)$ by considering matching of the main fluid layer to the surface boundary layer. Since the equations governing the surface boundary layer are all in terms of our scaled orthogonal curvilinear coordinates S and N, we will match the velocity components to the main fluid flow in terms of this coordinate system, and from now on we will consider G to be a function of S and t.

Approaching the surface, the tangential component of the velocity in the main flow (4.1.51)

is given by

$$\begin{aligned} u_{\text{B}} &= -c(\hat{\mathbf{t}}\cdot\hat{\mathbf{x}}) + \delta\left(\frac{\partial\phi}{\partial X}(\hat{\mathbf{t}}\cdot\hat{\mathbf{x}}) + \frac{1}{\varepsilon}\frac{\partial\phi}{\partial y}(\hat{\mathbf{t}}\cdot\hat{\mathbf{y}})\right), \\ &= -c + \delta\left(\frac{\partial\phi}{\partial X} + \delta\frac{\partial\phi}{\partial y}\frac{\partial\eta}{\partial S}\right), \\ &= -c + \delta\left(\frac{\partial\phi}{\partial S} + \delta\frac{\partial\phi}{\partial y}\frac{\partial\eta}{\partial S}\right) + \mathcal{O}(\delta^2\varepsilon^2), \end{aligned} \tag{4.1.57}$$

using the fact

$$\frac{\partial}{\partial X} = \frac{\partial}{\partial S} + \mathcal{O}(\delta^2\varepsilon^2),$$

and

$$\hat{\mathbf{t}}\cdot\hat{\mathbf{x}} = 1, \qquad \hat{\mathbf{t}}\cdot\hat{\mathbf{y}} = \delta\varepsilon\frac{\partial\eta}{\partial S},$$

from the definition of the tangential unit vector from earlier given in Equation 4.1.24. Similarly the normal velocity component in the main flow is given by

$$\begin{aligned} v_{\text{B}} &= -c(\hat{\mathbf{n}}\cdot\hat{\mathbf{x}}) + \delta\left(\frac{\partial\phi}{\partial X}(\hat{\mathbf{n}}\cdot\hat{\mathbf{x}}) + \frac{1}{\varepsilon}\frac{\partial\phi}{\partial y}(\hat{\mathbf{n}}\cdot\hat{\mathbf{y}})\right), \\ &= \delta\varepsilon\left(c\frac{\partial\eta}{\partial S} - \delta\frac{\partial\eta}{\partial S}\frac{\partial\phi}{\partial X} + \frac{1}{\varepsilon^2}\frac{\partial\phi}{\partial y}\right), \\ &= \delta\varepsilon\left(c\frac{\partial\eta}{\partial S} - \delta\frac{\partial\eta}{\partial S}\frac{\partial\phi}{\partial S} + \frac{1}{\varepsilon^2}\frac{\partial\phi}{\partial y}\right) + \mathcal{O}(\delta^2\varepsilon^2), \end{aligned} \tag{4.1.58}$$

where

$$\hat{\mathbf{n}}\cdot\hat{\mathbf{x}} = -\delta\varepsilon\frac{\partial\eta}{\partial S}, \qquad \hat{\mathbf{n}}\cdot\hat{\mathbf{y}} = 1,$$

from the definition of the normal unit vector given earlier in Equation 4.1.23.

In the surface boundary layer, the tangential component of the velocity close to the main flow is given by

$$-c + \delta\widetilde{U}_{\text{B}}$$

from Equation 4.1.43, where $\widetilde{U}_{\text{B}}$ is defined in Equation 4.1.41 to be

$$\widetilde{U}_{\text{B}} = \widetilde{U} - \frac{\alpha}{\sqrt{c}}\mathscr{T}\left[\widehat{T}_{\text{t}}\right].$$

Thus, looking at the tangential velocity components, the matching condition of the main

flow u_{B} to the surface boundary layer solution is given by

$$\lim_{y\to 0}\left[u_{\text{B}}\right] = \lim_{y\to 0}\left[-c+\delta\frac{\partial\phi}{\partial S}+\mathcal{O}(\delta^2)\right] = -c+\delta\widetilde{U}-\delta\frac{\alpha}{\sqrt{c}}\mathscr{T}\left[\widehat{T}_{\text{t}}\right]. \tag{4.1.59}$$

We see that the $-c$ terms match exactly. Then considering $\mathcal{O}(\delta)$ terms, in order to match we require

$$\lim_{y\to 0}\left[\frac{\partial\phi}{\partial S}\right] = \widetilde{U}-\frac{\alpha}{\sqrt{c}}\mathscr{T}\left[\widehat{T}_{\text{t}}\right],$$

and hence using Equation 4.1.56 we obtain

$$\lim_{y\to 0}\left[\frac{\partial G}{\partial S}-\frac{\varepsilon^2}{2}(1+y)^2\frac{\partial^3 G}{\partial S^3}+\mathcal{O}(\delta_{\text{B}}\varepsilon^2,\varepsilon^4)\right] = \widetilde{U}-\frac{\alpha}{\sqrt{c}}\mathscr{T}\left[\widehat{T}_{\text{t}}\right] \tag{4.1.60}$$

which at leading-order becomes

$$\frac{\partial G}{\partial S} = \widetilde{U}-\frac{\alpha}{\sqrt{c}}\mathscr{T}\left[\widehat{T}_{\text{t}}\right]. \tag{4.1.61}$$

Looking now at the normal component of velocity in the outer edge of the surface boundary layer, from Equation 4.1.43 we have

$$\delta V_{\text{B}} = \delta\varepsilon\left(\delta\frac{\partial\eta}{\partial\tau}-\frac{\delta_{\text{B}}\alpha}{c}\widehat{T}_{\text{t}}\right)+\delta\delta_{\text{B}}\varepsilon\left(N\frac{\partial\widetilde{U}_{\text{B}}}{\partial S}\right)_{N\to\infty}$$

and therefore, the matching condition of the main flow v_{B} to the surface boundary layer is given by

$$\begin{aligned}\lim_{y\to 0}\left[v_{\text{B}}\right] &= \delta\varepsilon\left(\delta\frac{\partial\eta}{\partial\tau}-\frac{\delta_{\text{B}}\alpha}{c}\widehat{T}_{\text{t}}\right)+\delta\delta_{\text{B}}\varepsilon\left(N\frac{\partial\widetilde{U}_{\text{B}}}{\partial S}\right)_{N\to\infty}\\ &= \delta\delta_{\text{B}}\varepsilon V_0+\delta\delta_{\text{B}}\varepsilon\left(N\frac{\partial\widetilde{U}_{\text{B}}}{\partial S}\right)_{N\to\infty}\end{aligned} \tag{4.1.62}$$

where

$$V_0 = \frac{\delta}{\delta_{\text{B}}}\frac{\partial\eta}{\partial\tau}-\frac{\alpha}{c}\widehat{T}_{\text{t}}.$$

In order to match we require

$$\lim_{y\to 0}\left[\delta\varepsilon c\frac{\partial\eta}{\partial S}-\delta^2\varepsilon\frac{\partial\eta}{\partial S}\frac{\partial\phi}{\partial S}+\frac{\delta}{\varepsilon}\frac{\partial\phi}{\partial y}\right]=\delta\delta_{\text{B}}\varepsilon V_0+\delta\delta_{\text{B}}\varepsilon\mathcal{U}$$
$$\Rightarrow\quad\lim_{y\to 0}\left[\varepsilon^2 c\frac{\partial\eta}{\partial S}-\delta\varepsilon^2\frac{\partial\eta}{\partial S}\frac{\partial\phi}{\partial S}+\frac{\partial\phi}{\partial y}\right]=\delta_{\text{B}}\varepsilon^2 V_0+\delta_{\text{B}}\varepsilon^2\mathcal{U}$$

using the definition of v_b given in Equation 4.1.58, and where

$$\mathcal{U}=\left(N\left(\frac{\partial\widetilde{U}}{\partial S}-\frac{\alpha}{\sqrt{c}}\mathscr{T}\left[\frac{\partial\widehat{T}_{\text{t}}}{\partial S}\right]\right)\right)_{N\to\infty}$$
$$=\left(N\frac{\partial^2 G}{\partial S^2}\right)_{N\to\infty}$$

using Equation 4.1.61. Hence, in the matching region we have

$$c\frac{\partial\eta}{\partial S}-\delta\frac{\partial\eta}{\partial S}\frac{\partial G}{\partial S}+\frac{\delta_{\text{B}}}{\sqrt{c}}\mathscr{T}\left[\frac{\partial^2 G}{\partial S^2}\right]-(1+y)\frac{\partial^2 G}{\partial S^2}+\mathcal{O}(\varepsilon^2,\delta\varepsilon^2)=\delta_{\text{B}}V_0+\delta_{\text{B}}\mathcal{U}. \quad (4.1.63)$$

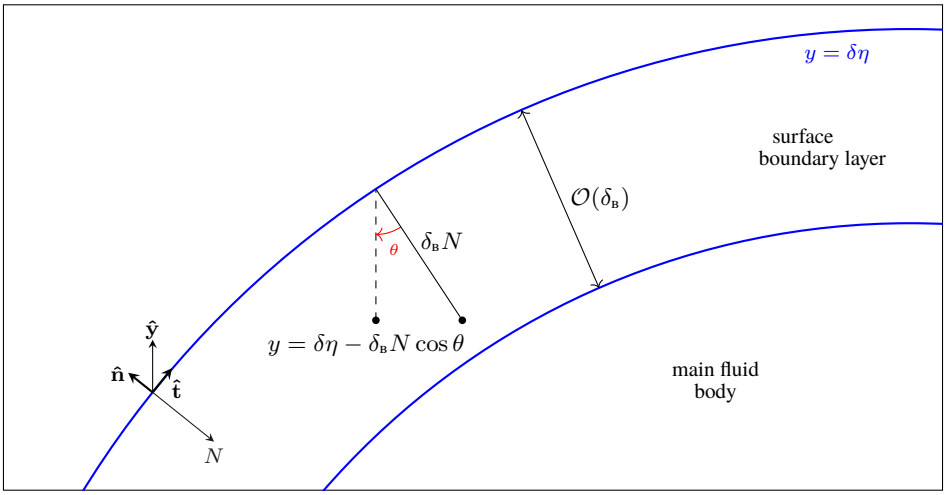

Figure 4.1.4: Sketch illustrating the relation between y and N in the matching region.

Up to now, in discussing the matching condition we have written $y\to 0$ as the matching region for the main layer. However, due to the behaviour of $\mathcal{U}$, the matching requires a more careful treatment. In the matching region, y and N are related by

$$y=\delta\eta-\delta_{\text{B}}N\cos\theta,$$
$$=\delta\eta-\delta_{\text{B}}N(\hat{\mathbf{n}}\cdot\hat{\mathbf{y}})$$

as illustrated by Figure 4.1.4. But to leading-order, $\hat{\mathbf{n}} \cdot \hat{\mathbf{y}} = 1$, so the relation between y and N in the matching region is

$$y = \delta\eta - \delta_{\text{B}} N. \tag{4.1.64}$$

Hence, in the matching region $N \to \infty$, $\delta_{\text{B}} N \to 0$, and Equation 4.1.63 becomes

$$c\frac{\partial \eta}{\partial S} - \delta \frac{\partial \eta}{\partial S}\frac{\partial G}{\partial S} + \frac{\delta_{\text{B}}}{\sqrt{c}}\mathscr{T}\left[\frac{\partial^2 G}{\partial S^2}\right] - (1 + \delta\eta - \delta_{\text{B}} N)\frac{\partial^2 G}{\partial S^2} + \mathcal{O}(\varepsilon^2) = \delta_{\text{B}} V_0 + \delta_{\text{B}} N \frac{\partial^2 G}{\partial S^2}.$$

It is seen that the terms proportional to N automatically match, leaving

$$\begin{aligned} & c\frac{\partial \eta}{\partial S} - \delta \frac{\partial \eta}{\partial S}\frac{\partial G}{\partial S} + \frac{\delta_{\text{B}}}{\sqrt{c}}\mathscr{T}\left[\frac{\partial^2 G}{\partial S^2}\right] - \frac{\partial^2 G}{\partial S^2} - \delta\eta\frac{\partial^2 G}{\partial S^2} = \delta\frac{\partial \eta}{\partial \tau} - \frac{\alpha\delta_{\text{B}}}{c}\widehat{T}_{\text{t}}, \\ \Rightarrow \quad & c\frac{\partial \eta}{\partial S} - \delta\frac{\partial}{\partial S}\left(\eta\frac{\partial G}{\partial S}\right) - \frac{\partial^2 G}{\partial S^2} + \frac{\delta_{\text{B}}}{\sqrt{c}}\mathscr{T}\left[\frac{\partial^2 G}{\partial S^2}\right] = \delta\frac{\partial \eta}{\partial \tau} - \frac{\alpha\delta_{\text{B}}}{c}\widehat{T}_{\text{t}}. \end{aligned}$$

Including the additional terms up to $\mathcal{O}(\varepsilon^6)$ from Equation 4.1.56 in the evaluation of $\frac{\partial \phi}{\partial y}$ gives

$$c\frac{\partial \eta}{\partial S} - \delta\frac{\partial}{\partial S}\left(\eta\frac{\partial G}{\partial S}\right) - \frac{\partial^2 G}{\partial S^2} + \frac{\delta_{\text{B}}}{\sqrt{c}}\mathscr{T}\left[\frac{\partial^2 G}{\partial S^2}\right] + \frac{\varepsilon^2}{3!}\frac{\partial^4 G}{\partial S^4} - \frac{\varepsilon^4}{5!}\frac{\partial^6 G}{\partial S^6} = \delta\frac{\partial \eta}{\partial \tau} - \frac{\alpha\delta_{\text{B}}}{c}\widehat{T}_{\text{t}}. \tag{4.1.65}$$

Similarly, including terms of the same order the tangential matching condition Equation 4.1.60 becomes

$$\frac{\partial G}{\partial S} - \frac{\varepsilon^2}{2!}\frac{\partial^3 G}{\partial S^3} + \frac{\varepsilon^4}{4!}\frac{\partial^5 G}{\partial S^5} + \mathcal{O}(\delta\varepsilon^2, \delta_{\text{B}}\varepsilon^2, \varepsilon^6) = \widetilde{U} - \frac{\alpha}{\sqrt{c}}\mathscr{T}\left[\widehat{T}_{\text{t}}\right]. \tag{4.1.66}$$

The reason for including these higher-order terms is discussed later in this section.

The aim going forward is to derive a differential equation governing the long-wavelength, shallow water fluid flow with an arbitrary stress condition at the fluid surface. In order to do this, we need to eliminate G and $\widetilde{U}$, and obtain a PDE for the surface elevation $\eta(S, \tau)$.

We currently have three equations of interest: the normal matching condition (4.1.65) which gives us information relating the surface elevation η to the leading-order potential G in the main flow, the tangential matching condition (4.1.66) which gives us information

relating G to the tangential fluid velocity at the surface $\widetilde{U}$, and also the tangential momentum equation (4.1.36) at the surface which relates η to $\widetilde{U}$. We will use these equations to eliminate G and $\widetilde{U}$ and derive the PDE for the surface elevation governing the fluid flow.

First, rearranging and differentiating Equation 4.1.66 with respect to S gives

$$\frac{\partial \widetilde{U}}{\partial S} = \frac{\partial^2 G}{\partial S^2} + \frac{\alpha}{\sqrt{c}}\mathscr{T}\left[\frac{\partial \widehat{T}_{\mathrm{t}}}{\partial S}\right] - \frac{\varepsilon^2}{2!}\frac{\partial^4 G}{\partial S^4} + \frac{\varepsilon^4}{4!}\frac{\partial^6 G}{\partial S^6}.$$

Then, combining this with Equation 4.1.65, in order to retain higher-order quantities, yields

$$\begin{aligned}\frac{\partial \widetilde{U}}{\partial S} = c\frac{\partial \eta}{\partial S} - \delta\left(\frac{\partial \eta}{\partial \tau} + \frac{\partial}{\partial S}\left(\eta\frac{\partial G}{\partial S}\right)\right) + \frac{\alpha\delta_{\mathrm{B}}}{c}\widehat{T}_{\mathrm{t}} + \frac{\delta_{\mathrm{B}}}{\sqrt{c}}\mathscr{T}\left[\frac{\partial^2 G}{\partial S^2}\right] \\ + \frac{\alpha}{\sqrt{c}}\mathscr{T}\left[\frac{\partial \widehat{T}_{\mathrm{t}}}{\partial S}\right] - \frac{\varepsilon^2}{2!}\frac{\partial^4 G}{\partial S^4} + \frac{\varepsilon^2}{3!}\frac{\partial^4 G}{\partial S^4} + \frac{\varepsilon^4}{4!}\frac{\partial^6 G}{\partial S^6} - \frac{\varepsilon^4}{5!}\frac{\partial^6 G}{\partial S^6},\end{aligned}$$

which simplifies to

$$\begin{aligned}\frac{\partial \widetilde{U}}{\partial S} = c\frac{\partial \eta}{\partial S} - \delta\left(\frac{\partial \eta}{\partial \tau} + \frac{\partial}{\partial S}\left(\eta\frac{\partial G}{\partial S}\right)\right) + \frac{\alpha\delta_{\mathrm{B}}}{c}\widehat{T}_{\mathrm{t}} + \frac{\delta_{\mathrm{B}}}{\sqrt{c}}\mathscr{T}\left[\frac{\partial^2 G}{\partial S^2}\right] \\ + \frac{\alpha}{\sqrt{c}}\mathscr{T}\left[\frac{\partial \widehat{T}_{\mathrm{t}}}{\partial S}\right] - \frac{\varepsilon^2}{3}\frac{\partial^4 G}{\partial S^4} - \frac{\varepsilon^4}{45}\frac{\partial^6 G}{\partial S^6}.\end{aligned}$$

Now we can eliminate G using the leading-order form of Equation 4.1.65

$$\frac{\partial^2 G}{\partial S^2} = c\frac{\partial \eta}{\partial S},$$

and hence we have

$$\begin{aligned}\frac{\partial \widetilde{U}}{\partial S} = c\frac{\partial \eta}{\partial S} - \delta\left(\frac{\partial \eta}{\partial \tau} + 2c\eta\frac{\partial \eta}{\partial S}\right) - c\frac{\varepsilon^2}{3}\frac{\partial^3 \eta}{\partial S^3} - c\frac{\varepsilon^4}{45}\frac{\partial^5 \eta}{\partial S^5} \\ + \frac{\alpha}{c}\left(\delta_{\mathrm{B}}\widehat{T}_{\mathrm{t}} + \sqrt{c}\,\mathscr{T}\left[\frac{\partial \widehat{T}_{\mathrm{t}}}{\partial S}\right]\right) + \delta_{\mathrm{B}}\sqrt{c}\,\mathscr{T}\left[\frac{\partial \eta}{\partial S}\right].\end{aligned} \tag{4.1.67}$$

It was discussed earlier in the surface boundary layer formulation that the case of most

interest is when $\alpha = \mathcal{O}(1)$. Therefore, at leading-order Equation 4.1.67 becomes

$$\begin{aligned} \frac{\partial \widetilde{U}}{\partial S} &= c\frac{\partial \eta}{\partial S} + \frac{\alpha}{\sqrt{c}}\,\mathscr{T}\left[\frac{\partial \widehat{T}_{\mathrm{t}}}{\partial S}\right] + \mathcal{O}(\delta, \delta_{\mathrm{B}}, \varepsilon^2), \\ \Rightarrow \quad \widetilde{U} &= c\eta + \frac{\alpha}{\sqrt{c}}\,\mathscr{T}\left[\widehat{T}_{\mathrm{t}}\right] \end{aligned} \tag{4.1.68}$$

This can now be used to remove terms involving $\widetilde{U}$ from the right-hand side of the tangential momentum equation (4.1.36) at the surface, as follows:

$$\begin{aligned} \frac{\partial \eta}{\partial S} - c\frac{\partial \widetilde{U}}{\partial S} &= -\delta\left(\frac{\partial \widetilde{U}}{\partial \tau} + \widetilde{U}\frac{\partial U}{\partial S}\right) - 2\delta_{\mathrm{B}}\varepsilon^2 c^{3/2}\,\mathscr{T}\left[\frac{\partial^3 \eta}{\partial S^3}\right] - \alpha\sqrt{c}\frac{\partial \widehat{T}_{\mathrm{t}}}{\partial S} + \beta\frac{\partial \widehat{T}_{\mathrm{n}}}{\partial S} \quad \text{(4.1.36)}, \\ &= -\delta\left(c\frac{\partial \eta}{\partial \tau} + \left(c\eta + \frac{\alpha}{\sqrt{c}}\,\mathscr{T}\left[\widehat{T}_{\mathrm{t}}\right]\right)\left(c\frac{\partial \eta}{\partial S} + \frac{\alpha}{\sqrt{c}}\,\mathscr{T}\left[\frac{\partial \widehat{T}_{\mathrm{t}}}{\partial S}\right]\right)\right) \\ &\quad - 2\delta_{\mathrm{B}}\varepsilon^2 c^{3/2}\,\mathscr{T}\left[\frac{\partial^3 \eta}{\partial S^3}\right] - \alpha\sqrt{c}\frac{\partial \widehat{T}_{\mathrm{t}}}{\partial S} + \beta\frac{\partial \widehat{T}_{\mathrm{n}}}{\partial S}, \\ &= -\delta c\left(\frac{\partial \eta}{\partial \tau} + c\eta\frac{\partial \eta}{\partial S} + \frac{\alpha}{\sqrt{c}}\left(\mathscr{T}\left[\widehat{T}_{\mathrm{t}}\right]\frac{\partial \eta}{\partial S} + \eta\,\mathscr{T}\left[\frac{\partial \widehat{T}_{\mathrm{t}}}{\partial S}\right]\right) + \frac{\alpha^2}{c}\mathscr{T}\left[\widehat{T}_{\mathrm{t}}\right]\mathscr{T}\left[\frac{\partial \widehat{T}_{\mathrm{t}}}{\partial S}\right]\right) \\ &\quad - 2\delta_{\mathrm{B}}\varepsilon^2 c^{3/2}\,\mathscr{T}\left[\frac{\partial^3 \eta}{\partial S^3}\right] - \alpha\sqrt{c}\frac{\partial \widehat{T}_{\mathrm{t}}}{\partial S} + \beta\frac{\partial \widehat{T}_{\mathrm{n}}}{\partial S}. \end{aligned} \tag{4.1.69}$$

We then use Equation 4.1.67 to eliminate $\frac{\partial \widetilde{U}}{\partial S}$ from the left-hand side, which yields

$$\begin{aligned} \frac{\partial \eta}{\partial S} - c\frac{\partial \widetilde{U}}{\partial S} &= \frac{\partial \eta}{\partial S} - c^2\frac{\partial \eta}{\partial S} + \delta c\left(\frac{\partial \eta}{\partial \tau} + 2c\eta\frac{\partial \eta}{\partial S}\right) + c^2\left(\frac{\varepsilon^2}{3}\frac{\partial^3 \eta}{\partial S^3} + \frac{\varepsilon^4}{45}\frac{\partial^5 \eta}{\partial S^5}\right) \\ &\quad - \alpha\delta_{\mathrm{B}}\widehat{T}_{\mathrm{t}} - \alpha\sqrt{c}\,\mathscr{T}\left[\frac{\partial \widehat{T}_{\mathrm{t}}}{\partial S}\right] - \delta_{\mathrm{B}}c^{3/2}\,\mathscr{T}\left[\frac{\partial \eta}{\partial S}\right]. \end{aligned} \tag{4.1.70}$$

Then we can combine Equation 4.1.69 and Equation 4.1.70 to give

$$\begin{aligned} &(1-c^2)\frac{\partial \eta}{\partial S} + \delta c\left(2\frac{\partial \eta}{\partial \tau} + 3c\eta\frac{\partial \eta}{\partial S}\right) \\ &\qquad = -c^2\left(\frac{\varepsilon^2}{3}\frac{\partial^3 \eta}{\partial S^3} + \frac{\varepsilon^4}{45}\frac{\partial^5 \eta}{\partial S^5}\right) - \delta_{\mathrm{B}}c^{3/2}\,\mathscr{T}\left[\frac{\partial \eta}{\partial S}\right] + \beta\frac{\partial \widehat{T}_{\mathrm{n}}}{\partial S} \\ &\qquad\quad - \frac{\alpha\delta}{\sqrt{c}}\left(\mathscr{T}\left[\frac{\partial \widehat{T}_{\mathrm{t}}}{\partial \tau}\right] + c\frac{\partial}{\partial S}\left(\eta\,\mathscr{T}\left[\widehat{T}_{\mathrm{t}}\right]\right) + \frac{\alpha}{\sqrt{c}}\,\mathscr{T}\left[\widehat{T}_{\mathrm{t}}\right]\mathscr{T}\left[\frac{\partial \widehat{T}_{\mathrm{t}}}{\partial S}\right] - \frac{\delta_{\mathrm{B}}}{\delta}\widehat{T}_{\mathrm{t}}\right). \end{aligned}$$

By considering leading-order terms we see that $c = 1 + \mathcal{O}(\delta)$. Here we define $c = 1$ and include evolution with time in the PDE on the slow time scale. Hence, finally the equation governing the shallow water long-wavelength fluid flow with an arbitrary stress

condition at the fluid surface are

$$2\frac{\partial \eta}{\partial \tau}+3\eta\frac{\partial \eta}{\partial S}+\frac{\varepsilon^2}{\delta}\left(\frac{1}{3}\frac{\partial^3 \eta}{\partial S^3}+\frac{\varepsilon^2}{45}\frac{\partial^5 \eta}{\partial S^5}\right)=\frac{\delta_{\text{B}}}{\delta}\mathscr{T}\left[\frac{\partial \eta}{\partial S}\right]+\frac{\beta}{\delta}\frac{\partial \widehat{T}_{\text{n}}}{\partial S}-\alpha\mathcal{R}, \quad (4.1.71)$$

where

$$\mathcal{R}=\mathscr{T}\left[\frac{\partial \widehat{T}_{\text{t}}}{\partial \tau}\right]+\eta\,\mathscr{T}\left[\frac{\partial \widehat{T}_{\text{t}}}{\partial S}\right]+\frac{\partial \eta}{\partial S}\mathscr{T}\left[\widehat{T}_{\text{t}}\right]+\alpha\,\mathscr{T}\left[\widehat{T}_{\text{t}}\right]\mathscr{T}\left[\frac{\partial \widehat{T}_{\text{t}}}{\partial S}\right]-\frac{\delta_{\text{B}}}{\delta}\widehat{T}_{\text{t}}. \quad (4.1.72)$$

This result is comparatively very similar to the result presented in Hammerton and Bassom (2013), the key difference being the definition of $\mathcal{R}$. In Hammerton and Bassom (2013), we propose that the parity of all terms involving the tangential surface stress parameter $\widehat{T}_{\text{t}}$ are incorrect, and that Equation 4.1.72 describes a corrected version.

As such, we expect the relevant effects to the solutions of Equation 4.1.71 (presented later in the thesis) will be substantial, and critical to explaining the unexpected behaviour of the solutions previously presented in Hammerton and Bassom (2013). This new derivation is therefore a key result of this chapter.

If the only surface stress acting is in the normal direction due to surface tension with a constant surface tension parameter, which we'll denote as σ_0, then the surface tension parameters can be expressed in their dimensionless form as

$$T_{\text{n}}=\delta\varepsilon^2\text{Eo}\frac{\partial^2 \eta}{\partial S^2}, \qquad T_{\text{t}}=0, \qquad \text{Eo}=\frac{\sigma_0}{\rho d^2 g}. \quad (4.1.73)$$

Using these values the equation governing a system with constant surface tension is given by

$$2\frac{\partial \eta}{\partial \tau}+3\eta\frac{\partial \eta}{\partial S}+\frac{\varepsilon^2}{\delta}\left(\frac{1}{3}-\text{Eo}\right)\frac{\partial^3 \eta}{\partial S^3}-\frac{\varepsilon^4}{45\delta}\frac{\partial^5 \eta}{\partial S^5}=\frac{\delta_{\text{B}}}{\delta}\mathscr{T}\left[\frac{\partial \eta}{\partial S}\right], \quad (4.1.74)$$

where Eo is an inverse Bond (Eötvös) number characterising the ratio of interfacial tension forces to gravitational forces (Davis and Acrivos, 1966). A high value of the Bond number indicates that the system is relatively unaffected by surface tension effects whereas a low value indicates that surface tension dominates. Equation 4.1.74 is a fifth-order KdV equation, with the addition of the integral transform $\mathscr{T}\left[\frac{\partial \eta}{\partial S}\right]$, which describes

a system with constant surface tension and a viscous boundary layer at the fluid bottom. Such a scenario is discussed in more depth in Section 4.2.

It should also be noted that when $\alpha = \delta_{\text{B}} = 0$ and $\widehat{T}_{\text{n}} = \frac{\partial^2 \eta}{\partial S^2}$, then the resulting equation is a fifth-order KdV equation for surface elevation $\eta(S, \tau)$. Whether or not we need to retain the fifth-order derivative depends on the size of Eo. When Eo is close to its critical value of $1/3$ then the size of the third-order derivative becomes comparable to the fifth-order derivative, and hence we need to retain it so that we have the correct balance between nonlinearity and dispersion in the dispersion relation. When Eo is much larger or smaller than $1/3$ the fifth-order derivative is then much smaller than the third-order derivative so it an be omitted.

4.2 Amplitude decay due to the viscous bottom boundary layer

Suppose now we have a system with a solitary wave in the absence of any tangential surface stress, subject to decay due to the effects from the viscous boundary layer at the bottom of the fluid. Such a scenario is governed by

$$2\frac{\partial \eta}{\partial \tau} + 3\eta\frac{\partial \eta}{\partial S} + a\frac{\partial^3 \eta}{\partial S^3} = \vartheta\, \mathscr{T}\left[\frac{\partial \eta}{\partial S}\right] \tag{4.2.1}$$

which is Equation 4.1.74 with

$$a = \frac{\varepsilon^2}{\delta}\left(\frac{1}{3} - \text{Eo}\right), \qquad b = 0, \qquad \text{and} \qquad \vartheta = \frac{\delta_{\text{B}}}{\delta}.$$

We consider the scenario when the amplitude-wavelength scaling is given by

$$\delta = \varepsilon^2 \left|\frac{1}{3} - \text{Eo}\right| = \mathcal{O}(\varepsilon^2),$$

so that $a = 1$, to remain consistent with the analyses in previous chapters. This assumption implies that

$$b = \frac{\varepsilon^2}{45\left|\frac{1}{3} - \text{Eo}\right|}$$

and we choose Eo such that $\varepsilon^2 \ll 1/3 - \text{Eo}$. Hence the fifth-order derivative is small compared with the other terms in Equation 4.1.74 and has been omitted by setting $b = 0$. We also impose that $\vartheta \ll 1$ so that the damping effects due to the no-slip condition are kept small.

Now, Equation 4.2.1 is effectively the KdV equation with the addition of the integral transform term governing the damping effects associated with the no-slip condition at the solid impermeable bottom boundary. It is noted here that we could evaluate the spatial derivatives with respect to the horizontal spatial coordinate x, rather than the tangential spatial coordinate S, since here we are ignoring any effects at the surface due to a surface boundary layer. However, to remain consistent with the rest of the chapter, we will continue to use S as our spatial coordinate, and τ as our time coordinate.

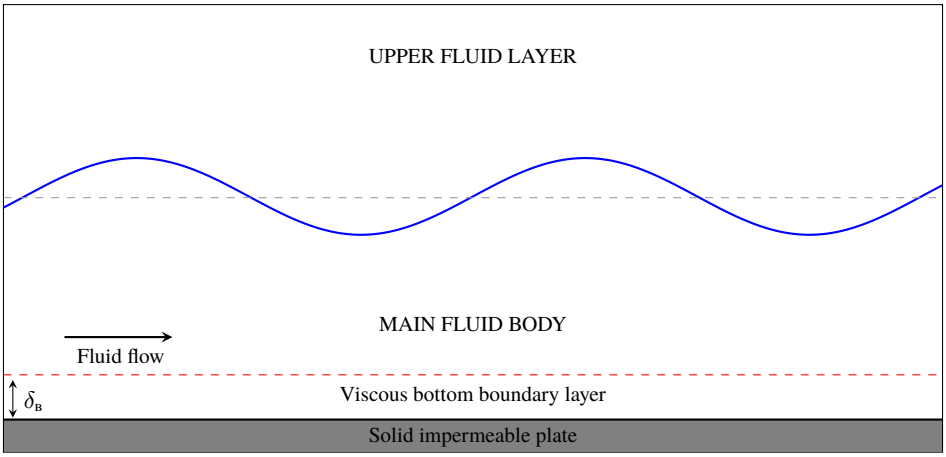

Figure 4.2.1: A system with a viscous bottom boundary layer.

As discussed earlier, this equation describes a system with constant surface tension meaning at leading-order we have no boundary layer effects at the fluid surface. Such a system is illustrated by Figure 4.2.1. We can however examine how the viscous bottom boundary layer affects a solitary wave solution using a similar analysis to that used in Chapter 3 for the KdV-Burgers' equation (3.1.2). We are particularly interested in modelling the amplitude decay.

We will first conduct a multi-scale analysis in an attempt to extract an analytical solution to the amplitude, at leading-order. We will then generate numerical solutions to Equa-

tion 4.2.1, using the solitary wave solution to the KdV equation (1.3.5) given by

$$\eta(S,0) = A_0 \operatorname{sech}^2\left(\sqrt{\frac{A_0}{2}}S\right) \tag{4.2.2}$$

as the initial condition. Finally, we will make comparisons between the asymptotically derived amplitude function and a numerically derived amplitude function.

4.2.1 Multiple scale analysis

We evaluate this problem in the same way as in Section 3.1 with the KdV-Burgers' system, and consider the multiple scale analysis similar to that seen in Mei (1989), and Keulegan (1948).

In this example, ϑ is the small parameter which controls the magnitude of decay associated with the boundary layer. We introduce a new slow time variable $\bar{\tau} = \vartheta\tau$, and expect the slowly decaying amplitude to behave as a function of $\bar{\tau}$ so that $A = A(\bar{\tau})$. Similar to Section 3.1, we attempt to derive an analytical form of A. First, we impose that $A > 0$ and hence we can write $|A| = A$. We then introduce a change of variables

$$z = S - \frac{1}{2}\int^{\bar{\tau}} A(\vartheta\tau')\,\mathrm{d}\tau'$$

so that derivatives in terms of the new variables are given by

$$\frac{\partial}{\partial S} = \frac{\partial}{\partial z}, \quad \text{and} \quad \frac{\partial}{\partial \tau} = -\frac{A}{2}\frac{\partial}{\partial z} + \vartheta\frac{\partial}{\partial \bar{\tau}},$$

and Equation 4.2.1 is rewritten in terms of new variables so that

$$2\vartheta\frac{\partial \eta}{\partial \bar{\tau}} - A\frac{\partial \eta}{\partial z} + 3\eta\frac{\partial \eta}{\partial z} + \frac{\partial^3 \eta}{\partial z^3} = \vartheta\mathscr{T}\left(\frac{\partial \eta}{\partial z}\right). \tag{4.2.3}$$

We now assume a solution in the form of an asymptotic expansion, expanding around small ϑ, which takes the form

$$\eta(z,\bar{\tau};\vartheta) = \eta_0(z,\bar{\tau}) + \vartheta\eta_1(z,\bar{\tau}) + \mathcal{O}(\vartheta^2).$$

Then, substituting this into Equation 4.2.3 and equating leading-order, $\mathcal{O}(\vartheta^0)$, terms we have

$$-A\frac{\partial \eta_0}{\partial z} + 3\eta_0\frac{\partial \eta_0}{\partial z} + \frac{\partial^3 \eta_0}{\partial z^3} = 0. \tag{4.2.4}$$

This is effectively Equation 1.3.3 in terms of the variable η_0, and therefore has a solution given by

$$\eta_0(z,\bar{\tau}) = A(\bar{\tau})\,\mathrm{sech}^2\left(\sqrt{\frac{A}{2}}z\right). \tag{4.2.5}$$

Next, we consider the next-order equation, $\mathcal{O}(\vartheta)$, which takes the form

$$-A\frac{\partial \eta_1}{\partial z} + 3\frac{\partial(\eta_0\eta_1)}{\partial z} + \frac{\partial^3 \eta_1}{\partial z^3} = \mathscr{T}\left[\frac{\partial \eta_0}{\partial z}\right] - 2\frac{\partial \eta_0}{\partial \bar{\tau}}. \tag{4.2.6}$$

The solution to $\eta_1(z,\bar{\tau})$ is difficult to solve exactly. Instead we use a similar technique to that used in Section 3.1 and rewrite Equation 4.2.4 and Equation 4.2.6 in terms of operators L_0 and L_1 which are defined as

$$L_0[U] = \frac{\partial}{\partial z}\left(-AU + \frac{3}{2}U^2 + \frac{\partial^2 U}{\partial z^2}\right), \tag{4.2.7}$$

where U is the leading-order solution, and

$$L_1[V] = \frac{\partial}{\partial z}\left(-AV + 3UV + \frac{\partial^2 V}{\partial z^2}\right), \tag{4.2.8}$$

respectively, where V is the solution at the next order. Using these operators, Equation 4.2.4 and Equation 4.2.6 become

$$L[\eta_0] = 0, \qquad \text{and} \qquad L[\eta_1] = \mathscr{T}\left[\frac{\partial \eta_0}{\partial z}\right] - 2\frac{\partial \eta_0}{\partial \bar{\tau}}.$$

It can be shown that L_0 and L_1 are adjoint operators using the same method seen in Section 3.1. In other words

$$\int_{-\infty}^{\infty} \eta_0 L_1[\eta_1]\mathrm{d}z = \int_{-\infty}^{\infty} \eta_1 L_0[\eta_0]\mathrm{d}z,$$

and hence we can derive a condition on η_0 such that

$$\int_{-\infty}^{\infty} \eta_0 \left(\mathscr{T}\left[\frac{\partial \eta_0}{\partial z}\right] - 2\frac{\partial \eta_0}{\partial \bar{\tau}} \right) \mathrm{d}z = 0. \tag{4.2.9}$$

Equation 4.2.9 is in terms of the leading-order solution η_0 only, and thus we have removed any dependence on η_1. The next step is to evaluate the integral, which removes any dependence on z. We can then derive an ordinary differential equation for A in terms of the slow-time variable $\bar{\tau}$.

First we consider the left-most part of the integral in Equation 4.2.9, with the transform term, given by

$$\int_{-\infty}^{\infty} \eta_0 \mathscr{T}\left[\frac{\partial \eta_0}{\partial z}\right] \mathrm{d}z \tag{4.2.10}$$

which, after substituting Equation 4.2.5, can be written as

$$-\frac{2A^2}{\sqrt{\gamma\pi}} \int_{-\infty}^{\infty} \operatorname{sech}^2\theta \int_0^{\infty} \frac{\tanh(\theta+Y)\operatorname{sech}^2(\theta+Y)}{\sqrt{Y}} \,\mathrm{d}Y \,\mathrm{d}\theta,$$

using the definition of the boundary layer transform Equation B.0.5, and where $\gamma = \frac{\sqrt{A}}{2}$ and $\theta = \gamma z$. This double integral is evaluated numerically using Maple and hence we can write Equation 4.2.10 as

$$\int_{-\infty}^{\infty} \eta_0 \mathscr{T}\left[\frac{\partial \eta_0}{\partial z}\right] \mathrm{d}z = -2k_1 \frac{A^2}{\sqrt{\gamma}}, \tag{4.2.11}$$

where the constant k_1 is given by

$$k_1 = \frac{1}{\sqrt{\pi}} \int_{-\infty}^{\infty} \operatorname{sech}^2\theta \int_0^{\infty} \frac{\tanh(\theta+Y)\operatorname{sech}^2(\theta+Y)}{\sqrt{Y}} \,\mathrm{d}Y \,\mathrm{d}\theta \quad \approx 0.3604151815.$$

Next we consider the remaining part of the integral in Equation 4.2.9 which is given by

$$-2\int_{-\infty}^{\infty} \eta_0 \frac{\partial \eta_0}{\partial \bar{\tau}} \,\mathrm{d}z. \tag{4.2.12}$$

We evaluate the derivative in time first to get

$$\frac{\partial \eta_0}{\partial \bar{\tau}} = \operatorname{sech}^2\theta \frac{\mathrm{d}A}{\mathrm{d}\bar{\tau}} - 2A\operatorname{sech}^2\theta\tanh\theta\left(\frac{z}{4\sqrt{A}}\frac{\mathrm{d}A}{\mathrm{d}\bar{\tau}} + \frac{\gamma}{2}A\right),$$

which can be simplified to

$$\frac{\partial \eta_0}{\partial \bar{\tau}} = \operatorname{sech}^2\theta \frac{\mathrm{d}A}{\mathrm{d}\bar{\tau}}(1 - \theta\tanh\theta) - \gamma A^2 \operatorname{sech}^2\theta\tanh\theta.$$

Then substituting back into the Equation 4.2.12 yields

$$\int_{-\infty}^{\infty} \eta_0 \frac{\partial \eta_0}{\partial \bar{\tau}}\,\mathrm{d}z = A\int_{-\infty}^{\infty} \operatorname{sech}^4\theta \frac{\mathrm{d}A}{\mathrm{d}\bar{\tau}}(1 - \theta\tanh\theta) - \gamma A^2 \operatorname{sech}^4\theta\tanh\theta\,\mathrm{d}z, \quad (4.2.13)$$

$$= \frac{A}{\gamma}\frac{\mathrm{d}A}{\mathrm{d}\bar{\tau}}\int_{-\infty}^{\infty} \operatorname{sech}^4\theta(1 - \theta\tanh\theta)\,\mathrm{d}\theta, \quad (4.2.14)$$

where the final term in Equation 4.2.13 is odd and therefore vanishes since

$$\int_{-\infty}^{\infty} \operatorname{sech}^4\theta\tanh\theta\,\mathrm{d}\theta = 0.$$

Then, evaluating the integral in Equation 4.2.14 yields

$$\int_{-\infty}^{\infty} \operatorname{sech}^4\theta(1 - \theta\tanh\theta)\,\mathrm{d}\theta = 1,$$

since

$$\int_{-\infty}^{\infty} \operatorname{sech}^4\theta\,\mathrm{d}\theta = \frac{4}{3}, \qquad \text{and} \qquad \int_{-\infty}^{\infty} \theta\operatorname{sech}^4\theta\tanh\theta\,\mathrm{d}\theta = \frac{1}{3},$$

using the integral results presented in Appendix A. Hence we have

$$\int_{-\infty}^{\infty} \eta_0 \frac{\partial \eta_0}{\partial \bar{\tau}}\,\mathrm{d}z = \frac{A}{\gamma}\frac{\mathrm{d}A}{\mathrm{d}\bar{\tau}}. \quad (4.2.15)$$

Substituting Equation 4.2.11 and Equation 4.2.15 back into the condition on η_0 (4.2.9) gives

$$-\frac{2k_1A^2}{\sqrt{\gamma}} - \frac{2A}{\gamma}\frac{\mathrm{d}A}{\mathrm{d}\bar{\tau}} = 0,$$

which simplifies to

$$\frac{\mathrm{d}A}{\mathrm{d}\bar{\tau}} + k_1 A\sqrt{\gamma} = 0. \quad (4.2.16)$$

This is a first-order ordinary differential equation for A in terms of $\bar{\tau}$ which, using $\gamma = \frac{\sqrt{A}}{2}$, can be rearranged to give

$$\frac{\mathrm{d}A}{\mathrm{d}\bar{\tau}} = -\frac{k_1 A^{5/4}}{\sqrt{2}}. \quad (4.2.17)$$

This equation is of separable type, and therefore can be solved using the method of separation of variables. After some work we eventually derive a leading-order analytical solution to the slowly decaying wave amplitude, given by

$$A(\bar{\tau}) = \frac{A_0}{\left(1 + A_0^{5/4} k_0 \bar{\tau}\right)^4}, \tag{4.2.18}$$

where A_0 is the initial wave amplitude, and

$$k_0 = \frac{\sqrt{2}}{8} k_1 \approx 0.063713005.$$

We see that increasing $\bar{\tau}$ causes a steady decrease in the amplitude $A(\bar{\tau})$ from its initial value $A(0) = A_0$.

4.2.2 Comparisons between the asymptotic and numerical solutions

We now find a numerical solution to Equation 4.2.1 for the surface elevation η to determine exactly how the bottom boundary affects the solitary wave. In the same way as before, we will also generate a numerical solution to the amplitude function and compare it with the asymptotically derived solution, Equation 4.2.18.

In order to set up a numerical scheme using the integrating factor method discussed in Section 2.3, we first need to consider how we can evaluate the Fourier transform of the boundary layer integral transform $\mathscr{T}[f(s)]$, so that we are able to advance using spectral methods. The Fourier transform of Equation B.0.5 is given in Hammerton and Bassom (2013) to be

$$\mathscr{T}\left[\mathrm{e}^{\mathrm{i}kS}\right] = \begin{cases} k^{-1/2} \exp\left(\mathrm{i}\left(kS + \frac{\pi}{4}\right)\right), & k > 0, \\ (-k)^{-1/2} \exp\left(\mathrm{i}\left(kS - \frac{\pi}{4}\right)\right), & k < 0. \end{cases} \tag{4.2.19}$$

We then use this result to evaluate the Fourier transform of Equation 4.2.1, which in terms of spectral variable k is given by

$$2\frac{\partial \widehat{\eta}}{\partial \tau} + \frac{3}{2}\mathrm{i}k\widehat{(\eta^2)} = -(\mathrm{i}k)^3 \widehat{\eta} + \mathrm{i}\vartheta |k|^{1/2} \exp\left(\mathrm{sgn}\left(\frac{\mathrm{i}\pi}{4}\right)\right) \widehat{\eta}. \tag{4.2.20}$$

In order to eliminate the numerically stiff linear terms from Equation 4.2.20 we introduce an integrating factor, as discussed in Chapter 2, given by

$$\widehat{E} = \exp\left(-\frac{1}{2}\Big((\mathrm{i}k)^3 + \mathrm{i}\vartheta k^{1/2}\mathrm{e}^{\mathrm{i}\pi/4}\Big)\right),$$

and multiply through. We then introduce a new variable

$$\widehat{v} = \widehat{E}\widehat{\eta}$$

and substitute into Equation 4.2.20 with the integrating factor, which yields

$$\begin{aligned}\frac{\partial \widehat{v}}{\partial \tau} + \frac{1}{2}\Big((\mathrm{i}k)^3 + \mathrm{i}\vartheta k^{1/2}\mathrm{e}^{\mathrm{i}\pi/4}\Big)\widehat{E}\widehat{\eta} + \frac{3}{4}\mathrm{i}k\widehat{E}\widehat{(\eta^2)} &= \frac{1}{2}\Big((\mathrm{i}k)^3 + \mathrm{i}\vartheta k^{1/2}\mathrm{e}^{\mathrm{i}\pi/4}\Big)\widehat{E}\widehat{\eta}, \\ \Rightarrow \quad \frac{\partial \widehat{v}}{\partial \tau} + \frac{3}{4}\mathrm{i}k\widehat{E}\widehat{(\eta^2)} &= 0 \end{aligned} \tag{4.2.21}$$

and then we advance $\widehat{v}$ in time using the fourth-order Runge-Kutta time step method defined in Chapter 2, using Python to generate the numerical solution. Figure 4.2.2 is a plot illustrating the effect of the bottom boundary layer on a solitary wave solution for two different values of ϑ. We observe from the plot that the damped solution exhibits similar behaviour to the solution with diffusive damping Figure 3.1.1 in that we see a decay in amplitude, wave speed and the formation of an elevated shelf behind the main wave peak, followed by a decaying oscillatory tail. The decaying tail is more clearly observed in Figure 4.2.3, which is a close-up of the tail region in Figure 4.2.2, for the case $\vartheta = 0.2$. Increasing the value of ϑ appears to result in increased damping and a more defined elevated shelf.

We then use the `max` algorithm in Python extract the numerical value of the amplitude. Figure 4.2.4 gives a comparison between the numerical and asymptotic amplitudes as a function of $\bar{\tau}$ describing the decay in amplitude due to the viscous bottom boundary layer. From the figure we can see that there is a good level of agreement between the numerical and asymptotic solutions, but the agreement diverges as time increases. This differs from the KdV-Burgers' diffusive case where the agreement got better with time after initially diverging.

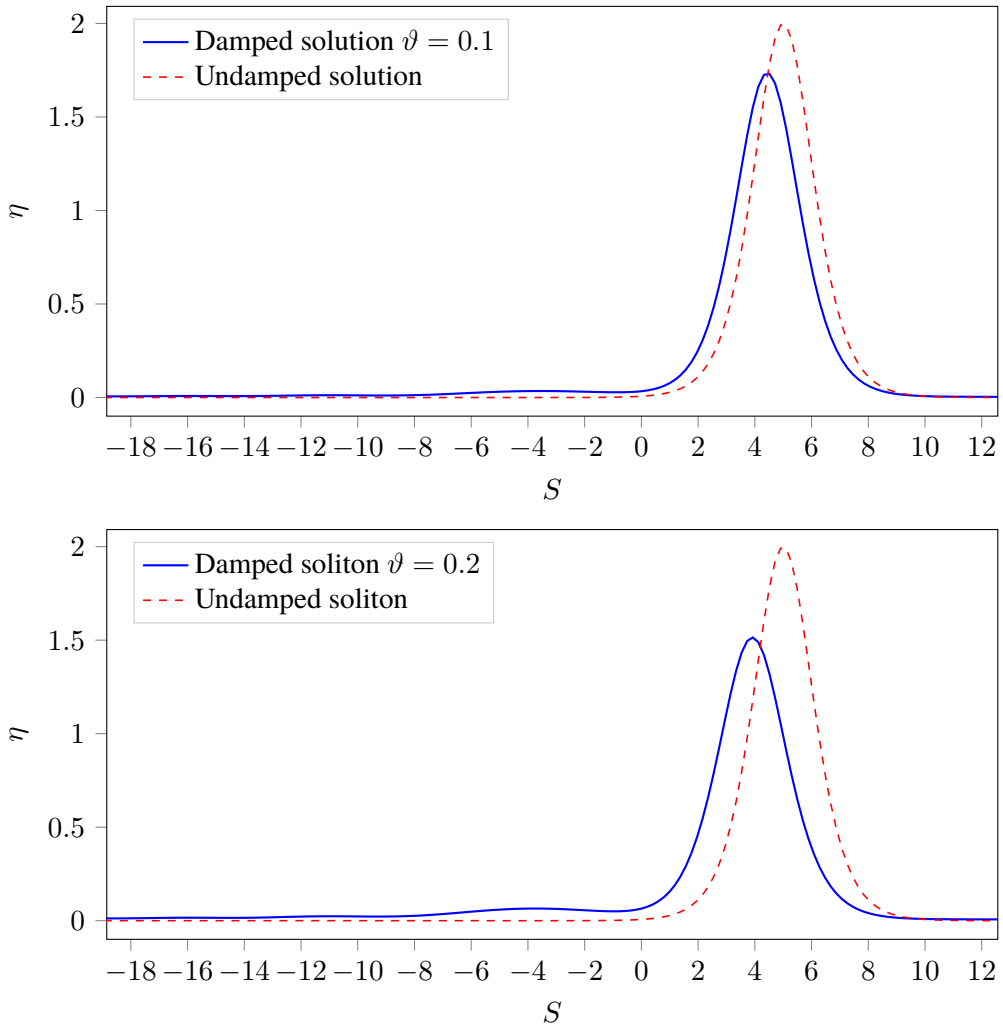

Figure 4.2.2: A plot of the damped numerical solution $\widehat{\eta}$ with $\vartheta = 0.1$ (top) and $\vartheta = 0.2$ (bottom), each plot with the undamped solitary wave (4.2.2), with parameter values $\tau_{\max} = 5$, initial amplitude $A_0 = 2$, and domain $S \in [-8\pi, 8\pi]$.

This is perhaps better illustrated by Figure 4.2.5 where we see a gradual increase in the difference between the two solutions.

At this point we could construct a similar analysis to that seen in Chapter 3, and attempt to evaluate the correction term at the next order. We could then use this to derive a more accurate asymptotic approximation to the amplitude. However, this is not explored here.

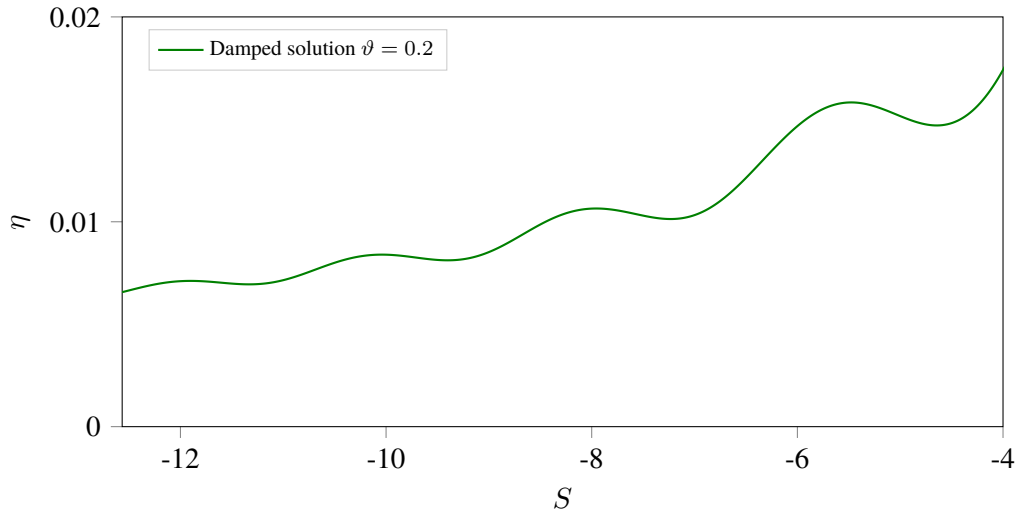

Figure 4.2.3: A close-up of the decaying oscillatory tail region of the damped numerical solution $\widehat{\eta}$, with parameter values $\tau_{\max} = 5$, $A_0 = 2$, $S \in [-4\pi, 4\pi]$ and $\vartheta = 0.2$.

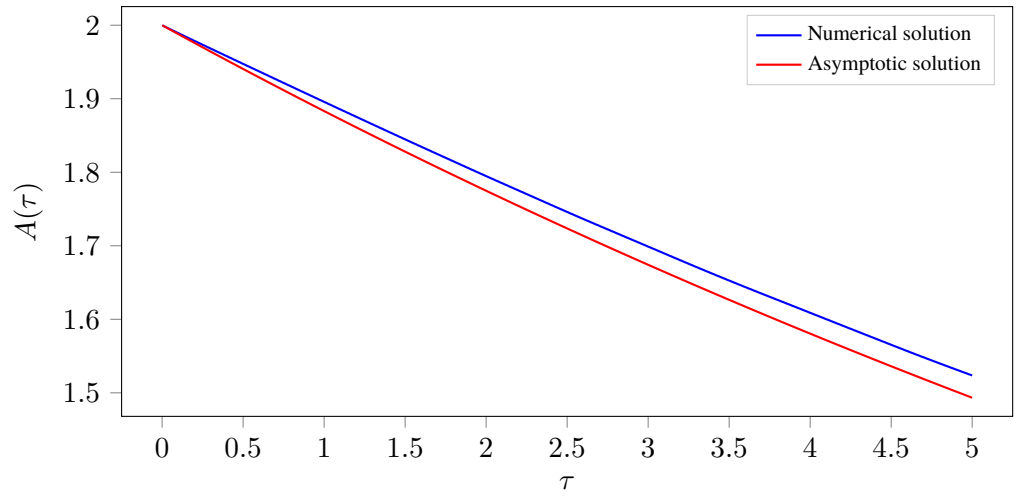

Figure 4.2.4: A comparison between the numerically derived amplitude and the leading-order asymptotic amplitude function, with parameters $\vartheta = 0.1$, $A_0 = 2$ and $\tau_{\max} = 2$.

4.3 Summary of chapter

A large part of this chapter was dedicated to the derivation of the equations governing the shallow water long-wavelength incompressible fluid system with arbitrary stress conditions at the fluid surface, given by Equation 4.1.71 and Equation 4.1.72.

By constructing a much more detailed analysis we were able to identify mistakes in Hammerton and Bassom (2013) and thus provide the corrections to the equations governing the system. We believe that this partly explains some of the unexpected behaviour seen

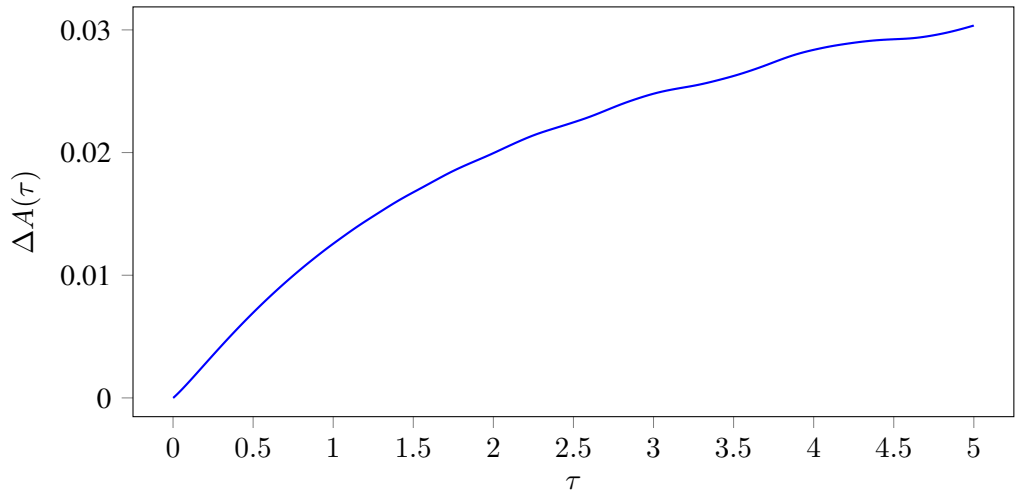

Figure 4.2.5: Difference between the numerically derived amplitude and the leading-order asymptotic amplitude function, with $\vartheta = 0.1$, $A_0 = 2$ and $\tau_{\max} = 2$.

in the solutions presented in the previous work, and allows us to use the new equations in Chapter 5 to provide more accurate numerical solutions to the scenario with an insoluble surfactant at the fluid interface.

In Section 3.1 we saw that the leading-order asymptotic approximation to the wave amplitude for the KdV-Burgers' system showed reasonable agreement with the numerically derived amplitude. However, there was a divergence between the two solutions which was the motivation for Subsection 3.2.2 where we obtained a much more accurate asymptotic approximation to the wave amplitude.

The system in Section 4.2, with decay due to the no-slip condition at the bottom boundary, showed a much better agreement between the numerical and asymptotic solutions for earlier times. This is shown more clearly in Figure 4.2.5. The percentage error at $\tau = 1$ for the bottom boundary layer scenario is approximately 0.6%, compared with 1% for the KdV-B scenario at the same time value. We therefore make no attempt to solve the correction term for the no-slip boundary layer system.

We now proceed, instead, to look at a scenario with a surface stress condition at the free surface.

5

The effect of an insoluble surfactant on the surface stress

Surfactants are chemical compounds that lower the interfacial surface tension between two fluids (or between a fluid and a solid), and can cause damping in both linear and nonlinear waves. Surfactants collect at an interface, or surface, and may be soluble or insoluble. Although clean or surfactant-free interfaces are often preferred for research studies, some surfactant contamination is always present in natural systems (Lapham et al., 2001).

Insoluble surfactants are easier to model as they are typically distributed along the fluid interface only, whereas soluble surfactants can be present in the main fluid body as well as at the surface which results in a much more complicated system to model. For air-water interfaces, as consistent with our previous analyses, examples of common soluble surfactants include soaps, and common insoluble surfactants include different types of oils. Surfactants are strongly adsorbed at an air-water interface, resulting in depression of the surface tension (Kosmulski, 2001).

The existence of solitary waves in a system with variable surface tension has been considered as a model problem by letting the surface tension parameter $\sigma^\star$ depend linearly on the surface curvature and demonstrating numerically that solitary waves with oscillating tails exist (Özuğurlu and Vanden-Broeck, 2006). In other words, the surface tension does not need to be constant for solitary waves to be present. However, no examination was given of a surface boundary layer, despite the variation in the surface tension parameter giving rise to a tangential stress at the fluid surface. The variation of the surface tension parameter was only taken into account in the normal stress balance at the surface.

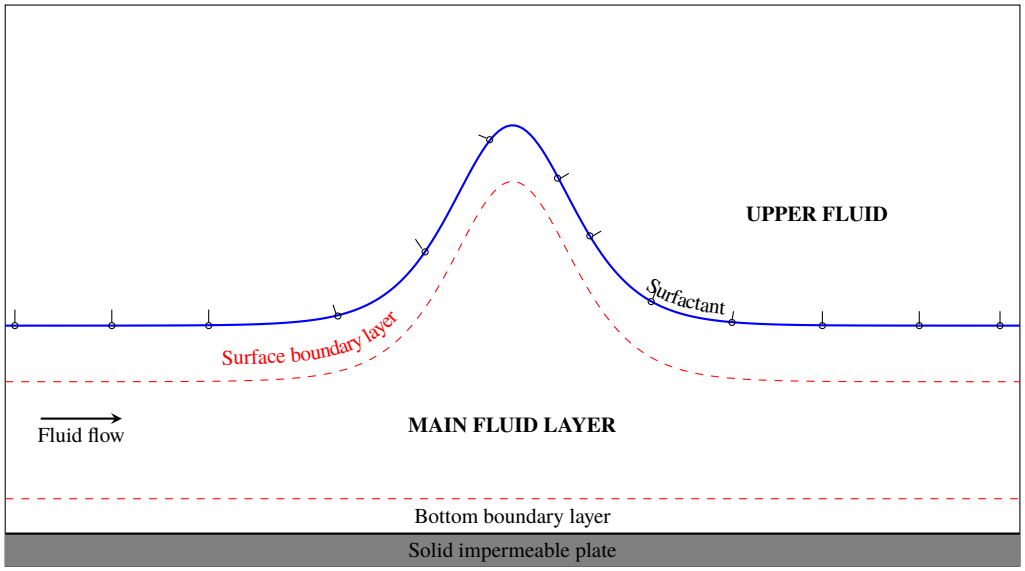

Figure 5.0.1: An interfacial travelling wave with a low concentration insoluble surfactant at the fluid interface.

Instead of pursuing the model problem, we focus on a more physically realistic scenario where variation of the surface tension parameter occurs due to the presence of an insoluble surfactant along a fluid interface. Such a scenario is illustrated by Figure 5.0.1.

First we construct a similar analysis to Hammerton and Bassom (2013) and derive equations governing the system with an insoluble surfactant at the free surface boundary. As discussed in Chapter 4, Hammerton and Bassom used a similar set up to the formulation presented in Section 4.1 where we consider a long-wavelength small-amplitude incompressible flow with a surface boundary layer due to a general surface stress condition together with a bottom boundary layer due to a no-slip condition on the fluid bottom.

In this chapter, the surface stress condition occurs due to the insoluble surfactant at the fluid surface. We solve for the surfactant using the same approach as (Hammerton and Bassom, 2013), and then present new numerical solutions to the system which will aim to address the unexplained behaviour seen in the earlier results; namely the rapid amplitude growth seen in the previous work. Finally we summarise the results presented in the chapter.

5.1 Formulation

For systems with a low concentration insoluble surfactant at the fluid interface, we assume that the surface tension parameter $\sigma^\star$ varies linearly with surfactant concentration denoted by $\Gamma^\star$. Due to the nature of surfactants in lowering the surface tension, we expect a relationship between the surface tension parameter $\sigma^\star$ and the surfactant concentration $\Gamma^\star$ such that an increase in the surfactant concentration will result in a decrease of surface tension $\sigma^\star$.

We begin with an advection-diffusion equation describing the surface concentration of the insoluble surfactant on the interface, given by Halpern and Frenkel (2003) to be

$$\frac{\partial}{\partial t^\star}(H\Gamma^\star) + \frac{\partial}{\partial x^\star}(H\Gamma^\star u^\star) = D_{\mathrm{s}}^\star \frac{\partial}{\partial x^\star}\left(\frac{1}{H}\frac{\partial \Gamma^\star}{\partial x^\star}\right) \tag{5.1.1}$$

in terms of surfactant concentration $\Gamma^\star$, horizontal spatial coordinate $x^\star$, time $t^\star$ and the horizontal fluid velocity at the surface $u^\star$, where the * notation denotes that a parameter is in its dimensional form, and $D_{\mathrm{s}}^\star$ represents surfactant diffusion. In addition to this

$$H = \sqrt{1 + \eta_{x^\star}^{\star\,2}}$$

where $y^\star = \eta^\star$ describes the surface position. The following scalings are used to non-dimensionalise

$$t^\star = t\sqrt{\frac{d}{g}}, \quad u^\star = u\sqrt{dg}, \quad x^\star = xd, \quad \Gamma^\star = \tilde{\Gamma}\Gamma_{\mathrm{m}},$$

where Γ_{m} is some constant scaling on the surfactant concentration. With these scalings, the dimensionless form of Equation 5.1.1 is given by

$$\frac{\partial(H\tilde{\Gamma})}{\partial t} + \frac{\partial(H\tilde{\Gamma}u)}{\partial x} = \frac{1}{\mathrm{Pe}}\frac{\partial}{\partial x}\left(\frac{1}{H}\frac{\partial \tilde{\Gamma}}{\partial x}\right). \tag{5.1.2}$$

with

$$\mathrm{Pe} = \frac{d\sqrt{dg}}{D_{\mathrm{s}}^\star}.$$

Here Pe is the Peclet number characterising the ratio between surfactant advection along

the fluid surface and the surfactant diffusion. Looking now at the long-wavelength, slow-time, small amplitude limit considered in Subsection 4.1.1, we have

$$x = s + \mathcal{O}(\delta^2\varepsilon), \quad S = \varepsilon s, \quad u = -c + \delta\widetilde{U}, \quad \tau = \widehat{\varepsilon}t$$

where S is the spatial coordinate parametrised at the surface, τ is the slow-time coordinate, and $\widetilde{U}$ is the scaled tangential fluid velocity at the surface. Since $\frac{\partial\eta}{\partial x} = \mathcal{O}(\delta\varepsilon) \ll 1$, then

$$H = 1 + \mathcal{O}(\delta\varepsilon)$$

and thus we impose $H = 1$. With these scalings the dimensionless advection-diffusion equation (5.1.2) then becomes

$$\widehat{\varepsilon}\frac{\partial\tilde{\Gamma}}{\partial\tau} + \varepsilon\frac{\partial}{\partial S}\left(-c\tilde{\Gamma} + \delta\tilde{\Gamma}\widetilde{U}\right) = \frac{\varepsilon^2}{\mathrm{Pe}}\frac{\partial^2\tilde{\Gamma}}{\partial S^2}.$$

From Equation 4.1.35 we have $\widehat{\varepsilon} = \delta\varepsilon$ so that nonlinearity in the wave amplitude equation occurs at leading-order, and hence the advection-diffusion equation governing the surfactant concentration $\tilde{\Gamma}$ is given by

$$\frac{\partial}{\partial S}\left(c\tilde{\Gamma} + \frac{\varepsilon}{\mathrm{Pe}}\frac{\partial\tilde{\Gamma}}{\partial S}\right) = \delta\left(\frac{\partial\tilde{\Gamma}}{\partial\tau} + \frac{\partial(\tilde{\Gamma}\widetilde{U})}{\partial S}\right). \tag{5.1.3}$$

To remain consistent with the long-wavelength, small amplitude system described in Subsection 4.1.1, we set $c = 1$. We are interested in the case where surfactant concentration tends to a constant as $\Gamma \to \pm\infty$. Hence, we consider small perturbations in the surfactant concentration about its far field behaviour and write

$$\tilde{\Gamma} = 1 + \delta\Gamma + \mathcal{O}(\delta^2). \tag{5.1.4}$$

Then, substituting this into Equation 5.1.3, rearranging and dividing through by δ, we have

$$\frac{\partial}{\partial S}\left(\Gamma + \frac{\varepsilon}{\mathrm{Pe}}\frac{\partial\Gamma}{\partial S} - \widetilde{U}\right) = \delta\left(\frac{\partial\Gamma}{\partial\tau} + \frac{\partial(\Gamma\widetilde{U})}{\partial S}\right). \tag{5.1.5}$$

If $\widetilde{U}$ is known then this equation determines Γ. However, the tangential fluid velocity at the surface $\widetilde{U}$ depends on the surface stress condition, so if the surface tension parameter

is a function of surfactant concentration then a system of equations must be solved relating η, Γ and $\widetilde{U}$.

The aim of this section is to determine how the presence of the surfactant will affect the surface elevation η, and thus an equation relating η to the surfactant concentration Γ is required. From Equation 4.1.68, the fluid velocity at the surface is given by

$$\widetilde{U} = \eta + \alpha \mathscr{T}\left[\widehat{T}_{\mathrm{t}}\right].$$

where $\widehat{T}_{\mathrm{t}}$ is the tangential surface stress component. Substituting this into Equation 5.1.5, we obtain an equation for the surfactant concentration Γ in terms of the surface elevation η and the tangential stress component $\widehat{T}_{\mathrm{t}}$, given by

$$\frac{\partial \Gamma}{\partial S} - \frac{\partial \eta}{\partial S} + \frac{\varepsilon}{\mathrm{Pe}}\frac{\partial^2 \Gamma}{\partial S^2} - \alpha \mathscr{T}\left[\frac{\partial \widehat{T}_{\mathrm{t}}}{\partial S}\right] = \delta\left(\frac{\partial \Gamma}{\partial \tau} + \frac{\partial}{\partial S}\left(\Gamma \mathscr{T}\left[\widehat{T}_{\mathrm{t}}\right] + \Gamma \tilde{\eta}\right)\right). \tag{5.1.6}$$

Writing $\varphi = \frac{\varepsilon}{\mathrm{Pe}}$, we first integrate with respect to S to get

$$\Gamma - \eta + \varphi \frac{\partial \Gamma}{\partial S} - \alpha \mathscr{T}\left[\frac{\partial \widehat{T}_{\mathrm{t}}}{\partial S}\right] = \mathcal{O}(\delta),$$

and then after rearranging, the $\mathcal{O}(\delta^0)$ equation is written as

$$\eta = \Gamma + \varphi \frac{\partial \Gamma}{\partial S} - \alpha \mathscr{T}\left[\widehat{T}_{\mathrm{t}}\right] \tag{5.1.7}$$

where $\Gamma \to 0$ as $S \to \pm\infty$. The normal and tangential surface stress balances are given by Halpern and Frenkel (2003) in their dimensional forms to be

$$T_{\mathrm{t}}^{\star} = \frac{1}{H}\frac{\partial \sigma^{\star}}{\partial x^{\star}}, \qquad T_{\mathrm{n}}^{\star} = -\frac{\sigma^{\star}}{H}\frac{\partial^2 \eta^{\star}}{\partial x^{\star 2}} \tag{5.1.8}$$

where $\sigma^{\star}$ is the surface tension parameter discussed earlier. For low surfactant concentrations, we use the standard assumption that the surface tension parameter $\sigma^{\star}$ varies linearly with surfactant concentration so that

$$\sigma^{\star} = \sigma_0 - k_0(\Gamma^{\star} - \Gamma_{\mathrm{m}})$$

where Γ_{m} denotes the surfactant concentration far from the disturbance (which is effectively the average concentration since $\tilde{\Gamma} \to 0$ as $S \to \pm\infty$), and where σ_0 is the surface tension parameter when $\Gamma^\star = \Gamma_{\mathrm{m}}$, and k_0 is a positive constant. We see that as the surfactant concentration $\Gamma^\star$ increases then the surface tension $\sigma^\star$ must decrease. Non-dimensionalising, and using Equation 5.1.4, gives

$$\begin{aligned}\sigma &= \frac{\sigma_0}{\rho d^2 g} - k_0\Gamma_{\mathrm{m}}(\tilde{\Gamma} - 1)\\ &= \mathrm{Eo} - \delta k_0 \Gamma_{\mathrm{m}}\Gamma\\ &= \mathrm{Eo} - \delta E\Gamma, \qquad E = k_0\Gamma_{\mathrm{m}}\end{aligned}$$

where Eo is an inverse Bond number and the constant E can be considered as a dimensionless Marangoni number which characterises the importance of the surfactant in the interfacial dynamics of the system. Substituting this into the non-dimensionalised form of Equation 5.1.8 yields

$$T_{\mathrm{t}} = -\delta\varepsilon E\frac{\partial\Gamma}{\partial S}, \qquad \text{and} \qquad T_{\mathrm{n}} = \delta\varepsilon^2(\mathrm{Eo} - \delta E\Gamma)\frac{\partial^2\eta}{\partial S^2}. \tag{5.1.9}$$

Then, from Equation 4.1.34, we have

$$\alpha = \frac{[T_{\mathrm{t}}]}{\delta\delta_{\mathrm{B}}\varepsilon} = \frac{E}{\delta_{\mathrm{B}}}, \qquad \text{and} \qquad \beta = \frac{[T_{\mathrm{n}}]}{\delta} = \varepsilon^2\mathrm{Eo},$$

where

$$[T_{\mathrm{t}}] = \delta\varepsilon E, \qquad \text{and} \qquad [T_{\mathrm{n}}] = \delta\varepsilon^2\mathrm{Eo} + \mathcal{O}(\delta^2\varepsilon^2). \tag{5.1.10}$$

Thus, in terms of the perturbation of surfactant concentration Γ, the surface stress components are given by

$$\widehat{T}_{\mathrm{t}} = -\frac{\partial\Gamma}{\partial S}, \qquad \widehat{T}_{\mathrm{n}} = \frac{\partial^2\eta}{\partial S^2},$$

where the $\mathcal{O}(\delta)$ change in $\widehat{T}_{\mathrm{n}}$ has been omitted, since it is not used in the following analyses. Then, substituting the tangential surface stress component into Equation 5.1.7, we have

$$\eta = \Gamma + \varphi\frac{\partial\Gamma}{\partial S} + \alpha\mathscr{T}\left[\frac{\partial\Gamma}{\partial S}\right], \qquad \varphi = \frac{\varepsilon}{\mathrm{Pe}}. \tag{5.1.11}$$

If the Peclet number $\mathrm{Pe} \ll \varepsilon$ then $\varphi \gg 1$, and hence $\frac{\partial\Gamma}{\partial S} \ll 1$, so the diffusion dominates

and we return to the case of a constant surfactant concentration and constant surface tension. However, when $\mathrm{Pe} = \mathcal{O}(\varepsilon)$ or larger then the surfactant evolves on the same time scale as the slow nonlinear evolution.

Now that we have derived a relation between Γ and η, and derived the surface stress components $\widehat{T}_{\mathrm{t}}$ and $\widehat{T}_{\mathrm{t}}$, we can use these, together with the equations governing the shallow water long-wavelength fluid flow with an arbitrary stress condition at the fluid surface, (4.1.71) and (4.1.72), to describe a scenario with a solitary wave subject to a low concentration insoluble surfactant present at the fluid surface. The governing equations for the surfactant system can be written in the form

$$\frac{\partial}{\partial\tau}\left(2\eta - \alpha\,\mathscr{T}\left[\frac{\partial\Gamma}{\partial S}\right]\right) + 3\eta\frac{\partial\eta}{\partial S} + a\frac{\partial^3\eta}{\partial S^3} + b\frac{\partial^5\eta}{\partial S^5} = \vartheta\,\mathscr{T}\left[\frac{\partial\eta}{\partial S}\right] - \alpha\mathcal{R} \tag{5.1.12}$$

and

$$\mathcal{R} = -\eta\,\mathscr{T}\left[\frac{\partial^2\Gamma}{\partial S^2}\right] - \frac{\partial\eta}{\partial S}\,\mathscr{T}\left[\frac{\partial\Gamma}{\partial S}\right] + \alpha\,\mathscr{T}\left[\frac{\partial\Gamma}{\partial S}\right]\mathscr{T}\left[\frac{\partial^2\Gamma}{\partial S^2}\right] + \frac{\delta_{\mathrm{B}}}{\delta}\frac{\partial\Gamma}{\partial S} \tag{5.1.13}$$

which must be solved together with the relation between η and Γ such that

$$\eta = \Gamma + \varphi\frac{\partial\Gamma}{\partial S} + \alpha\mathscr{T}\left[\frac{\partial\Gamma}{\partial S}\right] \tag{5.1.14}$$

where

$$a = \frac{\varepsilon^2}{\delta}\left(\frac{1}{3} - \mathrm{Eo}\right), \quad b = \frac{\varepsilon^4}{45\delta}, \quad \vartheta = \frac{\delta_{\mathrm{B}}}{\delta}, \quad \varphi = \frac{\varepsilon}{\mathrm{Pe}}, \quad \alpha = \frac{E}{\delta_{\mathrm{B}}}.$$

The system contains four positive dimensionless parameters. In no particular order, first we have α, a dimensionless value which describes the relative effects of surface tension and viscous forces and characterises the Marangoni stresses in the system (Elfring et al., 2016).

Then we have b which characterises the effect of higher-order dispersion term. This is only important when the inverse Eötvös number Eo is sufficiently close in value to its critical value of $1/3$ so that the constant coefficient, a, of the third-order dispersion term is the same order as b, the constant coefficient of the fifth-order dispersion term. In

other words, if a is small then the fifth-order term is needed in the dispersion balance, as discussed in Section 4.1.

The small parameter ϑ is the magnitude of the effect of viscous dissipation due to the bottom boundary layer, satisfying the no-slip condition at the rigid boundary. This parameter also governs the magnitude of dissipation due to the presence of surfactant at the fluid surface. In the latter part of this chapter where we consider the effects due to the surfactant in the absence of the viscous bottom boundary layer, we set the coefficient governing the magnitude of viscous dissipation due to the bottom boundary layer to be zero but retain the coefficient governing dissipation due to the surfactant. This is discussed in more detail later.

Finally, φ is an inverse Peclet number characterising the ratio between the surfactant advection along the fluid surface and the surfactant diffusion. In addition to these parameters, we also have the parameter a. The parity of a dictates whether we have positive elevated travelling wave solutions, or negative waves of depression, as discussed in Section 1.2. The size of a also determines whether we require the fifth-order derivative in the dispersion relation. In much of the following analysis, we impose that the coefficient $a = 1$ so that in the absence of effects due to surface stress and viscous dissipation we retain a general form of the KdV equation with positive amplitude elevated solitary wave solutions.

An interesting first test case that we examine is to set $\alpha = 0$ and consider the distribution of surfactant in a system with no dissipation due to a bottom boundary layer, and fifth-order derivative ignored. In this scenario, in a surfactant-free system, η would have the travelling wave solution

$$\eta = A\,\mathrm{sech}^2\left(\frac{\sqrt{|A|}}{2}\left(S - \frac{1}{2}A\tau\right)\right) \tag{5.1.15}$$

from before, where A represents the wave amplitude. Setting $\alpha = 0$ means that the tangential stress has no effect on the flow in the main body of fluid, nor on the surface elevation. Thus, the surfactant is passively advected and diffused along the fluid interface. The motivation for looking at this scenario is to see how the surfactant concentration

relates to the shape of the interface.

We start by setting $\alpha = 0$ and substituting the travelling solitary wave solution (5.1.15) for η into Equation 5.1.14, so the relationship between η and the surfactant concentration Γ is then given by

$$\varphi\frac{\partial\Gamma}{\partial S} + \Gamma = A\,\mathrm{sech}^2\left(\frac{\sqrt{|A|}}{2}(S - \frac{1}{2}A\tau)\right). \tag{5.1.16}$$

To solve this partial differential equation for $\Gamma(S,\tau)$, first we introduce a new variable

$$\theta = \frac{S - \frac{1}{2}A\tau}{\varphi}$$

and then rewrite Equation 5.1.16 in terms of θ, which gives us the ordinary differential equation

$$\begin{aligned}\frac{\mathrm{d}\Gamma}{\mathrm{d}\theta} + \Gamma &= A\,\mathrm{sech}^2\left(\frac{\varphi\sqrt{|A|}}{2}\theta\right),\\ &= A\,\mathrm{sech}^2(K_0\theta)\end{aligned} \tag{5.1.17}$$

where

$$K_0 = \varphi\frac{\sqrt{|A|}}{2}.$$

In general, it is not possible to write a closed form of the solution for Γ in terms of φ and A. However, we can find Γ for general φ and A using an integrating factor method so that

$$\Gamma = A\mathrm{e}^{-\theta}\int \mathrm{e}^{\theta}\,\mathrm{sech}^2(K_0\theta)\,\mathrm{d}\theta. \tag{5.1.18}$$

A closed form of the solution can be obtained for the special case

$$K_0 = 1 \quad\Rightarrow\quad \frac{\sqrt{|A|}}{2} = \frac{1}{\varphi},$$

given by

$$\Gamma = -A\mathrm{e}^{-\theta}\left(\mathrm{sech}\,\theta - 2\arctan\left(\mathrm{e}^{\theta}\right) + c\right), \tag{5.1.19}$$

where c is some constant of integration which must be zero since, using the boundary

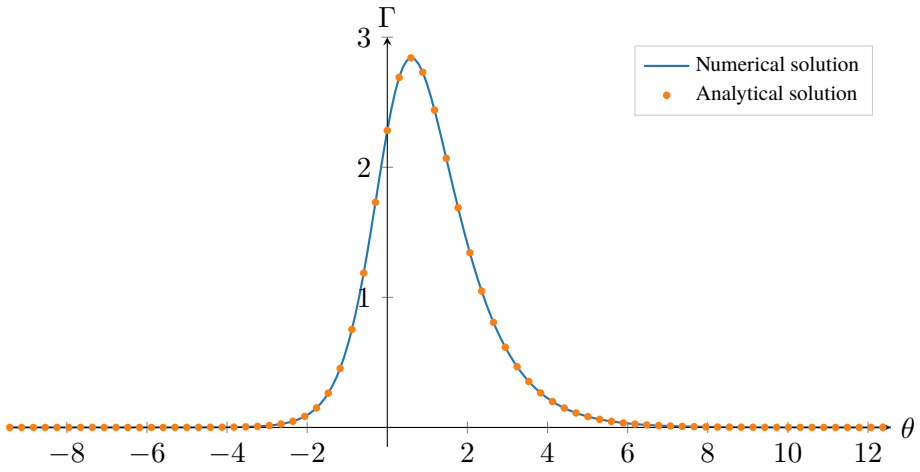

Figure 5.1.1: A comparison between the exact solution Equation 5.1.19, and the numerically obtained solution to the distribution of surfactant concentration Equation 5.1.18 using the integrating factor method, for the special case $\frac{\sqrt{|A|}}{2} = \frac{1}{\varphi}$.

conditions $\Gamma \to 0$ as $\theta \to \pm\infty$, we have

$$e^{-\theta}\operatorname{sech}\theta \to 2, \quad e^{-\theta}\arctan\left(e^{\theta}\right) \to 1, \qquad \text{as} \quad \theta \to -\infty$$

and

$$e^{-\theta}\operatorname{sech}\theta \to 0, \quad e^{-\theta}\arctan\left(e^{\theta}\right) \to 0, \qquad \text{as} \quad \theta \to \infty.$$

A plot comparing the exact solution of Γ for the special case $K_0 = 1$ with the numerically obtained solution to Γ using the integrating factor method is illustrated by Figure 5.1.1. The results obtained by numerically evaluating the integrating factor solution given in Equation 5.1.18 using Python, for various different values of φ and different wave amplitudes A, are illustrated by Figure 5.1.2 for waves with positive amplitude travelling to the right. Then the results for waves with negative amplitude travelling to the right, with similar variations of φ and A, are illustrated by Figure 5.1.3.

We observe from Figure 5.1.2 that elevated solitary wave disturbances, travelling to the right, appear to distribute the surfactant around the main disturbance with the maximum concentration centred on the front face of the wave. We also see that for larger values of φ, which represents large diffusion, the perturbation in surfactant concentration $\Gamma \to 0$ and thus we return to a case with constant surfactant concentration, as discussed earlier. We also observe that for smaller values of φ, the surfactant is distributed more uniformly

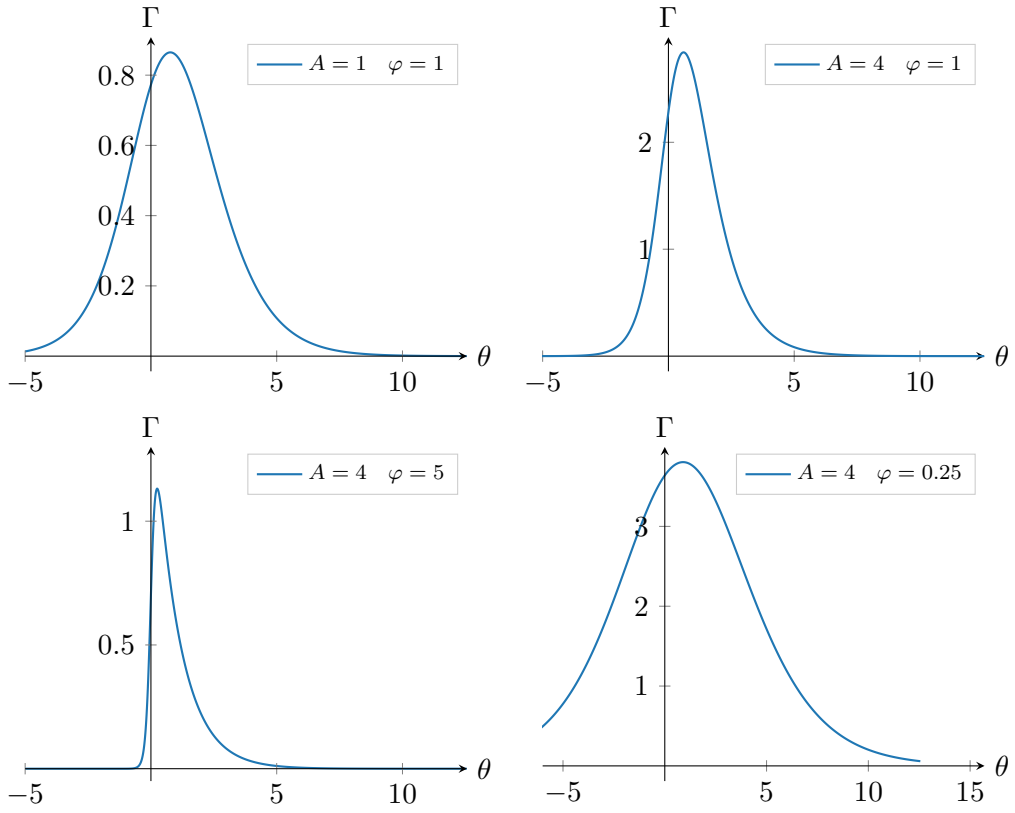

Figure 5.1.2: Distribution of the passive surfactant concentration Γ plot against θ with positive amplitude A (elevated waves travelling to the right) for different values of φ and A.

across the surface of the wave. We observe from Figure 5.1.3 that for waves of depression, travelling to the left, the surfactant appears to be distributed on the rear face of the wave. Similar to the case with waves with positive amplitude, as φ increases then $\Gamma \to 0$ which depicts a system with constant surface tension.

In the following analysis we turn instead to the case $\alpha > 0$ which describes a system where the surfactant is no longer acting passively, and thus the tangential surface stress directly affects both the fluid flow and the surface elevation.

5.2 Numerical analysis of the surfactant system

We will now construct a numerical scheme to solve Equation 5.1.12 and its associated equation (5.1.13) for the surface elevation function $\eta(S, \tau)$. First, grouping all non-linear

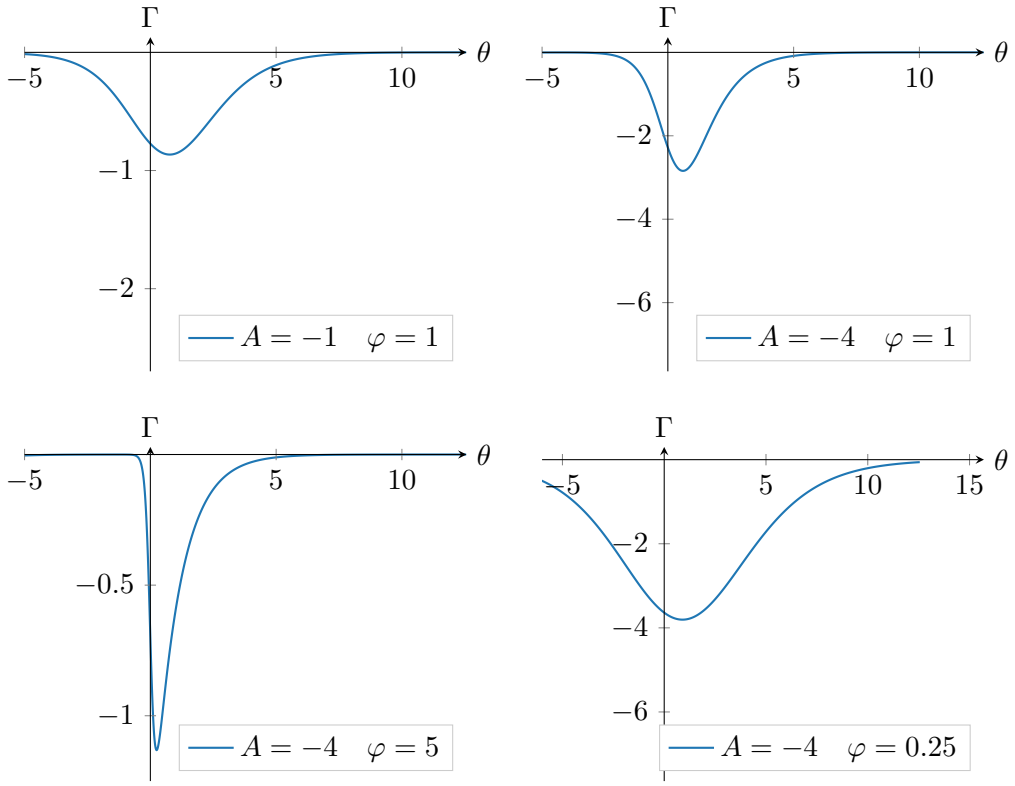

Figure 5.1.3: Distribution of the passive surfactant concentration Γ plot against θ with positive amplitude A (elevated waves travelling to the right) for different values of φ and A.

terms with the time derivative on the left-hand side, and all linear terms on the right-hand side yields

$$\frac{\partial}{\partial \tau}\left(2\eta - \alpha\,\mathscr{T}\left[\frac{\partial \Gamma}{\partial S}\right]\right) + \frac{\partial}{\partial S}\left(\frac{3}{2}\eta^2 + \frac{\alpha^2}{2}\left(\mathscr{T}\left[\frac{\partial \Gamma}{\partial S}\right]\right)^2 - \alpha\eta\,\mathscr{T}\left[\frac{\partial \Gamma}{\partial S}\right]\right) = -a\frac{\partial^3 \eta}{\partial S^3} - b\frac{\partial^5 \eta}{\partial S^5} + \vartheta\left(\mathscr{T}\left[\frac{\partial \eta}{\partial S}\right] - \alpha\frac{\partial \Gamma}{\partial S}\right) \tag{5.2.1}$$

and from Equation 5.1.11 we know that the relationship exists between η and Γ such that

$$\eta = \Gamma + \varphi\frac{\partial \Gamma}{\partial S} + \alpha\,\mathscr{T}\left[\frac{\partial \Gamma}{\partial S}\right]. \tag{5.2.2}$$

Now, if we set

$$L(\eta, \Gamma) = 2\eta - \alpha\,\mathscr{T}\left[\frac{\partial \Gamma}{\partial S}\right], \tag{5.2.3}$$

and

$$R(\eta, \Gamma) = -a\frac{\partial^3 \eta}{\partial S^3} - b\frac{\partial^5 \eta}{\partial S^5} + \vartheta\left(\mathscr{T}\left[\frac{\partial \eta}{\partial S}\right] - \alpha\frac{\partial \Gamma}{\partial S}\right)$$

then these can be substituted into Equation 5.2.1, which becomes

$$\frac{\partial L}{\partial \tau} + \frac{1}{2}\frac{\partial}{\partial S}\left(L^2 - \eta^2\right) + \alpha \frac{\partial}{\partial S}\left(\eta\, \mathscr{T}\left[\frac{\partial \Gamma}{\partial S}\right]\right) = R(\eta, \Gamma)$$

Next, Γ can be eliminated from the above using the substitution

$$\alpha \eta\, \mathscr{T}\left[\frac{\partial \Gamma}{\partial S}\right] = 2\eta^2 - \eta L$$

so we have

$$\frac{\partial L}{\partial \tau} + \frac{1}{2}\frac{\partial}{\partial S}\left(L^2 + 3\eta^2 - 2\eta L\right) = R(\eta, \Gamma). \tag{5.2.4}$$

and also

$$\begin{aligned} \eta &= \varphi \frac{\partial \Gamma}{\partial S} + \Gamma + 2\eta - L, \\ \Rightarrow \quad L &= \varphi \frac{\partial \Gamma}{\partial S} + \Gamma + \eta \end{aligned} \tag{5.2.5}$$

using Equation 5.2.3 and Equation 5.2.2.

Once again we will use the method presented in Milewski and Tabak (1999) and attempt to derive an integrating factor for the right-hand side of Equation 5.2.4, conveniently given by $R(\eta, \Gamma)$, and then advance the function L in time using a Runge-Kutta scheme detailed in Chapter 2.

First we take the Fourier transform of Equation 5.2.4 which yields

$$\frac{\partial \widehat{L}}{\partial \tau} + \frac{1}{2}\mathrm{i}k\left(\widehat{(L^2)} + 3\widehat{(\eta^2)} - 2\widehat{(\eta L)}\right) = \widehat{R} \tag{5.2.6}$$

where the hat notation describes a transformed variable, and k once again represents our spectral variable. Also, $\widehat{R}$ denotes the Fourier transform of $R(\eta, \tau)$ and is given by

$$\widehat{R} = \left(-a(\mathrm{i}k)^3 - b(\mathrm{i}k)^5 + \vartheta\mu(k)\right)\widehat{\eta} - (\mathrm{i}k)\alpha\vartheta\widehat{\Gamma}.$$

If we take the Fourier transform of Equation 5.2.3 and Equation 5.2.5 then we can evaluate

$\widehat{L}$ in two different ways:

$$\widehat{L} = 2\widehat{\eta} - \alpha\mu(k)\widehat{\Gamma}, \qquad \text{or} \quad \widehat{L} = (1 + \mathrm{i}k\varphi)\widehat{\Gamma} + \widehat{\eta}$$

where

$$\mu(k) = \mathrm{i}\,|k|^{\frac{1}{2}} \exp\left(\tfrac{\mathrm{i}\pi}{4}\mathrm{sgn}(k)\right).$$

In order to advance in time, we require that all variables need to be written in terms of $\widehat{L}$. We can write $\widehat{\eta}$ in terms of $\widehat{\Gamma}$ by taking the Fourier transform of Equation 5.2.2 to give

$$\widehat{\eta} = \big(1 + \mathrm{i}k\varphi + \alpha\mu(k)\big)\widehat{\Gamma}$$

so we have that

$$\widehat{L} = \big(2 + 2\mathrm{i}k\varphi + \alpha\mu(k)\big)\widehat{\Gamma}$$

and hence

$$\widehat{\Gamma} = \frac{\widehat{L}}{2(1 + \mathrm{i}k\varphi) + \alpha\mu(k)}, \qquad \text{and} \qquad \widehat{\eta} = \frac{1 + \mathrm{i}k\varphi + \alpha\mu(k)}{2(1 + \mathrm{i}k\varphi) + \alpha\mu(k)}\widehat{L}. \tag{5.2.7}$$

For simplicity we can write

$$\widehat{\Gamma} = \bar{q}(k)\widehat{L}, \qquad \text{and} \qquad \widehat{\eta} = \bar{p}(k)\widehat{L},$$

where

$$\bar{q}(k) = \frac{1}{2(1 + \mathrm{i}k\varphi) + \alpha\mu(k)}, \qquad \bar{p}(k) = \bar{q}(k)\big(1 + \mathrm{i}k\varphi + \alpha\mu(k)\big).$$

Then, substituting these into Equation 5.2.6, we have

$$\frac{\partial\widehat{L}}{\partial\tau} + \frac{1}{2}\mathrm{i}k\Big(\widehat{(L^2)} + 3\widehat{(\eta^2)} - 2\widehat{(\eta L)}\Big) = \big(\lambda(k)\bar{p}(k) + \nu(k)\bar{q}(k)\big)\widehat{L} \tag{5.2.8}$$

where

$$\lambda(k) = -a(\mathrm{i}k)^3 - b(\mathrm{i}k)^5 + \vartheta\mu(k), \qquad \nu(k) = -\mathrm{i}k\alpha\vartheta. \tag{5.2.9}$$

Here we note that in the above equations for $\lambda(k)$ and $\nu(k)$ we have assumed that both the

bottom and surface boundary layers have the same thickness (consistent with the analysis presented in Section 4.1). In the case when there is no effect due to the no-slip condition at the bottom boundary, the value of ϑ in the $\lambda(k)$ relation would be zero. However, simply setting $\vartheta = 0$ would omit any contribution from the final term in Equation 5.2.1, described by $\nu(k)$ in our numerical scheme, which governs dissipative effects due to the surfactant. We therefore modify $\lambda(k)$ and $\nu(k)$ to account for this, so that

$$\lambda(k) = -a(\mathrm{i}k)^3 - b(\mathrm{i}k)^5 + \vartheta_0\mu(k), \qquad \nu(k) = -\mathrm{i}k\alpha\vartheta_1$$

where ϑ_1 is fixed and

$$\vartheta_0 = \begin{cases} 0, & \text{(no effect from bottom boundary layer)}, \\ \vartheta_1, & \text{(no-slip condition at bottom boundary)}. \end{cases}$$

This is the equivalent of saying that the thickness of the bottom boundary layer $\delta_{\text{N}} = 0$ in the absence of the no-slip condition at the bottom boundary, or $\delta_{\text{N}} = \delta_{\text{B}}$ when we include the no-slip condition, i.e. the boundary layers have the same thickness as discussed in Section 4.1.

Before proceeding, we note that some of the nonlinear terms in Equation 5.2.8 still contain $\widehat{\eta}$. In order to numerically evaluate these nonlinear terms, we write these in terms of Fourier and inverse Fourier transforms, $\mathcal{F}$ and $\mathcal{F}^{-1}$ so that

$$\begin{aligned} \widehat{(\eta^2)} &= \mathcal{F}\Big[\mathcal{F}^{-1}[\widehat{\eta}] \cdot \mathcal{F}^{-1}[\widehat{\eta}]\Big] \\ &= \mathcal{F}\Big[\mathcal{F}^{-1}[\bar{p}(k)\widehat{L}] \cdot \mathcal{F}^{-1}[\bar{p}(k)\widehat{L}]\Big] \end{aligned}$$

and similarly,

$$\begin{aligned} \widehat{(\eta L)} &= \mathcal{F}\Big[\mathcal{F}^{-1}[\widehat{\eta}] \cdot \mathcal{F}^{-1}[\widehat{L}]\Big] \\ &= \mathcal{F}\Big[\mathcal{F}^{-1}[\bar{p}(k)\widehat{L}] \cdot \mathcal{F}^{-1}[\widehat{L}]\Big] \end{aligned}$$

$$\widehat{(L^2)} = \mathcal{F}\Big[\mathcal{F}^{-1}[\hat{L}] \cdot \mathcal{F}^{-1}[\widehat{L}]\Big].$$

Now that the numerical system is set up, we advance $\widehat{L}$ in time using the fourth-order

Runge-Kutta scheme discussed in Chapter 2. We can then recover the surface elevation $\eta(S, \tau)$ using Equation 5.2.7 and an inverse Fourier transform. Figure 5.2.1 is a plot of the

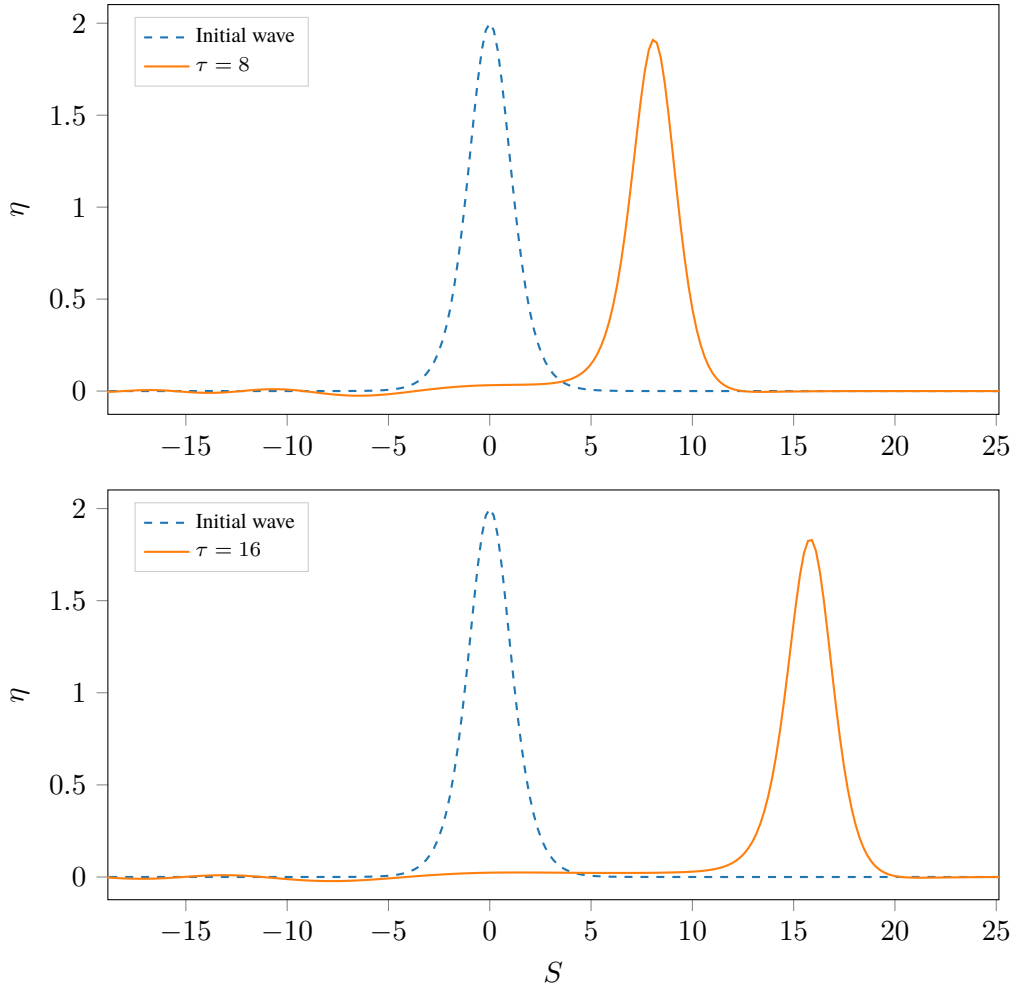

Figure 5.2.1: Solitary wave solution with surfactant present, at times $\tau = 0, 8$ and 16, with parameters: $\alpha = 0.2$, $A = 2$, $S \in [-8\pi, 8\pi]$, $b = 0$, $\vartheta = 0.2$ and no effect due to viscous dissipation at bottom boundary $\vartheta_0 = 0$.

numerical solution together with the initial condition, for a scenario with no effect due to viscous dissipation from the non-slip condition at the solid bottom boundary. All effects are therefore due to the surface boundary layer. We observe a change in wave form of the solitary wave solution, and a slight damping effect on the wave which agrees with the expected effects discussed in the description of surfactants given in Section 5.1. Even without boundary layer damping due to the no-slip condition on the bottom boundary, we see the formation of a decaying oscillatory tail and elevated shelf which we have consistently observed in previous results.

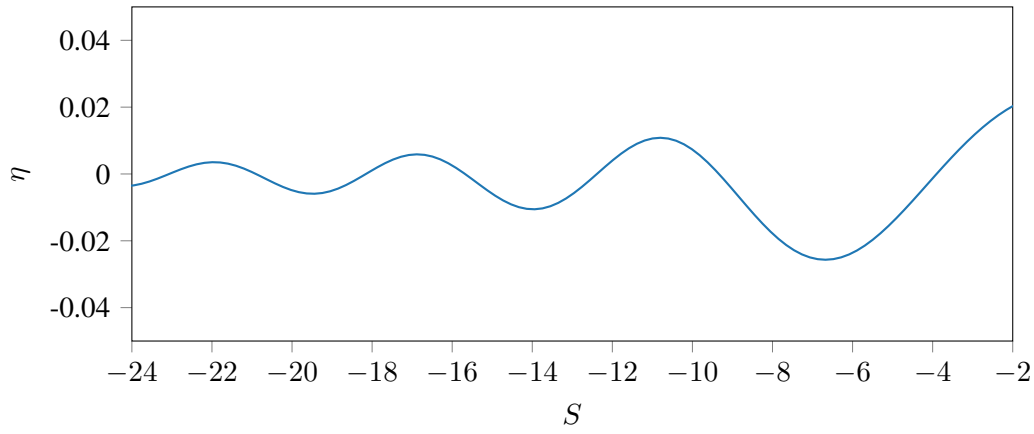

Figure 5.2.2: Close-up of the tail region for the surfactant solution at time $\tau = 16$, with parameters: $\alpha = 0.2$, $A = 2$, $S \in [-8\pi, 8\pi]$, $b = 0$, $\vartheta_1 = 0.2$, and no effect due to viscous dissipation at bottom boundary $\vartheta_0 = 0$.

The oscillating tail is perhaps easiest seen in Figure 5.2.2, a close up of the tail region from Figure 5.2.1. This change in wave form was not addressed in Hammerton and Bassom (2013), nor was the formation of the elevated shelf (although the shelf didn't appear to be present in the earlier results). Both the shelf and change in form are visible in Figure 5.2.3, a plot of the solitary wave with the effects due to the insoluble surfactant overlaid with the unaffected solitary wave solution, Equation 5.1.15. We observe from the figure that the surfactant has had a slight effect on the wave amplitude and wave speed, but the damping effect is not as strong as the damping due to the presence of the no-slip condition at the bottom boundary.

We can further demonstrate this deformation of the solitary wave form by numerically extracting the perturbation solution. In other words, if we were to construct an approximation in the form of an asymptotic expansion around small α, so that

$$\eta(S, \tau; \alpha) = \eta_0(S, \tau) + \alpha\eta_1(S, \tau) + \mathcal{O}(\alpha^2)$$

similar to that in Subsection 3.2.2, then the leading order solution η_0 would have the form

$$\eta_0(S, \tau) = A \operatorname{sech}^2\left(\frac{\sqrt{|A|}}{2}\left(S - \frac{1}{2}A\tau\right)\right)$$

and the numerically extracted perturbation solution would be approximately given by

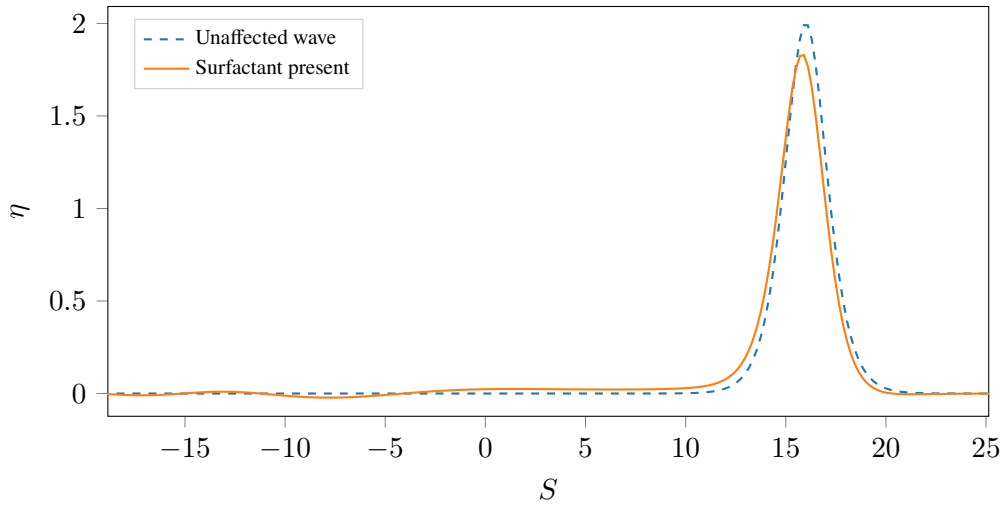

Figure 5.2.3: Comparison between the unaffacted solitary wave solution and the soliton with a surfactant present at time $\tau = 16$, with parameters: $\alpha = 0.2$, $A = 2$, $S \in [-8\pi, 8\pi]$, $b = 0$, $\vartheta_1 = 0.2$, and no effect due to viscous dissipation at the bottom boundary $\vartheta_0 = 0$.

$\eta_1(S,\tau) + \mathcal{O}(\alpha^2)$. Such a solution is illustrated by Figure 5.2.4 which has a similar structure to Figure 3.2.2, the perturbation solution from the KdV-Burgers' analysis given in Subsection 3.2.3. The solution appears to take the form of a core stationary solution followed by the decaying oscillating tail region, as we saw with the KdV-Burgers' perturbation solution, although the elevated shelf appears to be smaller in amplitude in comparison with the stationary core and tail regions.

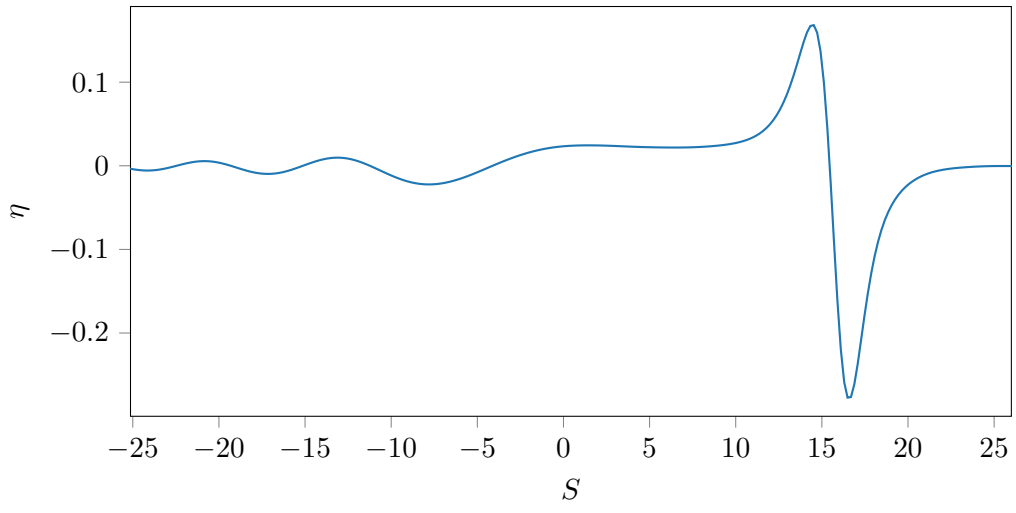

Figure 5.2.4: Numerical perturbation solution with surfactant present, at time $\tau = 16$, with parameters: $\alpha = 0.2$, $A = 2$, $S \in [-8\pi, 8\pi]$, $b = 0$, $\vartheta_1 = 0.2$ and $\vartheta_0 = 0$.

To summarise this particular result we first note that the surfactant has had a small damp-

ing effect on the wave amplitude (and by extension the wave speed). The structure of the wave form has also transformed so that visually the effects are similar to results we have seen in previous sections: a deformation of the initial soliton profile with the formation of a small-amplitude elevated shelf followed by a tail region with oscillatory decay.

We now look at the effect of including the no-slip condition at the solid bottom boundary in addition to the surfactant at the fluid interface.

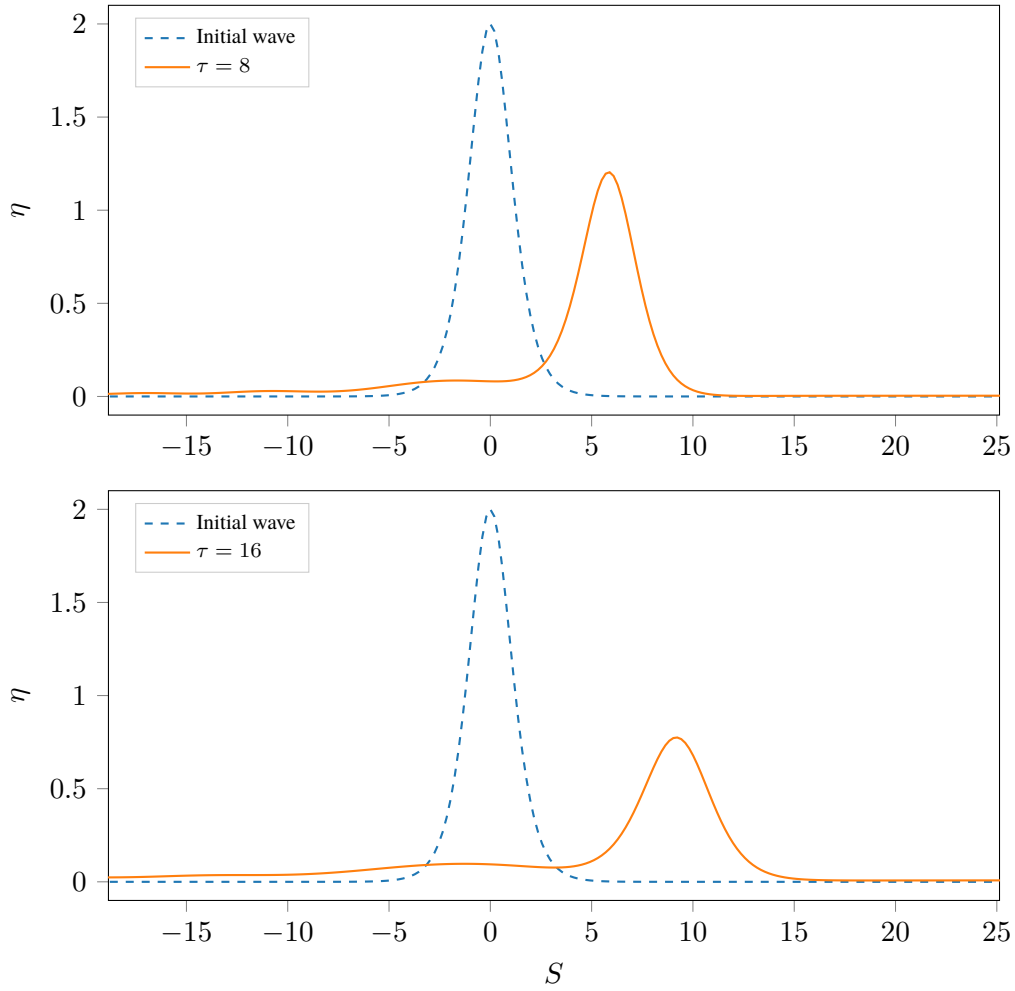

Figure 5.2.5: Solitary wave solution with surfactant present, at times $\tau = 0, 8$ and 16, with parameters: $\alpha = 0.2$, $A = 2$, $S \in [-8\pi, 8\pi]$, $b = 0$, and $\vartheta_0 = \vartheta_1 = 0.2$.

Figure 5.2.5 is a plot of the numerical solution alongside the initial solution, for a scenario with a moderate effect due to viscous dissipation from the non-slip condition at the solid bottom boundary. This has been achieved by setting the parameter characterising the effect of the base boundary layer to be $\vartheta_0 = 0.2$. We observe from the figure that the

solitary wave has been subject to increased amplitude decay and a larger decrease in the wave speed. We also observe a much more defined elevated shelf behind the peak disturbance which is expected given that we saw a similar effect in Section 4.2 where we only considered the effects due to the bottom boundary condition without any effects at the free surface.

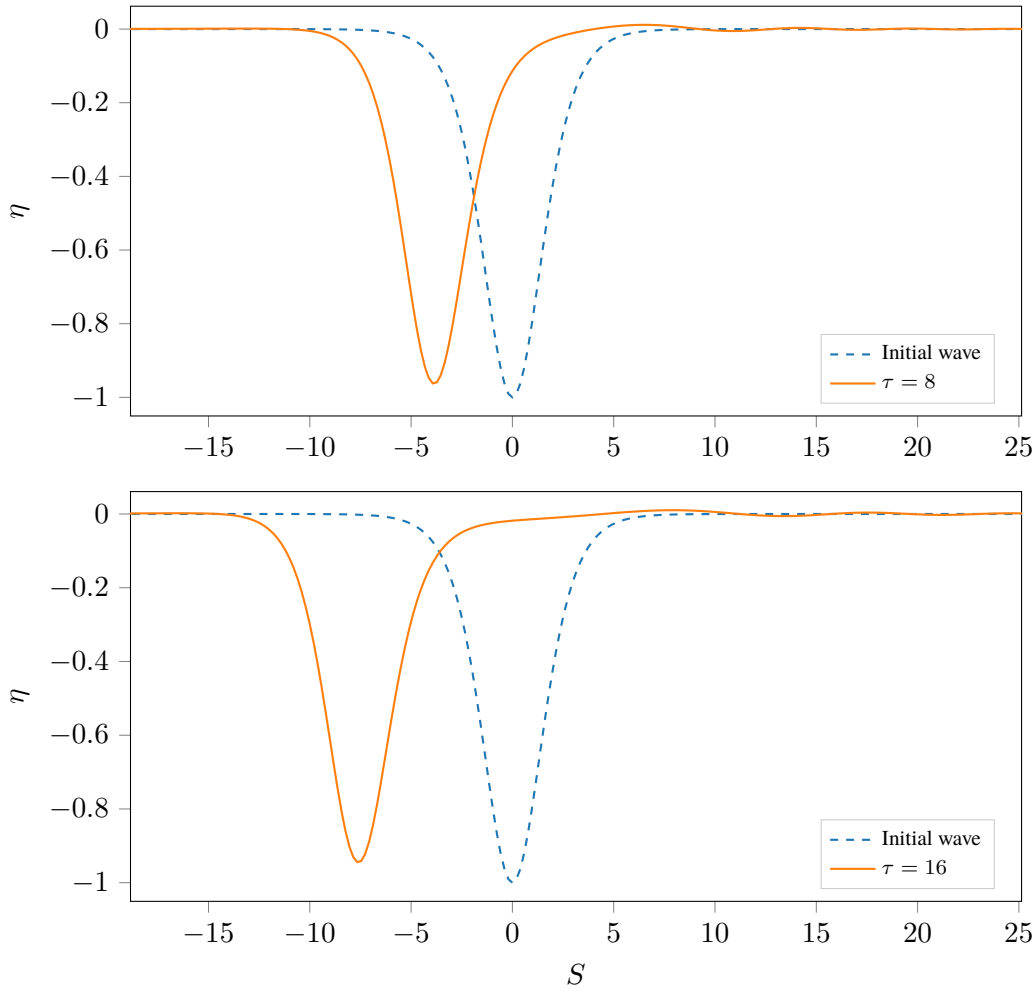

Figure 5.2.6: Solitary wave solution with surfactant present, at times $\tau = 0, 8, 16$, with parameters: $\alpha = 0.2$, $A = -1$, $S \in [-8\pi, 8\pi]$, $b = 0$, $\varphi = 1$, $\vartheta_0 = 0$ (no effect from no-slip condition) and $\vartheta_1 = 0.2$.

In addition to these results, we also note in particular the efficiency of the numerical scheme used. In the previous work presented by Hammerton and Bassom (2013), the numerical schemes would generate results in the order of 4-5 hours. Those results were generated using a basic form of the pseudospectral scheme in Subsection 3.2.3, but without the use of the integrating factor method described in Section 2.3 which has been used

throughout this report to generate all numerical results. As a direct comparison, with a negligible difference in hardware, the results presented in this report have taken around 4-5 seconds to generate. This is represents a huge improvement in efficiency and in return has allowed for a much more detailed comparison between results when using different parameters.

A much more interesting case is to use the exact parameter values pertaining to the results in Hammerton and Bassom (2013) which saw unexplained rapid increases in wave amplitude. The following parameter values were used, amplitude $A = -1$ (waves of depression with unit amplitude), $\alpha = 0.2$, domain $S \in [-8\pi, 8\pi]$, no effect due to the fifth-order term since $b = 0$, and the inverse Peclet number $\varphi = 1$. The results were presented for times $\tau = 0$, 8, and 16, and for $\vartheta_0 = 0$ (no effect due to the bottom boundary layer), $\vartheta_0 = \vartheta_1 = 0.1$ and $\vartheta_0 = \vartheta_1 = 0.2$.

In the case where the no-slip condition at the bottom boundary was ignored, $\vartheta_0 = 0$, the coefficient ϑ_1 governing the thickness of the upper boundary layer was also set to be zero in the results presented in Hammerton and Bassom (2013). This meant that there was no contribution from the final term in Equation 5.2.1. This term governs some of the dissipative effects associated with the presence of the surfactant and thus omitting it may have partly contributed to the rapid growth in amplitude seen in the Hammerton and Bassom (2013) results.

Using the same parameters (but not omitting the dissipative term) in the current analysis, we see from Figure 5.2.6 illustrating the case when $\vartheta_0 = 0$, $\vartheta_1 = 0.2$ that there is no rapid amplitude growth in the solutions, which was present in the solutions presented in Hammerton and Bassom (2013). In the solution for the case $\vartheta_0 = \vartheta_1 = 0.2$, illustrated by Figure 5.2.7, we see a much greater decay in the amplitude and wave speed which is expected with the no-slip condition present at the bottom boundary. It would appear then that the current work gives much more physically reasonable results than those demonstrated in the previous work.

At this point we note that a further check could be made to determine whether the current work describes an improvement over the previous results presented in Hammerton and

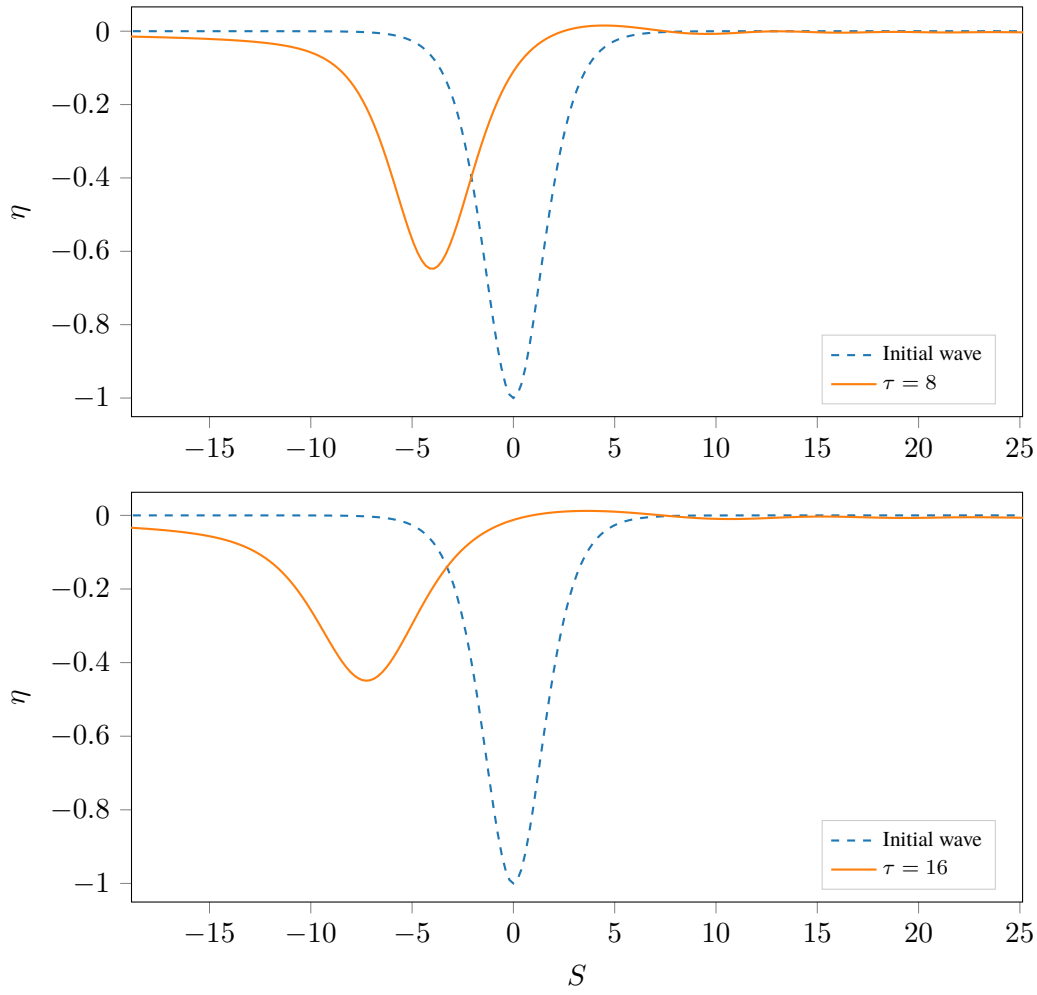

Figure 5.2.7: Solitary wave solution with surfactant present, at times $\tau = 0, 8, 16$, with parameters: $\alpha = 0.2$, $A = -1$, $S \in [-8\pi, 8\pi]$, $b = 0$, $\varphi = 1$, $\vartheta_0 = \vartheta_1 = 0.2$ (no slip condition at bottom boundary).

Bassom (2013). An energy conservation law could be constructed using

$$\frac{\partial}{\partial\tau}\left(2\eta - \alpha\,\mathscr{T}\left[\frac{\partial\Gamma}{\partial S}\right]\right) + \frac{\partial}{\partial S}\left(\frac{3}{2}\eta^2 + \frac{\alpha^2}{2}\left(\mathscr{T}\left[\frac{\partial\Gamma}{\partial S}\right]\right)^2 - \alpha\eta\,\mathscr{T}\left[\frac{\partial\Gamma}{\partial S}\right]\right) = -a\frac{\partial^3\eta}{\partial S^3} - b\frac{\partial^5\eta}{\partial S^5} + \vartheta\left(\mathscr{T}\left[\frac{\partial\eta}{\partial S}\right] - \alpha\frac{\partial\Gamma}{\partial S}\right), \tag{5.2.10}$$

together with the equivalent equation given in Hammerton and Bassom (2013). If the conservation argument indicated that energy was decreasing in Equation 5.2.10 which describes the system presented in the thesis, and that energy was increasing in the equations presented in the previous work, then this would be further indicative that the current

work is correct, and the previous work is wrong. However, an energy conservation law is not given here and we leave this open to future work.

5.3 Summary of chapter

In this chapter we constructed a similar analysis to Hammerton and Bassom (2013) for a system with an insoluble surfactant positioned at the free surface. While much of the formulation was the same, the equations governing the system (5.1.12) and (5.1.13) were different. This is largely due to working with the corrected form of Equation 4.1.71 from Chapter 4.

An additional scenario was explored where we were able to describe how the concentration of the surfactant relates to the shape of the interface in a system where the surfactant is passively advected and diffused along the interface. The results indicated that in the small-amplitude long-wavelength limit, the surfactant is largely distributed along the leading face of the solitary wave.

Finally we presented new numerical results for elevated travelling waves and recreated the results presented in Hammerton and Bassom (2013) for waves of depression using the same parameters. We were able to see from the new results that the insoluble surfactant caused a small amount of dissipation of the solitary wave. In addition the wave form changed so that it was somewhat consistent in shape with previous results for solitary waves affected by damping such as the diffusively damped solitary wave solutions presented in Chapter 3 and the solitary wave solutions damped by the no-slip condition presented in Chapter 4.

We also saw when attempting to recreate the results from the previous work that the new solutions no longer experienced rapid amplitude growth. This is much more in line with what we would expect to see in a physical experiment due to the decaying nature of surfactants. The efficiency of the numerical scheme used from Chapter 2 allowed us to provide closer comparisons and give a much more detailed illustrative analysis of the solutions, such as the close-up plots illustrating regions of particular interest.

6

Further applications, future work and concluding remarks

In this chapter we discuss other scenarios where the exact form of the surface stress is an important factor in the analysis. We then present solutions to an electrohydrodynamic system and discuss opportunities for possible extensions to this work. Finally we summarise the results presented in the thesis.

6.1 Other scenarios with a tangential stress condition

In the previous chapter we explored the effect of having a surfactant present at the fluid surface leading to a surface stress condition and the inclusion of a tangential surface stress component. For this scenario we considered Equation 4.1.71 and Equation 4.1.72, and calculated the surface stress components $\widehat{T}_{\mathrm{t}}$ and $\widehat{T}_{\mathrm{n}}$ according to a low concentration insoluble surfactant.

However, Equation 4.1.71 represents a generalised equation for an incompressible long-wavelength, small-amplitude hydrodynamic system with a surface stress condition at the fluid surface. As such, there are many other applications where this equation may be applicable in governing the system. Of particular note is a system in the presence of an electric field. The generated electric field modifies the surface tension at the fluid surface which alters the tangential surface stress. We explore such a system in greater depth in the following section.

In addition to an electrohydrodynamic system, there are many other scenarios with a tangential stress condition at the fluid surface. While no explicit physical application is given, Batyshchev (1991) considered asymptotic solutions of the wave motion of a fluid with specified tangential surface stresses constructed at high Reynolds numbers.

More recently Sumer et al. (2011) considered sediment transport experiments induced by a plunging solitary waves. Solitary waves are able to transport a large amount of sediment when approaching a beach, which sometimes causes serious beach erosion (Kim et al., 2016). In such a scenario any sediment present at the fluid surface is likely to modify the surface tension of the wave and result in a tangential stress condition at the surface. While such a scenario is not explored here, we believe we could draw parallels with the surfactant system and derive a similar set of equations to Equation 5.1.12 and Equation 5.1.13 which would govern the system.

Instead we proceed to consider a system subject to an electric field due to the presence of parallel electrodes positioned above the fluid and at the bottom boundary.

6.2 The effect of surface stress in electrohydrodynamic flows

In this section we consider a scenario with a fluid layer of finite depth in the presence of an electric field acting vertically through the fluid body. The electric field is generated due to parallel electric plates below and above the fluid with an arbitrary separation distance d. We focus on the limit $d \to \infty$ so that $\mathbf{E} \to E_0\mathbf{y}$ as $y \to \infty$, for some constant E_0. The propagation of travelling waves on the surface of the fluid layer along with the perturbation to the electric field is considered. Such a scenario is illustrated by Figure 6.2.1.

Nonlinear travelling waves in the presence of a normal electric field have been considered (Gonzalez and Castellanos, 1997; Papageorgiou and Vanden-Broeck, 2006) when the electric field is due to parallel electrodes with arbitrary separation distance comparable to the fluid depth. In the case of parallel electrodes with very large separation distance, a Korteweg-de Vries-Benjamin-Ono type equation is obtained for particular wavelength

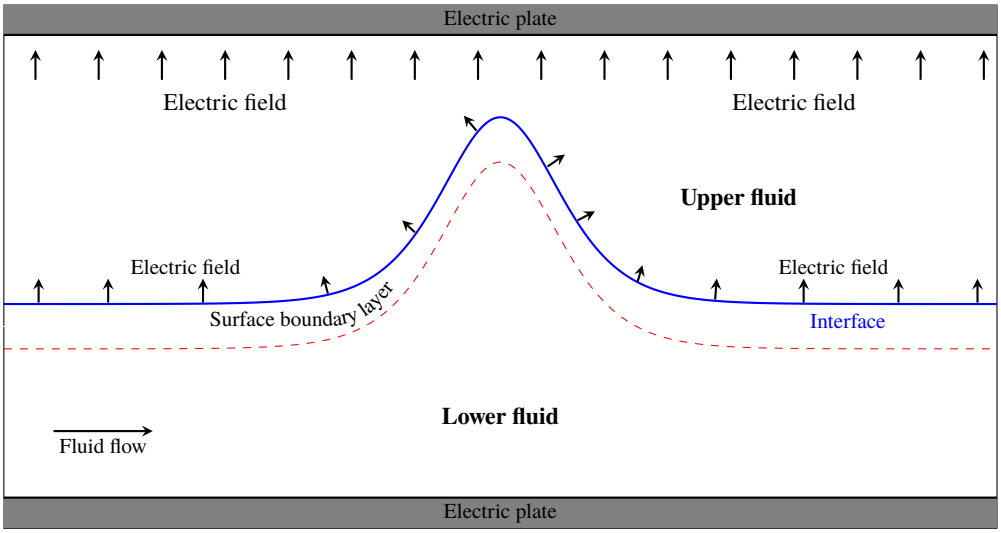

Figure 6.2.1: An illustration of an interfacial travelling wave with an electric field passing vertically through the fluid body.

and amplitude scalings. This notion was discussed in Gleeson et al. (2007), although explicit results were not given. Hammerton (2013) considered a similar scenario with two fluid layers where the lower fluid was assumed to be a perfect conductor and the upper fluid a perfect dielectric (not conducting), and the existence of solitary waves was discussed. A further example was provided in Hammerton and Bassom (2013) for travelling waves of depression and later Hammerton and Bassom (2014) consider small-amplitude disturbances on the surface of a fluid layer subject to a normal electric field.

6.2.1 Formulation

The general theory is formulated by considering the application of a vertical electric field when the two fluid layers have different electrical properties. If we use subscripts 1 and 2 to denote the lower and upper fluids respectively, the two fluids are taken to have permittivity ϵ_k and conductivity $\sigma_{c,k}$, where $k \in [1, 2]$, and the electric field intensity is given by $\mathbf{E}$.

Assuming we have an incompressible fluid, the governing equations for an electrohydrodynamic system are given by Melcher and Schwarz Jr (1968); Castellanos and Gonzalez

(1998) in their dimensional forms

$$\nabla^\star \times \mathbf{E}^\star = \mathbf{0}, \tag{6.2.1}$$

$$\nabla^\star \cdot (\epsilon \mathbf{E}^\star) = q^\star, \tag{6.2.2}$$

$$\frac{\partial q^\star}{\partial t} + \nabla^\star \cdot \mathbf{J}^\star = 0, \tag{6.2.3}$$

where $q^\star$ is the charge density, and $\mathbf{J}^\star$ is the current density given by

$$\mathbf{J}^\star = \sigma_{\mathrm{c}} \mathbf{E}^\star + q^\star \mathbf{u}^\star, \tag{6.2.4}$$

where we have assumed no charge diffusivity, and from (6.2.1) an electric potential $V^\star$ exists so that

$$\mathbf{E}^\star = \nabla V^\star.$$

At the interface we have the jump conditions

$$\left[\hat{\mathbf{t}} \cdot \mathbf{E}^\star\right]_2^1 = 0, \qquad \left[\hat{\mathbf{n}} \cdot \epsilon \mathbf{E}^\star\right]_2^1 = q_s, \tag{6.2.5}$$

where q_{s} is the surface charge density and $[\cdot]_2^1$ denotes a jump in quantity when crossing the interface from fluid 1 to fluid 2. The normal and tangential stress balances due to the electric field are

$$\bar{T}_{\mathrm{n}}^\star = \epsilon \hat{\mathbf{n}} \cdot \mathbf{f}^\star \cdot \hat{\mathbf{n}} \qquad \text{(normal stress balance)},$$

$$\bar{T}_{\mathrm{t}}^\star = \epsilon \hat{\mathbf{t}} \cdot \mathbf{f}^\star \cdot \hat{\mathbf{n}} \qquad \text{(tangential stress balance)},$$

where the stress tensor $\mathbf{f}^\star$ is given by

$$\mathbf{f}^\star = f_{ij}^\star = E_i^\star E_j^\star - \frac{1}{2} \left|\mathbf{E}^\star\right|^2 \delta_{ij}.$$

Hence the normal and tangential stress components exerted on the lower fluid due to the electric field are given by

$$\bar{T}_{\mathrm{n}}^\star = \frac{1}{2} \epsilon_k \left[(E_{\mathrm{n}}^\star)^2 - (E_{\mathrm{t}}^\star)^2 \right]_2^1, \qquad \bar{T}_{\mathrm{t}}^\star = -q_{\mathrm{s}} E_{\mathrm{t}}^\star, \tag{6.2.6}$$

respectively, where $E_{\mathrm{n}}^{\star}$ and $E_{\mathrm{t}}^{\star}$ are the respective normal and tangential components of the electric field.

To complete the system we also require an equation relating the surface charge density and the flux of charge onto the surface from the body of the fluids, and the flux along the surface. We consider the charge conservation equation (6.2.3) at the fluid interface which, using Equation 6.2.5 and substituting for Equation 6.2.4, becomes

$$\frac{\partial q_s}{\partial t} + \nabla_s(q_s \mathbf{u}_s) + \hat{\mathbf{n}} \cdot [\epsilon_0 \mathbf{E}^{\star}] = 0 \tag{6.2.7}$$

where $\mathbf{u}_s$ is the surface velocity, and ∇_s is the surface divergence such that

$$\nabla_s = \nabla^{\star} - \hat{\mathbf{n}} \cdot (\hat{\mathbf{n}} \cdot \nabla^{\star}).$$

In the surfactant analysis in Chapter 5 we used an advection-diffusion equation (5.1.1) to relate the surfactant concentration to the surface fluid velocity and then, after some work, we derived a relationship between the perturbation of surfactant concentration and the surface elevation. Equation 6.2.7 provides us with a similar relationship, this time between the surface charge density and fluid velocity and thus we can derive a relationship between the electric field and the surface elevation.

We now proceed to look at two cases. The first assumes that the lower fluid is a perfect conductor, or dielectric. The second case is the general case and makes no assumption on the lower fluid.

6.2.2 Results for a perfectly conducting lower fluid

In this example we assume that the lower fluid is a perfect conductor so $\mathbf{E}^{\star} = 0$ in this region, and the upper fluid is a perfect dielectric (non-conducting) subject to

$$\mathbf{E}^{\star} \to E_0 \hat{\mathbf{y}}, \quad \text{as} \quad y \to \infty.$$

where E_0 is some constant describing $\mathbf{E}^\star$ in the far field. With these assumptions, using the jump condition at the interface given by Equation 6.2.5 we have $[E_\mathrm{t}] = 0$. Hence, since the lower fluid is a perfect conductor, the tangential component of the electric field either side of the interface is zero, and thus from Equation 6.2.6 we have

$$\bar{T}_\mathrm{n}^\star = \frac{1}{2}\epsilon_0 (E_\mathrm{n}^\star)^2, \qquad \bar{T}_\mathrm{t}^\star = 0 \tag{6.2.8}$$

where ϵ_0 is the permittivity in the upper fluid. Assuming long-wavelength, small-amplitude disturbances on the surface of the lower fluid layer (the interface between the two fluids), we will use the same scalings on the fluid as in the surfactant analysis in Chapter 5. Then using Equation 4.1.71 in the absence of any tangential surface stress at the fluid interface, the partial differential equation governing the system in Cartesian coordinates is given by

$$2\frac{\partial \eta}{\partial t} + 3\eta\frac{\partial \eta}{\partial x} + \frac{\varepsilon^2}{\delta}\left(\frac{1}{3}\frac{\partial^3 \eta}{\partial x^3} + \frac{\varepsilon^2}{45}\frac{\partial^5 \eta}{\partial x^5}\right) = \frac{1}{\delta^2}\frac{\partial \widehat{T}_\mathrm{n}}{\partial x} + \frac{\delta_\mathrm{B}}{\delta}\mathscr{T}\left[\frac{\partial \eta}{\partial x}\right] \tag{6.2.9}$$

where $\widehat{T}_\mathrm{n}$ is the normal stress component with contribution T_n from the surface tension σ and contributions $\bar{T}_\mathrm{n}^\star$ from the electric field. We have also assumed a no-slip condition on the lower electric plate, the effects of which are governed by the final term in Equation 6.2.9. From Chapter 5 the contribution from the surface tension to the normal surface stress component is given in its dimensionless form by

$$T_\mathrm{n} = \delta\varepsilon^2 \mathrm{Eo}\frac{\partial^2 \eta}{\partial x^2},$$

where Eo is the Bond number and thus, if we combine this with the contribution from the vertical electric field $\bar{T}_\mathrm{n}^\star$ from Equation 6.2.8, which is to be non-dimensionalised, we have

$$\widehat{T}_\mathrm{n} = \delta\varepsilon^2 \mathrm{Eo}\frac{\partial^2 \eta}{\partial x^2} + \frac{1}{2}\epsilon_0 (E_\mathrm{n}^\star)^2.$$

Then, substituting this into Equation 6.2.9 we obtain

$$2\frac{\partial \eta}{\partial t} + 3\eta\frac{\partial \eta}{\partial x} + \frac{\varepsilon^2}{\delta}\left(\frac{1}{3} - \mathrm{Eo}\right)\frac{\partial^3 \eta}{\partial x^3} + \frac{\varepsilon^4}{45\delta}\frac{\partial^5 \eta}{\partial x^5} = \frac{\widehat{E}}{\delta^2} + \frac{\delta_\mathrm{B}}{\delta}\mathscr{T}\left[\frac{\partial \eta}{\partial x}\right] \tag{6.2.10}$$

where

$$\widehat{E} = \frac{\epsilon_0}{2}\frac{\partial}{\partial x}\left((E_{\mathrm{n}}^{\star})^2\right),$$

and the coefficients of the derivatives in η are identical to those in Section 4.1.

The velocity potential in the lower fluid is $\phi_1 = \phi$, and in the upper fluid $\phi_2 = 0$ since the fluid is considered to be hydrodynamically passive. These satisfy Laplace's equation, so we have

$$\nabla^2\phi \equiv \frac{\partial^2\phi}{\partial x^2} + \frac{\partial^2\phi}{\partial y^2} = 0.$$

Due to the presence of the electric field, we also have voltage potentials V_1 and V_2, where again the subscripts denote the lower and upper fluids, respectively. Then, since the lower fluid is a perfect conductor we have $\mathbf{E} = 0$ and hence $V_1 = \text{constant} = 0$. In addition to this, since the upper fluid is a perfect dielectric there is no charge density and the voltage potential in the upper fluid $V_2 = V^{\star}$ also satisfies Laplace's equation. Then we have

$$V^{\star} \to E_0 y^{\star}, \qquad \text{as} \quad y^{\star} \to \infty.$$

We use the same scalings as in Chapter 5 to non-dimensionalise

$$t^{\star} = t\sqrt{\frac{d}{g}}, \quad u^{\star} = u\sqrt{dg}, \quad x^{\star} = dx, \quad y^{\star} = dy, \quad \bar{T}^{\star} = \rho g h \bar{T}$$

and the scaling on the voltage potential in the upper fluid is given by

$$V^{\star} = dE_0 V,$$

where E_0 is some constant scaling parameter. Hence we have

$$E_{\mathrm{n}}^{\star} = \hat{\mathbf{n}} \cdot \nabla^{\star} V^{\star} = E_0 \hat{\mathbf{n}} \cdot \nabla V. \tag{6.2.11}$$

The wavelength of the surface disturbance is $\mathcal{O}(\varepsilon^{-1})$ so we rescale horizontal coordinate as

$$X = \varepsilon x,$$

and then using the expression (4.1.23) for the unit normal vector $\hat{\mathbf{n}}$ together with Equa-

tion 6.2.11, we have

$$E_{\mathrm{n}}^{\star} = -E_0 \left(\frac{\partial V}{\partial y} - \delta\varepsilon^2 \frac{\partial \eta}{\partial X} \frac{\partial V}{\partial X} \right), \qquad \text{on} \quad y = \delta\eta. \tag{6.2.12}$$

We then choose the scaling on the vertical coordinate y such that $Y = \varepsilon y$ so that V satisfies Laplace's equation X, Y

$$\nabla^2 V \equiv \frac{\partial^2 V}{\partial X^2} + \frac{\partial^2 V}{\partial Y^2} = 0.$$

The interface is then

$$y = \delta\eta \quad \Rightarrow \quad Y = \delta\varepsilon\eta,$$

with

$$V \to \frac{Y}{\varepsilon} \quad \text{as} \quad Y \to \infty, \qquad \text{and} \qquad V = 0 \quad \text{on} \quad Y = \delta\varepsilon\eta.$$

Thus we write

$$V = \frac{1}{\varepsilon}(Y + \delta\varepsilon\psi)$$

where ψ satisfies

$$\frac{\partial^2 \psi}{\partial X^2} + \frac{\partial^2 \psi}{\partial Y^2} = 0 \tag{6.2.13}$$

with

$$\psi \to 0, \quad \text{as} \quad Y \to \infty, \qquad \text{and} \qquad \psi = -\eta \quad \text{on} \quad Y = \delta\varepsilon\eta.$$

Hence Equation 6.2.12 in terms of ψ and Y becomes

$$E_{\mathrm{n}}^{\star} = -E_0 \left(1 + \delta\varepsilon \frac{\partial \psi}{\partial Y} - \delta^2\varepsilon^2 \frac{\partial \eta}{\partial X} \frac{\partial \psi}{\partial X} \right), \qquad \text{on} \quad Y = \delta\varepsilon\eta. \tag{6.2.14}$$

Finally we have

$$\begin{aligned} \bar{T}_{\mathrm{n}} &= \frac{\bar{T}_{\mathrm{n}}^{\star}}{\rho g h} = \frac{(E_{\mathrm{n}}^{\star})^2}{2\rho g h} = \frac{(E_{\mathrm{n}})^2}{2} \\ &= -\frac{E_b}{2} \left(1 + 2\delta\varepsilon \frac{\partial \psi}{\partial Y} + \mathcal{O}(\delta^2\varepsilon^2) \right) \end{aligned} \tag{6.2.15}$$

where E_b is an electric Bond number (or Weber number) given by

$$E_b = \frac{\varepsilon_0 E_0^2}{\rho g h}. \tag{6.2.16}$$

Then the contribution from the electric field $\widehat{E}$ in Equation 6.2.10 in terms of the dimensionless normal component E_{n}, and E_b, is

$$\widehat{E} = \frac{E_b}{2}\frac{\partial}{\partial x}\Big((E_{\mathrm{n}})^2\Big). \tag{6.2.17}$$

The problem reduces to solving Equation 6.2.13 together with Equation 6.2.15 in order to express the contribution from the electric field $\widehat{E}$ from (6.2.17) in terms of the surface elevation function η. Using a similar approach to Gleeson et al. (2007), we observe that the first-order derivatives $\frac{\partial \psi}{\partial X}$ and $\frac{\partial \psi}{\partial Y}$ in Equation 6.2.13 and Equation 6.2.15 are related by

$$\frac{\partial \psi}{\partial Y} = \mathcal{H}\left[\frac{\partial \psi}{\partial X}\right]$$

where $\mathcal{H}[f(X)]$ denotes the Hilbert transform, defined as the Cauchy principal value PV of the convolution integral

$$\mathcal{H}[f(X)] \equiv PV\left(\frac{1}{\pi}\int_{-\infty}^{\infty}\frac{f(S)}{X-S}\mathrm{d}S\right) \tag{6.2.18}$$

with the unique property that

$$\mathcal{H}[\,\mathcal{H}[f]] = -f.$$

If we apply this at the interface $Y = \delta\varepsilon\eta$, then $\psi = -\eta$ so

$$\frac{\partial \psi}{\partial Y} = -\,\mathcal{H}\left[\frac{\partial \eta}{\partial X}\right] = -\frac{1}{\varepsilon}\,\mathcal{H}\left[\frac{\partial \eta}{\partial x}\right]$$

and hence the contribution from the electric field at the interface is given by

$$\widehat{E} = \frac{E_b}{2}\left(-1 + 2\delta\,\mathcal{H}\left[\frac{\partial \eta}{\partial x}\right]\right) + \mathcal{O}(\delta^2\varepsilon). \tag{6.2.19}$$

Finally, substituting (6.2.19) back into Equation 6.2.10, the governing equation for the incompressible long-wavelength, small-amplitude electrohydrodynamic system is given

by

$$2\frac{\partial \eta}{\partial t}+3\eta\frac{\partial \eta}{\partial x}+a\frac{\partial^3 \eta}{\partial x^3}+b\frac{\partial^5 \eta}{\partial x^5}=\bar{p}\,\mathcal{H}\left[\frac{\partial^2 \eta}{\partial x^2}\right]+\vartheta\,\mathscr{T}\left[\frac{\partial \eta}{\partial x}\right] \tag{6.2.20}$$

where

$$a=\frac{\varepsilon^2}{\delta}\left(\frac{1}{3}-\mathrm{Eo}\right),\qquad b=\frac{\varepsilon^4}{45\delta},\qquad \bar{p}=\frac{E_b}{\delta},\qquad \vartheta=\frac{\delta_{\text{B}}}{\delta}.$$

If we set $b=\vartheta=0$ then the resulting equation is sometimes called the Korteweg-de Vries-Benjamin-Ono equation (Gleeson et al., 2007) as is it effectively a linear combination of the Korteweg-de Vries equation (2.1.1) and the Benjamin-Ono equation

$$\frac{\partial \eta}{\partial t}+\eta\frac{\partial \eta}{\partial x}=E_b\,\mathcal{H}\left[\frac{\partial^2 \eta}{\partial x^2}\right]. \tag{6.2.21}$$

a nonlinear partial differential equation that describes one-dimensional internal waves in deep water. We now proceed to obtain travelling wave solutions to Equation 6.2.20.

6.2.3 Numerical derivation of the travelling wave solution

The governing equation equation (6.2.20) derived above has no known exact solutions. In the next part of the analysis we will attempt to find numerical solutions using a Newton-Raphson type approximation, with the solitary wave solution given by

$$\eta=A\,\mathrm{sech}^2\left(\frac{\sqrt{|A|}}{2}\left(x-\frac{A}{2}t\right)\right) \tag{6.2.22}$$

taken as an initial guess. We begin with (6.2.20) in the case $\vartheta=0$ with no effect due to a no-slip condition on the solid lower electric plate,

$$2\frac{\partial \eta}{\partial t}+3\eta\frac{\partial \eta}{\partial x}+a\frac{\partial^3 \eta}{\partial x^3}+b\frac{\partial^5 \eta}{\partial x^5}=\bar{p}\,\mathcal{H}\left[\frac{\partial^2 \eta}{\partial x^2}\right] \tag{6.2.23}$$

which is a fifth-order KdV-Benjamin-Ono equation where as before we impose that $a=\pm 1$ depending on the parity of the amplitude, and the Hilbert transform $\mathcal{H}[f(X)]$ is defined in Equation 6.2.18. Setting $b=\bar{p}=0$ reduces Equation 6.2.20 to a KdV equation

with solitary wave solution given by Equation 6.2.22. Now, we make the substitution

$$\eta = AN(z), \qquad z = \frac{\sqrt{|A|}}{2}\left(x - \frac{A}{2}t\right), \tag{6.2.24}$$

so the initial guess becomes

$$N = \operatorname{sech}^2 z,$$

and the derivatives become

$$\frac{\partial}{\partial t} = \frac{\partial z}{\partial t}\frac{\partial}{\partial z} = -\frac{A\,|A|^{\frac{1}{2}}}{4}\frac{\partial}{\partial z}, \tag{6.2.25}$$

and

$$\frac{\partial}{\partial x} = \frac{\partial z}{\partial x}\frac{\partial}{\partial z} = \frac{|A|^{\frac{1}{2}}}{2}\frac{\partial}{\partial z}. \tag{6.2.26}$$

Then we substitute (6.2.25) and (6.2.26) into Equation 6.2.20 to get

$$-\frac{A\,|A|^{\frac{1}{2}}}{2}\frac{\mathrm{d}N}{\mathrm{d}z} + \frac{3A\,|A|^{\frac{1}{2}}}{4}\frac{\mathrm{d}\left(N^2\right)}{\mathrm{d}z} + a\frac{|A|^{\frac{3}{2}}}{8}\frac{\mathrm{d}^3N}{\mathrm{d}z^3} + b\frac{|A|^{\frac{5}{2}}}{32}\frac{\mathrm{d}^5N}{\mathrm{d}z^5} = \bar{p}\frac{|A|}{4}\mathcal{H}\left[\frac{\mathrm{d}^2N}{\mathrm{d}z^2}\right]$$

and this can be simplified to

$$\frac{\mathrm{d}N}{\mathrm{d}z} - \frac{3}{2}\frac{\mathrm{d}\left(N^2\right)}{\mathrm{d}z} = \frac{1}{2A}\left(a\frac{|A|}{2}\frac{\mathrm{d}^3N}{\mathrm{d}z^3} + b\frac{|A|^2}{8}\frac{\mathrm{d}^5N}{\mathrm{d}z^5} - \bar{p}\,|A|^{\frac{1}{2}}\mathcal{H}\left[\frac{\mathrm{d}^2N}{\mathrm{d}z^2}\right]\right).$$

We then integrate with respect to z which yields

$$N - \frac{3}{2}N^2 = \frac{1}{2A}\left(a\frac{|A|}{2}\frac{\mathrm{d}^2N}{\mathrm{d}z^2} + b\frac{|A|^2}{8}\frac{\mathrm{d}^4N}{\mathrm{d}z^4} - \bar{p}\,|A|^{\frac{1}{2}}\,\mathcal{H}\left[\frac{\mathrm{d}N}{\mathrm{d}z}\right]\right). \tag{6.2.27}$$

As with previous chapters in the report, we will use spectral methods to numerically evaluate Equation 6.2.27. Similar to the boundary layer integral transform Equation B.0.5, the Fourier transform of the Hilbert term is non-trivial and is given in Hammerton and Bassom (2013) by

$$\mathcal{F}\left[\mathcal{H}[f(x)]\right] = \begin{cases} -\mathrm{i}\widehat{f}(k), & k > 0 \\ \mathrm{i}\widehat{f}(k), & k < 0 \end{cases}$$

or more compactly,

$$\mathcal{F}\left[\mathcal{H}[f(x)]\right] = -\mathrm{i}\,\mathrm{sgn}(k)\widehat{f}(k),$$

where sgn denotes the signum function. We take the Fourier transform of Equation 6.2.27 which gives

$$\widehat{N} - \frac{3}{2}\widehat{(N^2)} + \frac{1}{2A}\left(ak^2\frac{|A|}{2} - bk^4\frac{|A|^2}{8} + \bar{p}k^2\frac{|A|^{\frac{1}{2}}}{|k|}\right)\widehat{N} = 0,$$

and this can be simplified to

$$\widehat{N} - \frac{3}{2}\widehat{(N^2)} + \frac{\gamma}{2}\left(\frac{1}{2}ak^2 - \frac{1}{8}bk^4|A| + \bar{p}k\,|A|^{-\frac{1}{2}}\,\mathrm{sgn}(k)\right)\widehat{N} = 0 \tag{6.2.28}$$

where $\gamma = \mathrm{sgn}(A)$. Then, writing N as a discrete Fourier transform

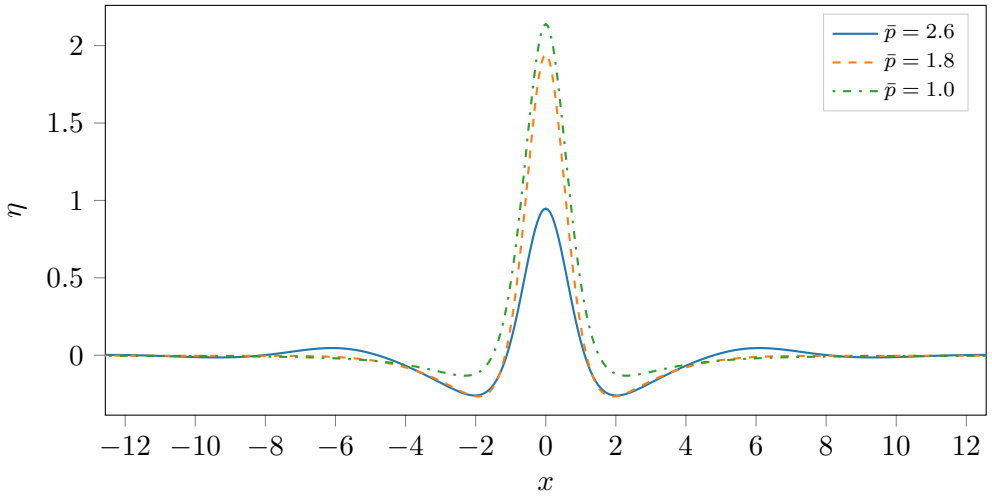

Figure 6.2.2: Initial travelling wave profiles for the KdV-Benjamin-Ono equation (6.2.20), with parameters $a = 1$, $A = 2$, $b = 0$, $\vartheta = 0$, $x \in [-4\pi, 4\pi]$, for different values of $\bar{p} = 1$, 1.8, and 2.6.

$$N(z) = \sum_{k=-n}^{n} c_k \mathrm{e}^{\mathrm{i}kz},$$

Equation 6.2.28 can be written

$$c_k - \frac{3}{2}\sum_s c_s c_{k-s} + \frac{\gamma}{2}\left(\frac{1}{2}ak^2 - \frac{1}{8}bk^4|A| + \bar{p}k\,|A|^{-\frac{1}{2}}\,\mathrm{sgn}(k)\right)c_k = 0 \tag{6.2.29}$$

with unknown coefficients c_k. The set of $n+1$ equations with $n+1$ unknowns is solved for c_k using a Newton-Raphson approximation method, iterating from the initial guesses for c_k, given by taking the Fourier coefficients of $N = \mathrm{sech}^2 z$.

Figure 6.2.2 illustrates the approximate travelling wave solution to Equation 6.2.20, with

no effect due to a no-slip condition on the bottom boundary so that $\vartheta = 0$, and no contribution from the fifth-order derivative so $b = 0$. We see that increasing the value of $\bar{p}$ results in a much smaller initial amplitude of the wave. We also see the formation of additional troughs and peaks, or ripples, either side of the main peak disturbance. In the case where $\bar{p} = 1$ the wave looks altogether similar to a sech^2 solitary wave solution to the KdV equation, with the addition of two small troughs either side of the main disturbance. As we increase $\bar{p}$ we see additional ripples, bigger troughs and a smaller middle peak.

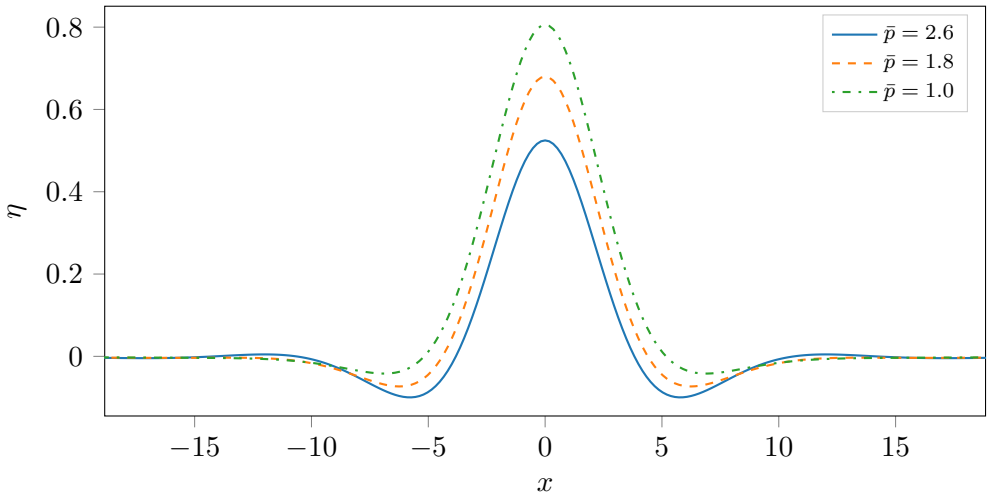

Figure 6.2.3: Initial travelling wave profiles for the fifth-order KdV-Benjamin-Ono equation (6.2.20), with parameters $a = 1$, $A = 2$, $b = 1$, $\vartheta = 0$, $x \in [-8\pi, 8\pi]$, for different values of $\bar{p} = 1$, 1.8, and 2.6.

Figure 6.2.3 illustrates travelling wave solutions using the same parameters but including the fifth-order derivative. We observe similar behaviour in these solutions to those in Figure 6.2.2 except that the main disturbance appears to be much wider with a smaller amplitude. In addition to this, we observe in Figure 6.2.4 that keeping the value of $\bar{p}$ fixed and decreasing the amplitude A results in the ripples becoming more comparable in size to the main central peak.

We now advance these solutions in time using the fourth order Runge-Kutta and integrating factor methods defined in Chapter 2, and then look at the effects of including the no-slip condition on the solid bottom electrode boundary. We begin with the case $\vartheta = 0$ where we choose to omit any effects due to a no-slip condition at the fluid bottom. Figure 6.2.5 illustrates such a scenario which demonstrates that the numerical solution obtained from solving Equation 6.2.28 using the Newton method is indeed a travelling

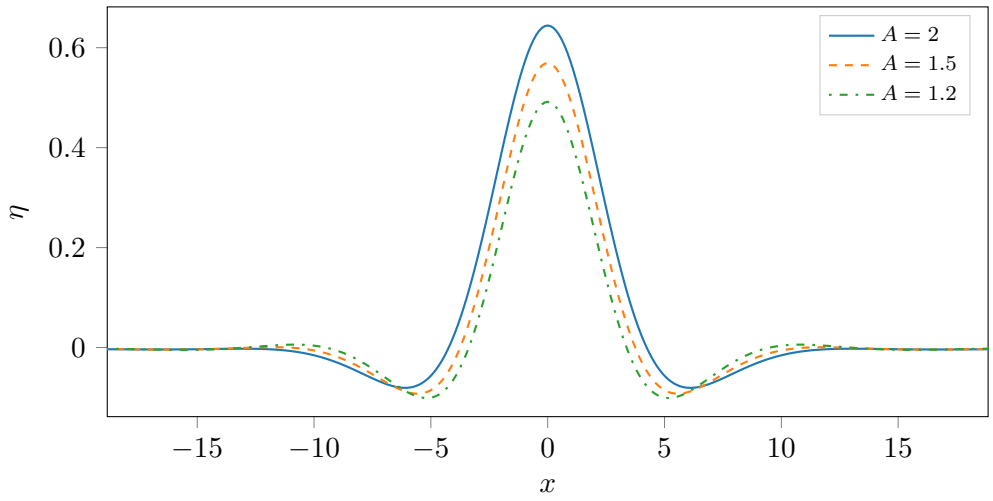

Figure 6.2.4: Initial travelling wave profiles for the fifth-order KdV-Benjamin-Ono equation (6.2.20), with parameters $a = 1$, $b = 1$, $\vartheta = 0$, $x \in [-8\pi, 8\pi]$, $\bar{p} = 2$ for different values the amplitude $A = 1.2$, 1.5, and 2.

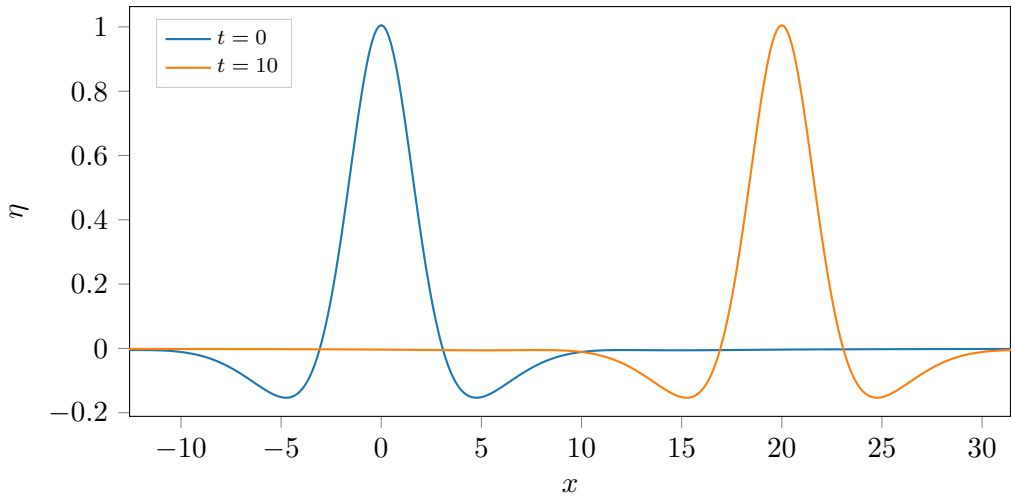

Figure 6.2.5: Numerical travelling wave solution to the KdV-Benjamin-Ono equation (6.2.20) at times $t = 0$ and $t = 10$, with parameters $a = 1$, amplitude $A = 2$ $b = 0$, $x \in [-8\pi, 8\pi]$, $\bar{p} = 2.2$ and no effect due to the no-slip condition at the fluid bottom, so $\vartheta = 0$.

wave solution to the KdV-Benjamin-Ono equation Equation 6.2.23. We observe that the wave travels without loss of amplitude or change in wave form.

Next we look at the case $\vartheta = 0.1$ which represents a small dissipative effect from the no-slip condition on the bottom electrode. We advance the numerical solution obtained from solving Equation 6.2.28 in time and increase ϑ from its zero value to $\vartheta = 0.1$ for times $t > 0$. Figure 6.2.6 illustrates such a scenario. We observe from the figure that the main disturbance has decayed in amplitude, as expected, and that an elevated shelf has

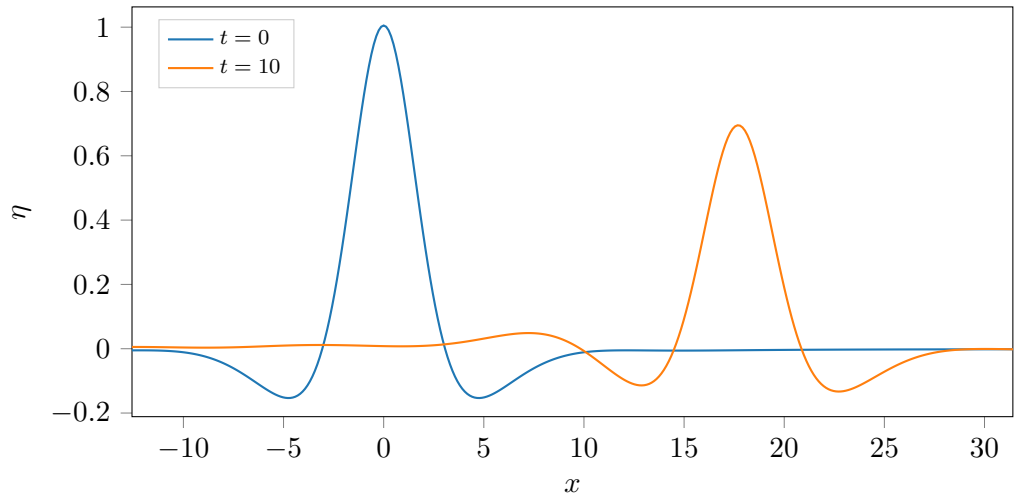

Figure 6.2.6: Numerical travelling wave solution to the KdV-Benjamin-Ono equation (6.2.20) at times $t = 0$ and $t = 10$, with parameters $a = 1$, amplitude $A = 2$ $b = 0$, $x \in [-8\pi, 8\pi]$, $\bar{p} = 2.2$ and a small effect due to the no-slip condition at the fluid bottom $\vartheta = 0.1$.

formed behind the left-hand trough. Although not visible in the figure, careful analysis of the results show that a decaying oscillatory tail has also formed similar to the KdV-B results in Chapter 3 and the surfactant analysis in Chapter 5. We see also that both ripples have become smaller in value, with the trough on the left-hand side decaying more than the trough to the right of the main peak.

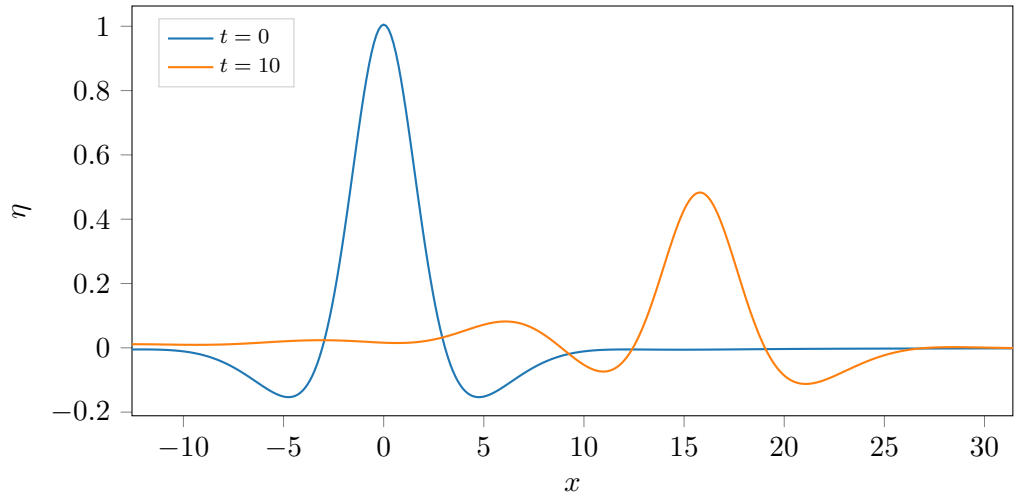

Figure 6.2.7: Numerical travelling wave solution to the KdV-Benjamin-Ono equation (6.2.20) at times $t = 0$ and $t = 10$, with parameters $a = 1$, amplitude $A = 2$ $b = 0$, $x \in [-8\pi, 8\pi]$, $\bar{p} = 2.2$ and moderate effect due to the no-slip condition at the fluid bottom $\vartheta = 0.2$.

Finally we look at the case $\vartheta = 0.2$ which represents a moderate dissipative effect from the no-slip condition on the bottom electrode. In the same way as before, we advance the

numerical solution obtained from Equation 6.2.28 in time and increase ϑ to $\vartheta = 0.2$ for times $t > 0$. Figure 6.2.7 illustrates such a scenario. We observe from the figure that the main disturbance has experienced a greater decay in amplitude, as expected, and that an elevated shelf has formed behind the left-hand trough, as before. We see also that both sets of ripples have become smaller in value again, with the trough on the left-hand side decaying more than the trough to the right of the main peak.

6.3 Extensions to the existing analyses

The case when the lower fluid is not a perfect conductor

In the previous results the lower fluid was assumed to be a perfect conductor. This represents a massive simplification to the model in that we had no tangential surface stress condition. If instead we do not impose that the lower fluid is perfectly conducting then the model becomes much more similar to the surfactant system and we would consider Equation 4.1.71 together with Equation 6.2.7 and a suitable tangential stress component $\widehat{T}_{\mathrm{t}}$ with contributions $\bar{T}_{\mathrm{t}} \neq 0$ from the electric field.

While such a scenario isn't explored here, we believe this to be an interesting possible extension to the existing model in Section 6.2 from which we could draw parallels with the surfactant analysis from Chapter 5.

A scenario with a soluble surfactant at the fluid interface

The surfactant system in Chapter 5 considered weakly nonlinear disturbances in the presence of an insoluble surfactant. One possible extension of this analysis may be to explore a similar system but instead consider the effects of a soluble surfactant at the fluid interface.

Insoluble surfactants are much easier to model than soluble surfactants which adsorb much more with the main fluid body. This makes the analysis much more complicated

and would add conditions on the equations governing the fluid flow of the main fluid body. While such a system isn't considered here, we believe this would make an interesting extension to the current model.

This notion has been explored experimentally for nonlinear gravity-capillary waves (Lapham et al., 2001) although the governing system of equations were absent from the analysis. Certainly the surface elevation equation with stress conditions (4.1.71) may be applicable although both the normal and tangential surface stress conditions would look different to those described in the insoluble case.

An electrohydrodynamic system with an insoluble surfactant

We have considered two scenarios in depth, a fluid with an insoluble surfactant at the fluid surface and a fluid in the presence of an electric field. As such, we believe that an interesting scenario would be to combine both of these systems. Although we pursue this model out of general interest, in real-world experiments it can often be difficult to remove all traces of surfactant on a fluid surface. Therefore one possible motivation for obtaining results for such a scenario would be an instance with an electrohydrodynamic system subject to *unintended* surfactant present at the fluid interface.

For a combined system we could assume the travelling wave solution to the electrohydrodynamic system which is affected by an insoluble surfactant for times $t > 0$. Alternatively we could consider an undisturbed sech^2 solitary wave solution affected by both an electric field generated through the fluid and the insoluble surfactant for times $t > 0$. In either case we can use the full system of equations given by

$$\frac{\partial}{\partial \tau}\left(2\eta - \alpha\,\mathscr{T}\left[\frac{\partial \Gamma}{\partial S}\right]\right) + 3\eta\frac{\partial \eta}{\partial S} + a\frac{\partial^3 \eta}{\partial S^3} = \bar{p}\,\mathcal{H}\left[\frac{\partial^2 \eta}{\partial S^2}\right] + \vartheta\,\mathscr{T}\left[\frac{\partial \eta}{\partial S}\right] - \alpha\mathcal{R}, \quad (6.3.1)$$

omitting the fifth-order derivative ($b = 0$), and where

$$\mathcal{R} = -\eta\,\mathscr{T}\left[\frac{\partial^2 \Gamma}{\partial S^2}\right] - \frac{\partial \eta}{\partial S}\,\mathscr{T}\left[\frac{\partial \Gamma}{\partial S}\right] + \alpha\,\mathscr{T}\left[\frac{\partial \Gamma}{\partial S}\right]\mathscr{T}\left[\frac{\partial^2 \Gamma}{\partial S^2}\right] + \frac{\delta_{\text{B}}}{\delta}\frac{\partial \Gamma}{\partial S} \quad (6.3.2)$$

as in Chapter 5.

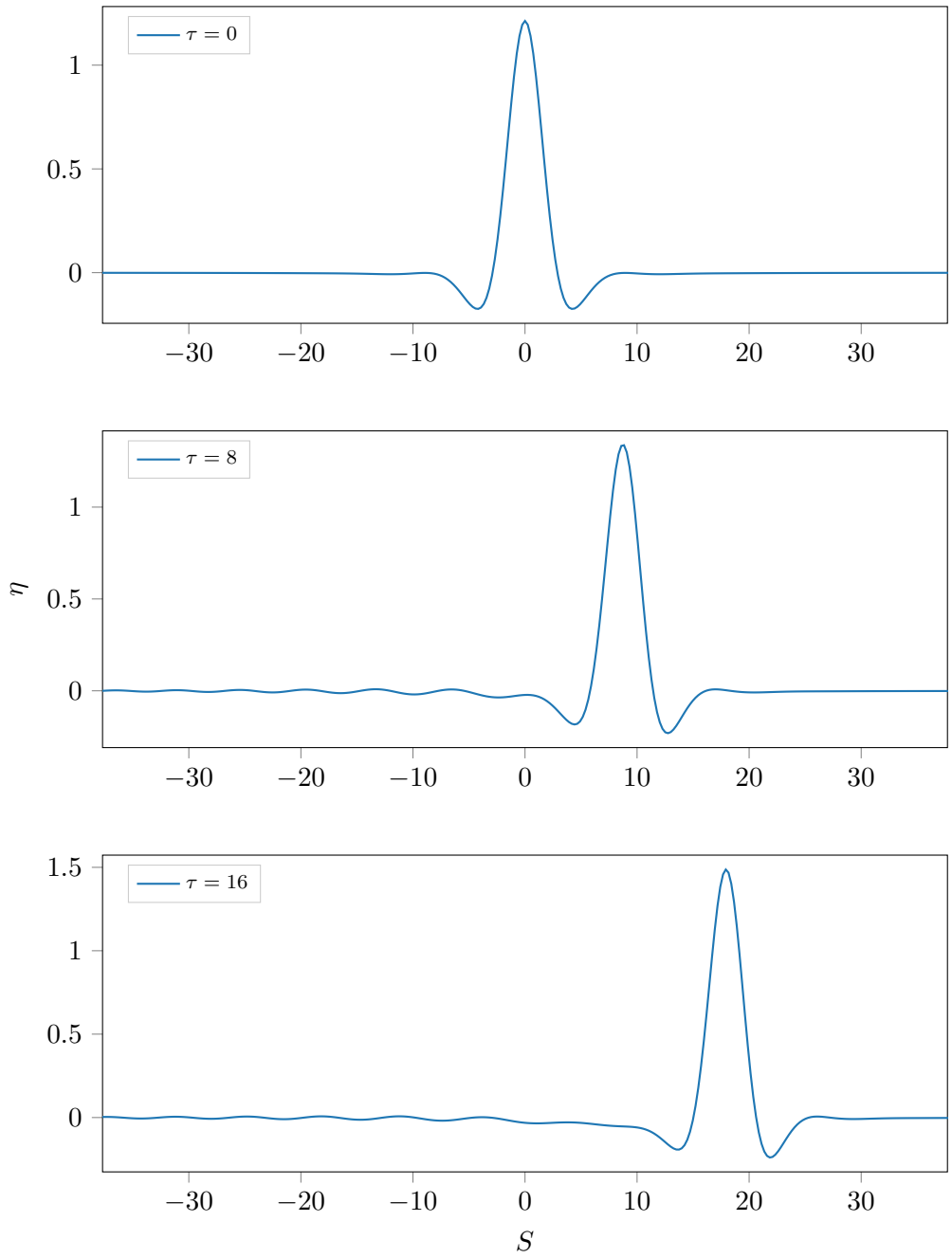

Figure 6.3.1: A numerical solution to the full system of equations (6.3.1) and (6.3.2) with the electrohydrodynamic travelling wave as an initial condition, with parameters: $x \in [-8\pi, 8\pi]$, $t = 0$, 8, and 16, $A = 2$, $\alpha = 0.4$, $a = 1$, $\bar{p} = 2.2$, and no effect due to no-slip condition $\vartheta = 0$.

Figure 6.3.1 is a numerical illustration generated using the integrating factor method defined Chapter 2 which shows the electrohydrodynamic travelling wave solution in the presence of a surfactant, for times $\tau = 0$, $\tau = 8$ and $\tau = 16$. In this system we have ignored the effects due to a no-slip condition at the solid bottom boundary.

We observe from the figure that the travelling wave has formed a noticeable oscillatory tail behind the ripple which sits to the rear of the main peak disturbance. We also see that for later times the ripple to the left of the main peak has decayed, whereas the main peak disturbance has grown in amplitude by small amount. It is not immediately clear from the figure itself, but upon further inspection we observe that the ripple to the right of the main peak has also decayed slightly in amplitude.

We note that although the main peak has increased slightly in amplitude, this is not attributed to a numerical instability or error causing rapid amplitude growth which was seen in Hammerton and Bassom (2013). One possible cause of this growth may be that the some of the fluid mass has been redistributed from the ripples either side of the main peak.

Figure 6.3.2 is a numerical illustration which shows the electrohydrodynamic travelling wave solution in the presence of a surfactant, for times $\tau = 0$, $\tau = 8$ and $\tau = 16$, with the inclusion of the no-slip condition at the solid bottom boundary. This figure has also been generated using the integrating factor scheme defined in Chapter 2. We observe from the figure that the travelling wave has again formed a noticeable oscillatory tail behind the ripple which sits to the rear of the main peak disturbance. We also see that another elevated ripple, or indeed perhaps the equivalent of a constant elevated shelf, has formed behind the trough ripple to the left of the main peak. This time the main peak has decayed, in addition to the ripples on either side. Once again, it is not immediately clear from the figure itself, but upon further inspection we observe that the ripple to the right of the main peak has also decayed slightly in amplitude.

6.4 Summary of chapter and concluding remarks

This chapter first discussed other scenarios where the governing equations for the system with an arbitrary surface stress condition may be applicable. While usage in previous work to our knowledge is limited to the surfactant and electric field systems, we believe that there are many more applications where it may be used such as the sediment transport

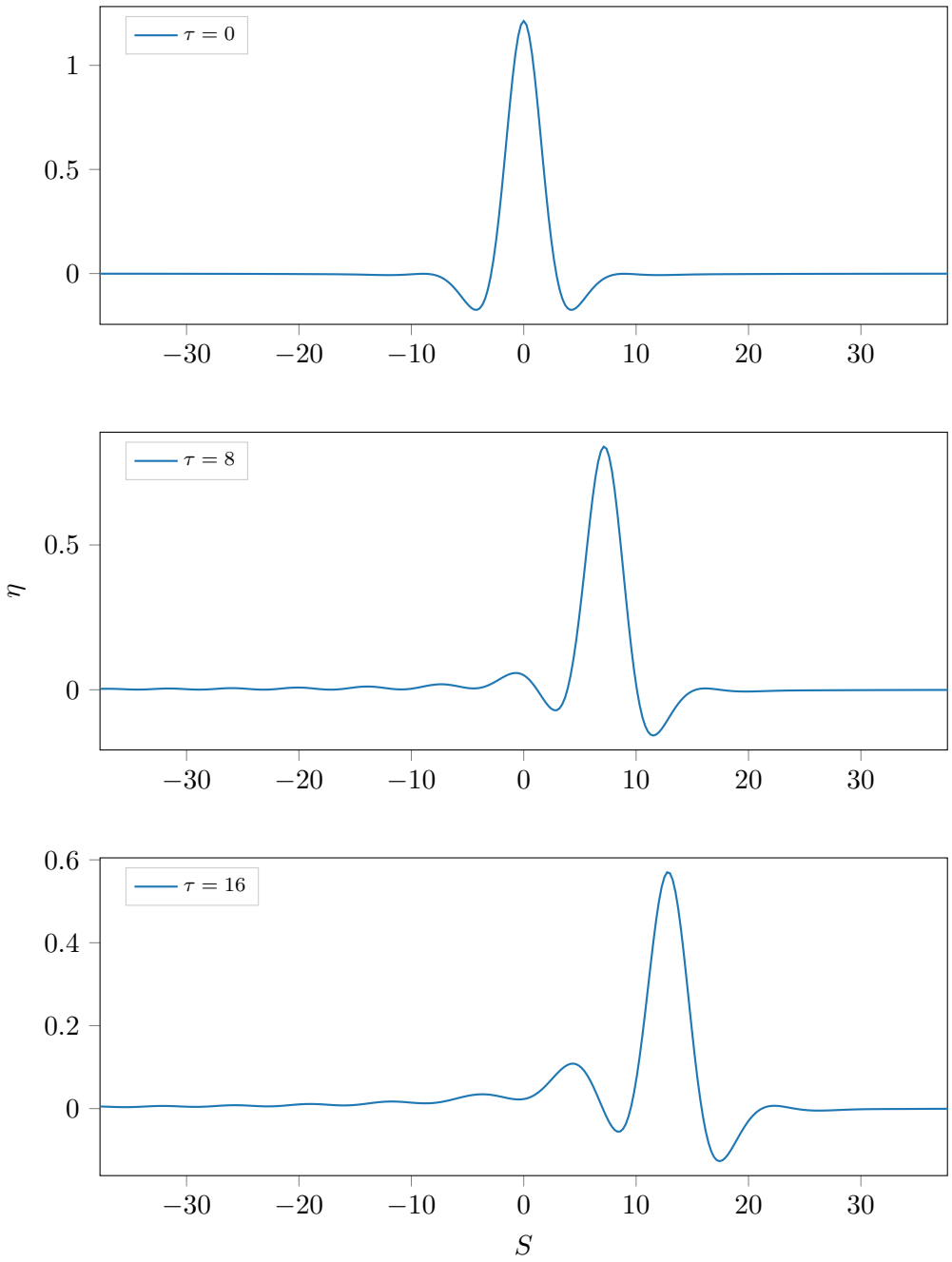

Figure 6.3.2: A numerical solution to the full system of equations (6.3.1) and (6.3.2) with the electrohydrodynamic travelling wave as an initial condition, with parameters: $x \in [-8\pi, 8\pi]$, $t = 0$, 8, and 16, $A = 2$, $\alpha = 0.4$, $a = 1$, $\bar{p} = 2.2$, and moderate effect due to no-slip condition $\vartheta = 0.2$.

scenario discussed in Section 6.1.

In Section 6.2 we revisited a scenario previously explored in Hammerton and Bassom (2013), Hammerton (2013), and Hammerton and Bassom (2014) as well as various other works such as Papageorgiou and Vanden-Broeck (2006) and Gleeson et al. (2007). We

have shown that travelling wave solutions are possible in an electrohydrodynamic system and in addition to this we provided numerical solutions and illustrations using various different parameters. We also presented illustrations for a scenario with a no-slip condition at the bottom boundary.

We note, in particular, certain parallels with the surfactant system. A relationship between the surface elevation function and the electric charge density can be derived using the electric charge conservation equation (6.2.7), in the same way that a relationship between the surfactant concentration and the surface elevation can be formed using the advection-diffusion equation (5.1.1). Both comparisons allowed us to deduce the surface stress conditions exhibited in each scenario.

While no surface stress conditions were explicitly given for the KdV-Burgers' system presented in Chapter 3, these could be derived for each physical scenario discussed in the chapter introduction. The governing equations for each physical system: the KdV-B system (Chapter 3), the system with boundary layer damping in Chapter 4, the surfactant system in Chapter 5 and the electrohydrodynamic system presented earlier in the present chapter; all represented small perturbations to the Korteweg-de Vries equation (1.3.1). This is a direct result of applying small magnitude interferences to the weakly nonlinear long-wavelength fluid system.

Each scenario presented in the thesis has considered a travelling solitary wave solution as an initial condition before applying the relative effects for times $t > 0$. While each scenario has different parameters characterising the relative effects along with its own intricate boundary conditions, direct comparisons between the results identified similarities in the transformation of the solitary wave profile. In each case we identified a slowly decaying oscillatory tail, a small amplitude elevated shelf behind the peak disturbance, and a gradual decay in ampltiude resulting also in a loss of wave speed.

This appears to be a general result for solitary wave dissipation, reaffirming previous work such as that presented by Karpman and Maslov (1978) and Grimshaw et al. (2003).

As such, it is our belief that the results presented in this thesis may be both useful and applicable to future research concerning the dissipation and the effect of surface stress

on solitary wave propagation.

Bibliography

Abramowitz, M.

1964. Handbook of mathematical functions with formulas, graphs, and mathematical tables, nbs. *Applied Math. Series*, 55:232.

Acheson, D.

1990. *Elementary Fluid Dynamics*, Oxford Applied Mathematics and Computing Science Series. Clarendon Press.

Atik, H., C.-Y. Kim, L. Van Dommelen, and J. Walker

2005. Boundary-layer separation control on a thin airfoil using local suction. *Journal of Fluid Mechanics*, 535:415–443.

Batchelor, G.

1989. A brief guide to two-phase flow. In *Theoretical and Applied Mechanics*, Pp. 27–40.

Batchelor, G. K.

2000. *An introduction to fluid dynamics*. Cambridge university press.

Batyshchev, V.

1991. The non-linear action of tangential stresses on the wave motion of a low-viscosity fluid. *Journal of Applied Mathematics and Mechanics*, 55(1):67–74.

Bona, J. L. and J. A. Tropp

2001. Cnoidal solutions to the pth-order korteweg-de vries equation.

Boussinesq, J.

1877. *Essai sur la théorie des eaux courantes*. Impr. nationale.

Brauer, K.

2000. The korteweg-de vries equation: history, exact solutions, and graphical representation. *University of Osnabrück/Germany1*.

Canepa, E., D. Lengani, F. Satta, E. Spano, M. Ubaldi, and P. Zunino

2006. Boundary layer separation control on a flat plate with adverse pressure gradients using vortex generators. In *ASME turbo expo 2006: Power for land, sea, and air*, Pp. 1211–1220. American Society of Mechanical Engineers Digital Collection.

Caputo, J.-G. and Y. A. Stepanyants

2003. Bore formation, evolution and disintegration into solitons in shallow inhomogeneous channels. *Nonlinear Processes in Geophysics*, 10(4–5):407–424.

Castellanos, A. and A. Gonzalez

1998. Nonlinear electrohydrodynamics of free surfaces. *IEEE Transactions on Dielectrics and Electrical Insulation*, 5(3):334–343.

Davis, R. and A. Acrivos

1966. The influence of surfactants on the creeping motion of bubbles. *Chemical Engineering Science*, 21(8):681–685.

Dewey Jr, C. F. and J. F. Gross

1967. Exact similar solutions of the laminar boundary-layer equations. In *Advances in heat transfer*, volume 4, Pp. 317–446. Elsevier.

Drazin, P. and R. Johnson

1989. *Solitons: An Introduction*. Cambridge University Press.

Elfring, G. J., L. G. Leal, and T. M. Squires

2016. Surface viscosity and marangoni stresses at surfactant laden interfaces. *Journal of Fluid Mechanics*, 792:712–739.

Feng, Z.-s. and Q.-g. Meng

2007. Burgers-Korteweg-de Vries equation and its traveling solitary waves. *Science in China Series A: Mathematics*, 50(3):412–422.

Gao, X.-Y.

2015. Variety of the cosmic plasmas: general variable-coefficient korteweg-de vries-burgers equation with experimental/observational support. *EPL (Europhysics Letters)*, 110(1):15002.

Gleeson, H., P. Hammerton, D. Papageorgiou, and J.-M. Vanden-Broeck

2007. A new application of the korteweg–de vries benjamin-ono equation in interfacial electrohydrodynamics. *Physics of Fluids*, 19(3):031703.

Gonzalez, A. and A. Castellanos

1997. Nonlinear waves in a viscous horizontal film in the presence of an electric field. *Journal of electrostatics*, 40:55–60.

Gradshteyn, I. and I. Ryzhik

1980. Tables of integrals, series and products: corrected and enlarged edition. *Academic Press: New York*.

Grimshaw, R., E. Pelinovsky, and T. Talipova

2003. Damping of large-amplitude solitary waves. *Wave Motion*, 37(4):351–364.

Grimshaw, R. and C. Yuan

2016. Depression and elevation tsunami waves in the framework of the korteweg–de vries equation. *Natural Hazards*, 84(2):493–511.

Halpern, D. and A. L. Frenkel

2003. Destabilization of a creeping flow by interfacial surfactant: linear theory extended to all wavenumbers. *Journal of Fluid Mechanics*, 485:191–220.

Hammerton, P.

2013. Existence of solitary travelling waves in interfacial electrohydrodynamics. *Wave Motion*, 50(4):676–686.

Hammerton, P. and A. P. Bassom

2013. The effect of surface stress on interfacial solitary wave propagation. *The Quarterly Journal of Mechanics and Applied Mathematics*, 66(3):395–416.

Hammerton, P. and A. P. Bassom

2014. The effect of a normal electric field on wave propagation on a fluid film. *Physics of Fluids*, 26:012107.

Harris, S. and D. Crighton

1994. Solitons, solitary waves, and voidage disturbances in gas-fluidized beds. *Journal of Fluid Mechanics*, 266:243–276.

Hereman, W.

2012. Shallow water waves and solitary waves. In *Mathematics of Complexity and Dynamical Systems*, Pp. 1520–1532. Springer.

Holloway, P. E., E. Pelinovsky, and T. Talipova

1999. A generalized korteweg-de vries model of internal tide transformation in the coastal zone. *Journal of Geophysical Research: Oceans*, 104(C8):18333–18350.

Holloway, P. E., E. Pelinovsky, T. Talipova, and B. Barnes

1997. A nonlinear model of internal tide transformation on the australian north west shelf. *Journal of Physical Oceanography*, 27(6):871–896.

Johnson, S. G.

2011. Notes on FFT-based differentiation.

Karpman, V. and E. Maslov

1978. Structure of tails produced under the action of perturbations on solitons. *Soviet Journal of Experimental and Theoretical Physics*, 48:252.

Kaup, D. J. and A. C. Newell

1978. Solitons as particles, oscillators, and in slowly changing media: a singular perturbation theory. *Proceedings of the Royal Society of London A: Mathematical, Physical and Engineering Sciences*, 361(1707):413–446.

Keulegan, G. H.

1948. Gradual damping of solitary waves. *J. Res. Natl. Bur. Stand*, 40(6):487–498.

Kim, D., K. Hwang, S. Lee, et al.

2016. Dynamic transport of suspended sediment by solitary wave: Experimental study. In *EGU General Assembly Conference Abstracts*, volume 18.

Korteweg, D. and F. de Vries

1895. On the change of form of long waves advancing in a rectangular canal, and on a new type of long stationary waves. *Philos. Mag.*, 39:422–443.

Kosmulski, M.

2001. *Chemical properties of material surfaces*. CRC press.

Kruskal, M., C. Gardner, J. Green, and R. Miura

1967. Method for solving korteweg–de vries equation. *Phys. Rev. Lett*, 19:1095–1098.

Lapham, G., D. Dowling, and W. Schultz

2001. Linear and nonlinear gravity-capillary water waves with a soluble surfactant. *Experiments in fluids*, 30(4):448–457.

LeVeque, R. J.

2006. Finite difference methods for differential equations.

LeVeque, R. J.

2007. *Finite difference methods for ordinary and partial differential equations: steady-state and time-dependent problems*, volume 98. Siam.

Longuet-Higgins, M. S.

1953. Mass transport in water waves. *Phil. Trans. R. Soc. Lond. A*, 245(903):535–581.

Macura, W. K.

2016. Numerical Stability. From MathWorld—A Wolfram Web Resource. Last visited on 6/4/2016.

Mathews, J. H., K. D. Fink, et al.

2004. *Numerical methods using MATLAB*, volume 4. Pearson Prentice Hall Upper Saddle River, NJ.

Mei, C. C.

1989. *The applied dynamics of ocean surface waves*, volume 1. World Scientific.

Melcher, J. R. and W. J. Schwarz Jr

1968. Interfacial relaxation overstability in a tangential electric field. *The Physics of Fluids*, 11(12):2604–2616.

Milewski, P. A. and E. G. Tabak

1999. A pseudospectral procedure for the solution of nonlinear wave equations with examples from free-surface flows. *SIAM journal on scientific computing*, 21(3):1102–1114.

Ott, E. and R. Sudan

1970. Damping of solitary waves. *Phys. Fluids*, 13:1432–1434.

Özuğurlu, E. and J.-M. Vanden-Broeck

2006. A note on solitary waves with variable surface tension in water of infinite depth. *The ANZIAM Journal*, 48(2):225–235.

Papageorgiou, D. T. and J.-M. Vanden-Broeck

2006. Numerical and analytical studies of nonlinear gravity-capillary waves in fluid layers under normal electric fields. *IMA journal of applied mathematics*, 72(6):832–853.

Pelinovsky, D. E. and R. H. Grimshaw

1997. Structural transformation of eigenvalues for a perturbed algebraic soliton potential. *Physics Letters A*, 229(3):165–172.

Pelinovsky, E. N., Y. Stepanyants, and T. Talipova

1993. Nonlinear dispersion model of sea waves in the coastal zone.

Russell, J. S.

1844. Report on waves. In *14th meeting of the British Association for the Advancement of Science*, volume 311, P. 390.

Smith, F.

1986. Steady and unsteady boundary-layer separation. *Annual review of fluid mechanics*, 18(1):197–220.

Sugimoto, N.

1996. Acoustic solitary waves in a tunnel with an array of helmholtz resonators. *The Journal of the Acoustical Society of America*, 99(4):1971–1976.

Sumer, B. M., M. B. Sen, I. Karagali, B. Ceren, J. Fredsøe, M. Sottile, L. Zilioli, and D. R. Fuhrman

2011. Flow and sediment transport induced by a plunging solitary wave. *Journal of Geophysical Research: Oceans*, 116(C1).

Trefethen, L. N.

2000. *Spectral methods in MATLAB*. Siam.

Vanden-Broeck, J.-M.

2010. *Gravity-capillary free-surface flows*. Cambridge University Press.

Wu, T. and C.-F. Chen

2000. Laminar boundary-layer separation over a circular cylinder in uniform shear flow. *Acta Mechanica*, 144(1-2):71–82.

Zabusky, N. J. and M. D. Kruskal

1965. Interaction of" solitons" in a collisionless plasma and the recurrence of initial states. *Physical review letters*, 15(6):240.

Appendices

A

Integral constraints and results used for the KdV-Burgers' Analysis

---

A.1 Integral constraints on the linear perturbation equation

In determining the solution of the linear perturbation equation (3.2.13), three integral constraints (3.2.22)-(3.2.24), are used. These constraints are derived in this appendix. For $R[\upsilon_0]$ and $L[F]$, given by Equation 3.2.16 and Equation 3.2.15 respectively, and $\upsilon_0 = \operatorname{sech}^2\theta$, it can readily be shown that when F and its derivatives tend to zero as $\theta \to \pm\infty$ then

$$\int_{-\infty}^{\infty} R[\upsilon]\,\mathrm{d}\theta = 2\mu_0 \qquad \int_{-\infty}^{\infty} L[F]\,\mathrm{d}\theta = 0$$

$$\int_{-\infty}^{\infty} \upsilon_0 R[\upsilon_0]\,\mathrm{d}\theta = \frac{3}{2}\mu_0 \int_{-\infty}^{\infty} \upsilon_0^2 + \left(\frac{\partial \upsilon_0}{\partial \theta}\right)^2 \mathrm{d}\theta \qquad \int_{-\infty}^{\infty} \upsilon_0 L[F]\,\mathrm{d}\theta = 0$$

$$\int_{-\infty}^{\infty} \theta L[F]\,\mathrm{d}\theta = \int_{-\infty}^{\infty} (12\upsilon_0 F - 4F)\,\mathrm{d}\theta \qquad \int_{-\infty}^{\infty} \theta R[\upsilon_0]\,\mathrm{d}\theta = 2\mu_1$$

Integrating Equation 3.2.19 with respect to θ and the product of Equation 3.2.19 with $\upsilon_0(\theta)$ then gives

$$\frac{\mathrm{d}}{\mathrm{d}\tilde{t}}\left(\int_{-\infty}^{\infty} F\,\mathrm{d}\theta\right) = 2\mu_0, \qquad \frac{\mathrm{d}}{\mathrm{d}\tilde{t}}\left(\int_{-\infty}^{\infty} \upsilon_0 F\,\mathrm{d}\theta\right) = 2\left(\mu_0 - \frac{8}{15}\right).$$

Then, noting that $F(\theta, 0) = 0$, the first two integral constraints are obtained:

$$\int_{-\infty}^{\infty} F\,\mathrm{d}\theta = 2\mu_0\tilde{t}, \qquad \int_{-\infty}^{\infty} \upsilon_0 F\,\mathrm{d}\theta = 2\left(\mu_0 - \frac{8}{15}\right)\tilde{t}.$$

Similarly,

$$\begin{aligned}\frac{\mathrm{d}}{\mathrm{d}\tilde{t}}\left(\int_{-\infty}^{\infty}\theta F\,\mathrm{d}\theta\right) &= 12\int_{-\infty}^{\infty}v_0 F\,\mathrm{d}\theta - 4\int_{-\infty}^{\infty}F\,\mathrm{d}\theta - \mu_1\int_{-\infty}^{\infty}v_0\,\mathrm{d}\theta,\\ &= 24\left(\mu_0 - \frac{8}{15}\right)\tilde{t} - 8\mu\tilde{t} - 2\mu_1.\end{aligned}$$

Integrating with respect to the transformed time variable $\tilde{t}$ then gives the final integral constraint required.

A.2 Useful integral results

In the main body Subsection 3.2.2, a number of integrals involving hyperbolic functions are used. All of the integrals can be evaluated using standard techniques and their values are given in this appendix for convenience. Using the shorthand notation $T = \tanh\theta$ and $S = \operatorname{sech}^2\theta$, we have

$$\begin{aligned}&\int_{-\infty}^{\infty}S^2\,\mathrm{d}\theta = 2, && \int_{-\infty}^{\infty}S^4\,\mathrm{d}\theta = \frac{4}{3}, && \int_{-\infty}^{\infty}S^6\,\mathrm{d}\theta = \frac{16}{15},\\ &\int_{-\infty}^{\infty}\theta^3 S^2 T\,\mathrm{d}\theta = \frac{\pi^2}{4}, && \int_{-\infty}^{\infty}\theta^2 S^2\,\mathrm{d}\theta = \frac{\pi^2}{6}, && \int_{-\infty}^{\infty}\theta S^2 T\,\mathrm{d}\theta = 1,\\ &\int_{-\infty}^{\infty}\theta S^4 T\,\mathrm{d}\theta = \frac{1}{3}, && \int_{-\theta_{\mathrm{M}}}^{\infty}(1-T)\,\mathrm{d}\theta = 2\theta_{\mathrm{M}}, && \int_{-\theta_{\mathrm{M}}}^{\infty}\theta(1-T)\,\mathrm{d}\theta = \frac{\pi^2}{12} - \theta_{\mathrm{M}}^2.\end{aligned}$$

A.3 Convolution integrals involving Airy functions

If we define the convolution $H = f * \mathrm{Ai}$ and

$$F(z) = \int_{-\infty}^{z}H(z')\,\mathrm{d}z',$$

and also

$$I_1(z) = \int_{-\infty}^{z}F(z')\,\mathrm{d}z', \qquad I_2(z) = \int_{-\infty}^{z}z'F(z')\,\mathrm{d}z',$$

then it is postulated that as long as $f(x)$ decays sufficiently rapidly as $|x| \to \infty$ so that

$$C_0 = \int_{-\infty}^{\infty} f(x)\,\mathrm{d}x, \quad C_1 = \int_{-\infty}^{\infty} xf(x)\,\mathrm{d}x, \quad C_2 = \int_{-\infty}^{\infty} x^2 f(x)\,\mathrm{d}x,$$

then

$$F \sim C_0, \qquad I_1(z) \sim C_0 z - C_1, \qquad I_2(z) \sim \frac{1}{2}\left(C_0 z^2 - C_2\right), \tag{A.3.1}$$

as $z \to \infty$. This corresponds to Equation 3.2.30 with an appropriate change of variables. Here it is verified that the result is true when $f(x) = 1$ for $a < x < b$ and zero elsewhere. Since all the results are linear in $f(x)$, then this validates the result for all piecewise constant functions with compact support.

We begin by defining the function

$$I_{\mathrm{A}} = \int_{-\infty}^{\infty} \mathrm{Ai}(z')\,\mathrm{d}z'$$

from which it follows that

$$\begin{aligned}
q(z) &= \int_{-\infty}^{z} I_{\mathrm{A}}(z')\,\mathrm{d}z' = zI_{\mathrm{A}} - \mathrm{Ai}' \\
r(z) &= \int_{-\infty}^{z} q(z')\,\mathrm{d}z' = \frac{1}{2}(z^2 I_{\mathrm{A}} - z\mathrm{Ai}' - \mathrm{Ai}) \\
s(z) &= \int_{-\infty}^{z} z'q(z')\,\mathrm{d}z' = \frac{1}{3}(z^3 I_{\mathrm{A}} - z^2\mathrm{Ai}' - z\mathrm{Ai} + I_{\mathrm{A}}).
\end{aligned}$$

Taking the limit as $z \to \infty$, and using the asymptotic forms for Airy functions (Abramowitz, 1964) gives

$$I_{\mathrm{A}} \sim 1, \quad q \sim z, \quad r \sim \frac{1}{2}z^2 \quad \text{and} \quad s \sim \frac{1}{3}(z^3 + 1).$$

Hence we have

$$H(z) = \int_a^b \mathrm{Ai}(z - y)\,\mathrm{d}y = I_{\mathrm{A}}(z - a) - I_{\mathrm{A}}(z - b),$$

and therefore

$$F(z) = q(z - a) - q(z - b).$$

Thus $F \sim b - a$ and similarly, after some working,

$$I_1 \sim (b-a)z - \frac{1}{2}(b^2 - a^2), \qquad I_2 \sim \frac{1}{2}(b-a)z^2 - \frac{1}{6}(b^3 - a^3).$$

Finally, substituting for $f(x)$ in the expressions for C_i,

$$C_0 = b - a, \qquad C_1 = \frac{1}{2}(b^2 - a^2), \quad \text{and} \quad C_2 = \frac{1}{3}(b^3 - a^3),$$

and thus the results for Equation A.3.1 are validated.

This proof has been constructed using a piecewise constant, but it can also be demonstrated numerically that the same limiting forms apply when $\phi(x)$ from Subsection 3.2.2 decays exponentially as $|x| \to \infty$. However, proof of this is not attempted here.

B

Derivation of the vorticity transform

Consider from Chapter 5 the tangential momentum equation (4.1.32) at the surface $N = 0$,

$$\frac{\widehat{\varepsilon}}{\varepsilon}\frac{\partial \widetilde{U}}{\partial \tau} - c\frac{\partial \widetilde{U}}{\partial S} + \delta U\frac{\partial \widetilde{U}}{\partial S} + \frac{\partial \eta}{\partial S} - \frac{1}{\delta}\frac{\partial T_{\mathrm{n}}}{\partial S} - 2\delta_{\mathrm{B}}^2\varepsilon^2\frac{\partial^2 \widetilde{U}}{\partial S^2} = \frac{1}{\delta}\frac{\partial \widetilde{\omega}_i}{\partial N}\bigg|_{N=0}$$

where $\widetilde{U}(S) = \tilde{u}(S,0)$. To evaluate the right-hand side, we want to find $\frac{\partial \widetilde{\omega}_i}{\partial N}\big|_{N=0}$ and thus we need to solve Equation 4.1.31 subject to the condition at the surface

$$\widetilde{\omega}_i(S,0) = f_i(S)$$

and the matching condition $\widetilde{\omega}_i \to 0$ as $N \to \infty$ and $|S| \to \infty$. From Equation 4.1.31, the leading order vorticity equation for each component $\widetilde{\omega}_i$ has the form

$$\frac{\partial^2 \widetilde{\omega}_i}{\partial N^2} = -c\frac{\partial \widetilde{\omega}_i}{\partial S}.$$

We set $\widetilde{\omega}_i(S,0) = f_i(S)$ where the appropriate f_i follows from Equation 4.1.28. First, we take the Fourier transform with respect to S to give

$$\frac{\partial^2 \Omega}{\partial N^2} = -c(\mathrm{i}k)\Omega$$

where $\Omega = \mathcal{F}[\omega]$. If we write $\lambda^2 = -c\mathrm{i}k$ then we have a second order differential equation for Ω in the form

$$\frac{\partial^2 \Omega}{\partial N^2} - \lambda^2\Omega = 0$$

with solutions given by

$$\Omega = P\mathrm{e}^{\lambda N} + Q\mathrm{e}^{-\lambda N}$$

for some constants P and Q to be determined. Now, since $\lambda^2 = -c\mathrm{i}k$, we have

$$\lambda = \pm\sqrt{ck}\mathrm{e}^{-\mathrm{i}\pi/4} = \begin{cases} \sqrt{\frac{c|k|}{2}}(1-\mathrm{i}), & k > 0 \\ -\sqrt{\frac{c|k|}{2}}(1+\mathrm{i}), & k < 0 \end{cases}$$

We know that $\Omega \to 0$ as $N \to \infty$, so $P = 0$. Then at $N = 0$ we have

$$\Omega = F(k), \quad \text{where} \quad F(k) = \mathcal{F}[f(S)]$$

so $Q = F(k)$ and hence we can write

$$\Omega(N,k) = \sqrt{2\pi}F(k)G(N,k)$$

where Ω and F are the Fourier transforms of ω and f, respectively, and

$$G(N,k) = \begin{cases} \frac{1}{\sqrt{2\pi}}\exp\left(-\mu(1-\mathrm{i})N\right), & k > 0 \\ \frac{1}{\sqrt{2\pi}}\exp\left(-\mu(1+\mathrm{i})N\right), & k < 0 \end{cases} \tag{B.0.1}$$

where $\mu = \sqrt{\frac{c|k|}{2}}$. The solution can then be written as a convolution

$$\omega(N,S) = \int_{-\infty}^{\infty} f(s+\upsilon)g(N,\upsilon)\,\mathrm{d}\upsilon \tag{B.0.2}$$

where $g(N,S)$ is the inverse Fourier transform of $G(N,k)$ so that

$$g(N,S) = \frac{1}{2\pi}\int_0^{\infty} \mathrm{e}^{-\mu N}\left(\mathrm{e}^{\mathrm{i}(kS+\mu N)} + \mathrm{e}^{-\mathrm{i}(kS+\mu N)}\right)\,\mathrm{d}k$$

We switch from $\mathrm{d}k$ to $\mathrm{d}\mu$ for simplicity. Since $c > 0$ and $\mu > 0$, then

$$k = \frac{2\mu^2}{c} \quad \Rightarrow \quad \mathrm{d}k = \frac{4\mu}{c}\mathrm{d}\mu$$

and hence

$$\begin{aligned} g(N,S) &= \frac{2}{\pi c}\int_0^\infty \mu \mathrm{e}^{-\mu N}\left(\mathrm{e}^{\mathrm{i}\mu\left(\frac{2S}{c}\mu+N\right)}+\mathrm{e}^{-\mathrm{i}\mu\left(\frac{2S}{c}\mu+N\right)}\right)\,\mathrm{d}\mu \\ &= \frac{4}{\pi c}\int_0^\infty \mu \mathrm{e}^{-\mu N}\cos\left(\tfrac{2s}{c}\mu^2+\mu N\right)\,\mathrm{d}\mu \end{aligned}$$

Then we set

$$\mu = \frac{x}{N} \quad \text{so} \quad \mathrm{d}\mu = \frac{\mathrm{d}x}{N},$$

and also set $a = \frac{2S}{cN}$, so that

$$g(N,S) = \frac{4}{c\pi N^2}\left(c(a)-s(a)\right)$$

where

$$\begin{aligned} c(a) &\equiv -\int_0^\infty x\mathrm{e}^{-x}\cos(x)\cos\left(ax^2\right)\,\mathrm{d}x \\ s(a) &\equiv \int_0^\infty x\mathrm{e}^{-x}\sin(x)\sin\left(ax^2\right)\,\mathrm{d}x \end{aligned}$$

Using results from Gradshteyn and Ryzhik (1980), we can deduce that $g(N,S)=0$ for $S>0$, and

$$\begin{aligned} \omega(N,S) &= \int_0^\infty f(S+\upsilon)g(N,\upsilon)\,\mathrm{d}\upsilon \\ g(N,\upsilon) &= \frac{cN}{4\pi\upsilon^{3/2}}\exp\left(\frac{-cN^2}{4\upsilon}\right) \end{aligned} \tag{B.0.3}$$

and also as

$$N\to 0, \quad \omega(N,S)\to f(S).$$

Then if we integrate $g(N,\upsilon)$ with respect to N we have

$$\begin{aligned} \int_0^\infty g(N,\upsilon)\,\mathrm{d}N &= \sqrt{\frac{c}{\pi}}\frac{1}{2\upsilon^{3/2}}\int_0^\infty N\exp\left(\frac{-cN^2}{4\upsilon}\right)\,\mathrm{d}N \\ &= \frac{1}{\sqrt{c\pi\upsilon}} \end{aligned}$$

Therefore, if we substitute into Equation B.0.2 we have

$$\begin{aligned}\int_0^\infty \omega \,\mathrm{d}N &= \int_0^\infty f(S+\upsilon)\left(\int_0^\infty g\,\mathrm{d}N\right)\mathrm{d}\upsilon \\ &= \frac{1}{\sqrt{c\pi}}\int_0^\infty \frac{f(S+\upsilon)}{\upsilon^{1/2}}\,\mathrm{d}\upsilon \\ &= \frac{1}{\sqrt{c}}\mathscr{T}[f] \end{aligned} \tag{B.0.4}$$

where

$$\mathscr{T}[\varsigma(X)] \equiv \frac{1}{\sqrt{\pi}}\int_0^\infty \frac{\varsigma(X+Y)}{\sqrt{Y}}\,\mathrm{d}Y. \tag{B.0.5}$$

Direct evaluation of the convolution integral for $\frac{\partial\omega}{\partial N}$ converges as $N \to 0$, but not for $N = 0$, so it is better evaluated by integrating the original equation from $N = 0$ to $N = \infty$.

$$\left.\frac{\partial\omega}{\partial N}\right|_{N=0} = c\int_0^\infty \frac{\partial\omega}{\partial S}\,\mathrm{d}N = \sqrt{c}\,\mathscr{T}\left[\frac{\mathrm{d}f}{\mathrm{d}S}\right] \tag{B.0.6}$$

Integrating Equation 4.1.31 yields

$$-c\int_0^\infty \frac{\partial\widetilde{\omega}_i}{\partial S}\,\mathrm{d}N = \int_0^\infty \frac{\partial^2\widetilde{\omega}_i}{\partial N^2}\,\mathrm{d}N = -\left.\frac{\partial\widetilde{\omega}_i}{\partial N}\right|_{N=0}$$

and hence, from Equation B.0.6,

$$\left.\frac{\partial\widetilde{\omega}_i}{\partial N}\right|_{N=0} = \sqrt{c}\,\mathscr{T}\left[\frac{\mathrm{d}f_i}{\mathrm{d}S}\right] \tag{B.0.7}$$

▲